|| Shree Ganeshaya Namah ||

DIAGNOSTIC MARKERS FOR SCHISTOSOME-MEDIATED LIVER DISEASE

Bhagyashree Manivannan (Uradey)

A thesis
Submitted to the Victoria University of Wellington
In fulfilment of the requirements for the degree of
Doctor of Philosophy
In Cell and Molecular Biosciences

March 2010

ABSTRACT

Chronic schistosomiasis presents with either a moderate or a severe form, termed intestinal (INT) or hepatosplenic (HS) schistosomiasis, respectively. The *Schistosoma mansoni*-associated hepatomegaly is estimated in 8.5 million people and ultimately results from liver granulomas induced by trapped parasitic eggs. The CBA/J mouse model replicates these two human disease forms and was used to understand the progressive pathology that leads to HS and to identify potential biomarkers. In this model 20% of infected mice spontaneously develop hypersplenomegaly syndrome (HSS) by 20 weeks of infection while the remaining 80% develop moderate splenomegaly syndrome (MSS). Using this model, we compared the liver protein patterns of control mice and mice infected for 6, 8, 12, or 20 (MSS and HSS) weeks. Two-dimensional differential in gel electrophoresis (2D-DIGE) was used to identify protein pattern variations and protein spots were identified using matrix adsorption laser desorption ionisation-time of flight (MALDI-TOF) mass spectrometry. In the first experiment, we found 124 protein spot unique changes for MSS and HSS compared to control mice of which 80 were identified and 35 changes were specific for HSS. In the second experiment, comparison between various time points with control mice revealed 76 significant protein spot changes of which 44 were identified using MALDI-TOF mass spectrometry. Importantly, we found that the abundance of liver keratin D, transferrin isoforms, collagen isoforms, hydroxyproline and *Schistosoma mansoni*-phosphoenolpyruvate carboxykinase increased while epoxide hydrolase isoforms, peroxiredoxin 6 and major urinary protein (MUP) isoforms decreased significantly with infection. To verify the changes in the liver 2D-DIGE analysis, candidate liver protein markers were measured in mouse serum using targeted biochemical assays. The mouse serum analysis showed MUP levels were

decreased, while transferrin, connective tissue growth factor (CTGF), keratin D, hydroxyproline were increased in HSS mice compared to control mice or MSS mice supporting the liver 2D-DIGE analysis. Using targeted assays, serum samples from INT and HS patients were tested for the candidate liver protein markers: keratin D, CTGF, hydroxyproline and transferrin. The human serum analysis showed keratin D levels increased for HS compared to INT and normal sera. The CTGF levels were high in INT compared to HS and normal sera, while transferrin remained unchanged in INT and HS similar to normal sera. Additionally, in severe HS disease, serum hydroxyproline emerged as a strong indicator of fibrosis. We believe that these findings will have direct value in the development of diagnostic tools for early detection of hepatosplenic schistosomiasis in humans.

ACKNOWLEDGMENTS

|| **Pranamya Shirasha Devam Gauriputram Vinayakam** ||

|| **Bhaktavaasam Smaren.h Nityam Aayuh Kamarthasiddhaye** || 1 ||

"One should bow the head and offer obeisance before the son of Gauri, Vinayaka, whose abode is the devotees, and remember Him always for the purpose of positive accomplishments."

I am grateful to my supervisor **Dr. Anne LaFlamme** for her precious advise and guidance for my PhD study. I sincerely thank my co-supervisor **Dr. Bill Jordan** for imbibing me with his biochemistry and proteomics knowledge.

I express my gratitude towards **Dr. Pisana Rawson** without whose help proteomic techniques were impossible**.** I am grateful to **Danyl McLauchlan** and **Dr. Nokuthaba Sibanda** for their help in bioinformatics and statistics respectively. I would like to thank all at Cell and Molecular Biology laboratory (KK601) and Centre for Biodiscovery proteomics facility (KK714), Victoria University of Wellington, New Zealand.

I thank **Dr. Evan Secor** for his advise and support for my work at Centers for Disease Control and Prevention, Atlanta, USA and for providing the CBA/J mice liver and sera samples and the human serum samples for my project. My sincere thanks to **Peter Augostini,** CDC, Atlanta for sharing his knowledge about the snails (*Biomphalaria glabrata)* and CBA/J mice liver and serum collection for the study.

I dedicate my work to **Aai-Baba** (my mother and father) and **Yadvendra** (my brother) for their encouragement and enthusiasm, **Amma-Aappa** (my in-laws) and my husband,

Manivannan for their help and support through out. Thanks to all my friends and relatives in India.

Finally, my special thanks to the funding sources, which made my project possible: Vice-Chancellor's Strategic Research Scholarship, Wellington Medical Research Foundation Research Grant, University Research Fund, Wellington Medical Research Foundation Travel Grant 2008, American Society of Tropical Medicine and Hygiene Travel Award 2008, New Zealand Postgraduate Study Abroad Awards 2009, J.L. and Kathleen Stewart Research Experience Awards 2009, VUW Faculty Strategic Research Grant 2009.

|| Vakratunda Mahakaya Suryakotisamaprabha
Nirvighnam Kuru me Deva Sarvakaryeshhu Sarvada ||

"O Ganapati, One with a curved trunk, a large body, and a brilliance equal to a crore suns!
O God, please make all my undertakings free from obstacles always."

TABLE OF CONTENTS

LIST OF TABLES

CHAPTER 1

CHAPTER 3

CHAPTER 4

CHAPTER 5

APPENDIX A

APPENDIX C

APPENDIX E

LIST OF FIGURES

CHAPTER 1

CHAPTER 2

CHAPTER 3

CHAPTER 4

CHAPTER 5

APPENDIX F

APPENDIX G

ABBREVIATIONS

%LBW	percent liver to body weight ratio
%SBW	percent spleen to body weight ratio
10-FTHDH	10-formyl tetrahydro folate dehydrogenase
2D-DIGE	two-dimensional differential in-gel electrophoresis
ATPase alpha	ATP synthase-H+ transporting mitochondrial-F1 complex-alpha subunit-isoform 1
ATPase beta	ATP synthase-beta subunit
AVR	average volume ratio between study groups
BA-DHAK	bifunctional ATP-dependent dihydroxyacetone kinase
BHMT	betaine-homocysteine s-methyltransferase
BSA	bovine serum albumin
BVA	biological variation analysis
C	control
CAA	circulating anodic antigen
CCA	circulating cathodic antigen
CHAPS	3-[(3-cholamidopropyl) dimethylammonio]-1-propanesulfonate
CHCA	α-cyano-4-hydroxycinnamic acid
CRIs	cross-reactive idiotypes
CTGF	connective tissue growth factor
DMDH	dimethylglycine dehydrogenase
ELISA	Enzyme Linked Immunosorbent Assay
FBPase	fructose-1, 6-bisphosphatase 1
FDR	false discovery rate

GSTPi	glutathione S-transferase class pi
H	HSS
HBV	hepatitis B virus
HCA	hierarchical cluster analysis
HCV	hepatitis C virus
HS	hepatosplenic schistosomiasis
HSS	hypersplenomegaly syndrome
IFN-γ	interferon-gamma
INT	intestinal schistosomiasis
IPA	Image Pattern A
IPB	Image Pattern B
IPC	Image Pattern C
IPD	Image Pattern D
IPE	Image Pattern E
Keratin D	cytokeratin 18 or keratin 18
M	MSS
MALDI-TOF	matrix assisted laser desorption-ionization time of flight
MSS	moderate splenomegaly syndrome
MUP	major urinary protein
Mw	molecular weight
PCA	principle component analysis
PEPCK	phosphoenolpyruvate carboxykinase
pI	isoelectric pH
PVDF	polyvinylidene difluoride

r square	r square for linear regression
RBP1	retinol binding protein-1
SDS-PAGE	sodium dodecyl sulphate- polyacrylamide gel electrophoresis
SEM	standard error of mean
Sm-PEPCK	*Schistosoma mansoni*-phosphoenolpyruvate carboxykinase
TGF-β	transforming growth factor-beta

CHAPTER1: INTRODUCTION

1.1 Background

In 1851, Theodor Bilharz first identified the cause of urinary schistosomiasis and thus schistosomiasis is known as bilharzia or bilharziosis in many countries. Endemic in Africa, South America and Asia, the spread of schistosomiasis is due to the freshwater snails that carry the parasite. Also known as snail fever, human schistosomiasis is caused by five helminth species: *Schistosoma mansoni, Schistosoma haematobium, Schistosoma japonicum, Schistosoma intercalatum,* and *Schistosoma mekongi* and of these 5 species, *S. mansoni* is the focus of this thesis. The worms are called blood flukes because they live in the vascular system of humans and other vertebrates like dogs, pigs, cows, water buffaloes, horses. The life cycle of the worms involves two hosts: fresh water snails, which are the intermediate hosts, carrying the asexual stage and humans (and other vertebrates) which are the definitive hosts carrying the sexual stage (Figure 1.1). Different genera of snails act as intermediate hosts for each of the five *Schistosoma spp.* and are listed in Table 1.1.

TABLE 1.1 Fresh water snails act as intermediate hosts for different species of schistosomes.

No.	Schistosoma *spp.*	Snail *gen.*
1.	*Schistosoma mansoni*	*Biomphalaria spp.*
2.	*Schistosoma haematobium*	*Bulinus spp.*
3.	*Schistosoma japonicum*	*Oncomelania spp.*
4.	*Schistosoma intercalatum*	*Bulinus spp.*
5.	*Schistosoma mekongi*	*Neotricula spp.*

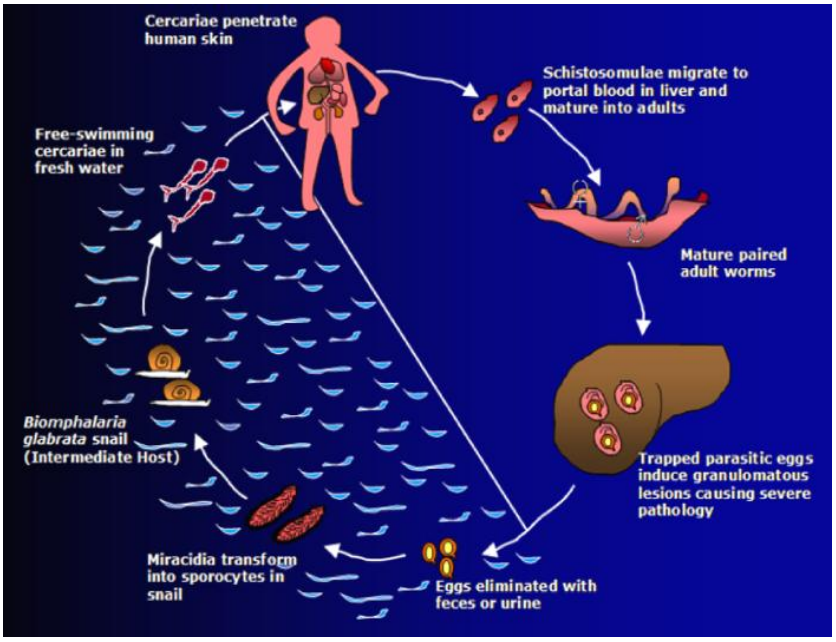

FIGURE 1.1 Life cycle of *Schistosoma mansoni*. In the human vascular system, adult worms mate and lay eggs. Parasite eggs exit the host through feces and urine. On sensing fresh water, the miracidia are released from the eggs and penetrate the snail. Within 3-5 weeks, they asexually multiply into hundreds of fork-tailed cercariae. The cercariae leave the snail and swim to a human, where they penetrate the skin. Inside the definitive host, cercariae transform into schistosomulae and travel to the heart, lungs and portal veins, where they develop into adult worms. (Picture drawn is based on my microscopic observations and readings.)

1.2 Geographic distribution

Schistosomiasis is endemic in 74 countries, mostly African, Asian, Eastern Mediterranean, Caribbean and South American countries (Figure 1.2) and is the second most devastating parasitic disease after malaria in terms of the world health budget. Currently, 200 million people have schistosomiasis and 600 million people are at the risk of infection (Chitsulo *et al.*, 2000). In particular, *Schistosoma mansoni* infects almost 83 million people causing

intestinal or hepatic schistosomiasis (Crompton, 1999). It is estimated that approximately 40% of the 200 million people affected with schistosomiasis worldwide remain asymptomatic (80 million) and 60% become symptomatic (120 million). Of the symptomatic patients approximately 10% develop severe hepatosplenic disease (20 million) (Chitsulo *et al.*, 2000) with 8.5 million people suffering from life threatening *S. mansoni* hepatosplenic disease alone (Van der Werf *et al.*, 2003).

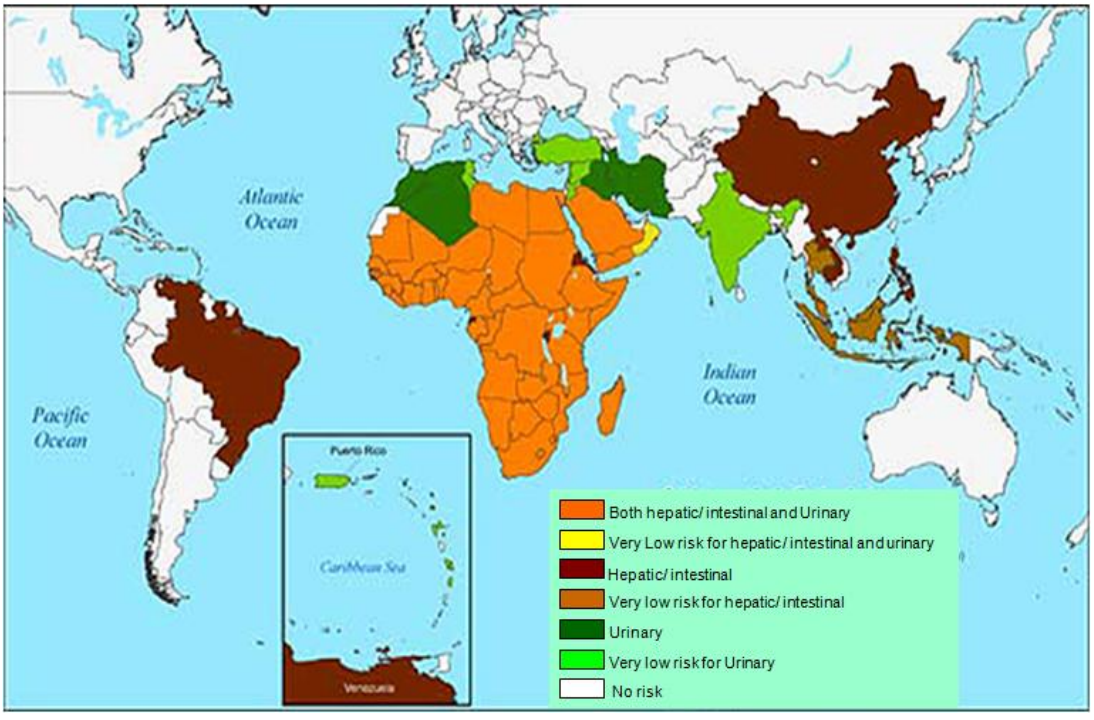

FIGURE 1.2 Global distribution of schistosomiasis, 2007 (Map courtesy: Centers for Disease Control and Prevention, USA).

In addition to the infection of persons living in endemic areas, travellers are at risk of schistosomiasis due to bathing, wading or swimming in fresh waters in these endemic areas. A report by GeoSentinel Surveillance Network 1997-2008, USA on *Schistosome*-endemic area travellers shows that, of 828 travellers evaluated for schistosomiasis 49%

were diagnosed with schistosomiasis (Nicolls *et al.,* 2008). The data questions the effectiveness of pre-travel intensive schistosomiasis education programs and emphasises the importance of research programs for biomarkers, vaccine and drug development. Thus, tourism and immigration from endemic areas results in cases of schistosomiasis even in the developed world. Finally, researchers warn that global warming will lead to the shifting of isotherms, lines that connect areas with the same temperature, and this shifting may ultimately facilitate spread of infectious diseases to new places and novel habitats. Current records indicate that intestinal schistosomiasis which previously occurred only at altitudes below 1,400 metres above sea level, now occurs at 1,682 metres above sea level (Githeko, 2009), suggesting the shift has already begun.

1.3 Schistosomiasis mortality and morbidity

Schistosomiasis-associated mortality is about 280,000 people per year (0.08% of the deaths worldwide). The majority of these mortalities due to *S. mansoni* infections occurring in 52 countries (Pearce and MacDonald, 2002) include both intestinal schistosomiasis and hepatosplenic schistosomiasis. Figure 1.3 shows the cartogram for deaths due to schistosomiasis in the year 2002 (approximately seven deaths per million people). However, this information does not include estimates of deaths that may be due to schistosomiasis-associated pathologies such as bladder cancer, cirrhosis of the liver, or colon cancer (www.worldmapper.org/images/largepng/393.png) and so underestimates the true number of deaths due to schistosomiasis.

In general, the morbidity related to schistosomiasis is classified into overt or end-organ morbidity (direct) or subtle systemic morbidity (indirect). Consequence of egg deposition

is the most severe and accounts for the overt or end-organ morbidity characterised by hepatic fibrosis, portal hypertension and their clinical complications. In S. *mansoni* infections end-organ morbidity includes bleeding oesophageal varices, haematemesis and *S. mansoni*-associated hepatomegaly that is estimated in 8.5 million people (Van der Werf *et al.*, 2003).

Subtle morbidity includes stunted growth, decreased cognitive performance and anaemia observed in intestinal and hepatosplenic schistosomiasis. These subtle forms of morbidity are a consequence of chronic infection with either malnutrition and/or iron deficiency occurring simultaneously. Pregnant women, young children, growing adolescent children and persons with co-morbid diseases are most susceptible to subtle forms of morbidity (Olds and Dasarathy, 2001). Details of the clinical features of these morbidities are described in subsequent sections. Epidemiological data shows that although chemotherapy provides protection for schistosomiasis there is a high risk of re-infection (Magnussen, 2003). Additionally, the use of anti-schistosomal drugs influences development, physical fitness and working ability in adults and in children (Olds and Dasarathy, 2001) thus contributing to schistosomiasis associated morbidity.

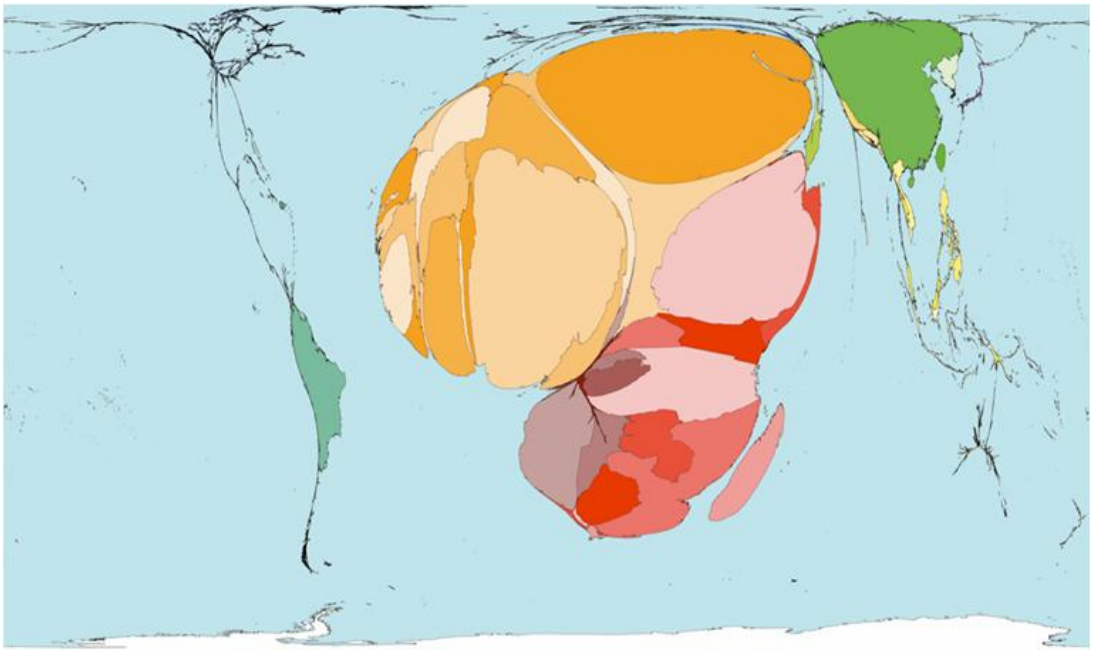

FIGURE 1.3 Cartogram shows schistosomiasis deaths in 2002, highest being in the sub-Saharan Africa (yellow, orange and red), followed by South Americas (blue) and lowest in Asian countries mainly China (green) (Map courtesy: www.worldmapper.org).

1.4 Clinical features of schistosomiasis

1.4.1 Acute toxaemic schistosomiasis

The acute phase of schistosomiasis occurs at 6-8 weeks after infection coincides with the onset of egg laying by the adult worms and is mostly seen in travellers, army personnel and peace workers. Acute schistosomiasis is characterised by "katayama fever", cough, headache, rash, diarrhoea, weight loss and eosinophilia, diffuse abdominal pain and toxaemia especially upon first exposure to the parasite egg antigen. Katayama fever is believed to be due to the high worm and egg antigen stimuli that result from egg-specific immune response and is rare in chronically exposed people. Although the eggs are excreted through urine and faeces, half are lodged in the liver microvasculature inducing a strong immune response that directs granulomatous lesion development. Additionally,

peripheral-blood mononuclear cells produce large quantities of tumour-necrosis factor (TNF), interleukin-1 (IL-1) and IL-6 (Pearce and MacDonald, 2002) during acute schistosomiasis. Abdominal ultrasound shows hepatosplenomegaly and periportal and peripancreatic lymphadenomegaly (lymph nodes enlarge temporarily). These changes are transient and non-specific and may resolve (Corachan, 2002). While, most clinical manifestations are benign; some are severe and can result in severe morbidity or death. However, the exact mechanism by which acute toxaemic schistosomiasis causes death is not fully understood.

1.4.2 Chronic clinical features of schistosomiasis

The chronic phase occurs at approximately 4-5 years or more post-infection presenting with severe granulomatous lesions in the liver, intestine, spleen, lungs, brain and male and female pelvic organs. Liver fibrosis and hepatosplenomegaly due to granulomatous lesions are the most important features of chronic schistosomiasis. The chronic disease may also cause blood in stool, abdominal pain, oesophageal varices and haematemesis and if untreated and lead to death (King and Dangerfield-Cha, 2008, Strauss, 2002). The common features (granulomas, fibrosis and hepatosplenomegaly) are detailed in the subsequent sections.

1.4.2.1 Granulomas

Granulomatous lesions result from schistosome eggs that get trapped in tissues. In *S. mansoni* infection, the major sites of egg deposition are the liver and intestine. Egg induced granuloma formation is a delayed type hypersensitivity (type IV hypersensitivity) reaction towards hepatotoxic components secreted by the entrapped egg (Doughty *et al.*,

1984). The granuloma that forms around the egg consists of a number of different types of cells: T and B lymphocytes, macrophages, epitheloid cells, mast cells, fibroblasts and eosinophils (Figure 1.4). The immune cells contribute to the formation of the granuloma and interactions with surrounding hepatocytes and in particular CD4 cells have been shown to be essential in granuloma formation (Jankovic *et al.*, 1998). The interactions are highly complex, and occur both by direct cell to cell interactions and a wide variety of cytokines, resulting in severe pathology (Rumbley *et al.*, 1998). Many studies have contributed to the understanding of granulomatous immune responses and modulation in schistosomiasis with varying results. Previous studies have demonstrated a pivotal role for IFN-gamma in the early granulomatous response to schistosoma eggs (Rezende *et al.*, 1997). In *S. mansoni*-infected gene knockout mice deficient in either CD8 lymphocytes or IFN-gamma demonstrated that neither of these immunologic components plays roles in granuloma formation and or immune responses during the acute or chronic stage of infection (Yap *et al.*, 1997). A study in mice demonstrated that *S. mansoni* infection induced IL-2 and IFN-gamma (Th1 cytokines) just before parasite egg laying and initiated liver granuloma formation during the acute disease. Whereas after egg laying and during the chronic disease the embedded parasite eggs induced IL-4 and IL-5 (Th2 cytokines) (Cheever *et al.*, 1992) thus illustrating the importance of immune responses in the pathogenesis of liver granulomas during schistosomiasis.

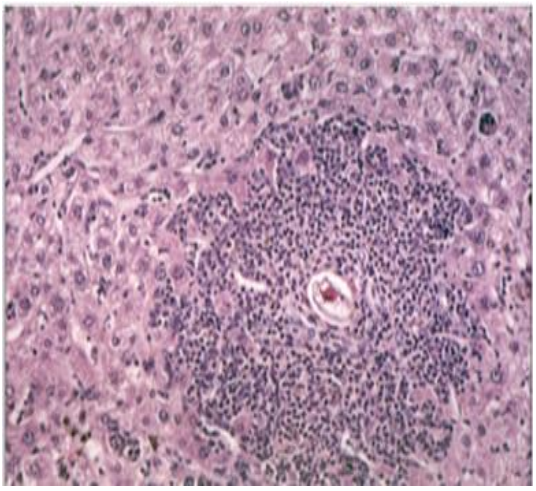

FIGURE 1.4 Haematoxylin and eosin (H&E) stained section of liver parenchymal granuloma with *S. mansoni* egg at its centre. The granuloma around the egg consists of different types of immune cells like macrophages, eosinophils, T cells. (Image courtesy of Dr. Anne La Flamme)

1.4.2.2 Intestinal schistosomiasis

In 90% of infected individuals, the disease symptoms and egg-associated inflammation recede resulting in intestinal schistosomiasis (INT) with potential gastrointestinal haemorrhage. Nearly 80 million people have INT (Rowland, 1971) caused by *S. mansoni* endemic in 52 countries (Kogulan and Lucey, 2007). INT remains asymptomatic most of the time with subtle morbidity either due to nutrient deficient food (anaemia, impaired cognitive development and growth retardation) and/ or due to functional difficulties (educational impairment and productivity loss). Importantly, patients with INT have lower titres of IgM, IgG and IgA antibodies to *S. mansoni* carbohydrate antigens than those with hepatosplenic disease (Nyame *et al.*, 2003). Moreover, intestinal granulomas are smaller and contain less collagen fibres when compared to hepatic granulomas (Santos *et al.*,

1992). Yet, despite these known differences, it is not known what factor(s) drive the development of intestinal versus the more severe hepatosplenic disease.

1.4.2.3 Hepatic fibrosis

S. mansoni infection is an important cause of hepatic fibrosis. Hepatic fibrosis is a wound healing process in the liver, triggered by chronic injury due to inflammatory responses and accumulation of extracellular matrix proteins (especially collagen) being overproduced, not degraded, or both. Advanced hepatic fibrosis is asymptomatic but can lead to portal hypertension or cirrhosis and ultimately failure to build and replace destroyed liver cells resulting in liver dysfunction and liver failure. Schistosomiasis research has been directed on identifying biomarkers for hepatic fibrosis and determining the underlying mechanisms that lead to hepatic fibrosis. Studies have characterised collagen isoforms in liver biopsies indicating increased deposition of collagen I, III and B forms in portal triads and fibrotic septa (Biempica *et al.*, 1983). Another study demonstrated increased levels of serum procollagen peptides and collagen type VI suggesting their importance for the assessment of degree of hepatic fibrosis in schistosomiasis (Shahin *et al.*, 1992). Increase in other cytoskeletal proteins like actin in schistosome infections show the intensity of liver damage caused by the parasite during pathogenesis of schistosomiasis (Andrade *et al.*, 1992, Harvie *et al.*, 2007).

Measurement of liver hydroxyproline in liver fibrosis and cirrhosis requires needle liver biopsies which is an invasive technique and has shown sampling variability (Lee *et al.*, 2005). Alternatively, serum hydroxyproline content has been measured in liver fibrosis associated with chronic HCV infections (Attallah *et al.*, 2007) and therefore proves to be promising for schistosomiasis hepatic fibrosis. Additionally, recent studies have focussed

on connective tissue growth factor (CTGF) and transforming growth factor -β (TGF-β) in fibrosis. Studies show increased CTGF and TGF-β in HCV fibrosis (Kovalenko *et al.*, 2009) and increased CTGF in idiopathic portal hypertension (Morikawa *et al.*, 2007). Another study associates CTGF variants with schistosomiasis fibrosis (Dessein *et al.*, 2009). During acute *S. mansoni* infection, hepatic inflammation is controlled by TGF-β and IL-10 (Herbert *et al.*, 2008), while in the chronic stage IL-13 and TGF-β appear to be most important in the fibrotic process (Kaviratne *et al.*, 2004).

Many schistosomiasis studies have also focussed on the intermediate filament proteins that support the liver infrastructure and are hepatoprotective. Intermediate filament protein keratin 18 (cytokeratin 18) fragments have been studied extensively in liver fibrosis related to non-alcoholic steatohepatitis in children (Vos *et al.*, 2008) and adults (Yilmaz, 2009) but not in human schistosomiasis fibrosis. These studies indicate a definitive role of hepatic inflammation and hepatocellular apoptosis in inducing liver fibrosis. Additionally, studies indicate mutations in keratin 18 predisposes the liver to fibrosis during hepatocellular diseases (Ku *et al.*, 2003). Studies have demonstrated increased abundance of vimentin in hepatosplenic schistosomiasis (Andrade *et al.*, 1992) and in acute schistosomiasis (Harvie *et al.*, 2007). Laminin, another intermediate filament protein is increased in human hepatosplenic schistosomiasis compared to hepatointestinal schistosomiasis (Andrade *et al.*, 1992, Parise and Rosa, 1992) indicating a definitive role of these proteins in severe disease.

Imaging techniques are used commonly for assessing schistosomiasis morbidity. Ultrasound is one such technique which is cheap, non-invasive and easily portable; some

studies have established hepatic fibrosis grading system based on the ultrasound image pattern (IP) analysis, viz. A, B, C, D, E, F. Image patterns A, B represent normal livers and C, D, E, F represent increasing levels of fibrosis (Mohamed-Ali *et al.*, 1999). Mwinzi and co-workers assessed the ultrasound image patterns for degree of liver fibrosis in schistosomiasis patients. The authors' assigned patients with a normal liver texture as IPA, IPB was indicative of patients with a small degree of fibrosis, but no definitive pathology. IPC showed "ring echoes" that appeared as pipe stems in a perpendicular scan. IPD characterised by a "ruff" around the main portal vein and bifurcation. IPE showed a "ruff" extending into the liver parenchyma with patches of fibrosis (Mwinzi *et al.*, 2004). This same image pattern assessment was used in our study for human serum analysis.

1.4.2.4 Hepatosplenic schistosomiasis

Hepatosplenic disease caused by *S. mansoni* is characterised by hepatosplenomegaly, Symmers' or "clay pipestem" fibrosis, portal hypertension, and oesophageal varices, which may lead to haematemesis and death. The marked features of hepatosplenic schistosomiasis are renal failure with anaemia, abdominal distension, hepatosplenomegaly, pedal oedema, and ascites seen in adults and children. In 10% infected individuals, the disease presents with severe hepatic and Symmers' fibrosis, portal hypertension and portal-systemic venous shunts due to hepatic granulomas and gastrointestinal bleeding; these contribute to life-threatening severe hepatosplenic schistosomiasis (HS). Patients, both adults and children (Figure 1.5) with HS present relatively normal liver function, but increased hydroxyproline levels and collagen synthesis (Warren 1978). Hepatosplenic schistosomiasis associated morbidity is a consequence of egg deposition in other tissues in addition to the liver and intestine, aggravating disease pathology. Morbidities due to egg

deposition in three most common tissues (reproductive organs, central nervous system, lungs) are discussed below.

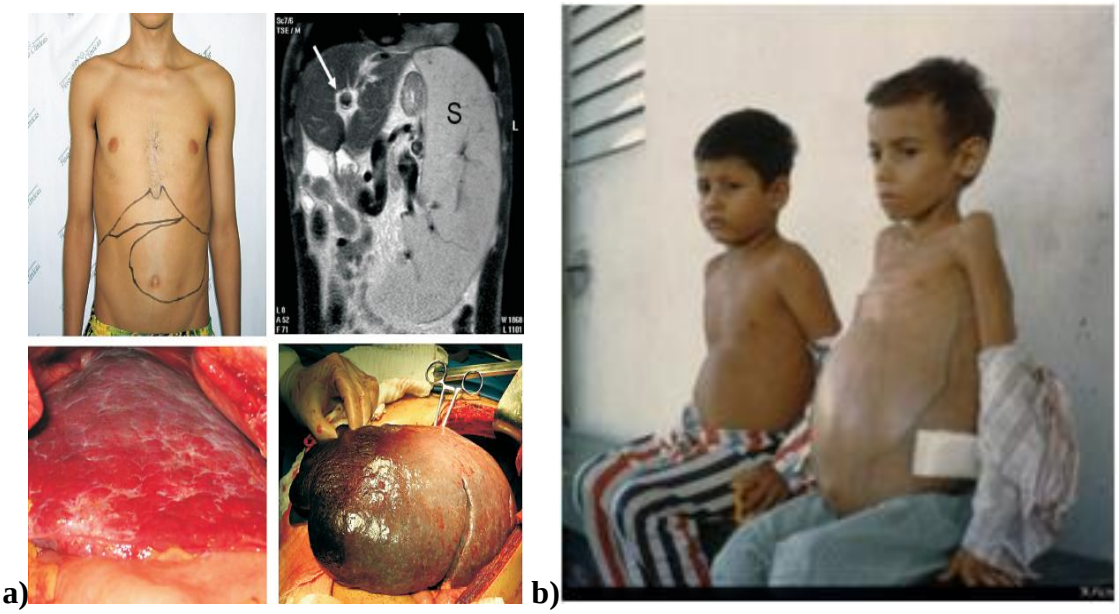

FIGURE 1.5 a) Magnetic resonance imaging and surgery of a 21-year-old patient with hepatosplenic schistosomiasis. On the upper right hand side, a coronal section of the abdomen captured by magnetic resonance imaging, showing periportal fibrosis (white arrow) and a huge spleen (S). During surgery, the nodular surface of the liver (on the left) and the spleen (on the right) is evident. (Image courtesy: Drummond *et al.*, 2006) **b)** Puerto Rican children with abdominal distension suffering from hepatosplenic schistosomiasis (Image courtesy: Tropical Disease Research, WHO).

1.4.2.4.1 Genital schistosomiasis

Lodging of the parasite eggs in the internal genital organs presents with ulcerative lesions in the female lower reproductive tract (cervix, valva and vagina) with ovaries mainly affected by *S. haematobium* infections in 50-80% women and *S. mansoni* infections in 5-

27% women. It is documented that female genital schistosomiasis facilitates the bidirectional transmission of sexually transmitted diseases as HIV-1 and human papillomavirus (Feldmeier *et al.*, 1998, Poggensee *et al.*, 2000). Another study indicates 49% of infected women had impaired fertility (Takougang *et al.*, 2008) supporting a report which lists lesions of the ovaries and fallopian tubes, fibrotic scars, hormonal disturbances and viral co-infections as the leading causes that explain infertility in schistosome-infected women (Feldmeier *et al.*, 1998). In male patients the parasite eggs get lodged in the epididymis, testicles, spermatic chord, seminal vesicles and prostate glands with haemospermia (blood in the ejaculate) which is the most important symptom of male genital schistosomiasis observed in travellers and men from endemic areas (Feldmeier *et al.*, 1999). The epidemiology and pathogenesis of haemospermia during schistosomiasis is still unknown and therefore there is no definitive evidence that male genital schistosomiasis affects fertility although case reports indicate possibilities of testicular tumours (Lopes *et al.*, 2003, Mortati Neto *et al.*, 2004) suggesting that the disease outcome for male patients may be fatal.

1.4.2.4.2 Central nervous system schistosomiasis

Parasitic egg deposition in the central nervous system involves focal and generalised seizures, headache, myeloradiculopathy with lower limb and back pain and bladder dysfunction. Spinal schistosomiasis due to *S. mansoni* infection presents as transverse myelitis (Kogulan and Lucey, 2007) and is due to eggs trapped in the lower vertebral plexus affecting the lower spinal cord. Asymptomatic deposition of *S. mansoni* eggs in the brain and meninges is more frequent in hepatosplenic compared to intestinal schistosomiasis. Additionally, some patients with central nervous system schistosomiasis

present with epilepsy. While initially high, the mortality rate for patients with schistosomal myelopathy has fallen from 72% to 11.5% since 1965 due to early treatment options (Scrimgeour and Gajdusek, 1985), but the risk for central nervous system schistosomiasis still persists.

1.4.2.4.3 Pulmonary schistosomiasis

Also known as, schistosomal cor pulmonale, pulmonary schistosomiasis develops in 5% of hepatosplenic *S. mansoni* infections. It is characterised by larval pneumonitis with a cough, mild wheezing, low-grade fever and pulmonary hypertension. Destruction of the wall of pulmonary arterial branches is common, and fibrin deposition causes thickening of the pulmonary artery walls. These acute lesions are due to schistosomal granulomata in the lung. It is observed that the incidence of schistosomal cor pulmonale is higher in women than in men but the reason for this difference is unknown. Death in patients with pulmonary schistosomiasis is often a result of congestive heart failure (Lopes de Faria, 1954).

1.5 Laboratory diagnosis

1.5.1 Stool or urine analysis

The most common method for diagnosis of schistosomiasis is microscopic identification of eggs in stool or urine, also known as the stool smear Kato-Katz method (Santos *et al.*, 2005). The difference in the egg morphology helps to differentiate between the *Schistosoma spp*. and has been described by the Division of Parasitic Diseases, Centers for Disease Control, USA. The eggs of *S. haematobium* are spindle-shaped with a terminal spine. *S. intercalatum* have prominent terminal spine and equatorial (central) bulge. *S.*

japonicum eggs are oval with less conspicuous spine whereas *S. mansoni* eggs are spindle-shaped with a lateral prominent spine. Lastly, *S. mekongi* eggs are oval and have a small knob on the side. The different egg morphologies are shown in Figure 1.6. While this method is the most common it is also insensitive and low intensity infections are hard to detect.

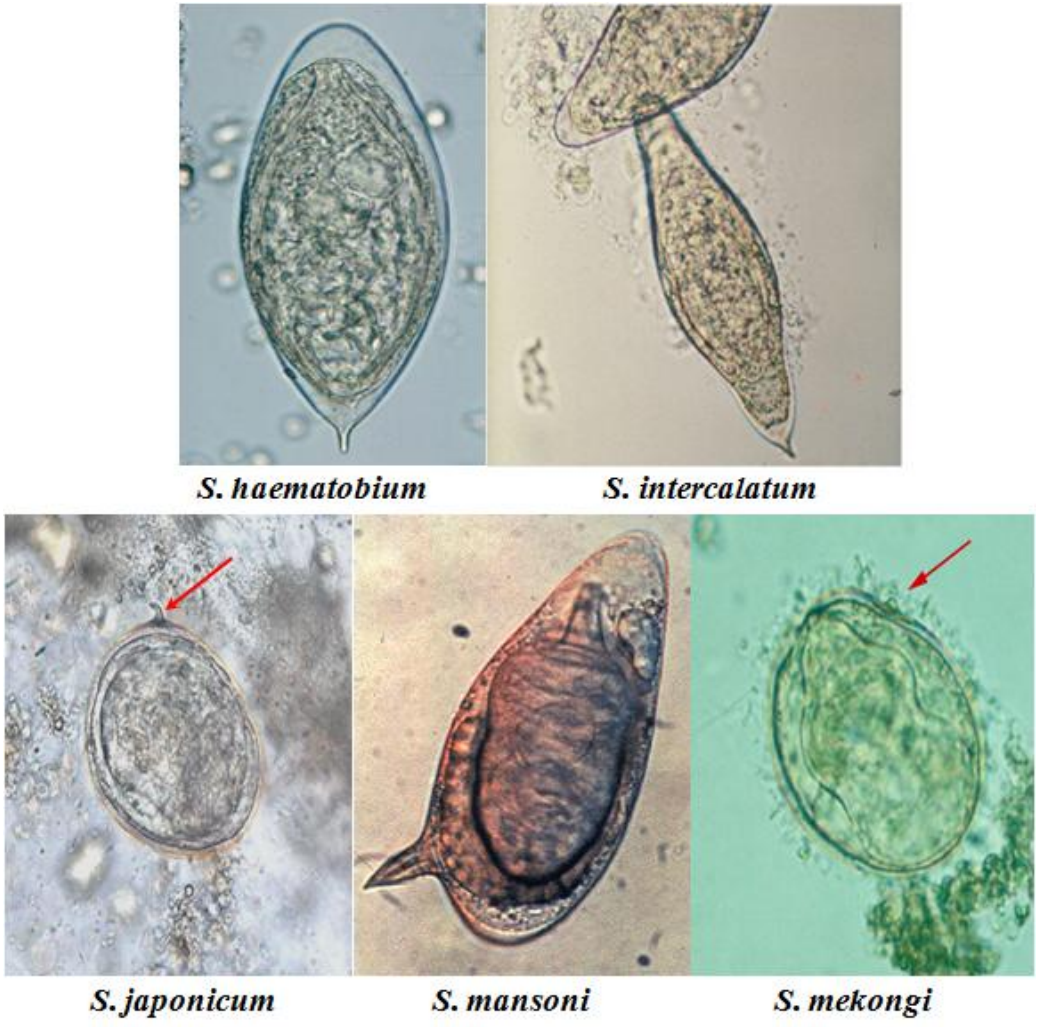

FIGURE 1.6 Egg morphology of *Schistosoma spp.* The five species: *S. haematobium*, *S. intercalatum*, *S. japonicum*, *S. mansoni*, and *S. mekongi* have distinct egg structures (*spp*. arranged alphabetically, Image courtesy: Division of Parasitic Diseases, Centers for Disease Control and Prevention).

1.5.2 Immunoassays

Recent use of antigen preparations for the detection of infection-specific antibodies has made schistosomiasis diagnosis easier. These antigen reagents are prepared by homogenising worms from infected tissue followed by subcellular organelle fractionation to generate vesicles from the broken endoplasmic reticulum called microsomes (nonexistent in live cells or tissues) which are rich in worm antigens. Therefore, the prepared antigen is called microsomal antigen. Thus, serum antibodies can be detected that are highly specific for *S. mansoni* adult worm microsomal antigen, with similar tests available for *S. haematobium*, and *S. japonicum*. These antigens are used in Enzyme Linked Immunosorbent Assay (ELISA) to detect infection. Antibodies from the infected serum recognise GP30 from adult worm antigen with *S. mansoni* infection, GP18, GP23 or GP29 identifies *S. japonicum*, and GP23 identifies *S. haematobium* infections (Al-Sherbiny *et al.*, 1999). For *S. mansoni* infections, the assay sensitivity is 99%, for *S. haematobium* infection it is 95% and for *S. japonicum* infection the assay sensitivity is <50% (Courtesy: Division of Parasitic Diseases, Centers for Disease Control and Prevention, USA).

The ELISA techniques for quantitative determination of circulating anodic antigen (CAA) and circulating cathodic antigen (CCA) in serum and urine samples are used to detect infection for *S. mansoni* and *S. haematobium* (Al-Sherbiny *et al.*, 1999). CAA and CCA have been studied extensively in mouse models but little in human immunodiagnostic applications. Detection of these antigens is not sensitive in low intensity infections. Also, the amount of CAA or CCA detected in the circulation or in the urine does not reflect the

actual production by the worms during infection and can be a result of host metabolic activities (Dam *et al.*, 1996). In addition to low sensitivity in low infections, the CCA and CAA tests are costly. Finally, none of these antibody tests can detect difference between past and current infection and are possible only when the individual has the prolonged schistosome infection.

1.5.3 Parasite DNA detection

In the last few years, a rapid 2-step polymerase chain reaction (PCR) has been is being used to detect *S. mansoni* DNA in human urine, faecal and serum samples and is 10 times more sensitive than the Kato-Katz examination (Pontes *et al.*, 2002). This PCR technique can detect infections as early as 3-4 weeks (Sandoval *et al.*, 2006) although its efficacy needs to be tested for acute human schistosomiasis infections. This test should allow a more reliable diagnosis of schistosomiasis infection especially with low intensity infections as it has low costs and easy protocols. Unfortunately, while it will diagnose schistosomiasis infection, it will be unable to determine whether the schistosomiasis is intestinal or hepatosplenic. This distinction must be made separately by imaging techniques, which are currently only useful during late stage of disease.

1.5.4 Radio Imaging

Ultrasound is an economical and non-invasive technique for assessment of schistosomiasis morbidity but it underestimates liver fibrosis and is ineffective at detecting early liver pathology during the chronic stage. Even when performed by experienced clinicians the reproducibility of ultrasound measurements are unsatisfactory in the early stages of fibrosis (Chiavaroli and Grima, 2008). Computed tomographic scanning and magnetic

resonance imaging are other conventional imaging techniques used for schistosomiasis morbidity detection. Unfortunately, these techniques like ultrasound are unable to provide a definitive diagnosis during early stages of schistosomiasis.

In *Schistosomiasis mansoni,* ultrasound shows fibrotic bands along the portal veins (Figure 1.7). Computed tomography shows low-attenuation bands around the large portal vein branches in the central part of the liver with marked enhancement (Figure 1.8). Magnetic resonance imaging shows periportal fibrous thickening in the central part of the liver with shrunken and irregular liver (Figure 1.5). The use of magnetic resonance imaging for diagnosis of chronic schistosomiasis disease of the spinal cord has increased the importance of this imaging technique (Drummond *et al.*, 2006) for assessment of schistosomiasis morbidity; however, this technique is very expensive.

Ultrasound is a commonly used technique and therefore many authors have described various methods for the gradation of liver fibrosis during schistosomiasis infection. In 1992, Abdel-Wahab and co-workers described a grading method for ultrasound assessment of periportal fibrosis for hepatosplenic schistosomiasis patients according to the thickness of the portal tracts: grade I = 3-5 mm, grade II ≥ 5-7 mm, and grade III ≥ 7 mm (Abdel-Wahab *et al.*, 1992). Another method demonstrated by Mohamed-Ali and co-workers graded the ultrasound detectable periportal fibrosis as F0, FI, FII and FIII based on the thickening of the peripheral periportal branch wall, secondary portal branches and the fibrosis reaching the surface of the liver (Mohamed-Ali *et al.*, 1999). In two separate studies, the authors used similar image pattern grading method of A through F, depending on the extent of visible fibrotic tissue around the portal branch and throughout the

parenchyma. Grades A and B were considered to be normal livers, whereas grades C, D, E, and F represented increasingly severe manifestations of the schistosomiasis disease (Booth *et al.*, 2004, Mwinzi *et al.*, 2004). Details of the grading technique used by Mwinzi and co-workers are described in section 1.4.2.3 (hepatic fibrosis) (2004). These studies indicate that a standard and definitive grading method for schistosomiasis ultrasound imaging patterns needs to be considered to allow immediate treatment solutions.

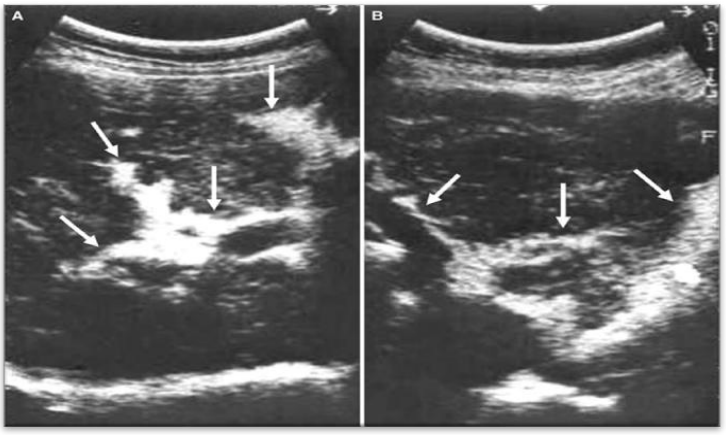

FIGURE 1.7 Ultrasound of *S. mansoni* infected 40-year-old man. Sonogram of the right (A) and left hepatic lobe (B) shows hyper-echoic, thick, fibrous bands along the portal vein branches (arrows) (Image courtesy: Manzella *et al*., 2008).

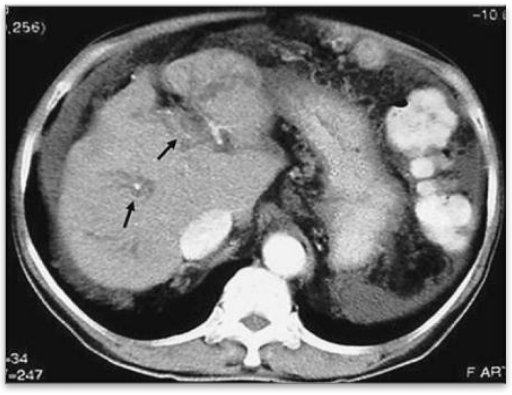

FIGURE 1.8 Computed tomography of a 69-year-old man with *S. mansoni* infection. Post-contrast CT image shows low-attenuation rings or bands around the portal vein branches (arrows). Note shrunken liver with undulated surface and ascites due to advanced liver cirrhosis (Image courtesy: Manzella *et al*., 2008).

1.6 Treatment and prevention

1.6.1 Anti-schistosomal drugs

Anti-schistosomal drugs or anthelmintics are chemotherapeutic agents used to treat schistosomiasis. Currently, praziquantel ($C_{19}H_{24}N_2O_2$), oxamniquine ($C_{14}H_{21}N_3O_3$), metrifonate ($C_4H_8Cl_3O_4P$) and artemisinins ($C_{15}H_{22}O_5$) are available for treatment, with praziquantel and oxamniquine being the drugs of choice. Praziquantel is the most common and has a cure rate greater than 85%. Infections with *S. mansoni* and *S. haematobium* are treated with a single dose of 40 mg/kg/d and *S. japonicum* and *S. mekongi* with 60 mg/kg/d of praziquantel. Although a single dose is effective, the treatment becomes long-term considering the high rates of re-infection. No vaccine or prophylactic chemotherapy is currently available. Additionally, co-infections in schistosomiasis especially HIV-1, HPV, malaria and many other infectious diseases pose a greater challenge to scientists. However, Utzinger and co-workers have described a negative association between infection intensity and praziquantel cure rates especially for *S. mansoni* infections (Utzinger *et al.*, 2000) suggesting that host-related factors and pre-patent infections affect incomplete parasite clearance and thus treatment failures.

1.6.2 Control measures

Molluscicides are pesticides against the intermediate snail host for schistosomes. Spread of schistosomiasis is prevented by using molluscicides and other biological agents to eliminate fresh water snails. However, snail susceptibility and/ or resistance phenotypes have hindered this process (Lardans and Dissous, 1998) and indicate that the use of molluscicides alone will not be effective. Proper education about schistosomiasis and related diseases has improved the status of prevention strategies. Regular health checkups, sanitation and improved water irrigation systems are some of the preventive measures applied in endemic areas. Unfortunately, in recent years, studies have reported that new dams, irrigation systems and reservoirs as well as the movement, growth and settlement of populations in new areas has reduced the previous effectiveness of schistosomiasis prevention programs (Jassim *et al.*, 1987).

1.7 Animal schistosomiasis studies

1.7.1 Mouse studies

Experimental schistosome infection of laboratory animals has been described in rabbits, primates, rodents and mice such as BALB/c or C57BL/6. Mouse models are often used for experiments, as they are easy to handle and amenable to genetic manipulation (i.e. transgenic mice or knock-out mice). Experimental *S. mansoni* infection models have been used to reproduce and study the anatomopathologic and pathophysiologic features of the infection as well as for the study of immunity and treatment. Various models have shown that development of schistosomiasis causes liver dysfunction by altering the metabolic processes through the up-regulation or down-regulation of enzymes (Harvie *et al.*, 2007, Pearce, 2005, Wynn *et al.*, 2004). Granulomas play an important role in the development of severe pathology in schistosomiasis and have been studied for the immunopathology

(Freeman Jr *et al.*, 1996, Montesano *et al.*, 2002, Stadecker, 1999). Comprehensive research in experimental murine models has contributed more broadly to the understanding of granulomatous inflammation and Th2-mediated fibrosis of the liver (Cheever *et al.*, 2002). Experimental schistosomiasis has also become a model for Th2 immune response development and regulation.

1.7.2 C57BL/6 mouse model

The C57BL/6 mouse model is a general multipurpose model. Availability of immunological reagents such as specific antibodies, recombinant proteins, specific cell types, soluble molecules (cytokines, chemokines, and circulating antibodies), etc. makes these mice suitable for immunological research purposes. These mice are commonly genetically modified for production of transgenic or gene deficient strains to examine the involvement of specific immune mediators. For example, in IL-4 deficient mice on the C57BL/6 background it was shown that IL-4 plays a protective role during schistosomiasis by controlling the regulation and generation of reactive oxygen and nitrogen intermediates in the liver (La Flamme *et al.*, 2001). Most mice studies use the C57BL/6 mouse model (Cheever and Barral-Netto, 1985, Harvie *et al.*, 2007) which display significantly smaller granulomas than other mouse strains (Rutitzky *et al.*, 2001). The inability of the C57BL/6 mice to survive chronic infections was studied by Colley *et al*. and led to the discovery that C57BL/6 granulomas were consistently half the volume of their counterpart lesions in CBA/J mice (Colley and Freeman Jr., 1980). Many researchers consider that C57BL/6 mice have comparable results to intestinal schistosomiasis while CBA/J mice results are more similar to hepatosplenic schistosomiasis patients (Stadecker, 1999, Stadecker *et al.*, 2004), although this comparison is hotly debated.

Using animal models for schistosomiasis studies raises an important point regarding the intensity of experimental schistosome infections. The infection intensities in these studies is generally high and infections are given as a single exposure to cercariae. In contrast most schistosome infections in humans are acquired gradually over years. Additionally, most humans exposed to schistosomiasis are born to mothers who are or have been infected hence in utero exposure to schistosome antigens or to idiotypic or anti-idiotypic antibodies may modify the response to subsequent infection in humans. Chronic human schistosomiasis is not reproducible in most animal models; therefore the relevance of these studies to human infection must be carefully considered (Cheever *et al.*, 2002).

1.7.3 CBA/J mouse model

One model that reproduces the clinical forms of human hepatosplenic schistosomiasis with the same spectrum of the disease is the CBA/J mouse (Henderson *et al.*, 1993). After infection 20% of CBA/J mice present with hypersplenomegaly syndrome (HSS) which resembles HS and 80% of the mice develop the moderate splenomegaly syndrome (MSS) similar to INT. HSS mice have enlarged livers with discoloured and coarse appearance due to granulomas. Liver from control mice are pink when compared to either MSS or HSS livers (Figure 1.9a). Moreover, the spleens from HSS mice are almost 5 times heavier compared to the control mice (Figure 1.9b). These prominent differences in pathology make HSS mice different from MSS mice.

Anti-soluble egg antigen antibodies from MSS mice have distinct cross-reactive idiotypes (CRIs) and lymphocyte stimulatory abilities. These distinctive CRIs are also found in

patients with INT and are believed to regulate the immunopathogenesis of chronic infection in humans and mice. In contrast, CRI cannot be detected in HSS mice or HS patients. CRIs can be detected as early as 6 weeks post infection; thus, CRIs have the ability to predict chronic pathology. The early appearance of CRIs in infected male CBA/J mice and human patients anticipates no development of severe disease, whereas infected male CBA/J mice and human patients with no CRIs present with early death in mice or severe chronic disease in humans (Montesano *et al.*, 2002).

Being an ideal model for schistosomiasis fibrosis, researchers have investigated the mechanisms and pathology of fibrosis in CBA/J mice. A previous study used the CBA/J mouse model to study liver fibrogenesis in *S. japonicum* infections and demonstrated marked abscess, inflammatory responses and fibrosis in the liver (Hirata *et al.*, 1993). Work in CBA/J neonatal mice exposed to CRI preparations showed that there is modulation of immune responses and liver fibrosis in such a manner that animals survive successive *S. mansoni* infections (Montesano *et al.*, 1999). Another study investigated the immunopathogenesis and immunoregulation of CBA/J mice with MSS and HSS chronic pathologic syndromes and demonstrated the mice have distinct and different degrees of fibrosis (Freeman Jr *et al.*, 1996). Together these studies support the relevance of this model for investigating chronic human schistosomiasis.

a) Liver pathology in murine schistosomiasis

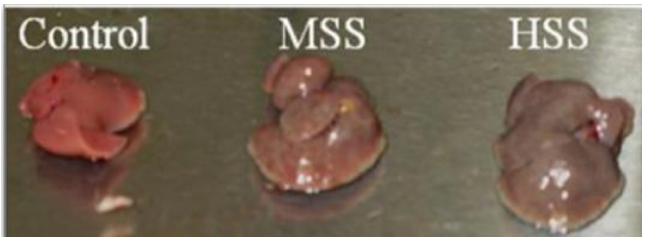

b) Spleen pathology in murine schistosomiasis

FIGURE 1.9 The CBA/J mouse model mimics the human form of the disease. After infection, 20% of the CBA/J mice present with hypersplenomegaly syndrome (HSS) which resembles HS and remaining 80% of the mice develop the moderate splenomegaly syndrome (MSS) similar to INT. **a)** Granulomas in the liver show coarse appearance, note the colour variation from pink to pale for normal through MSS to HSS liver. **b)** The spleen presents with moderate splenomegaly for MSS and hypersplenomegaly for HSS mice compared to control mice.

1.7.4 Animal fibrosis studies

Mouse studies have been used extensively to study various aspects of schistosome-induced fibrosis. There is increased synthesis of collagen isoforms due to schistosomiasis fibrosis (Dunn *et al.*, 1977) and liver hydroxyproline is increased during experimental *S. mansoni* infection (El-Meneza *et al.*, 1989). Also, liver enzymes like galactosylhydroxylysyl glucosyltransferase, hydroxylysyl galactosyltransferase and prolyl hydroxylase are increased post 6-week infection (Bolarin *et al.*, 1985). These parameters were measured to evaluate molecular mechanisms related to liver collagen synthesis

during schistosomiasis and to understand the damage caused by hepatic fibrosis. In addition to collagen, intermediate filaments are important for structural stability and provide scaffolding function. They form complex signalling platforms and interact with various kinases, adaptor, and apoptotic proteins. Among the intermediate filament proteins, vimentin and cytokeratin 18 (keratin 18 or keratin D) play an important role in liver stability during schistosomiasis (Boehme *et al.*, 1989, Chiarini *et al.*, 2006). Previous studies have described the changes induced by schistosome infection on cytoskeletal composition during both the acute (Harvie *et al.*, 2007) and chronic ((Silva *et al.*, 2004)) stages and have highlighted changes in collagen, vimentin, actin and cytokeratin. Mechanisms leading to liver fibrosis are unclear (in mice as well as in humans) but it is thought to be caused by hepatic stellate cell activation and their transition to myofibroblast-like cells (Xu *et al.*, 2009).

1.7.5 Animal co-infection studies

Schistosomiasis is a tropical disease that co-exists with many other infectious diseases. In particular, schistosomiasis and malarial or HIV-1 co-infections pose a major problem as poly-parasitism affects host immunity and ultimately vaccine effectivity. The effects of co-infection with schistosomiasis-malaria in BALB/c mice demonstrated aggravated malaria severity, as shown by increased parasitemia (the quantitative content of parasites in the blood) and severe gross pathology of liver and spleen (Kanyugo *et al.*, 2009). In an HIV study, when *S. mansoni*-infected rhesus monkeys were exposed to simian-human immunodeficiency virus, the animals demonstrated eosinophilia, higher IL-4 and IL-10 mRNA levels compared to parasite negative control animals, consistent with a Th2-type response to schistosome infection. In the same study when the animals were inoculated

intravenously with a high titre simian-human immunodeficiency virus stock, animals with schistosomiasis developed early viral replication that was significantly elevated compared to that of control animals (Secor, 2005). The above experimental studies are indicative of comprehensive strategies applied to integrate research programs for the control or elimination of schistosomiasis.

1.8 Human schistosomiasis studies

Many human studies have focused on immunological aspects and late stage morbidities of the disease. Induced immune responses are mainly due to host response to parasitic antigens and at later stages of the disease are largely due to eggs embedded in the granulomas (De Morais *et al.,* 2008). Epidemiological studies in endemic areas, combined with animal experiments, have led to the view that host genetics, infection intensity, schistosome antigen and co-infection status all influence the development of the immune response and disease severity (Pearce and MacDonald, 2002). The large number of factors that influence the development and severity of disease make the research related to discovery of drug targets and biomarkers quite complex.

Research focused on schistosomiasis morbidity includes hepatic fibrosis, portal hypertension, cognitive function studies, and assessment of anaemia. Portal hypertension measured by hyperdynamic circulation using electron paramagnetic resonance spectroscopy (Battista *et al.,* 1997), and fibrosis detected by liver biopsies (Camacho-Lobato and Borges, 1998) are invasive techniques. Ultrasound is conventional and non-invasive and can detect severe fibrosis as well as hepatosplenomegaly. However, ultrasound only detects at a late stage and is not sensitive enough to detect the earlier

stages (Pereira *et al.*, 1998). Hepatic fibrosis due to schistosomiasis has been discussed in a previous section 1.4.2.2 and is one of the major topics targeted by human studies because of its importance in morbidity. Epidemiological studies indicate the effectiveness of control and prevention measures but it is difficult to follow individuals and patients in endemic locations where disease spread is rapid and education limited.

1.8.1 Co-infection studies

In most countries of sub-Saharan Africa, and in many other tropical and subtropical countries, at least five to six tropical diseases occur in the same region. As a result a considerable proportion of the population is co-infected with one or more pathogens. Multiple infections adversely affect childhood growth, cause micronutrient deficiencies, and lead to extensive organ pathology. The susceptibility of children and pregnant women to co-infections is the rationale behind an increased focus on research programs related to vaccines and drugs. Likewise, co-infections in schistosomiasis are common and influence immune responses and response to treatments. The most common or well-studied co-infections with schistosomiasis include malaria, HIV, tuberculosis and viral hepatitis are discussed in the following sections.

1.8.1.1 Malaria and schistosomiasis

Malaria and schistosomiasis are two major parasitic diseases in developing countries and are co-endemic, resulting in varied pathologies. Children are more vulnerable to co-infections and present with impairment in growth and development. *Plasmodium falciparum* infected adults and children with schistosomiasis infection show increased malaria morbidity in children in contrast to the effects seen in co-infected adults indicate

that schistosomiasis co-infection can unbalance the regulation of inflammatory factors (Diallo *et al.*, 2004). Co-infections in children with *P. falciparum* and *S. mansoni* result in lower percentages of activated T cells and T regulatory memory cells (Mouk *et al.*, 2009). Recently, researchers have found a cross-reactive antigen, SmLRR shared between *S. mansoni* and *P. falciparum* sera from both humans and rats infected with either parasite species and is a promising therapeutic target (Helmby, 2007). A better understanding of the interactions between these two parasites might prove invaluable in the development and evaluation of new vaccine candidates or therapeutic strategies.

1.8.1.2 HIV-1 and schistosomiasis

HIV-1 and AIDS are prevalent in Africa and the pathology is aggravated in schistosomiasis co-infections. Granuloma formation and pathology during schistosomiasis is dependent on, and mediated by, CD4 cells responding to egg antigens. Likewise, CD4 cells are critical in HIV-1/AIDS to maintain cell-mediated immunity. Experiments *in vitro* have shown that CD4 cells of persons with active schistosomiasis have higher distribution of specific cell surface chemokine receptors that make them more susceptible to HIV infections (Secor *et al.*, 2003). Also, *S. mansoni* infected subjects with HIV-1 showed more rapid liver fibrosis (Mwinzi *et al.*, 2004). These studies demonstrate that schistosomiasis increases the susceptibility to HIV-1/AIDS or aggravates the progression of HIV-1 disease (Secor *et al.*, 2004). Finally, human co-infection studies become complex because individuals cannot be studied longitudinally without treating their schistosome or HIV-1 infections. Thus, the need to develop and use animal models is highlighted.

1.8.1.3 Tuberculosis and schistosomiasis

In Africa, tuberculosis is highest among HIV-1 infected individuals and helminth infections. *S. mansoni* infection suppresses anti-mycobacterial immune responses through enhanced production of cytokines like TGF-β and IL-10, and promotes active tuberculosis development among HIV-1-infected Ugandans (Brown *et al.*, 2006). In spite of the high incidence of these two infections in Africa, *S. mansoni* and *Mycobacterium tuberculosis* co-infections are rare. Recently a study demonstrated that schistosoma infection induces a cellular Th2 immune response and mycobacterial induced immunity is Th1 cell-mediated. This imbalance in the lymphocyte population could enhance susceptibility to mycobacterial diseases in co-infected individuals (Basile *et al.*, 2007) and thus result in a fatal outcome. This possibility emphasises the need for research into schistosome vaccine and drugs.

1.8.1.4 Hepatitis and schistosomiasis

Human studies on co-infection with Hepatitis B virus (HBV) and *S. mansoni* indicate aggravated disease pathology specifically associated with the liver. Some studies indicate the association of HBsAg (surface antigen of the hepatitis B virus), anti-HBsAg, anti-HBc (antibody to hepatitis B core antigen) with haematemesis and macronodular cirrhosis in patients with hepatosplenic schistosomiasis (Conceição *et al.*, 1998). Another study correlated the presence of HBsAg in hepatosplenic schistosomiasis patients with aggravated chronic liver disease and chronic inflammation of the portal spaces (Lyra *et al.*, 1976). While some studies maintain that there is no association of HBV and schistosomiasis (Abdella Eltoum *et al.*, 1991), research also suggests a synergistic role of

HBV infection with *S. mansoni* in the development of chronic hepatic schistosomiasis (Kojiro *et al.*, 1986).

Schistosomiasis and hepatitis C virus (HCV) co-infections lead to severe fibrosis due to virological and immunologic interactions. Hepatosplenic schistosomiasis patients with HCV have significantly higher serum TNF-α than schistosomiasis patients, showing that HCV co-infection aggravates the liver pathology (Morais *et al.*, 2006). Some studies indicated that use of liver function tests (alanine aminotransferase, aspartate aminotransferase, albumin, alkaline phosphatase, gamma-glutamyl transferase) is able to differentiate chronic schistosomiasis, HCV and co-infection (Fahim *et al.*, 2000). In 2004, a study demonstrated that *S. mansoni* induced Th2 dominance down-regulates the Th1 cytokine profile in HCV infection (el-Kady *et al.*, 2004). Furthermore, some studies suggest that schistosome and HCV co-infections have higher incidence of hepatocellular carcinoma and mortality rates due to liver-related diseases (Kamal *et al.*, 2001). Nonetheless, a study in Ethiopian population claims that HCV has no association with *S. mansoni* infection but HBV co-infection can predict levels of hepatic periportal thickening/fibrosis (Berhe *et al.*, 2007).

1.8.2 Schistosomiasis and cancer

Schistosomiasis infection generates free radicals and immune-generated toxic oxygen compounds triggering carcinogenic activities during the disease (Mostafa *et al.*, 1999). There is evidence that *S. japonicum* causes development of liver cancer in Japan and colorectal cancer in China. In schistosomiasis due to *S. haematobium*, the intensity of infection, the degree of haematuria and proteinuria, and the pathological changes in the

urinary bladder and ureters have been shown to induce malignancy leading to bladder cancer (Mostafa *et al.*, 1999). Urinary schistosomiasis accounts for 16% of bladder cancer cases in an Egyptian population (Bedwani *et al.*, 1998) suggesting carcinogenic effects of the helminths during schistosomiasis. There is no direct evidence that *S. mansoni* plays a role in the carcinogenesis but case reports link it to liver, colorectal and prostate cancer (Vennervald and Polman, 2009). In addition, *S. mansoni* infections clearly causes increased incidence of hepatocellular carcinoma in HCV patients (Kamal *et al.*, 2000).

S. haematobium is the only helminth that has been proven to be definitely carcinogenic in humans, although other *schistosome spp*. also may facilitate malignant transformations. Helminth infection-related cancers involve chronic inflammation which induces many complex mechanisms like host immune system modulation, intracellular communication inhibition and disruption of propagative and anti-propagative pathways. In addition, there is genomic instability, oxidation and damage of DNA, induction and propagation of malignant stem cell progeny (Mayer and Fried, 2007). A study demonstrated that *S. mansoni* infection alters the function of p53 protein in schistosomal colitis-associated colorectal cancer (Madbouly *et al.*, 2007). Additionally, experimental work indicates somatic and metabolic antigens from *S. mansoni* induce reticular-cell hyperplasia and plasmocytic differentiation predisposing the spleen to the development of follicular lymphoma (Andrade and Abreu, 1971). Moreover, another study showed liver DNA had promutagenic methylation damage with increasing intensities of *S. mansoni* infection. The authors indicate that carcinogenic and/or toxic substances in schistosome eggs, schistosomulae and adult worms may have carcinogenic effects (Badawi *et al.*, 1993).

Together these studies support a role for schistosome-mediated mechanisms and tissue damage in the development of cancer.

1.8.3 Schistosomiasis and chronic renal failure

Chronic renal failure is a marked feature of *Schistosomiasis haematobium* and also occurs in *S. mansoni* infections. In *S. haematobium,* direct egg deposition causes bladder pathology in 50% cases with increased bladder damage associated with parasite genetics, intensity of infection, proteinuria and haematuria (Brouwer *et al.,* 2003). In addition to causing glomerular lesions due to schistosomal antigens and circulating immune complexes (antigen-antibody complexes) being deposited in the renal glomeruli, schistosome infections do cause schistosomal nephropathy which is a leading cause of progressive renal diseases (El-Koraie *et al.,* 2002). Circulating immune complexes due to *Schistosomiasis mansoni* are heterogeneous in size and composition leading to different types of glomerular lesions in chronic schistosomiasis (Brito *et al.*, 1979) and acute schistosomiasis (Lawley *et al.*, 1979). Furthermore, *S. mansoni*-induced mesangiocapillary glomerulonephritis is an important cause of nephrotic syndrome and chronic renal failure (Martinelli *et al.,* 1989). Investigating the immunochemical composition of the complexes and the pathophysiology involved in the initiation of renal injury could help to solve the mystery behind the mechanism of the schistosomal specific nephropathies and initiation of anti-schistosomal treatment.

1.8.4 Schistosomiasis, allergies and autoimmune diseases

Recently, there has been growing appreciation in developed countries that chronic worm infections can prevent or suppress autoimmune and allergic disorders. Studies have shown that the prevalence of allergies and autoimmune diseases is negatively correlated to the prevalence of worm infections, potentially due to improved hygienic conditions. Although the development of allergies and auto-immunity are influenced by both genetic background and environment/lifestyle, studies have directly demonstrated that human schistosomiasis decreases immune responses to allergens and clinical manifestations of asthma in people living in helminth endemic areas (Araujo and De Carvalho, 2006). Other studies (La Flamme *et al.,* 2003b, Sewell *et al.,* 2003) demonstrate that exposure to *S. mansoni* eggs or chronic *S. mansoni* infection reduces incidence and delays progression of experimental autoimmune encephalomyelitis, an animal model for multiple sclerosis. A recent study with multiple sclerosis and worm infections demonstrates that parasite infections induce regulatory T cells generating immune modulators that alter the progression of multiple sclerosis (Correale and Farez, 2007). Additionally, infection with schistosoma helminth or exposure to schistosoma eggs significantly reduces the incidence of insulin dependent diabetes mellitus (IDDM), an autoimmune disease resulting in the destruction of insulin producing cells (Cooke *et al.,* 1999). Thus, schistosome infection modulates the immune responses involved in pathology related to allergies and autoimmune diseases, and this approach is being investigated by researchers for parasitic molecules that might prove beneficial in treating the autoimmune and allergic diseases.

1.9 Diagnostic markers or biomarkers for schistosomiasis

In the light of global warming, climate change has lead to shifting of the isotherms that have caused the plant and animal species to adapt to new climates and colonizing new,

warmer habitats. These changes have facilitated the spread of schistosomiasis to new regions and highlighted the need for new prevention and treatment solutions (Githeko, 2009). Recently, there have been significant advances in the decoding of the *S. mansoni* genome, transcriptome and proteome, which may uncover targets for new therapies for schistosomiasis (Berriman *et al.,* 2009). Research focussed on new treatment solutions include chemotherapeutic strategies, integrated community-based interventions and clinical trials and accessible quality-assured diagnostic markers either related to schistosomiasis infection, host immunity and disease associated morbidity.

1.9.1 Infection and immunity markers

Although sensitive and specific tests have been developed to detect schistosome-specific antibodies, the tests are too vague. Serologic tests for anti-schistosomal antibodies cannot distinguish between past and current infections. In contrast, antigens excreted by worms and eggs are present during active infection and can be detected. Assays measuring circulating antigens like circulating anodic antigen (CAA) and circulating cathodic antigen (CCA) have been demonstrated in serum and urine but demand further validation in sero-epidemiological studies. The recent development of the dipstick ELISA for CAA and CCA is proving to be a useful method for detecting and quantifying infection especially in epidemiological studies (Ouma *et al.,* 2001). A study reported that schistosomal carbohydrate antigens could be used as targets for vaccination and/or serodiagnosis of chronic schistosomiasis in humans (Nyame *et al.,* 2003). Re-infection studies in schistosomiasis demonstrated increased levels of protective molecules like IgE which resist re-infection while increased IgG4 was related to high risk of re-infection (Deelder,

1992) this information can help in the treatment of patients in sero-epidemiological studies and vaccine trials.

The development of the PCR for detecting *S. mansoni* DNA in human faecal and serum samples (Pontes *et al.*, 2002) is a breakthrough for clinicians struggling to effectively treat schistosomiasis although it requires rigorous testing for efficacy and validation for epidemiological and clinical settings. A study by Caldas *et al.* demonstrated the importance of cross-reactive idiotypes (CRIs) during pathology modulation in schistosomiasis (Caldas *et al.*, 2008) suggesting it is important in directly mediating the disease outcome. Additionally, CRIs can be used to detect severe schistosomiasis morbidity at an early stage in the infection and thereby help in treatment strategies (Montesano *et al.*, 2002). Importantly, schistosomiasis infection triggers immune responses and therefore infection and immunity markers have to be used in combination.

1.9.2 Markers of morbidity

The primary markers of schistosomiasis morbidity are liver fibrosis and differential antibody levels in hepatosplenic compared to intestinal schistosomiasis. To address the problem of hepatic fibrosis in hepatosplenic schistosomiasis, researchers have identified connective tissue metabolites, carboxyterminal procollagen IV peptide as a potential biomarker that could be used in endemic areas (Kardorff *et al.*, 1999). New research has used various other approaches to develop diagnostic markers including genomics, proteomics, transcriptomics and metabonomics. Urinary metabolic profiles of *S. mansoni* infected mice showed changes in the tricarboxylic acid cycle, glycolysis and amino acid metabolism suggesting that these are a part of the biological responses to parasitic

infections. This study showed that decreases in citrate, succinate, 2-oxoglutarate, taurine, 2-oxoisocaproate, 2-oxoisovalerate and increases in pyruvate and tryptophan may be diagnostic for chronic schistosomiasis (Wang *et al.*, 2004). Another study found elevated levels of peripheral blood cholylglycine (marker of portal blood in the systemic circulation), procollagen-III-peptide (cleavage product of collagen synthesis) and neopterin (macrophage product) in hepatosplenic schistosomiasis and suggests the use of these tests for clinical assessment (Zwingenberger *et al.*, 1988). In spite of the extensive work on diagnostic markers for hepatosplenic schistosomiasis, markers identified using mouse models and human studies applied in clinical and epidemiological studies have failed to produce viable and robust biomarkers so far.

1.10 Aim of the study

The aim of this study was to identify diagnostic markers for hepatosplenic schistosomiasis. Early diagnosis of hepatosplenic patients can focus treatment on these patients. Eradication of the disease using chemotherapy has never been achieved due to moving populations, high re-infection rates and post-morbidity leaving sufficient scope for research in various aspects of the disease (like vaccines, drug development and diagnostic markers). Previous study by our group in the C57Bl/6 mice at 8-week infection showed differential expression of proteins like transferrin isoforms, cytokeratin isoforms, vimentin, dimethyl dehydrogenase and selenium binding protein using two-dimensional electrophoresis (Harvie *et al*., 2007). In the present study, we intend to use the CBA/J mouse model and 2D-DIGE coupled with MALDI-TOF mass spectrometry. The CBA/J mouse model is a reproducible mouse model that presents both pathological forms of the chronic disease: moderate splenomegaly syndrome (MSS) similar to INT and

hypersplenomegaly syndrome (HSS) similar to HS in humans. This model was used to identify candidate protein markers of HSS, and Dr. Evan Secor, Centres for Disease Control and Prevention, Atlanta, USA provided the CBA/J mouse liver and serum samples for the proteome analyses as well as the human serum samples for biomarker verification.

The specific aims for this study were:

1. Compare liver protein abundance in chronically (20-week) infected MSS and HSS mice to determine the distinct differences between the two late stage disease forms and to identify candidate liver protein markers unique to HSS and MSS.
2. Analyse changes in liver protein abundance over time post-infection to identify candidate liver protein markers in liver samples from CBA/J mice infected for 6, 8, 12 weeks and compare it with the abundance of proteins from 20 week infected mice and control CBA/J mice. This approach will identify differentially expressed proteins as early marker proteins, late marker proteins, and marker proteins which are consistently expressed through the progression of the hepatosplenic disease.
3. Analyse mouse candidate liver protein markers, associated with the pathogenesis of schistosomiasis, in serum samples from infected mice and humans to develop the candidate liver protein markers as diagnostic markers for hepatosplenic disease.

CHAPTER 2: MATERIALS AND METHODS

2.1 Mouse model, liver and serum sample collection

Male CBA/J mice were obtained from The Jackson Laboratory and were maintained at the American Association for Accreditation of Laboratory Animal Care, Centers for Disease Control and Prevention, Atlanta, USA (CDC) in accordance with institutional guidelines and federal regulations. Mice were infected by subcutaneous injection of 45 cercariae of a Puerto Rican strain of S. *mansoni* that had been maintained in *Biomphalaria glabrata* snails. At 20-week of infection, animals were sacrificed and classified as having MSS or HSS, based on percent spleen body weight and gross pathological appearance at CDC. Liver and serum samples were collected from the three study groups (uninfected age-matched controls, MSS and HSS; n = 5 per group) and snap frozen at -80 °C. A second set of liver and serum samples similarly treated was collected for uninfected age-matched controls (n=5) and mice infected for 6-week (n=10), 8-week (n=10), 12-week (n=10), 20-week (n=10) and all samples snap frozen at -80°C. Although the sets were collected separately, samples from each set were collected within the same time period to avoid bias due to collection time. Mice liver and serum samples sent by Dr. Secor were used for proteomics experiments at the Victoria University of Wellingtons' Proteomics Facility. The Victoria University of Wellington Animal Ethics Committee approved all experiments.

2.2 Human serum samples

Human serum samples were collected from car washers with intense *S. mansoni* infections in Kisumu, Kenya (Karanja *et al.*, 2002). Study participants were occupationally exposed

car washers above 18 years of age. On approval by the participants, sera were tested for antibodies to HIV-1. The modified Kato Katz technique was used to quantify *S. mansoni* eggs in the faecal specimens expressed as eggs per gram. The CD4 cell counts were evaluated in persons with schistosomiasis liver pathology (Mwinzi *et al.*, 2004). The HIV-1 and CD4 cell counts were done by Mwinzi *et al.* (2004).

Assessment of schistosomiasis morbidity was done using a portable Aloka SSD-620 ultrasound machine with a 3.5 megahertz convex probe (Aloka Co., Ltd., Tokyo, Japan) and schistosome-induced pathology in the liver was evaluated according to the Niamey classification (Richter *et al.*, 2000, Richter *et al.*, 1992). The image pattern (IP) specifications have been discussed in Chapter 1 (section 1.2.4.3 hepatic fibrosis) and are based on the degree of liver fibrosis detected by ultrasound done by trained ultrasonographers in Kisumu. In our study, patients with image pattern IPA were classified as INT, image patterns IPC, IPD, IPE were classified as HS, and more specifically IPD and IPE were severe HS. Twenty three INT serum samples and fourteen HS serum samples were selected for the study with similar eggs per g (Figure 2.1). Thirteen age and sex matched controls were included from CDC. I used targeted assays for liver and serum hydroxyproline, transferrin (ELISA), CTGF (ELISA) and keratin D (western blot) measurements which were done at CDC. The institutional review boards of the Centers for Disease Control and Prevention, U.S. Department of Health and Human Services, and The Kenya Medical Research Institute approved all the human sera experiments.

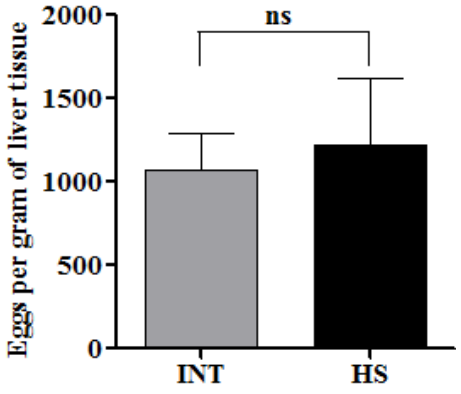

FIGURE 2.1 Egg count per g of faeces in the two study groups INT and HS, mean ± SEM, serum samples with similar EPG between the groups.

2.3 Extraction of protein from murine liver tissue

Each liver sample was homogenised using disposable 1.5 mL polypropylene pestle with standard lysis buffer. For every 10 mg of tissue weighed 100 µL standard lysis buffer was added containing 30 mM Tris-HCl (Sigma-Aldrich, St. Louis, MO, USA), 2 M thiourea (MERCK, Darmstadt, Germany), 7 M urea (MERCK), 4% (w/v) 3-[(3-cholamidopropyl) dimethylammonio]-1-propanesulfonate (CHAPS) (Sigma-Aldrich). Homogenates were vortexed for 10 min, and centrifuged at 13,000 rpm for 10 min and supernatants were collected for proteomic analysis. Liver total protein concentration was determined using a 2D-Quant Kit (GE Healthcare Bio-Sciences AB, Uppsala, Sweden) (Beddek *et al.*, 2008) and a modified Bradford Assay (Viswanathan *et al.*, 2006). Lysates were stored at -20^{o}C until further use.

2.3.1 Modified Bradford assay

Stock standard albumin (concentration 2.5 mg/mL) was prepared using 0.0125 gm bovine serum albumin (Sigma-Aldrich) in 5 mL standard lysis buffer. Working standards were

prepared with serial dilutions from 2.5 mg/mL to 2.0 mg/mL, 1.5 mg/mL, 1.0 mg/mL and 0.5 mg/mL using standard lysis buffer. Standards and protein samples, 2 µL each were added to 10 mL tubes inclusive of 2 µL standard lysis buffer as blank. A volume of 1600 µL MilliQ deionised water (Millipore Corporation, 290 Concord Road, Billerica, MA 01821, USA) was added to each tube and mixed with 400 µL Bradford reagent (0.005% Coomassie blue G-250, 5% methanol, and 10% orthophosphoric acid) (Viswanathan *et al.*, 2006). A volume of 200 µL of the above mixture was dispensed into a 96-well flat bottom plate and read on Molecular Devices Plate Reader (Molecular Devices, Orleans Drive, Sunnyvale, CA 94089-1136, USA) at 595 nm within 60 min of assay.

2.3.2 2-D Quant kit

A 2-D Quant Kit (GE Healthcare) was used to quantify lysates and serum samples for total protein concentration prior to two-dimensional differential in gel electrophoresis (2D-DIGE) as per the manufacturer's guidelines. A standard curve was prepared using 2 mg/mL bovine serum albumin (BSA) standard solution provided with the kit. The standard curve was generated with 0, 5, 10, 15, 20, 25 µL standard solution making up the volume with standard lysis buffer. Duplicates and double diluted samples were included in the assay. A volume of 500 µL precipitant was added to each tube (including the standard curve tubes). Tubes were vortexed briefly and incubated for 2–3 min at room temperature. Next, 500 µL co-precipitant was added to each tube and mixed briefly by vortexing or inversion. The tubes were centrifuged 10,000 x g for 5 min and then immediately the supernatants were decanted. The above process of addition of precipitant, co-precipitant, mixing, vortexing and decanting the supernatant was repeated. To avoid resuspension or dispersion of the pellets, the tubes were centrifuged again to bring any remaining liquid to

the bottom of the tube. A micropipette was used to remove the remaining supernatant from the tube with no residual liquid in the tube. A volume of 100 µL copper solution and 400 µL MilliQ ((Millipore Corp., USA)) was added to each tube. The tubes were vortexed to dissolve the precipitated protein and 1 mL working colour reagent was added to each tube, mixed, and incubated for 15–20 min at room temperature. The absorbance was read at 480 nm (Molecular Devices, USA) within 40 min of the addition of working colour reagent.

2.4 2D-DIGE with Minimal CyDyes

The Minimal CyDye Kit (GE Healthcare) was used to label the liver lysates using the manufacturer's recommended protocol. Lysates were thawed, vortexed and centrifuged before labelling and the pH was adjusted to 8.5 by addition of 1.5 M Tris-HCl pH 8.5. The internal standard, a pool of all liver lysates or serum samples (10 µg per sample, 5 Control +5 MSS + 5 HSS) was labelled using Cy2; individual samples were labelled with Cy3 and Cy5 (Figure 2.1). Ten µg of protein was labelled with 80 pmol of each of the amine reactive CyDyes reconstituted in anhydrous dimethylformamide (Sigma-Aldrich) for 30 min, at 4 °C in the dark. The reaction was quenched by the addition of 1 µL 10 mM lysine. Labelled liver lysate and serum samples were combined for electrophoresis as indicated in experimental design 1, 2 and 3 that are listed in Appendix A. Additional information about DIGE chemistry is discussed in Appendix F.

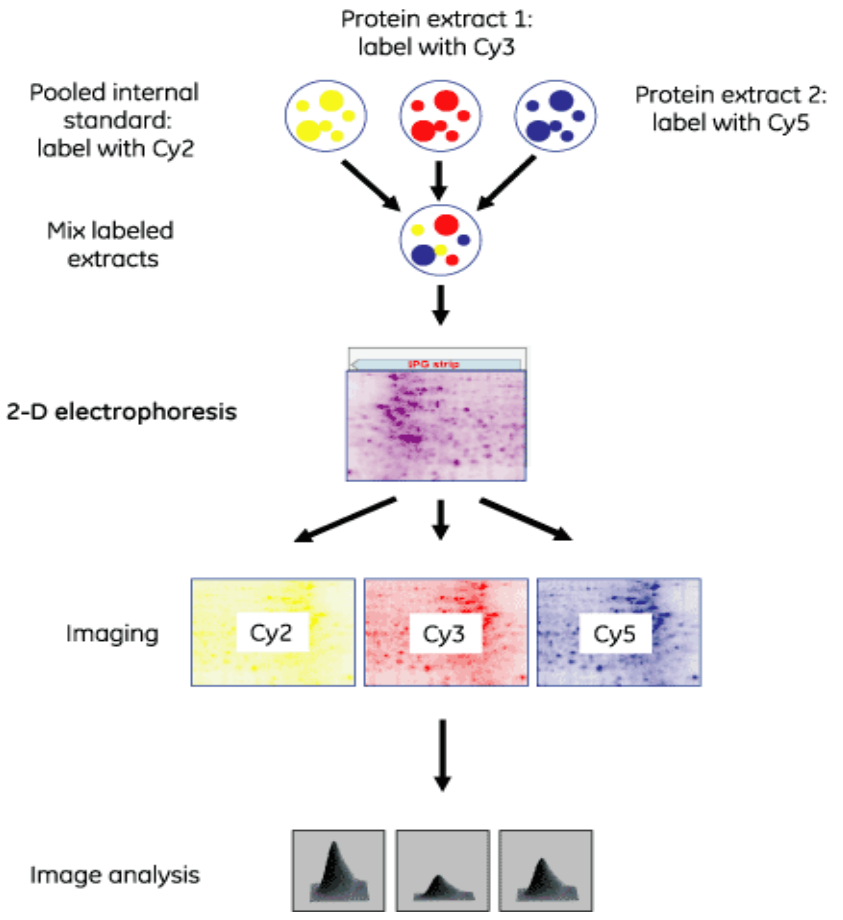

FIGURE 2.2 Minimal CyDye Kit (GE Healthcare) was used to label the liver and serum samples. The flow diagram illustrates the procedure followed for combined samples electrophoresed on one SDS-PAGE precast gel and protein abundance patterns analysed using DeCyder software-Biological variation analysis. (Courtesy: GE Healthcare)

2.5 Electrophoresis

2.5.1 Isoelectric focusing for pI 4-7 IPG DryStrips

The 7 cm Immobiline DryStrips, pI 4 to 7 were placed in contact with the 30 µg labelled protein sample diluted to 125 µL with rehydration buffer containing 2 M thiourea, 7 M urea, 2% IPG buffer 3-10 (GE Healthcare), 2% dithiothreitol (DTT), 4% (w/v) CHAPS and 0.5% bromophenol blue. The strips were subjected to first dimension separation using

an IPGphor™ system (GE Healthcare, Figure 2.4) with the following protocol: temperature 20^{o}C; current 50 μA per strip.

Setting	Voltage (v)	Time (h)
S1-Step	300	0:30
S2-Gradient	1000	0:30
S3-Gradient	5000	1:25
S4-Step	5000	0:25
	Total time: 2:50 h	

2.5.2 Isoelectric focusing for pI 6-11 IPG DryStrips

The 7 cm IPG 6-11 strips (GE Healthcare) were subjected to overnight rehydration without the CyDye labelled sample, using 125 μL rehydration buffer containing 2 M thiourea, 4 M urea, 1% IPG Buffer 6-11 (GE Healthcare), 2% (w/v) CHAPS, 10% isopropanol, 2.5% DTT, 5% glycerol and 0.5% bromophenol blue. Labelled samples were diluted to 100 μL with rehydration buffer and incubated overnight in the dark at room temperature. A Multiphor II™ system (GE Healthcare, Figure 2.4) was used to focus IPG 6-11 strips using the following protocol: temperature 20 ^{o}C; current 2 mA per strip.

Setting	Voltage (v)	Time (h)
S1- Step	200	0:01
S2-Gradient	3500	1:30
S3-Gradient	3500	1:04
	Total time: 2:35 h	

Samples were loaded by cup loading at the anodic end. The focused strips were equilibrated at room temperature for 10 min in equilibration buffer (50 mM Tris pH 8.8, 6 M urea, 30% glycerol, 2% SDS, 0.5% bromophenol blue) with 1% DTT followed by an

equilibration at room temperature for 10 min in equilibration buffer with 2.5% w/v iodoacetamide.

2.5.3 Two-dimensional gel electrophoresis

The equilibrated strips were electrophoresed on NuPAGE® Novex 4-12% Bis-Tris ZOOM® Gels, 1.0 mm IPG well (Invitrogen, Carlsbad, CA) using NuPAGE® MOPS SDS Running Buffer with the addition of 0.5 mL NuPAGE® Antioxidant (Invitrogen) in the inner chamber. To prevent the CyDyes from photo-degradation, all the work was carried out in minimal light conditions.

2.6 Scanning of CyDye labelled images

Gels were scanned using a Fujifilm FLA-5100 (Fuji Photo Film Co., Tokyo, Japan). The Cy2, Cy3, and Cy5 images were scanned sequentially. A 473 nm laser and a BPB1/ 530DF20 emission filter were used to scan Cy2 images. A 532 nm laser and a PBG/570DF20 emission filter were used to scan the Cy3 images. A 635 nm laser and a DBR1/R665 emission filter were used for the Cy5 images. All gels were scanned at 50 μm resolution and 16 bits (Beddek *et al.*, 2008).

2.7 Image analysis using DeCyder software

DIGE gels were analysed for differentially expressed proteins using DeCyder^{TM} 2-D 6.5 software (GE Healthcare). The internal standard was included in all gels and assisted in linking protein spots in-gel giving accurate quantitation and minimising the effects of variation between gels and each gel was matched to the standard. The Biological Variation Analysis (BVA) module was used for matching multiple gels, comparing protein spots and

calculating statistics for difference in protein spot abundance (Appendix B). The spot detection limit was set to 2500. The difference in protein spots between gels is expressed using the average volume ratio between the study groups. '+' indicating the increase in average volume ratio and '-' indicating the decrease in average volume ratio (Table 3.1, Table 4.2, Table 4.3, Table 5.1).

The False Discovery Rate (FDR) is a statistical method to interpret the proportion of false positives among those proteins that are thought to be significantly changed. Due to the high-dimensionality of the data, the FDR feature was applied as multiple test correction to minimise false positive discovery of protein spots and keep the overall error rate low. The data was analysed according to the guidelines for a target power of 0.8 (i.e. a two-fold change in average volume ratio can be accepted using four replicates with one-way analysis of variance (1-ANOVA) ≤ 0.01) (Karp and Lilley, 2005, Karp *et al.*, 2005).

Multivariate analysis was performed by using the DeCyder-Extended Data Analysis module with the Principle Component Analysis (PCA) and Hierarchical Cluster Analysis (HCA) features. PCA and HCA reduced the multidimensionality of the protein spot data across gel images and analysed the protein spots with 2-fold change and 1-ANOVA ≤ 0.01. Additional information on the DeCyder software analysis is illustrated in Appendix B.

2.8 Spot Picking and enzymatic digestion

2.8.1 Preparative gels for spot picking

The preparative gels (75 μg protein per gel from Control, MSS and HSS liver lysate and serum samples each) NuPAGE® Novex 4-12% Bis-Tris ZOOM® Gels, 1.0 mm IPG well

(Invitrogen) were fixed in 50% ethanol, 3% orthophosphoric acid for 1 h followed by three washes with MilliQ deionized water (Millipore Corp., USA) of 30 min each. The gels were then incubated in a staining solution containing 17% ammonium bicarbonate, 34% methanol, 3% orthophosphoric acid for 1 h before addition of 0.06% Coomassie G-250. After a day the gels were washed with MilliQ deionised water three times for 30 min each before scanning. Soluble Egg Antigen (SEA) was prepared using 55,000 *S. mansoni* eggs homogenised using glass tissue grinder T4018-15 (Pyrex®, Corning Inc., MA, USA) and protein concentration determined as stated earlier (Section 2.3.1).

2.8.2 Scanning of gels

The gels were scanned using a Molecular Dynamics Scanner, Personal Densitometer SI (Sunnyvale, CA, USA), with 50 micron and 12 bit resolution.

2.8.3 Spot excision and digestion

Spots were excised from the preparative gels using a 1.5 mm Spot Picker Plus (The Gel Company, San Francisco, USA) and transferred to v-bottom shaped 96-well polypropylene plate (Greiner Bio-One, Germany) containing 100 µL MilliQ in each well.

2.8.3.1 Manual method for tryptic digestion of spots

A step wise procedure was followed for the destaining of gel plugs and in-gel tryptic digestion done manually.

Step	Function	Cycles	Solutions used	Volume required	Time (min)
1	Washing	2	MilliQ	100 µL	10
2	Destaining	1	50% ACN and 50 mM NH_4HCO_3	100 µL	960
		1	50% ACN and 50 mM NH_4HCO_3	100 µL	30
3	Dehydration	1	100% ACN	100 µL	20
4	Drying (In laminar flow hood)	1	-	-	30
5	Digestion	1	Trypsin (trypsin 0.05 µg in 10 µL of 20 mM NH_4HCO_3)	10 µL	300
6	Peptide Recovery	2	50% ACN and 0.1% TFA	10 µL	15
		1	100% ACN	20 µL	15

2.8.3.2 Ettan Digester method for tryptic digestion of spots

The Ettan™ Digester (GE Healthcare) was used with the following protocol. The gels plugs were destained by washing four times for 30 min each with 100 µL 50 mM ammonium bicarbonate (Sigma-Aldrich), 50% methanol (MERCK) and dried at room temperature for 60 min. Ten µL trypsin (0.05 µg/10 µL in 20 mM ammonium bicarbonate) (trypsin modified sequencing grade, Roche Diagnostics, Germany) was added to each well and the digestion was carried out for 5 h at room temperature. The tryptic digests were transferred to a fresh plate and the gel plugs washed with 10 µL 0.1% TFA (Sigma-Aldrich) in 50% ACN (MERCK) for 20 min two times each. At each peptide recovery cycle the peptides were transferred into a fresh plate. The digestion and wash solutions were collected and combined. All the solutions were made fresh prior to use and were filtered

and degassed. The tryptic peptides were dried overnight completely in a laminar flow hood.

2.9 Protein identification using mass spectrometry

2.9.1 Preparation of matrix

The dried tryptic digests were resuspended in 1 µL of 10 mg/mL α-cyano-4-hydroxycinnamic acid (Sigma-Aldrich) solution prepared in a 50% (v/v) solution of ACN/aqueous 0.25% TFA and spotted onto a MALDI plate and air dried prior to mass spectrometry.

2.9.2 Collection and analysis of spectra

All tryptic digests were analysed by MALDI-TOF (Voyager-DE Pro MALDI-TOF Mass Spectrometer, Applied Biosystems, Foster City, CA) mass spectrometry. The spectra were collected over the range *m/z* 800– 3500 with approximate laser intensity of 2062, which changed ± 200 according to the size of the protein spot, and 120 laser shots were used. Spectra were processed using Data Explorer software (v 5.1, Applied Biosystems) to generate monoisotopic peptide masses which were used to identify proteins using Mascot Server, ProFound, v2.1.03 against the complete NCBInr and schistosome database updated 03/27/2007. Complete cysteine modification by iodoacetamide, methionine partial modification by oxidation, 50 ppm peptide tolerance and one missed trypsin cleavage were included as search parameters. Criteria for a match included number of 5 or more peptides matched, sequence coverage (correct cleavage sites, i.e. does the peptides terminate with: R or K) and difference in probability between first and second match should be 1×10^{-3} (Beddek *et al.*, 2008). Protein spots identified using ProFound search

engine were validated against two other protein search engines: Matrix Science Peptide Mass Fingerprint and XProteo v1.2.2.

2.9.3 Calibration of spectra

2.9.3.1 External calibration

External calibration was performed using the Calibration Mixture 2 of the Sequazyme^{TM} peptide mass standards kit (Applied Biosystems) containing angiotensin I (m/z 1297.51); and fragments of adrenocorticotropic hormone 1–17 (m/z 2094.46), 18–39 (m/z 2466.72). One µL Calibration Mixture 2 was mixed with 100 µL CHCA matrix prepared as indicated above and spotted in between protein spots on the MALDI plate. Spectra for the Calibration Mixture 2 were acquired with the same laser intensity and number of laser shots as for the protein spots.

2.9.3.2 Internal calibration

Internal calibration was performed by using monoisotopic autolytic tryptic peaks (m/z = 805.41 and 2163.05).

2.10 Western blots

2.10.1 One-dimensional electrophoresis

To validate the DIGE experiment data, liver lysate and serum samples were treated with NuPAGE LDS sample buffer (4X) and NuPAGE reducing agent (10X) at 70 ^{0}C for 10 min and separated by one-dimensional electrophoresis on a NuPAGE® BT Gel (Invitrogen). Liver lysates (20 µg/well) control mice (n=3), MSS mice (n=3), HSS mice (n=3) and soluble egg antigen (20 µg/well) were separated on a NuPAGE® BT Gel

(Invitrogen) for mouse liver PEPCK, MUP and transferrin western blots. The western blot for mouse serum transferrin was carried out using a serum dilution of 1:50 with phosphate buffered saline pH 7.4 for control (n=5), 8-week infected (n=10), 12-week infected (n=10) and MSS (n=5), and HSS (n=5) groups. A protein concentration of 10 μg/well for each serum sample was separated on NuPAGE® BT Gel (Invitrogen).

2.10.2 Western blot for mouse liver PEPCK, MUP, transferrin

The proteins were transferred onto Hybond™-LFP a low-fluorescent, hydrophobic polyvinylidene difluoride (PVDF) membrane (GE Healthcare) using a transfer buffer (39 mM glycine, 48 mM Tris base, 0.037% (w/v) SDS, 20% (v/v) methanol) and probed with antibodies against mouse phosphoenolpyruvate carboxykinase (PEPCK), mouse major urinary protein (MUP) or mouse and serum transferrin. The proteins were transferred at 25 V for 2.5 h at 4 ^{0}C. The membranes were blocked 1 h at room temperature using 5% non-fat dry milk in Tris-buffered saline (TBST: 0.5 M Tris, 1.5 M NaCl, 0.1% Tween 20 (Sigma-Aldrich), pH 7.4) for PEPCK and 1% casein (MERCK) in TBST for MUP and transferrin. The membranes were washed three times for 5 min with TBST and probed with the primary polyclonal antibodies (PEPCK rabbit polyclonal antibody, MUP goat polyclonal antibody and transferrin goat polyclonal antibody (Santa Cruz Biotechnology, Inc., Santa Cruz, CA, USA) at a 1: 600 dilution overnight at 4 °C followed with three washes for 5 min with TBST. The membranes were then incubated for 2 h with secondary Cy5-labelled anti-rabbit and anti-goat antibodies respectively (Jackson ImmunoResearch Laboratories, West Grove, PA, USA) with dilution 1: 2000 at room temperature. Mouse anti-actin monoclonal antibody (CHEMICON International, Inc., Millipore, CA, USA) was used as a loading control with Cy3-labelled anti-mouse antibody (Jackson

ImmunoResearch Laboratories). Protein bands were visualised using a Fujifilm FLA-5100 scanner (Fuji Photo Film Co.). ImageQuant™ 5.2v (GE Healthcare) software was used to analyse protein band volumes.

2.10.3 Western blot for serum keratin D (cytokeratin 18) and transferrin

Mouse and human serum samples with protein 10 μg/well were separated by one-dimensional electrophoresis using Bio-Rad Laboratories Criterion™ Precast Gel (Bio-Rad Laboratories, Inc., Hercules, CA, USA) for 1 h at 200 V. The proteins were transferred at 25 V for 1 h at 25 ^{0}C onto Immobilon™-P PVDF Membrane (Millipore Corp., Sigma Aldrich, USA) using a transfer buffer (192 mM glycine, 25 mM Tris base, 0.037% (w/v) SDS, 20% (v/v) methanol) and probed with antibodies against keratin D/ cytokeratin 18. The membranes were blocked 1 h at room temperature using 1% casein in phosphate-buffered saline (PBST: 0.1 M PBS, 0.1% Tween 20 (Sigma-Aldrich), pH 7.4). The membranes were washed three times for 5 min each with PBST and probed with cytokeratin 18 goat polyclonal antibody (Santa Cruz Biotechnology, Inc., Santa Cruz, CA, USA) at 1: 600 dilution overnight at 4 °C followed with three washes for 5 min each with PBST. The membrane was incubated for 2 h at room temperature with secondary Cy5-labelled anti-goat antibody (Jackson ImmunoResearch Laboratories, West Grove, PA, USA) with 1: 2000 dilution. GAPDH rabbit polyclonal antibody (Santa Cruz Biotechnology, Inc.) was used as a loading control with Cy3-labelled anti-rabbit antibody (Jackson ImmunoResearch Laboratories). Mouse serum was diluted 1:50 with phosphate buffered saline pH 7.4 for transferrin western blot analysis. Ten μg/μL/well sample from control (n=5), 8-week (n=10), 12-week (n=10) and MSS (n=5) and HSS (n=5) infected mice was separated on SDS-PAGE gel, transferred to Hybond™-LFP PVDF membrane

(GE Healthcare) and probed with goat anti-transferrin polyclonal antibody (Santa Cruz Biotechnology, Inc.) followed by Cy5-labelled anti-goat IgG (Jackson ImmunoResearch Laboratories). Fluorescence intensity of protein bands was visualised using a Fujifilm FLA-5100 scanner (Fuji Photo Film Co.) and protein band volumes were analysed using ImageQuant™ 5.2v (GE Healthcare) software.

2.11 Serum connective tissue growth factor (CTGF) development assay

A human CTGF-ELISA Development Kit (Leinco Technologies, Inc., MO, USA) was used to measure CTGF. A 96-well microplate (Immulon 2B, Nunc, Thermo Fisher Scientific, Inc., Rochester, NY, USA) was coated with 50 µL capture antibody (rabbit anti-human polyclonal antibody, conc. 1 µg/mL) in 10 mL PBS (1: 200) pH 7.2 overnight at room temperature. The plate was washed 4 times with 300 µL wash buffer per well and blotted dry. The microplate was blocked with 300 µL blocking buffer (1% bovine serum albumin in PBS pH 7.2) for 1 h at room temperature. The standard (recombinant human-CTGF) preparation was achieved by dilution of 3 µL kit standard (1000, 000 pg/mL) with 747 µL diluent to generate a standard of concentration 4000 pg/mL (1:250). The 4000 pg/mL standard was serially double diluted to generate a standard curve. After washing the plate as done previously, 100 µL standards (in triplicate) and serum samples (in duplicate) were added to each well and incubated at room temperature for 2 h. After 4 washes, 100 µL detection antibody (biotinylated antigen-affinity purified rabbit anti-human CTGF, concentration 0.25 µg/ml) was added per well (1: 200). With an incubation of 2 h at room temperature and after 4 washes, 100 µL ultra-avidin-horseradish peroxidise-conjugate per well (1:2000) was added. An incubation of 20 min in the dark at room temperature was followed by 4 washes. A volume of 100 µL TMB horseradish

peroxidase-substrate solution was added to each well and incubated at room temperature for 20 min. To stop the reaction 50 µL 1 M H_2SO_4 was added and colour development was monitored for 30 min with a plate reader at 450 nm (Molecular Devices, USA).

2.12 Liver hydroxyproline assay

Weighed liver samples were hydrolysed in 5 mL of 6 M HCl for 18 h at 110 °C in tightly sealed glass tubes (Montesano *et al.*, 2002). After cooling, 40 mg Dowex / Norit mixture (Sigma-Aldrich) and 5 ml distilled water were added to each hydrolysate. The mixture was centrifuged for 15 min at 2000 rpm at 25 °C, and the supernatant fluid was filtered through #1 Whatman 9.0 cm filter paper into a clean tube. A volume of 2 mL of the filtrate was neutralised by adding one drop of 1% phenolphthalein and then titrated against 10 M NaOH until pink and neutralised using 3 M HCl till the filtrate turned yellow. The final volume was adjusted to 4 mL with MilliQ. To make a stock standard (400 µg/mL), 40 mg hydroxyproline (Calbiochem Corporation, La Jolia, CA, USA) was dissolved in 100 mL MilliQ water. One mL stock and 9 mL MilliQ were mixed to prepare a working standard (40 µg/mL). A standard curve was generated with concentrations 0, 10, 20, 30, 40 µg/mL respectively using MilliQ water for dilutions. To 200 µL of neutralised liver hydrolysate or the above standards, 400 µL isopropanol was added and mixed. A volume of 200 µL freshly prepared oxidant solution (chloramine-T/citrate buffer, pH 6.0) was added with mixing and incubated at 25 °C for 4 min. To the above mixture, 2500 µL freshly prepared Ehrlich's Reagent Solution was added, mixed, and incubated at 60 °C for 25 min. The tubes were cooled and the absorbance read at 570 nm using a microplate reader (Molecular Devices, USA). Hydroxyproline levels were expressed as µg.

2.13 Serum hydroxyproline assay

One hundred microlitres of serum was hydrolysed using 400 µL 6 M HCl for 3 h at 120 °C in tightly sealed glass tubes (Uji *et al.*, 1994). After cooling, 10 mg Dowex / Norit mixture (Sigma-Aldrich) was added to each hydrolysate. The mixture was centrifuged for 15 min at 4000 rpm at 25 °C, and the supernatant fluid was filtered through Millex^{R}-GV, Low Protein Binding Durapore (PVDF) membrane, 0.22 µm filter (Millipore, USA) unit into a clean 1.5 mL tube. Fifty microliter filtrate was neutralised by adding 1 µL of 1% phenolphthalein and then titrated against 10 M NaOH until pink and neutralised using 3 M HCl till the filtrate turned yellow. The final volume was adjusted to 100 µL with MilliQ. The standard was prepared similarly as for liver hydroxyproline assay. A volume of 12.5 µL neutralised hydrolysate and standards were added to each well of a 96-well microplate and mixed followed by 25 µL isopropanol. Freshly prepared oxidant solution (chloramine-T/citrate buffer, pH 6.0), 12.5 µL was added to each well with mixing and incubated at 25 °C for 4 min. Ehrlich's Reagent solution was freshly prepared and 155 µL was added to each well, mixed, and incubated at 60 °C for 25 min. The plate was cooled and the absorbance read at 570 nm using a microplate reader (Molecular Devices, USA). Hydroxyproline levels were expressed as µg per mL serum.

2.14 Serum transferrin assay

A serum transferrin assay kit (Alpha Diagnostic Intl., Inc., San Antonio, TX, USA) was used for human serum transferrin measurement. All reagents were brought to room temperature before use. Human serum samples were diluted to 1:20000 using sample diluent. A volume of 300 µL wash buffer was added to each well for 30 min before sample addition to activate the pre-coated plate. The plate was washed 4 times and patted

dry. One hundred microlitres of standards diluted human serum samples or controls were added each to pre-determined wells and incubated for 60 min at room temperature. After washing the plates 4 times, 100 µL diluted anti-human transferrin-horseradish peroxidise-conjugate (1: 1000) was added to each well and incubated for 30 min. The plate was washed 5 times before adding 100 µL TMB substrate (Kirkegaard and Perry Laboratories, Inc., Gaithersburg, MD, USA) and incubated for 15 min in the dark. A volume of 100 µL of 2 M H_2SO_4 was added to stop the enzyme reaction. The absorbance was read at 450 nm (Molecular Devices, USA) within 30 min of addition of H_2SO_4.

2.15 Bicinchoninic acid (BCA) protein determination assay

BCA protein assay (Pierce, Pierce Chemical, Rockford, Illinois, USA) was used for mouse and human serum total protein measurements. 1X PBS pH 7.4 was used for standard preparations and sample dilutions. Fresh working BCA reagent was prepared by mixing 5 mL BCA Reagent A (Pierce, USA) with 100 µL BCA Reagent B (Pierce, USA) to form a clear green solution. The dilution for each sample was 1:10. The final volume of each sample in the microplate was set to 20 µL. The standard curve for the assay was generated by using 2 mg/mL albumin standard (Pierce, USA). The serial dilutions from 2.0 to 0.25 mg/mL were done using 1X PBS. Twenty microliter from each of the albumin standards and the diluted mouse and human serum samples was assayed in 96-well microplate. A volume of 150 µL freshly prepared BCA reagent was added to each well and mixed. The plate was incubated in a 37-40 ^{0}C water bath for 20 min and absorbance read at 570 nm (Molecular Devices, USA).

2.16 Statistical Analysis

Individual protein spot volumes extracted from the DeCyder software and western blot band volume data acquired form Image Quant and human serum samples data from CDC, Atlanta were analysed using GraphPad Prism (v4.0, GraphPad, San. Diego, CA, USA). Protein spot Gene Ontology functional data was generated manually using UniProtKB database and plotted using SPSS (v16.0.1, SPSS Inc, Chicago, Illinois, USA). Multiple regression analyses were performed using SPSS. For statistical analysis spot volumes with skewed distribution (for five study groups: transferrin, RBP1, keratin D, interleukin2, MUP, *Sm*-PEPCK, peroxiredoxin6, GSTPi) were logarithmically ($\log_e$) transformed to satisfy the assumption of normality according to the statistics applicable to 2D-DIGE dataset spot volumes (Chich *et al.*, 2007).

Details of reagents and experimental procedures are listed in Appendix D.

CHAPTER 3: DIFFERENTIAL PATTERNS OF MURINE LIVER PROTEINS AT 20-WEEK POST-INFECTION (MSS AND HSS)

3.1 Introduction

In 90% of infected individuals egg-associated inflammation recedes resulting in INT while 10% present with HS. The CBA/J mouse model reproduces these forms of the disease found in infected humans. Liver proteomic signatures from control (uninfected), MSS and HSS CBA/J mice were compared to identify differential protein patterns for 20-week infection. 2D-DIGE was used to study protein patterns and the candidate liver protein markers were identified using matrix adsorption laser desorption ionisation-time of flight (MALDI-TOF), correlated to the development of hypersplenomegaly syndrome and verified using western blot techniques to confirm the association pattern. The experimental design 1 for DIGE experiments is listed in Appendix A.

3.2 Results

All of the 20-week *S. mansoni*-infected CBA/J mice had enlarged, fibrotic and granulomatous livers, and were classified as MSS or HSS by percent spleen to body weight ratio and gross pathologic characteristics. The average percent spleen to body weight ratio for uninfected mice was 0.272, for MSS mice 0.578 and for HSS mice it was 2.314 (Figure 3.1). The spleen to body weight ratio for MSS was 2 times and HSS was 8.5 times more than the control mice. This ratio is a robust measure of the pathology associated with HSS.

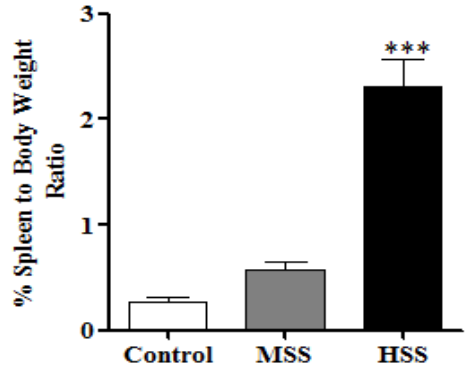

FIGURE 3.1 Comparison of percent spleen to body weight ratio from fifteen CBA/J mice (5 controls, 5 MSS, 5 HSS), 1-ANOVA $p \leq 0.01$. ***$p \leq 0.001$ HSS compared to MSS and control mice by Newman-Keuls Multiple Comparison Test.

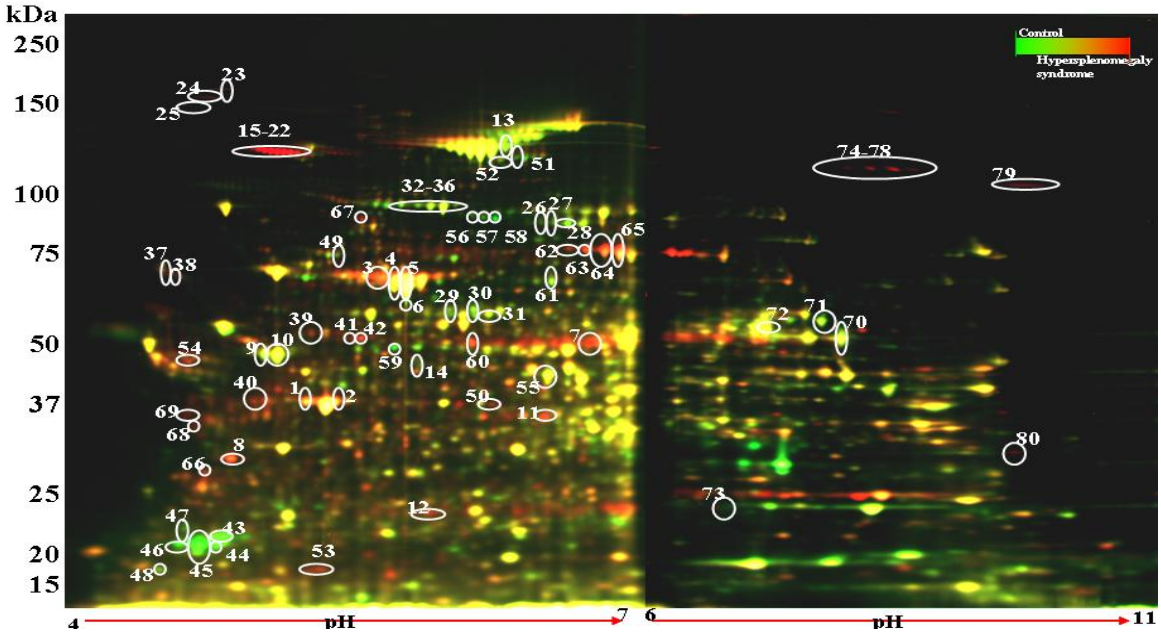

FIGURE 3.2: A pseudocolour map of total liver proteins from uninfected and HSS mice separated by 2D-DIGE. Liver lysate from control/uninfected liver was labelled with Cy5 (green), lysates from 20-week infected HSS liver was labelled with Cy3 (red) and a pooled internal standard of liver lysates from all mice in the study (n=15) was labelled with Cy2

(blue; not shown). Isoelectric focusing was performed on 7 cm IPG strips, pI 4-7 and pH 6-11 and proteins were then separated using SDS-PAGE. The image overlays of Cy5 and Cy3 labelled proteins appear yellow. The numbers correspond to the numbers (No.) of protein spots in Table 3.1. Note that the MUP (protein spots 45-49) are green showing high abundance in control mice and collagen (protein spots 16-23) are red showing high abundance in HSS mice.

Figure 3.2 is a pseudocolour map of superimposed 2D-DIGE images for pI 4-7 and 6-11 IPG DryStrips; and compares control liver lysate to 20-week infected HSS liver lysate. The DeCyder software detected 2550 spots each in the 4-7 and 6-11 pI range using the BVA module. The number of protein spots that changed for 4-7 and 6-11 pI ranges were 295 and 129, respectively. Furthermore, 134 and 38 protein spots in 4-7 and 6-11 pI ranges showed $\geq$ 2-fold change in average volume ratio with ANOVA $p \leq 0.01$; these were designated as proteins of interest. Application of false discovery rate (FDR) to remove false positives gave a total of 107 and 17 protein spots for each pI range respectively (although the application of FDR eliminated the false positive protein spots, we believe that these eliminated protein spots may be important in the pathogenesis of schistosomiasis). The 124 spots were subjected to MALDI-TOF mass fingerprinting and matched to database sequences, resulting in the identification of 80 protein spots listed in Table 3.1 (Figure 3.2 and Table A1). Additional information of the identified protein spots is listed in Appendix C.

The identified 80 protein spots were assessed according to the Gene Ontology molecular function categories. In particular, structural proteins, immune response proteins and acute

phase proteins showed increased abundance while the proteins related to energy metabolism; choline metabolism and xenobiotic metabolism were decreased in abundance (Figure 3.3). These specific protein spot changes will be discussed in the following sections in the context of these functional categories.

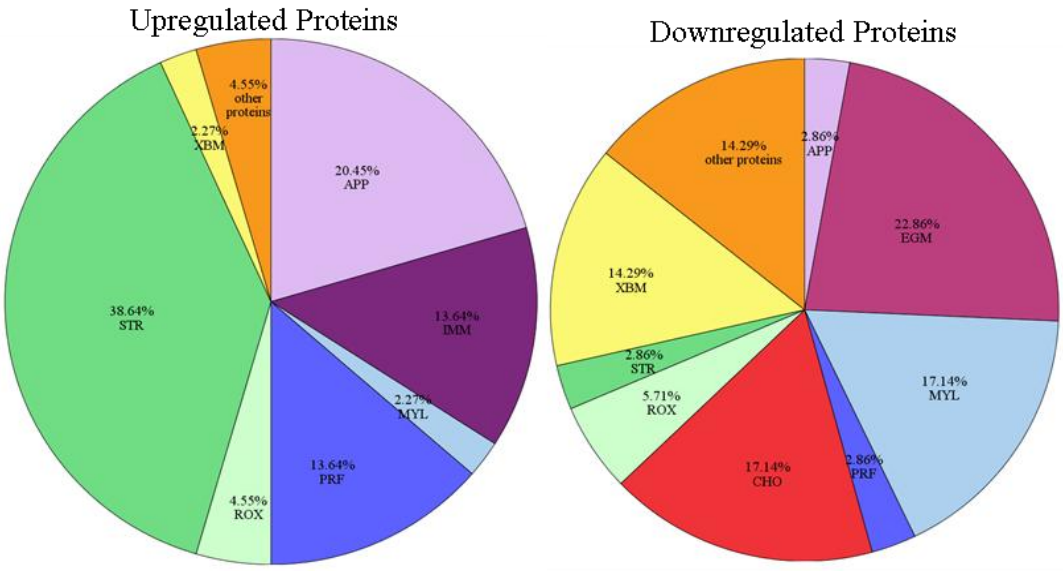

FIGURE 3.3 Distribution of protein abundance by Gene Ontology molecular function categories, during the development of chronic schistosomiasis. APP, acute phase protein; CHO, Choline Metabolism; EGM, energy metabolism; IMM, immune response; MYL, methylation; PRF, protein folding; ROX, redox reactions; STR, structural protein; XBM, xenobiotic metabolism.

TABLE 3.1: Experiment design 1: Identified protein spot comparisons for 20-week infected mice (MSS and HSS) with control mice for pI ranges 4-7 and 6-11 with 2-fold change, 1-ANOVA $p \leq 0.01$ and FDR.

Spot No.	***Protein ID (pI 4-7)***	***AVR[1] H/C***	***AVR[1] M/C***	***AVR[1] H/M***	***gi Number***	***pI[1]***	***Mw[1] (kDa)***	***Func.[2]***	***Ref.[1]***
1	Actin	+2.12	+1.81	+1.17	809561	5.8	39.45	STR	(Harvie *et al.*, 2007)
2	Actin	+2.39	+2.04	+1.17	49868	5.8	39.45	STR	(Harvie *et al.*, 2007)
3	Albumin	+3.26	+1.88	+1.73	19353306	5.8	70.73	APP	(Harvie *et al.*, 2007)
4	Albumin	+2.84	+1.71	+1.66	33859506	5.8	70.73	APP	(Harvie *et al.*, 2007)
5	Albumin	+2.83	+1.73	+1.63	19353306	5.8	70.73	APP	(Harvie *et al.*, 2007)
6	Albumin	-2.13	-1.51	-1.41	26341396	5.5	67.04	APP	(Harvie *et al.*, 2007)
7	Aldehyde dehydrogenase 9	+2.87	+1.90	+1.51	9910128	6.6	54.47	ROX	(Dragani *et al.*, 1996, Vasiliou *et al.*, 2000)
8	Annexin 5	+4.52	+2.17	+2.08	6753060	4.8	35.78	SIG	(Mulla *et al.*, 2004)
9	ATP5 beta synthetase (ATPS)	-2.05	-1.88	-1.09	23272966	5.2	56.65	EGM	(Capuano *et al.*, 1997, Harvie *et al.*, 2007)
10	ATPS	-2.13	-1.72	-1.24	23272966	5.2	56.65	EGM	(Capuano *et al.*, 1997, Harvie *et al.*, 2007)
11	Betaine homocysteine methyltransferase 2	+3.80	+2.54	+1.50	62533211	6.0	40.28	MYL	(Forestier *et al.*, 2003, Sun *et al.*, 2007)
12	Brain and reproductive organ-expressed protein	+3.04	+2.08	+1.46	38173925	5.7	43.95	APO	(Chen, 2008, Li *et al.*, 2004)
13	Carbamoyl phosphate synthase	-2.60	-1.87	-1.39	73918911	6.5	165.8	EGM	(Harvie *et al.*, 2007, Thome-Kromer *et al.*, 2003)
14	Chaperonin containing TCP-1 theta subunit (Chaperone CCT8)	-2.85	-1.78	-1.60	5295992	5.4	60.06	PRF	(Agaton *et al.*, 2003, Harvie *et al.*, 2007)
15	Collagen 6a1	+17.8	+12.2	+1.45	12805443	5.8	44.76	STR	(Saber *et al.*, 1983, Stickel *et al.*, 2001)

16	Collagen 6a1	+47.8	+32.3	+1.48	12805443	5.8	44.76	STR	(Saber *et al.*, 1983, Stickel *et al.*, 2001)
17	Collagen 6a1	+55.8	+36.2	+1.54	12805443	5.8	44.76	STR	(Saber *et al.*, 1983, Stickel *et al.*, 2001)
18	Collagen 6a1	+47.8	+31.9	+1.50	12805443	5.8	44.76	STR	(Saber *et al.*, 1983, Stickel *et al.*, 2001)
19	Collagen 6a1	+34.7	+24.2	+1.43	12805443	5.8	44.76	STR	(Saber *et al.*, 1983, Stickel *et al.*, 2001)
20	Collagen 6a1	+21.0	+15.5	+1.36	12805443	5.8	44.76	STR	(Saber *et al.*, 1983, Stickel *et al.*, 2001)
21	Collagen 6a1	+10.2	+7.81	+1.30	12805443	5.8	44.76	STR	(Saber *et al.*, 1983, Stickel *et al.*, 2001)
22	Collagen 6a1	+5.38	+4.94	+1.09	12805443	5.8	44.76	STR	(Saber *et al.*, 1983, Stickel *et al.*, 2001)
23	Collagen XIV	+5.13	+2.40	+2.13	30420885	5.0	194.3	STR	(Saber *et al.*, 1983, Stickel *et al.*, 2001)
24	Collagen XIV	+4.27	+2.78	+1.54	30420885	5.0	194.3	STR	(Saber *et al.*, 1983, Stickel *et al.*, 2001)
25	Collagen XIV	+7.13	+3.61	+1.97	30420885	5.0	194.3	STR	(Saber *et al.*, 1983, Stickel *et al.*, 2001)
26	Dimethylglycine dehydrogenase (DMDH)	-2.04	-1.71	-1.20	59808083	7.8	97.44	CHO	(Harvie *et al.*, 2007)
27	DMDH	-2.21	-1.74	-1.27	59808083	7.8	97.44	CHO	(Harvie *et al.*, 2007)
28	DMDH	-2.34	-1.76	-1.33	59808083	7.8	97.44	CHO	(Harvie *et al.*, 2007)
29	Epoxide hydrolase (EH)	-2.46	-1.78	-1.38	15929294	5.9	63.07	XBM	(Murray *et al.*, 1993)
30	EH	-2.41	-2.03	-1.19	15929294	5.9	63.07	XBM	(Murray *et al.*, 1993)
31	EH	-2.82	-1.85	-1.52	15929294	5.9	63.10	XBM	(Murray *et al.*, 1993)
32	Formyl tetrahydrofolate dehydrogenase (10-FTHFDH)	-2.52	-1.49	-1.69	20380027	5.6	99.55	MYL	(Krupenko and Oleinik, 2002, Vasiliou *et al.*, 2000)
33	10-FTHFDH	-2.56	-1.43	-1.79	20380027	5.6	99.55	MYL	(Krupenko and Oleinik, 2002, Vasiliou *et al.*, 2000)
34	10-FTHFDH	-2.28	-1.54	-1.48	23271467	5.6	99.55	MYL	(Krupenko and Oleinik, 2002, Vasiliou *et al.*,

									2000)
35	10-FTHFDH	-2.36	-1.51	-1.56	20380027	5.6	99.55	MYL	(Krupenko and Oleinik, 2002, Vasiliou *et al.*, 2000)
36	10-FTHFDH	-2.47	-1.70	-1.46	23271467	5.6	99.55	MYL	(Krupenko and Oleinik, 2002, Vasiliou *et al.*, 2000)
37	Glucosidase II β	+3.53	+2.47	+1.43	57013837	4.4	59.74	PRF	(Altmann, 2007, Rudd *et al.*, 2001)
38	Glucosidase II β	+2.47	+2.13	+1.16	57013837	4.4	59.74	PRF	(Altmann, 2007, Rudd *et al.*, 2001)
39	Group specific component	+2.89	+1.81	+1.60	51172612	5.4	55.18	APP	(Meier *et al.*, 2006, Schiødt, 2008)
40	Keratin D	+2.43	+1.52	+1.60	293682	5.3	47.47	STR	(Boehme *et al.*, 1989, Salmhofer *et al.*, 1994)
41	Lymphocyte cytosolic protein 1 (Plastin 2)	+4.17	+3.06	+1.36	26326929	5.2	70.77	PRF	(Strathmann *et al.*, 2007)
42	Plastin 2	+3.24	+2.45	+1.32	26326929	5.2	70.77	PRF	(Strathmann *et al.*, 2007)
43	Major urinary protein (MUP)	-8.11	-1.69	-4.80	53271	4.8	17.71	PHE	(Dragani *et al.*, 1989)
44	MUP	-7.54	-1.50	-5.02	12851568	4.8	17.71	PHE	(Dragani *et al.*, 1989)
45	MUP	-10.3	-2.61	-3.96	13276755	4.8	17.71	PHE	(Dragani *et al.*, 1989)
46	MUP	-5.56	-2.35	-2.37	494384	4.8	17.71	PHE	(Dragani *et al.*, 1989)
47	MUP	-3.51	-1.50	-2.34	38488789	4.8	21.73	PHE	(Dragani *et al.*, 1989)
48	Myosin light polypeptide 6	-2.15	-1.68	-1.28	33620739	4.6	17.09	STR	(Wegrzyn *et al.*, 2006)
49	NADH dehydrogenase (Ubiquinone) Fe-S protein 1	-2.12	-1.75	-1.21	21704020	5.5	80.76	EGM	(Blanc *et al.*, 2005)
50	Protein disulfide-isomerase A3, Erp57	+3.17	+1.94	+1.63	26353794	5.8	57.12	ROX	(Harvie *et al.*, 2007, Santos *et al.*, 2007)
51	Pyruvate	-3.44	-2.17	-1.58	26346581	6.1	103.8	EGM	(Hammond and Balinsky, 1978, Harvie

	carboxylase								*et al.*, 2007)
52	Pyruvate carboxylase	-2.35	-1.72	-1.36	26346581	6.1	103.8	EGM	(Hammond and Balinsky, 1978, Harvie *et al.*, 2007)
53	Retinol binding protein Type- I	+2.73	+1.91	+1.43	21730472	5.1	15.86	APP	(Uchio *et al.*, 2002)
54	Ribonuclease/angio genesis inhibitor	+2.15	+2.16	-1.00	14577933	4.6	51.21	IMM	(Chu *et al.*, 2003)
55	S-Adenosyl homocysteine hydrolase	-2.10	-1.68	-1.25	63471580	6.1	48.08	MYL	(Leal *et al.*, 2008)
56	Sarcosine dehydrogenase (SARDH)	-2.16	-1.35	-1.59	26352359	6.4	57.84	CHO	(Lim *et al.*, 2002)
57	SARDH	-2.80	-1.46	-1.92	26352359	6.4	57.84	CHO	(Lim *et al.*, 2002)
58	SARDH	-6.43	-3.23	-1.99	26352359	6.4	57.84	CHO	(Lim *et al.*, 2002)
59	Selenium binding protein 2 (SBP2)	-3.66	-2.40	-1.53	188848341	5.8	53.16	XBM	(Harvie *et al.*, 2007, Henkel *et al.*, 2006)
60	SBP2	+2.99	+1.63	+1.84	18848341	6.0	52.90	XBM	(Harvie *et al.*, 2007, Henkel *et al.*, 2006)
61	Succinate dehydrogenase Fp subunit	-2.33	-1.81	-1.29	15030102	6.2	59.27	EGM	(Blanc *et al.*, 2005)
62	Transferrin	+2.83	+1.43	+1.98	62027488	7.0	78.87	APP	(Harvie *et al.*, 2007)
63	Transferrin	+4.17	+1.66	+2.52	62027488	7.0	78.87	APP	(Harvie *et al.*, 2007)
64	Transferrin	+4.72	+1.71	+2.76	62027488	7.0	78.87	APP	(Harvie *et al.*, 2007)
65	Transferrin	+4.60	+1.68	+2.74	62027488	7.0	78.87	APP	(Harvie *et al.*, 2007)
66	Tropomyosin 3	+2.19	+1.61	+1.37	26341416	4.7	27.88	STR	(Harvie *et al.*, 2007, Otogawa *et al.*, 2009)
67	Valosin containing protein	+4.76	+3.68	+1.29	26350783	5.1	80.70	PRF	(Yamamoto *et al.*, 2003)
68	Vimentin	+2.31	+2.67	-1.16	31982755	4.9	53.73	STR	(Boehme *et al.*, 1989, Harvie *et al.*, 2007)
69	Vimentin	+2.54	+2.68	-1.06	31982755	4.9	53.73	STR	(Boehme *et al.*, 1989, Harvie *et al.*, 2007)

No.	Protein ID (pI 6-11)	AVR[1] H/C	AVR[1] M/C	AVR[1] H/M	gi Number	pI[1]	Mw[1] (kDa)	Func.[2]	Ref.[1]
70	Aldehyde dehydrogenase A1	-2.62	-2.02	-1.41	32484332	8.3	55.08	ROX	(Dragani *et al.*, 1996, Vasiliou *et al.*, 2000)
71	Catalase 1	-3.00	-2.61	-1.15	15004258	7.8	60.01	ROX	(Gharib *et al.*, 1999, Harvie *et al.*, 2007)
72	Glutamate dehydrogenase	-2.76	-2.12	-1.30	26354278	8.6	61.60	EGM	(Morand *et al.*, 2005, Van Waes and Lieber, 1977)
73	Glutathione S-transferase Pi class	-3.27	-2.05	-1.59	2624496	8.3	23.52	XBM	(Harvie *et al.*, 2007, Hayes *et al.*, 1991)
74	MHC class I H2 Q4 like	+5.01	+3.23	-1.55	51770518	7.3	71.74	IMM	(Grzych *et al.*, 1991, Hernandez *et al.*, 1997)
75	MHC class I H2 Q4 like	+8.09	+4.88	-1.66	51770518	7.3	71.74	IMM	(Grzych *et al.*, 1991, Hernandez *et al.*, 1997)
76	MHC class I H2 Q4 like	+12.2	+7.29	-1.67	51770518	7.3	71.74	IMM	(Grzych *et al.*, 1991, Hernandez *et al.*, 1997)
77	MHC class I H2 Q4 like	+18.3	+11.6	-1.58	51770518	7.3	71.74	IMM	(Grzych *et al.*, 1991, Hernandez *et al.*, 1997)
78	MHC class I H2 Q4 like	+17.2	+10.4	-1.66	51770518	7.3	71.74	IMM	(Grzych *et al.*, 1991, Hernandez *et al.*, 1997)
79	*Sm*-Phosphoenol pyruvate carboxykinase	+14.4	+8.05	-1.79	74828716	6.8	71.46	GLN	(Asahi *et al.*, 2000)
80	Prohibitin-2	+3.25	+1.61	+2.02	61556754 (76363295)	9.8	33.29	PRF	(Asamoto and Cohen, 1994, Mishra *et al.*, 2005)

[1]**AVR**: average volume ratio between study groups (C, control; M, MSS; and H, HSS); **pI:** isoelectric pH; **Mw:** molecular weight; **Ref:** references refer to association of protein with various diseases.

[2]**Func (Functions):** APO, anti-apoptotic; APP, acute phase protein; CHO, Choline Metabolism; EGM, energy metabolism; GLN, gluconeogenesis; IMM, immune response;

MYL, methylation; PHE, pheromone; PRF, protein folding; PRM, protein metabolism; ROX, redox reactions; SIG, cell signalling; STR, structural protein; XBM, xenobiotic metabolism.

3.2.1 Acute phase proteins

Nine negative acute phase protein spots (4 transferrins, 3 albumins, 1 retinol binding protein, 1 group specific component) increased in abundance due to schistosome infection, while one spot in particular for albumin decreased in abundance. The greatest changes were found with the transferrin spots. Overall transferrin abundance increased from 2.8 to 4.7 fold for HSS mice and as spot volumes for transferrin isoforms changed with schistosome infection. Specifically spots 63, 64 and 65 increased significantly by 4-fold and 2-fold for HSS when compared to control and MSS mice (Table 3.1 and Figure 3.2, Figure 3.4) indicating a disease form specific change.

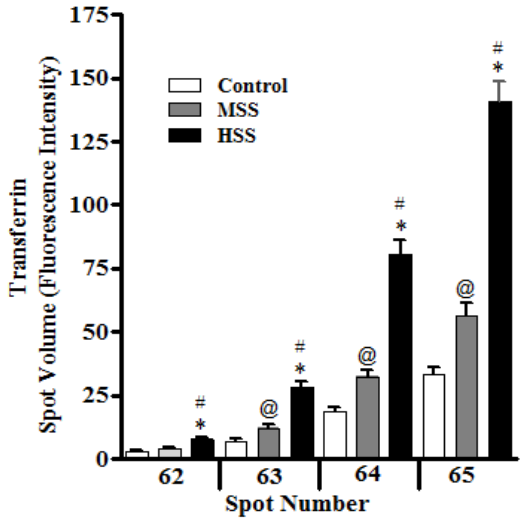

FIGURE 3.4 Comparison of spot volumes of transferrin spots, 1-ANOVA $p \leq 0.01$ for all spots. *$p \leq 0.001$ HSS compared to control, # $p \leq 0.01$ compared to MSS, $^{@}p \leq 0.05$ MSS compared to control by Newman-Keuls Multiple Comparison Test.

The spot volume data for albumin isoforms, another negative acute phase protein, showed three spots (spot 3, 4, 5; Figure 3.5) with increased abundance while one spot (spot 6) decreased with abundance. Group specific component (GSC) spot (Spot 29, Figure 3.2, Table 3.1) showed increased abundance in HSS mice alone. Similarly, retinol binding protein-1 (RBP1) spot (Spot 53, Figure 3.2, Table 3.1, Figure 3.7) showed increased abundance in HSS mice. The spot volume comparison for RBP1 showed 2-fold increase for HSS and MSS mice and was statistically significant. Ideally, negative acute phase proteins decrease with any infection and/or pathology, but our results are in contrast with this pattern and suggest that these changes during schistosomiasis are unique.

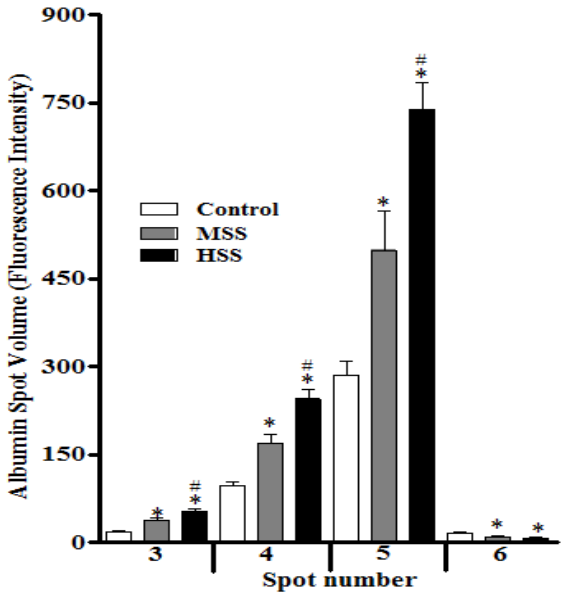

FIGURE 3.5 Comparison of spot volumes of albumin spots, 1-ANOVA $p \leq 0.01$ for all spots. *$p \leq 0.01$ compared to control, #$p \leq 0.05$ compared to MSS by Newman-Keuls Multiple Comparison Test.

3.2.2 Structural proteins

Overall, the extracellular matrix and cytoskeletal proteins increased in abundance. A total of 16 structural protein spots increased in abundance in response to schistosome infection. As expected collagen 6a1 spot volumes were increased by 5-fold to 55-fold and collagen XIV spot volumes increased from 4-fold to 7-fold significantly. Taking all the spot volumes together for collagen 6a1 protein, the increase was almost 300-fold for HSS mice and 165-fold for MSS mice when compared to control mice (Figure 3.2, Figure 3.6 and Table 3.1). These changes are in line with the known fibrotic changes that occur during chronic infection.

Like collagen, two actin spots (spots 1, 2) and two vimentin (spots 68, 69) spots (Figure 3.2, Table 3.1, Figure 3.7) increased in abundance from 2-fold to 2.6-fold. A single keratin D spot (spot 40) increased in the severe disease. Spot volume comparison for keratin D between control, MSS and HSS was significant (1-ANOVA $p \leq 0.05$, Figure 3.8). These results are likely due to the granulomatous response to the eggs embedded in the liver which involved increased deposition of extracellular matrix components like collagen, actin, vimentin and keratin D.

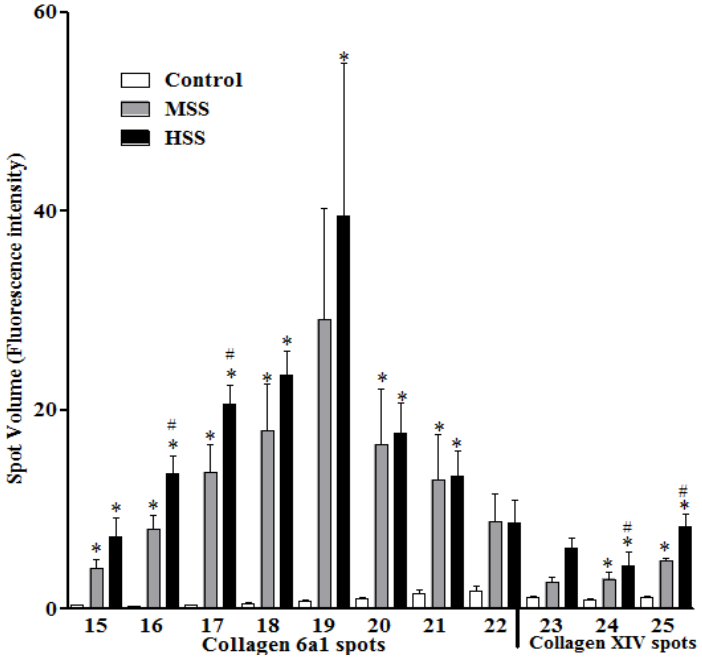

FIGURE 3.6 Comparison of spot volumes of collagen spots, 1-ANOVA $p \leq 0.01$ for all spots. *$p \leq 0.05$ compared to control, #$p \leq 0.05$ compared to MSS by Newman-Keuls Multiple Comparison Test.

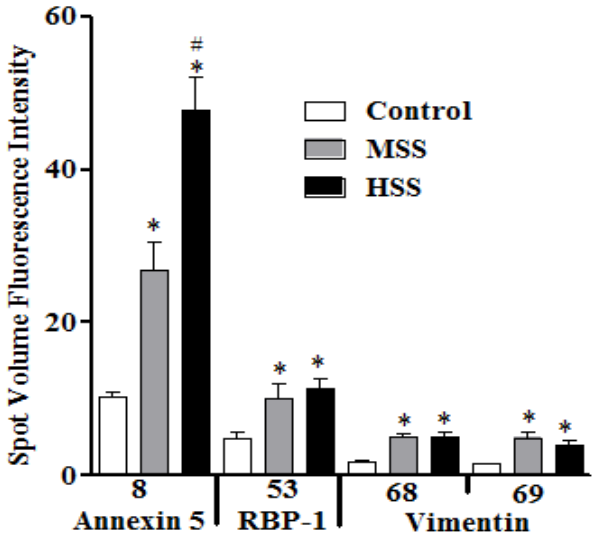

FIGURE 3.7 Comparison of spot volumes of various liver protein spots, 1-ANOVA $p \leq 0.01$ for all spots. *$p \leq 0.05$ compared to control, #$p \leq 0.05$ compared to MSS by Newman-Keuls Multiple Comparison Test. RBP-1=Retinol Binding Protein 1.

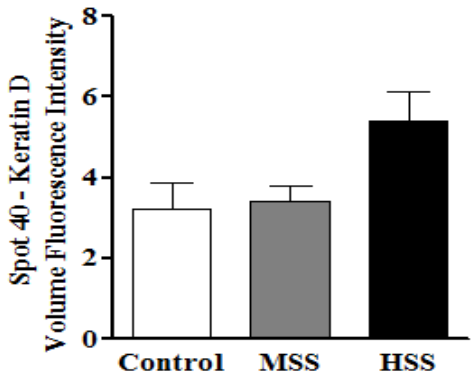

FIGURE 3.8 Comparison of spot volume for spot 40-Keratin D, 1-ANOVA $p \leq 0.05$ for all spots. Newman-Keuls Multiple Comparison Test for comparison between groups was not significant.

3.2.3 Energy metabolism proteins

There was a decrease in seven protein spots related to energy metabolism. Two spots with ATP synthase-beta subunit (ATPase beta) activity showed 2-fold decreased abundance (spots 9, 10, Figure 3.2, Table 3.1). Additionally, two spots of pyruvate carboxylase, one spot of NADH dehydrogenase (ubiquinone) Fe-S protein 1, one spot of glutamate dehydrogenase (GLDH) and one spot of carbamoyl phosphate synthase 1 were decreased in abundance by above two fold (Table 3.1). Based on these results it can be presumed that energy metabolism capacity is decreased during 20-week schistosomiasis infection.

3.2.4 Choline metabolism proteins

There was decreased abundance of two proteins associated with choline catabolism, dimethylglycine dehydrogenase (DMDH, spots 26-28) and sarcosine dehydrogenase (SARDH, spots 56-58**)** (Figure 3.2, Table 3.1, Figure 3.9). These six protein spots decreased significantly in MSS and HSS mice compared to control mice and indicate that

infection but not disease form-specific changes. These decreases could mean that there are alternative pathways for choline utilisation during schistosome infection.

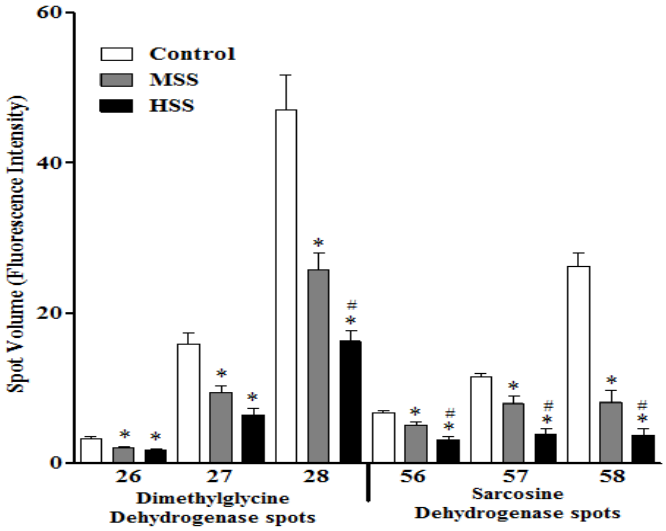

FIGURE 3.9 Comparison of spot volumes of dimethylglycine dehydrogenase and sarcosine dehydrogenase spots, 1-ANOVA $p \leq 0.01$ for all spots. *$p \leq 0.05$ compared to control, #$p \leq 0.05$ compared to MSS by Newman-Keuls Multiple Comparison Test.

3.2.5 Xenobiotic metabolism proteins

During disease and infection, xenobiotic metabolising proteins are increased providing protection to the host from harmful molecules such as free radicals. The overall decreased abundance of these protein spots in schistosomiasis infection may be explained by decreased synthesis during disease condition and may indicate an impaired ability to deal with oxidative stress. Five spots decreased and two spots increased in abundance related to xenobiotic metabolism. Catalase (Spot 71, Figure 3.2, and Table 3.1) was decreased by 3-fold in HSS mice and 2-fold in MSS mice. Two spots of selenium binding protein-2 (SBP2) were identified, one with increased activity (+2.99, pI 6.0) and other with

decreased activity (-3.66, pI 5.8). Glutathione S-transferase Pi (GSTPi) was decreased by above 3-fold in HSS and above 2-fold in MSS mice. Three epoxide hydrolase spots showed decreased abundance by 2-fold for HSS mice and two spots for MSS mice. Also, two spots with aldehyde dehydrogenase activity were identified, one spot with pI 6.6 showed increased expression of 2.8-fold while one spot with pI 8.3 showed 2.6 and 2.0-fold decreased activity in HSS and MSS mice respectively (Figure 3.2, Table 3.1).

3.2.6 DNA methylation-related proteins

Protein spots related to DNA methylation showed overall decreased abundance. Five spots decreased in abundance and two spots showed increased abundance. One spot of betaine-homocysteine S-methyltransferase (BHMT) was identified (Figure 3.2, Table 3.1, spot 11). The acidic spot showed 2.5 to 3.8-fold increase in abundance in schistosome infection. One spot with S-adenosylhomocysteine hydrolase (SAH) activity was increased by 2-fold. Five spots of 10-formyl tetrahydrofolate dehydrogenase (10-FTHDH) were decreased by above 2-fold in HSS mice alone (Figure 3.2, Table 3.1, spot 32-36). The proteins discussed in this category are associated with metabolic processes that are involved in synthesis of methyl groups. These methyl groups are used for methylation of DNA, which is necessary for the proper functioning of the DNA. The decreased abundance of these proteins in our study may suggest an imbalance in DNA methylation and function.

3.2.7 Immune response proteins

Given the involvement of the immune response in schistosomiasis, it is not surprising that significant changes occurred in this functional category. In MSS and HSS mice, there was a 2-fold to 18-fold significant increased abundance of MHC class I histocompatibility

antigen H2 Q4 alpha chain precursor like (MHC Class 1 H2Q4 like protein) (Figure 3.2, Table 3.1 spots 74-78, Figure 3.10). Two spots 75 and 76 are particularly interesting due to the significantly increased abundance in HSS when compared to MSS mice, and may be worth studying indepth as a severe disease specific marker. Two other immune-related proteins, lymphocyte cytosolic protein 1 (plastin-2) and prohibitin-2 were significantly increased in the study. The two plastin-2 spots increased by 3.2 to 4.2 fold for HSS and MSS mice, while just one spot of prohibitin-2 increased by 3.2-fold for HSS mice (Figure 3.2, Table 3.1, Figure 3.11). Overall immune response protein spots showed increased abundance from 2-fold to 18-fold in MSS and HSS mice when compared to control mice.

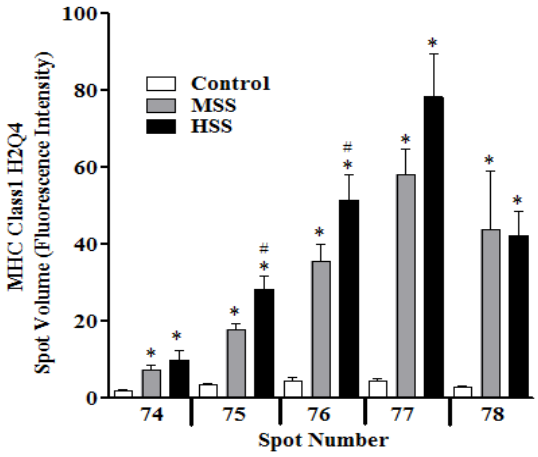

FIGURE 3.10 Comparison of spot volumes of MHC class I histocompatibility antigen H2 Q4 alpha chain precursor spots, 1-ANOVA $p \leq 0.01$ for all spots. *$p \leq 0.05$ compared to control, #$p \leq 0.05$ compared to MSS by Newman-Keuls Multiple Comparison Test.

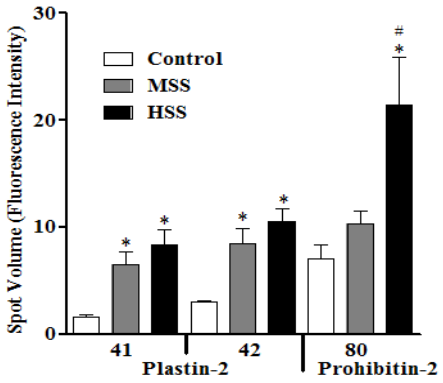

FIGURE 3.11 Comparison of spot volumes of plastin-2 and prohibitin-2 spots, 1-ANOVA $p \leq 0.01$ for all spots. *$p \leq 0.01$ compared to control, #$p \leq 0.05$ compared to MSS by Newman-Keuls Multiple Comparison Test.

3.2.8 Other liver proteins

Several proteins that changed significantly but did not fall into discrete functional categories were annexin 5, chaperonin containing TCP-1 theta subunit, glucosidase II beta subunit and major urinary protein isoforms. The annexin 5 spot volume comparison showed the protein increased by 2.1 to 4.5-fold in HSS and MSS, although the increase for HSS was significantly higher than MSS mice (Figure 3.7). Brain and reproductive organ-expressed protein was increased by 3-fold in HSS mice and by 2-fold in MSS mice (Figure 3.2, Table 3.1, spot 12). We identified two proteins involved in protein folding as chaperonin containing TCP-1 theta subunit (chaperone CCT8) and glucosidase II beta subunit. One spot with chaperone CCT8 activity decreased in abundance and two spots of glucosidase II beta subunit increased in abundance by 2.4 to 3.5-fold.

Major urinary proteins (MUP) are type of pheromone proteins synthesised in the liver. Male mice excrete MUPs under hormonal control to co-ordinate social behaviour. We found five MUP spots (Figure 3.2, spots 43-47) decreased by 2 to 10-fold specifically in

HSS mice while MSS mice showed only two spots with 2.6-fold decreased abundance. MUP spot volume comparison for 5 spots showed significantly high decrease for HSS mice when compared to MSS and control mice (Figure 3.12).

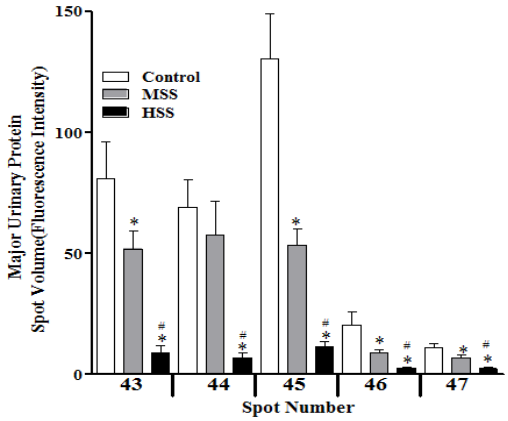

FIGURE 3.12 Comparison of spot volumes of major urinary protein spots, 1-ANOVA $p \leq 0.01$ for all spots. *$p \leq 0.05$ compared to control, # $p \leq 0.05$ compared to MSS by Newman-Keuls Multiple Comparison Test.

3.2.9 Parasite proteins

Schistosoma mansoni- phosphoenolpyruvate carboxykinase (*Sm*-PEPCK, Mw 71.46 and pI 6.8; Figure 3.2, spot 79 and Figure 3.13, Table 3.1) was the only parasitic protein identified in the study. The *Sm*-PEPCK abundance increased above 14-fold in HSS and 8-fold in MSS livers. With the purpose of verifying, confirming and locating *Sm*-PEPCK, soluble egg antigen (SEA) proteome was investigated for pI ranges 3-10, 4-7 and 6-11. Proteomic signatures from control and infected liver samples were compared with SEA proteome to determine the parasite generated proteins (non-host-derived factors) that contribute to the severe disease pathology. Spots 32, 33, 36 in Figure 3.14 were identified as *Sm*-PEPCK using schistosome genome databases. Additionally, the schistosome

genome and proteome helped verify that the identified protein spots were either parasite or host derived. Additional information of the identified protein spots using preparative gels is listed in Appendix C.

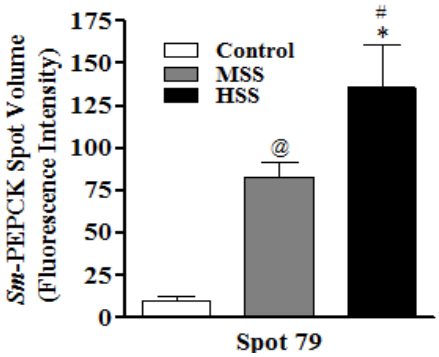

FIGURE 3.13 Comparison of spot volumes of *Sm*-PEPCK for control, MSS and HSS, 1-ANOVA $p \leq 0.01$ for all spots. *$p \leq 0.001$ compared to control, $^{@}p \leq 0.01$ compared to control, #$p \leq 0.05$ compared to MSS by Newman-Keuls Multiple Comparison Test. Spectrum for Sm-PEPCK shown in Appendix C (Figure C9).

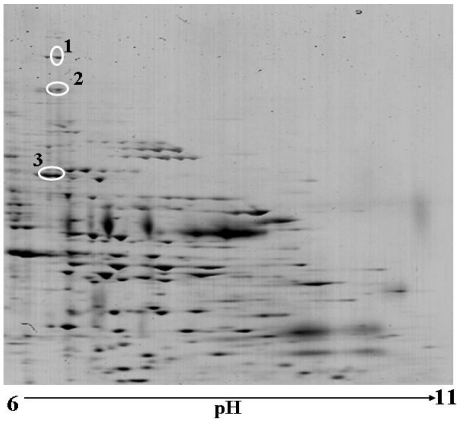

FIGURE 3.14 The SEA proteomic signature pI range 6-11 (75 µg protein) showing spots 1, 2 and 3 identified as *Sm*-PEPCK.

3.2.10 Multivariate analysis

To visualise differences in the most statistically significant protein spots associated with each mouse in the study the principle component analysis (PCA) and hierarchical cluster analysis (HCA) was performed. PCA compared the protein spot map data from the control, MSS and HSS mice. This supervised analysis showed close clustering of the individual 2D-DIGE spot maps within each group and thus revealed that the control, MSS, and HSS mice have distinct and distinct liver protein patterns (Figure 3.15 and Figure 3.16). The protein spots within the ellipse shows 72 protein spots representing 95% significance level, while the 8 protein spots outside the ellipse are very strongly differentially expressed proteins (collagen spots and major urinary protein spots). Protein spots within the ellipse in the light blue circle were upregulated in MSS and HSS mice when compared to the control mice. Protein spots within the ellipse in the dark blue circle were downregulated in MSS and HSS mice when compared to control mice. The protein spots for the pI range 4-7 had outliers outside the ellipse; these were strongly differentially expressed proteins, within the light blue circle were the collagen isoforms and in the dark blue circle it was the MUP isoforms. The PCA for the pI range 4-7 clearly defines and differentiates between the study groups: control, MSS and HSS (Figure 3.15). In contrast, the PCA for the pI range 6-11 is not conclusive as for pI 4-7. The plot shows cluster of MSS and HSS mice together, which may be due to the poor resolution of the protein spots for the pI range 6-11 (Figure 3.16).

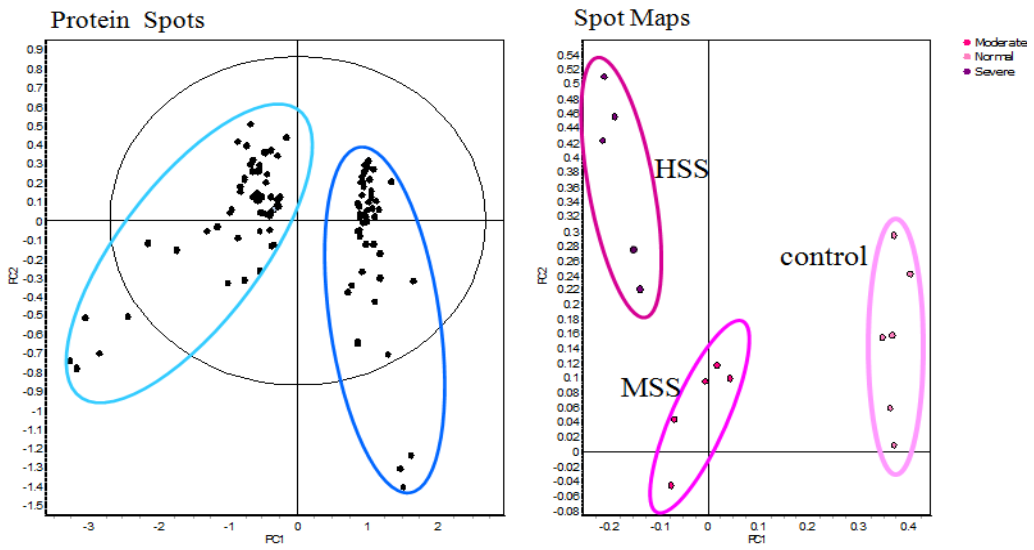

FIGURE 3.15 Principle component analysis scatter plot for protein spots in the pI range 4-7 with 2-fold change and 1-ANOVA ≤ 0.01, FDR. Protein spots within the ellipse show highly abundant (light blue circle, infected mice compared to control mice) and lowly abundant (dark blue circle, infected mice compared to control mice) protein spots. Spot maps (2D-DIGE images) show the best separation of the moderate and severe disease from the control (uninfected) CBA/J mice.

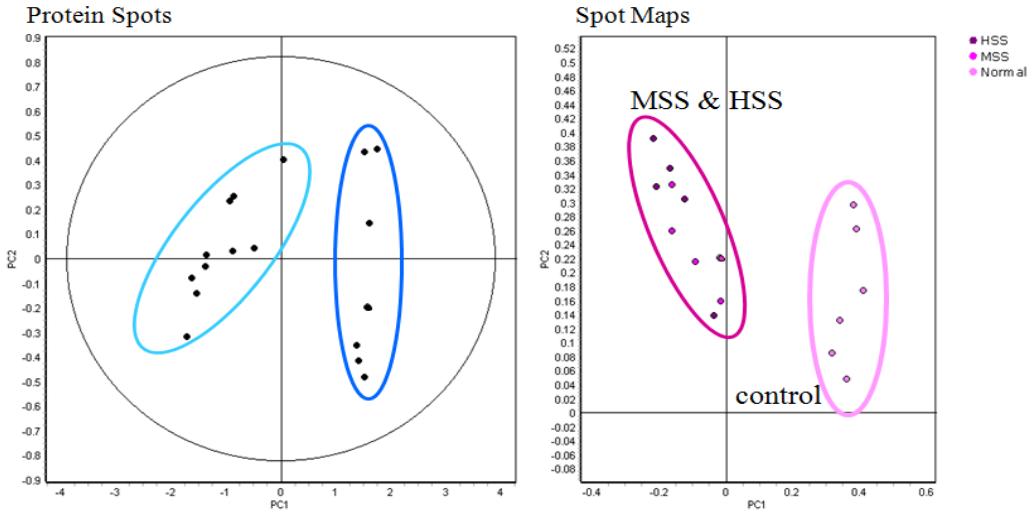

FIGURE 3.16 Principle component analysis scatter plot for protein spots in the pI range 6-11 with 2-fold change and 1-ANOVA ≤ 0.01, FDR. Protein spots within the ellipse

show highly abundant (light blue circle, infected mice compared to control mice) and lowly abundant (dark blue circle, infected mice compared to control mice) protein spots. Spot maps (2D-DIGE images) show the best separation of the moderate and severe disease from the control (uninfected) CBA/J mice.

The HCA is an unsupervised multivariate analysis depicted by a dendrogram and heat map, this analysis gave an overview of the different proteins and study groups with similar expression profiles grouped together (Figure 3.17 and Figure 3.18). As seen on the left hand side of the heat map, the proteins with similar functional groups are clustered together while the 2D-DIGE spot maps with similar protein expression are segregated into experimental groups as stated in this study. The HCA for the pI range 4-7 and 6-11 showed well defined separation of the control, MSS and HSS mice, supporting the %SBW difference between the three groups. The heat map best describes the distinct pattern of proteins during schistosomiasis disease.

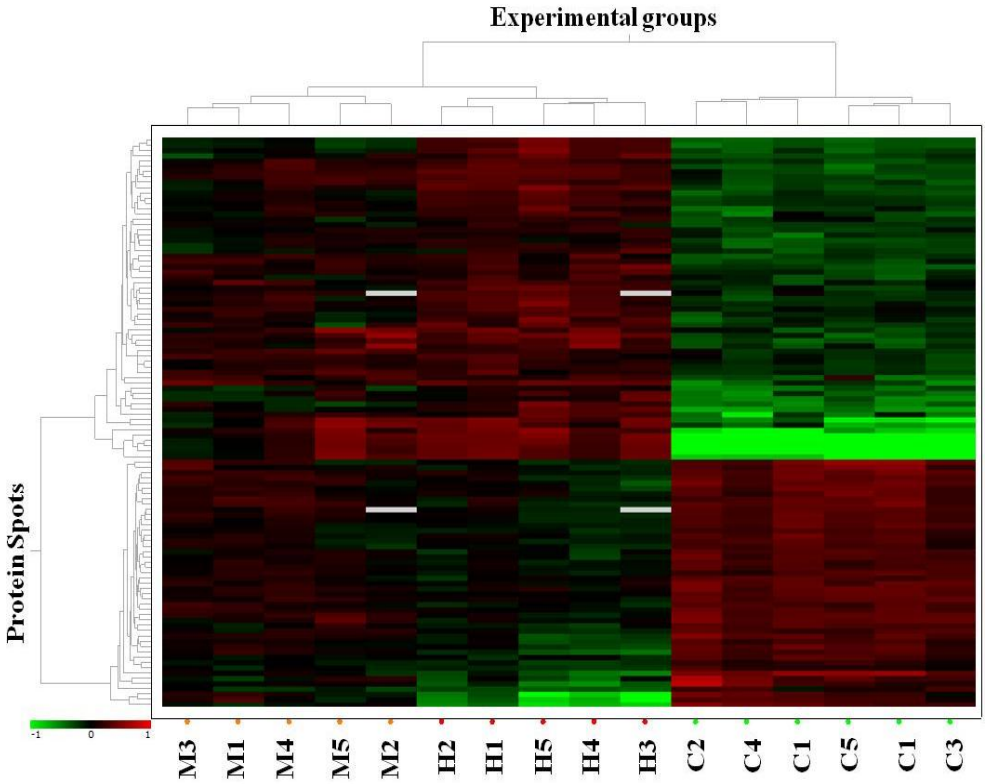

FIGURE 3.17 Hierarchical cluster analysis dendrogram and heat map for 108 protein spots in the pI (4-7) range (C, control; M, MSS; H, HSS mice). The dendrogram and heat map illustrates the distinct protein pattern between the three study groups: control, MSS and HSS mice with clustering of proteins with similar physiology. The colour scale goes from green (more abundant protein spots) to black (no change in protein abundance) to red (less abundant protein spots) with a heat map interval of 1 representing 10-fold increased abundance and -1 representing 10-fold decreased abundance.

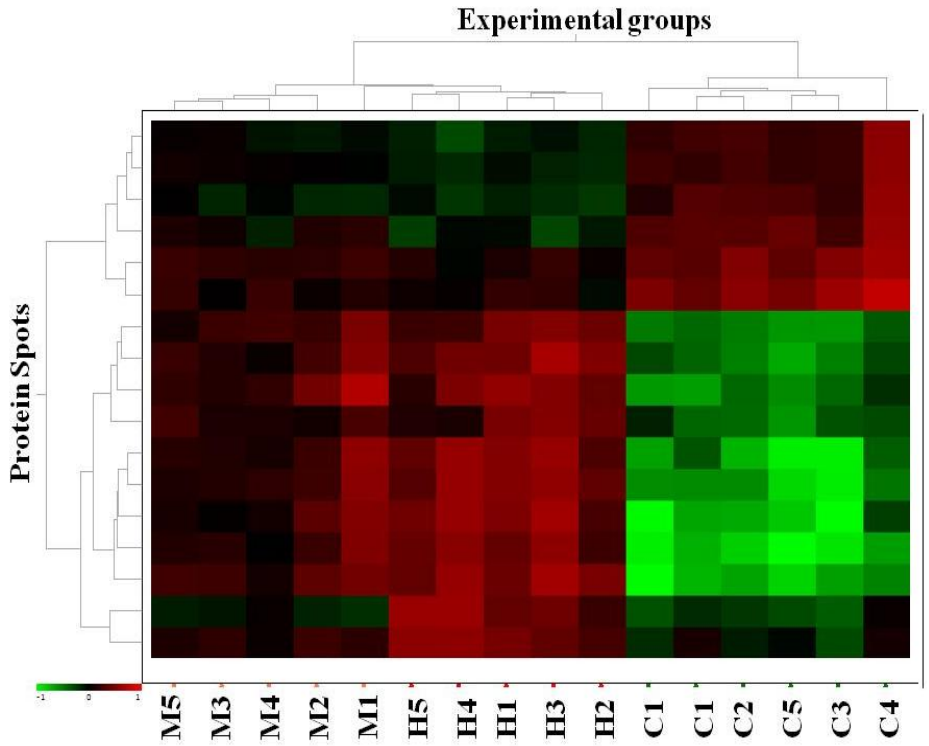

FIGURE 3.18 Hierarchical cluster analysis dendrogram and heat map for 17 protein spots within the pI (6-11) range (C, control; M, MSS; H, HSS mice). The dendrogram and heat map illustrates the distinct protein pattern between the three study groups: control, MSS and HSS mice with clustering of proteins with similar physiology. The colour scale goes from green (more abundant protein spots) to black (no change in protein abundance) to red (less abundant protein spots) with a heat map interval of 1 representing 10-fold increased abundance and -1 representing 10-fold decreased abundance.

3.2.11 Protein verification by western blot analysis

To verify the changes in the abundance of *S. mansoni*-phosphoenolpyruvate carboxykinase (*Sm*-PEPCK), mouse major urinary protein (MUP) and mouse liver transferring, western blot analysis was performed for liver lysates from control, MSS, and HSS mice (Figure 3.19a). Liver lysates from 3 mice per group were analysed and probed for the expression of MUP, PEPCK, transferrin or actin as a loading control. The antibody

used to detect PEPCK was known to recognise mouse PEPCK but its reactivity to *Sm*-PEPCK was unknown, and thus soluble schistosome egg antigen (SEA) was included to test its specificity. Although there was no reaction with the schistosome protein, there was increased abundance of mouse PEPCK in MSS and HSS (Figure 3.19b). The 2D-DIGE analysis failed to identify the mouse PEPCK either because the protein spot was not resolved satisfactorily on the gel or the spot volume for mouse PEPCK was just below the 2-fold, 1-ANOVA ≤ 0.01, FDR criteria set for the analysis in our study.

The MUP band intensity was decreased for MSS and HSS mice compared to control mice. In addition, 21 kDa and 17 kDa MUP bands (Figure 3.19a and Table 3.1) further add support to the 2D-DIGE results that showed variation among MUP spots 43-47 (Figure 3.2). The transferrin protein bands intensity for HSS mice was significantly higher ($p \leq 0.05$) compared to MSS and control mice (Figure 3.19b) and supported the 2D-DIGE results for transferrin spots 62-65 (Figure 3.2 and Figure 3.16). The band volume data for mouse PEPCK, MUP and mouse transferrin is suggestive of a distinct protein pattern associated with the HSS mice compared to MSS and control mice.

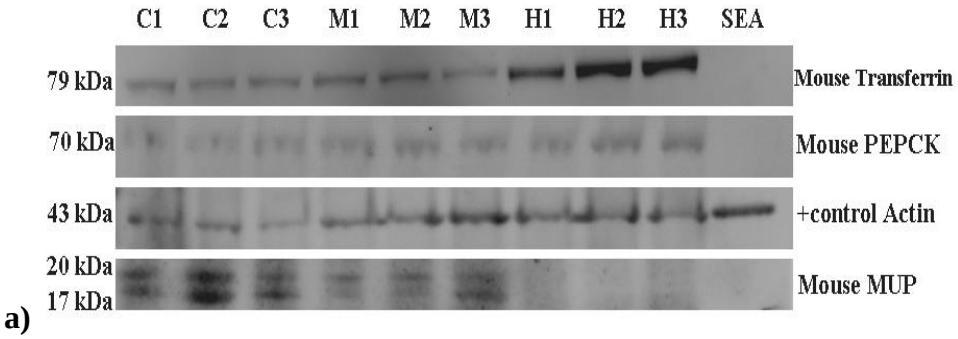

a)

b)

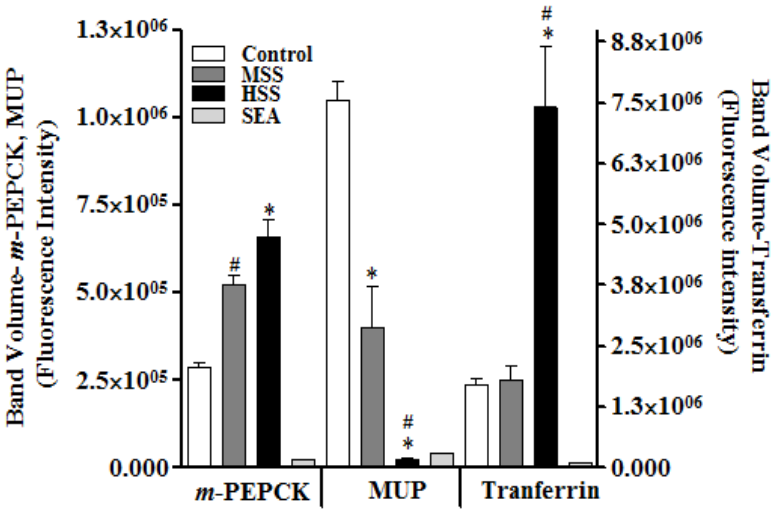

FIGURE 3.19 Liver lysate western blot analysis of MUP, PEPCK and transferrin. a) Lysates (20 μg/well) form control (C; n=3), MSS (M; n=3), and HSS (H; n=3), liver samples and soluble egg antigen (SEA; 20 μg/well) were separated on SDS-PAGE gel, transferred to PVDF membrane and probed with rabbit anti-murine PEPCK polyclonal antibody, goat anti - MUP, goat anti-transferrin polyclonal antibody , or mouse anti-actin monoclonal antibody followed by Cy5-labelled anti-goat, anti-rabbit IgG and Cy3-labelled anti-mouse IgG respectively. b) Protein band fluorescence intensity of HSS mice liver lysate compared with control and MSS mice liver lysate. Shown are the means ±SEM, *p ≤ 0.05 compared to control, #p ≤ 0.05 compared to MSS by Newman-Keuls Multiple Comparison Test. Western blot images included in Appendix G.

3.3 Discussion

The aim of this work was to identify changes in chronically infected mice that were unique to the severe disease form. Using 2D-DIGE we identified 80 significant changes and found that MSS, HSS and control mice had distinct proteomic signatures. The average percent spleen to body weight ratio for the control, MSS and HSS mice was similar to

previous findings (Henderson *et al.*, 1993) and supported the 2D-DIGE data. A previous has used the 2DE approach to understand the impact of infection on 8-week *S. mansoni*-infected C57BL/6 mice and reported impairment of multiple functional pathways in the liver during schistosomiasis (Harvie *et al.*, 2007). These findings were consistent with the results in our study and therefore the functional pathways were assessed similar to the study of Harvie *et al*. (Figure 3.3 and Table 3.1). In particular, structural proteins, immune response proteins and acute phase proteins showed increased abundance while the proteins related to energy metabolism; choline metabolism and xenobiotic metabolism were decreased in abundance. Similar to our findings, a murine *Schistosomiasis mansoni* study demonstrated reduced levels of the tricarboxylic acid cycle intermediates (energy metabolism) and disturbance in amino acid metabolism (Wang *et al.*, 2004) indicating that there are changes in biological processes during parasitic infections. In the following sections, specific proteins of interest related significantly to the pathophysiology of the disease will be discussed.

3.3.1 Acute phase proteins

Acute phase proteins are a group of proteins that increase or decrease during inflammation in response to infection and cell injury. In this study we compared the average volume ratios for transferrin, albumin, group specific component and retinol binding protein 1 between control, MSS and HSS mice. **Transferrin** is a negative acute phase protein and decreased serum levels have been reported in patients with liver diseases (Otegbayo *et al.*, 2005) while high levels are linked to alcoholic fatty liver disease (Potter *et al.*, 1985). In patients with hepatosplenic (Saif *et al.*, 1977) and urinary schistosomiasis (Arinola, 2004, Salawu and Arinola, 2004) both increased (Salawu and Arinola, 2004) and decreased

(Arinola, 2004, Saif *et al.*, 1977) serum levels have been reported. Previous work in C57BL/6 mice has shown increased liver transferrin at 8-week *S. mansoni* infection (Harvie *et al.*, 2007), and similarly, our study showed a significant 2.5 to 4.6-fold increase in 4 transferrin spots in CBA/J mice with HSS but not MSS mice (Figure 3.2-spots 62-65; Figure 3.4; Figure 3.19 and Table 3.1). The increased abundance of transferrin may be attributed to the growth of schistosome worms since a previous study found that schistosomes require iron and bind host transferrin for development (Clemens and Basch, 1989). The increased abundance of transferrin isoforms was confirmed by western blot analysis. The band volume fluorescence intensity for transferrin in HSS mice was significantly higher when compared to control and MSS mice (Figure 3.19). The increased transferrin in HSS mice is a feature of that disease form and thus has potential as a biomarker for HS.

Albumin is a major transport protein that increased with infection specifically for hepatosplenic disease and is a novel finding in our study (Figure 3.2, Table 3.1, Figure 3.5). This findings is in contrast to previous studies which indicate a decrease in albumin due to hepatocellular diseases in murine schistosomiasis (Saber *et al.*, 1983) One reason for increased abundance of albumin may be that albumin is required in the circulation to maintain oncotic pressure, for transport of toxins and other metabolites generated during infection. Another reason for the increase of albumin is the increased consumption by schistosome larvae during their development in the host (Arinola, 2004).

Another acute phase reactant, the **group specific component** (also called α-2-globulin Gc-globulin or vitamin D-binding protein) is a multifunctional protein from the albumin

family and its main physiological role is to scavenge actin. It has also been described as an acute phase reactant (Dahl *et al.*, 2001). GSC is synthesised in the liver and decreased serum levels have been documented in hepatotoxicity and acute liver failure due to hepatic insufficiency (Meier *et al.*, 2006, Schiødt, 2008). In comparison, our study showed high GSC levels in HSS mice and this may be due to scavenging activity towards high intracellular actin levels reported in this study.

Retinol binding protein 1 regulates uptake, intracellular trans-intracellular transport and esterification of retinol. It is also a negative acute phase protein extensively studied in liver fibrosis due to hepatoxicity and metabolic syndromes. In 2002, Uchio and co-workers, working with male murine models of liver fibrosis showed that RBP1 expression increased in response to hepatic fibrogenesis and plays a major role in hepatic tissue repair (Uchio *et al.*, 2002). Thus, schistosomiasis induced fibrosis could account for the increased RBP1 levels in HSS (Figure 3.7). Together the acute phase proteins identified in our study were negative phase reactants, yet conversely showed increased abundance a unique feature of our study.

3.3.2 Structural proteins

Hepatosplenic schistosomiasis is marked by periportal fibrosis and is the major cause of pathology of this disease. Increases in deposition of collagen including collagen 6a and XIV is suggestive of fibrosis and has been documented previously in murine schistosomiasis (Saber *et al.*, 1983), human alcoholic cirrhosis (Stickel *et al.*, 2001), and human hepatosplenic schistosomiasis (Camacho-Lobato and Borges, 1998, Shahin *et al.*, 1992). In our study similar results were obtained, with 11 collagen spots that increased in

volume from 2-fold to 55-fold (Figure 3.2, Table 3.1). The PCA analysis confirmed the differential expression of five collagen spots during disease (protein spots outside the ellipse in the light blue circle, Figure 3.15). Extensive fibrosis is triggered by molecules like TGF-β induce CTGF expression and increased collagen synthesis. CTGF is a profibrogenic molecule that is overexpressed in many fibrotic lesions and promotes hepatic stellate cell adhesion, proliferation, locomotion, and collagen production in hepatic fibrosis similar to processes seen in hepatosplenic schistosomiasis. CTGF is strongly expressed during liver fibrogenesis. Hepatic stellate cells are the major cellular sources of CTGF in the liver (Paradis *et al.*, 1999). Given the known connection between CTGF and fibrosis, it can be a new therapeutic target for this disease (Rachfal and Brigstock, 2003). Importantly it can be detected in serum and may predict the development of schistosomiasis fibrosis (Kovalenko *et al.*, 2009). Moreover, the amino acid hydroxyproline is found in collagen and is synthesised by hydroxylation of proline in pre-formed collagen. Detection of hydroxyproline followed by acid hydrolysis of liver can be used as a measure of hepatic collagen (Cetre-Sossahc. C. B. , 2007). During hepatic fibrosis there is increased abundance of hydroxyproline which may be due to its requirement in collagen synthesis (Dunn *et al.*, 1977) or impaired collagen degradation (Takahashi *et al.*, 1980). The increased collagen isoforms (Figure 3.6) in our study therefore would be expected to correlate to increased hydroxyproline levels.

We found a 2-fold increase in **actin** levels in schistosome infection suggestive of changes in the hepatocellular composition during schistosomiasis. Harvie *et al.*, have shown similar findings in the C57BL/6 mice with increase of up to 20-fold at 8-weeks of infection (2007). **Vimentin** is an intermediate cytoskeletal filament that increased in both

MSS and HSS above 2.5-fold. This increase is similar to previous studies (Boehme *et al.*, 1989, Harvie *et al.*, 2007) (Figure 3.7). **Tropomyosin** is one of the actin-associated proteins that modulate the interaction between actin and myosin to stabilise the actin filament structure. The 2-fold increase of tropomyosin 3 in our study is similar to the findings in ketotic livers (Xu and Wang, 2008). Another study in progressive liver fibrosis is suggestive of tropomyosin as a new marker of activated stellate cells and a useful diagnostic marker for liver fibrosis (Otogawa *et al.*, 2009).

The intermediate filament cytoskeletal protein, **keratin D** (type-I) in mouse liver corresponds to keratin 18 (type I, acidic pI) in human liver and is associated with liver diseases (Strnad *et al.*, 2008). In toxicity, induced liver damage a study demonstrated post-translational modifications that were associated with phosphorylation and proteolytic degradation of keratin filaments (Salmhofer *et al.*, 1994). These authors investigated the structural disturbances caused by modification of keratin in alcoholic hepatitis. Our study showed that similar protein change develops in severe schistosome-mediated liver disease. Indeed, increased levels of keratin D were associated with HSS but not MSS, which is a finding unique to our study (Figure 3.2, Figure 3.8). Furthermore, research in patients with schistosomiasis infection showed autoantibodies to keratin (Boehme *et al.*, 1989) which together with the findings in this study may indicate that the development of a response to modified cytoskeletal proteins such as keratin is a feature of the disease pathology.

Overall, we found different isoforms of collagen, actin and vimentin increased from 2 to 50-fold as well as one keratin D spot due to schistosome infection, suggesting induction of different mechanisms during schistosome infection that contribute to the deposition of

these extracellular components and intermediate filament proteins. If investigated further, the specific isoforms can be used as unique markers for schistosomiasis.

3.3.3 Energy metabolism proteins

We found decreased abundance of three proteins and increased abundance of one protein related to energy metabolism. A study showed decreased enzymatic activity of **ATPase beta** in hepatocellular carcinomas (Capuano *et al.*, 1997). In our study we have a similar finding with the levels of ATPase beta decreased by 2-fold, indicative of hepatic response similar to carcinogenesis occurring in schistosome infection during the development of the severe disease. Different isoforms of **carbamoyl phosphate synthase 1**, a urea cycle enzyme, are dysregulated in liver pathobiology, carcinogenesis and hepatotoxicity (Thome-Kromer *et al.*, 2003), similarly we found one spot with decreased carbamoyl phosphate synthase 1 activity. This decrease in carbamoyl phosphate synthase 1 was also a particularly marked finding in Harvie *et al*.

Glutamate dehydrogenase (GLDH) is widely used to assess liver dysfunction along with other liver function tests. GLDH is down-regulated by 6-fold in fructose-fed insulin resistant hamster liver, a form of liver injury (Morand *et al.*, 2005) but circulating levels increase in liver necrosis (Van Waes and Lieber, 1977). We found 2-fold GLDH decrease in schistosomiasis liver tissue; this may be due to its infiltration into the circulating system as previously reported (Camacho-Lobato and Borges, 1998). **Valosin-containing protein (VCP)** also called AAA-ATPase p97 is involved in export of proteins through the endoplasmic reticulum into the cytosol and inhibits apoptosis. Its expression increases in various carcinomas (Yamamoto *et al.*, 2003). Similarly, we found 3 to 5- fold increases in

VCP activity in MSS and HSS mice indicating that apoptosis could be a mechanism involved in schistosomiasis pathology. Taken together the results for proteins related to energy metabolism are suggestive of disturbance in this biological process during schistosomiasis.

3.3.4 Choline metabolism

The mitochondrial dehydrogenases, dimethylglycine dehydrogenase (DMDH) and sarcosine dehydrogenase (SARDH) catalyse the final steps of choline metabolism converting dimethylglycine to sarcosine, and then sarcosine to glycine. The predicted native masses of the proteins are 97.3 and 101.7 kDa respectively for DMDH and SARDH corresponding to their positions on the gels. Both proteins have predicted post-translational modifications including phosphorylation that would potentially give rise to isoforms that differ in isoelectric point. In HSS livers, three DMDH spots (spots 26-28, Figure 3.2, Figure 3.9) showed greater than 2-fold loss with a smaller non-significant decrease in MSS compared to controls (Table 3.1). Three SARDH isoforms (Figure 3.2, Table 3.1 spots 56-58) also decreased more than 2-fold in HSS with smaller decreases in MSS. The greatest loss of more than 6-fold in HSS mice, was for the most basic (spot 58) of the three SARDH isoforms (Figure 3.9). The loss of DMDH has been reported previously in 8-week *S. mansoni* infection (Harvie *et al*., 2007) and the loss of SARDH in hepatocellular carcinoma (Lim *et al.*, 2002). Our research found 2 to 6.4- fold decreases in the SARDH spots, suggesting similar hepatic responses in schistosomiasis and hepatocarcinogenesis. Furthermore, SARDH may be useful to differentiate between HSS and MSS since the average volume ratio decrease for three SARDH spots in HSS is large as opposed to MSS suggestive of an isoform pattern specific for severe disease.

Additionally, schistosomes use host lipids for survival as they do not make sterols or fatty acids *de novo*. Choline is crucial for phosphatidylcholine biosynthesis in schistosome development, especially females (Ancelin *et al.*, 1987). The decreased SARDH and DMDH reported in our study could mean increased choline diversion towards phosphatidylcholine biosynthesis.

3.3.5 Xenobiotic metabolism proteins

Schistosome worms and eggs in the host liver microvasculature induce alterations in the redox balance and invites oxidative stress from immune-generated radicals (La Flamme *et al.*, 2001). Moreover, the release of toxic heme and ferrous ions generated due to consumption of haemoglobin by schistosome larvae (Brindley *et al.*, 1997) contributes to the increase in xenobiotic molecules. Our study showed decreased abundance of xenobiotic metabolising proteins (Figure 3.3) similar to the study by Harvie *et al.,* 2007. Xenobiotic metabolising proteins provide protection form oxidant stress and a decrease of the proteins during disease state indicates increased abundance of toxic molecules in the host which can be fatal. We found decreased activity of catalase, protein disulphide-isomerase A3, selenium binding protein 2, glutathione S-transferase Pi, epoxide hydrolase and aldehyde dehydrogenase.

Catalase is one such protein that protects the cell from the toxic effects of hydrogen peroxide by breaking it down to molecular oxygen and water with no generation of free radicals. Previous studies have demonstrated decreased activity of this enzyme in schistosome infected liver during 6-week infection (La Flamme *et al.*, 2001) and 8-week infection (Gharib *et al.*, 1999), this correlates with the findings in our study where the

decrease is above 3-fold. Another protein that regulates the redox status of MHC class 1 during antigen presentation is **protein disulphide-isomerase A3** (Santos *et al.*, 2007) and increased activity has been recorded previously in 8-week CBL57/6 *S. mansoni* infection (Harvie *et al.*, 2007) consistent to the finding in our study. We report a single PDIA3 spot with increased abundance in HSS mice concomitant with high levels of MHC class 1 protein.

Selenium binding protein 2 (SBP2) is down-regulated in liver fibrosis possibly due to portal hypertension (Henkel *et al.,* 2006) which leads to increased cell proliferation (Giometti *et al.*, 2000), similar to the finding in our study. We found one SBP2 spot decreased by above 3-fold with pI 5.8, Mw 53.16. The reason for the upregulation of spot pI 6.0, Mw 52.90 needs to be evaluated, but is similar to the previous findings in liver of *HFE*-deficient mice (human haemochromatosis protein gene-deficient mice) with downregulated SBP2 (Petrak *et al.*, 2007).

The **glutathione S-transferase** (GST) enzyme family is associated with the detoxification of endogenous and exogenous toxins. In our study, we found among the proteins of interest (2-fold change, 1-ANOVA $p \leq 0.01$, before FDR was applied) there were GST enzymes that were significantly associated with schistosomiasis pathology. These include GST class mu1 (GSTmu1), GST class mu3 (GSTmu3) and GST class Pi (GSTPi) protein spots. However, with the FDR criteria for the DIGE analysis, only GSTPi showed significant change. The GSTPi spot (spot 73, Figure 3.2, Table 3.1) decreased in MSS and HSS mice and this decrease may represent variation in protein abundance during the chronic stage. In contrast, increased levels of GSTPi have been reported in tumor tissues

(Hayes *et al.*, 1991) and acute schistosomiasis (Harvie *et al.*, 2007). We found GSTmu1 protein spot decreased by 2-fold in both MSS and HSS mice compared to control mice. A GSTmu3 protein spot showed increased abundance in HSS mice alone (the average volume ratio for HSS/control=+3.45, HSS/MSS=+3.33 and MSS/control=+1.04). Among the GST family, the class mu enzymes are the most efficient in detoxifying mutagenic epoxides and studies have shown increased abundance of these enzymes in human hepatocellular carcinoma (Murray *et al.*, 1993) and rat hepatocellular carcinoma (Qi *et al.*, 2008). Other studies have also demonstrated increased abundance of GST mu1 and mu3 in hepatotoxicity (Ward *et al.*, 2006) and GST mu1 in acute schistosomiasis (Harvie *et al.*, 2007). The results for GST mu3 in our study are similar to previous studies and were more specific for HSS mice while the results for GST mu1 are in contrast to previous findings. Our study revealed some interesting and important patterns for the GST enzymes during schistosomiasis but require further investigation.

Aldehyde dehydrogenases (ALDH) are a family of enzymes that protect the body from aldehydes. (Dragani *et al.*, 1996) described the down regulation of ALDH in murine lung tumours which is supported by the study from Sun *et al*. that showed a 2.5-fold decrease in ALDH in human hepatocellular carcinoma (Sun *et al.*, 2007). Earlier studies have documented the decrease in expression of ALDH but our study indicates a spot with increase ALDH abundance in hepatosplenic disease. If studied further it can possibly explain the exact mechanism involved in the pathogenesis of severe disease. Altogether, the decreased abundance of xenobiotic metabolising proteins in our study suggests that schistosome infection induces certain biological responses that decrease the synthesis of these proteins during disease and leave the liver vulnerable to chronic oxidative damage.

3.3.6 DNA methylation-related proteins

The results in our study showed that schistosome infection affects the abundance of DNA methylation-related proteins including betaine homocysteine methyltransferase (BHMT), S-adenosylhomocysteine hydrolase (SAH) and formyltetrahydrofolate dehydrogenase (10-FTHDH) and this may cause imbalance in DNA methylation. **BHMT** is an enzyme involved in the methylation cycle in the liver, one spot with BHMT activity was upregulated and is in contrast to earlier work which demonstrated that BHMT is down-regulated in hepatocellular carcinoma (Sun *et al.*, 2007) (Figure 3.2, Table 3.1, spot 11). **SAH** has been described as a potential molecular target for anti-parasitic drugs due to its role in methylation reactions (Grillo and Colombatto, 2008). We found one downregulated SAH spot during schistosomiasis similar to a previous study that demonstrated decreased activity of the SAH in tumour tissues (Leal *et al.*, 2008). **10-FTHDH** enzyme is involved in detoxification, one-carbon metabolism and DNA methylation (Vasiliou *et al.*, 2000). The decreased activity of the enzyme in five protein spots may relate to decreased detoxification in the schistosomiasis disease as well as downregulation of DNA methylation. Previous work by Krupenko and co-workers stated that 10-formyl tetrahydrofolate dehydrogenase is involved in several cellular processes and is down-regulated in tumour tissues (Krupenko and Oleinik, 2002). All of the above results may suggest pro-cancerous activities that are specifically induced during severe schistosomiasis and may promote cancer development.

3.3.7 Immune response proteins

Schistosome eggs are well characterised inducers of immune responses (Henderson *et al.*, 1993) and therefore liver-derived immune related proteins were evaluated. Our study

identified several immune related proteins that were significantly altered during chronic infection. These proteins include MHC class I histocompatibility antigen H-2 Q4 alpha chain precursor like protein, plastin 2 and prohibitin 2. The increased abundance of **MHC class I histocompatibility antigen H-2 Q4 alpha chain precursor like protein** (MHC Class 1 H2Q4 like protein), a non-classical MHC class Ib-like molecule may reflect increased or altered immune recognition to parasite-derived products (Figure 3.2, Table 3.1 spots 74-78, Figure 3.10). While Hernandez *et al.* showed that classical MHC Class II but not MHC class I molecules are involved in granuloma formation in early stage disease (Hernandez *et al.*, 1997), our data suggests a possible role for the non-classical MHC class 1 H2 Q4 like protein in the development of schistosome-induced immune responses.

Plastin-2 is an actin-binding protein expressed in monocytes, B lymphocytes and myeloid cells. A recent study showed increase abundance of lymphocyte cytosolic protein 1 in chemically induced mouse liver tumours (Strathmann *et al.*, 2007), and another study reports 3-fold increase of lymphocyte cytosolic protein 1 transcripts using affymetrix microarray profiling in C57BL/6J mice with traumatic brain injury (Israelsson *et al.*, 2008). Albeit the technique, mouse model and tissue studied differ, we have similar findings with two lymphocyte cytosolic protein 1 spots (Figure 3.2, spot 41, 42, Figure 3.11) showing increased protein abundance (3 to 4-fold). Taken together, the increased levels of this protein are associated with tissue injury and stress conditions, and suggest effects on stress metabolism in moderate and severe schistosomiasis.

Prohibitin-2 (B-cell receptor-associated protein 37) is closely related and complexed with prohibitin 1 (p32). It plays a role in tumour suppression and cell cycle regulation as well

as inducing apoptosis (Guo *et al.*, 2007). Prohibitin gene expression increases in rat bladder carcinomas and prohibitin interacts with tumor-suppressor-gene proteins (Asamoto and Cohen, 1994), it has been highlighted as a possible therapeutic target (Mishra *et al.*, 2005). Our study showed 3.25-fold increase in HSS (spot 80-Figure 3.2, Table 3.1, Figure 3.11) but not MSS mice and may indicate its involvement in cell proliferation and/or apoptosis during severe disease. Finally, the increased abundance of immune response proteins provides support to the idea that similar pathological mechanisms may be occurring during schistosome-mediated liver disease, stress induced tissue injury and carcinogenesis.

3.3.8 Other liver proteins

In this study we identified hepatic proteins that were differentially expressed during schistosome infection and a subset of these may have been altered due to simultaneous hepatocarcinogenesis or other liver complications or due to hepatotoxicity. The annexins are a family of such proteins described in cancerous cells and tissues and **annexin 5** in particular increases during carcinogenesis. The 5-fold increase in annexin 5 (Figure 3.7) may possibly mean that liver injury in schistosome infection follows the same course as development of hepatocellular carcinoma. A recent study suggests annexin 5 as a tumourogenic protein (Mulla *et al.*, 2004) which can be a possibility with the findings in our study in mice with *S. mansoni* infection.

Brain and reproductive organ-expressed protein (BRE) inhibits the mitochondrial apoptotic pathway and is a stress modulating protein. These activities could be the reason for its increase in schistosomiasis as they may enhance cellular survival during disease

state (Li *et al.*, 2004). Additionally, a class of proteins called molecular chaperones are present in various compartments of the cell assisting in the proper folding of various proteins in health and disease. Chaperonin containing TCP-1 theta subunit **(Chaperone CCT8)** functions during actin and tubulin folding. An increase in chaperone CCT8 in tumour cells has been recorded by (Agaton *et al.*, 2003) using affinity proteomics. Our results associate decreased levels of the protein with HSS mice similar to the findings of 8-week infected mice (Harvie *et al.*, 2007) and in contrast to the results in tumour cells that showed strong expression of chaperone CCT8 (Agaton *et al*., 2003). Moreover, studies have demonstrated increased abundance of glycosylation during immunologic responses to infections and allergy (Altmann, 2007, Rudd *et al.*, 2001). In particular, **glucosidase II beta subunit** an enzyme involved in the glycosylation, allows folding and incorporation of glucosides in many secreted and membrane-bound proteins. Our study showed 2.5 to 3.5-fold increases in two glucosidase II beta subunit spots, certainly a distinctive feature of this study. Together, the 2D-DIGE data for annexin 5, chaperone CCT8 and glucosidase II beta subunit protein spots demonstrated that hepatic responses to schistosome infection and the importance of the follow-up of these proteins in human schistosomiasis may possibly be useful for diagnosis.

Major urinary protein (MUP) is from the lipocalin family and functions as a pheromone transporter in mouse urine. MUP has similarity to human epididymal-specific lipocalin-9 but more elaborate studies are needed to understand the relationship between this protein in mice and humans (Virtanen and Kinnunen, 2008). Previous research has demonstrated decreased abundance of MUP as an early event in the development of mouse liver tumours and hence may be used as a tumour marker in mouse hepatocarcinogenesis

(Dragani *et al.*, 1989). We found five MUP spots (Figure 3.2, spots 43-47) decreased 2 to 10-fold specifically in HSS livers while these same spots in MSS livers show only a moderate decrease in expression comparatively and these differences were verified by western blot. The PCA analysis confirmed the differential expression of three MUP spots during disease (protein spots outside the ellipse in the dark blue circle, Figure 3.15).The band volumes for HSS mice MUP bands were significantly high when compared to control and MSS mice (Figure 3.19). This is the first report of a specific alteration in this protein during schistosomiasis (Figure 3.2, Figure 3.11, Figure 3.12 and Table 3.1). The large decrease of MUP in HSS livers lends further support to the possibility of early stage responses to pro-cancerous activities in hepatosplenic schistosomiasis. Since MUP is significantly decreased in HSS mice and has similarity to human lipocalin 9 it would be worth investigating in mouse and human sera.

3.3.9 Parasite proteins

The only parasite protein identified in our study was *Sm*-PEPCK. This enzyme is responsible for the glucose metabolism in schistosomes. PEPCK carboxylates phosphoenolpyruvate to oxaloacetate that is then converted to malate for the parasites' energy needs (Mehlhorn, 2009). Given that miracidia contain *Sm*-PEPCK mRNA 60 times the adult level and sporocysts contain 10 times the adult level, it has been suggested that immature and mature schistosomes can synthesise glucose via gluconeogenesis or glycerol via glyceroneogenesis, using glutamine as a precursor (Yang *et al.*, 2009). Additionally, many parasitic proteins are glycosylated or phosphorylated and these modifications play an important part in the host immune responses (Cummings and Nyame, 1996) or during schistosome development and growth (Tarrab-Hazdai *et al.*,

2005). Thus, the pattern for the spots described from the SEA proteomics signatures (Figure 3.14, spots 32, 33, 36) suggests that the protein may be post-translationally modified as indicated by changes in the molecular weight and pI of the protein spots.

A study by Asahi *et al.* proposes that *Schistosoma mansoni* phosphoenolpyruvate carboxykinase (*Sm*-PEPCK) is a novel antigen for schistosome infection and suggests its potential as a disease specific protein marker (Asahi *et al.*, 2000). While mice do express a murine PEPCK, the results from the proteomic analyses have matched the protein spot to the parasite and not the mouse PEPCK. Thus due to the large increase of 8-fold to 13-fold in *Sm*-PEPCK (Figure 3.2, Table 3.1, Figure 3.10), we agree with the conclusions of Asahi *et al*. that this protein is a good candidate for development as a biomarker for schistosome infection. Furthermore, the western blot PEPCK results propose that in addition to the increase in *Sm*-PEPCK detected by DIGE, the liver enzyme also increased in abundance (Figure 3.19), thereby a potential for enhanced gluconeogenesis in infected liver through increased activity of the hepatic enzyme. These results suggest that PEPCK of mouse origin as well as *Sm*-PEPCK incresed in MSS and HSS mice, and that further studies will need to be designed to target *Sm*-PEPCK specifically.

3.3.10 Multivariate analysis

The results of the supervised (PCA) and unsupervised (HCA) multivariate analysis (Figure 3.15, 3.16, 3.17 and 3.18) indicate that MSS and HSS mice have distinct proteomic signatures that reflect the pathology in schistosomiasis. The close clustering of the control mice separated from the MSS mice clustering together and HSS mice grouped together in PCA and HCA indicate the strong differential protein abundance between the three study

groups which supports previous work (Freeman Jr *et al.*, 1996, Henderson *et al.*, 1993). Further analysis of the unique protein changes may provide insight into the molecular changes that drive the two chronic disease forms. Although previous schistosomiasis studies have analysed gene expression and metabolic profiles, none of the studies have studied protein spot abundance profiles using multivariate analysis like PCA and HCA.

3.4 Conclusion

The use of the CBA/J mouse model allowed us to explore the changes in various protein isoforms and variants associated with MSS and HSS disease forms. The liver 2D-DIGE profiles depicted a distinct picture of protein patterns expressed between MSS and HSS and revealed an increased abundance of proteins associated with the energy metabolism, choline metabolism and xenobiotic metabolism. The uniqueness of this study lies in the fact that lymphocyte cytosolic proteins 1 isoforms, sarcosine dehydrogenase isoforms, prohibitin 2, transferrin isoforms, and MUP have not previously been associated with hepatosplenic schistosomiasis. Additionally, *Sm*-PEPCK proves to be a promising candidate for detection of schistosome infection. It is anticipated that these proteins may be valuable as potential diagnostic biomarkers that may assist in early detection and treatment of schistosomiasis patients in the future.

CHAPTER 4: LIVER PROTEIN ABUNDANCE AT VARIOUS TIMES POST-INFECTION IN MURINE SCHISTOSOMIASIS

4.1 Introduction

Although MSS and HSS are identified pathologically at 20-weeks post infection, these forms can be distinguished immunologically as early as 6 weeks after infection due to the development of cross-reactive idiotypes (CRIs) in MSS mice (Montesano *et al.*, 2002). Unfortunately, the CRIs reagent is not appropriate for commercial development. However, because these forms show distinct immunological differences very early after egg laying begins, it is likely that other distinctive changes may be identified that can differentiate MSS from HSS earlier than 20 weeks. To identify differential protein abundance patterns driving the segregation of the two chronic pathologic forms, liver proteomic signatures from CBA/J mice infected for 6, 8, 12 weeks were compared with the abundance of proteins from 20-week infected mice and control CBA/J mice. This proteomic approach helped identify proteins expressed differentially and consistently at early stages of the disease as well as those expressed only at the late stage of the disease. The 20-week infected samples were classified as MSS (n=5) and HSS (n=5) according to liver pathology as described in Chapter 3 and the six groups (control, 6-week, 8-week, 12-week, MSS, HSS) were studied for protein pattern changes. At 20-week post-infection, 20% CBA/J mice present with HSS and 80% with MSS disease. In the present experiment we used 10 mice/group for the 6, 8 and 12 week time point infections, so that it can be

expected that approximately 2 mice/group will develop HSS. Experimental design 2 for DIGE experiments is listed in Appendix A.

4.2 Results

4.2.1 Comparison between %SBW for experimental design 2 and 1

Experimental design 2 was used to perform this 5 time point experiment. A comparison of the percent spleen to body weight ratio (%SBW) of control and 20-week infected mice from experimental design 2 with experimental design 1 was done to assess similarity of samples. The two experiments showed similar results for the three groups despite being from independent experiments suggesting that this mouse model is highly reproducible (Figure 4.1). The differential patterns of protein abundance from control/uninfected (n=5), 6-week (n=10), 8-week (n=10), 12-week (n=10), MSS (n=5) and HSS (n=5) (or 20-week infected mice, n=10) mice infected with *S. mansoni* was assessed using 2D-DIGE. The differentially expressed protein spot volumes detected for the control, MSS and HSS mice were similar to the protein spots in experimental design 1, supporting the robustness of our experimental system and previous results (Chapter 3). (The spot volume haemoglobin results from experimental design 2 and 1 were similar, results discussed in Appendix E.)

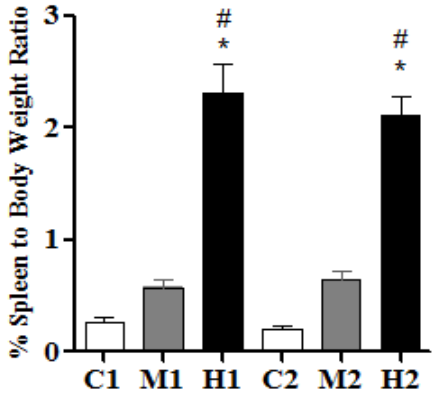

FIGURE 4.1 Percent spleen to body weight ratio comparisons for animals in experimental design 2 and experimental design 1. C_1, M_1, H_1=control, MSS, HSS respectively from experimental design 1 and C_2, M_2, H_2=control, MSS, HSS respectively from experimental design 2, 1-ANOVA $p \leq 0.01$. *$p \leq 0.001$ compared to control, #$p \leq 0.001$ compared to MSS by Newman-Keuls Multiple Comparison Test. Pairing of the animals between the two sets for control, MSS, HSS mice was statistically significant with $p \leq 0.0001$.

4.2.2 Correlations between splenomegaly and hepatomegaly

Comparison of the %SBW between the six study groups showed HSS mice were statistically different ($p \leq 0.0001$) from the other five groups (Figure 4.2). Percent liver to body weight ratio, a measure of hepatomegaly, was elevated in the five groups when compared to control mice (Figure 4.3). %SBW was log transformed to normalise the data. Linear regression analyses demonstrated significant correlations between percent liver to body weight ratio levels and %SBW at 6, 8, 12 and 20 week of infection (Figure 4.4) with r square value showing a strong effect of the liver on the spleen during the pathogenesis in hepatosplenic schistosomiasis. At 8-week, 12-week and 20-week infection the liver showed almost 90%, 94% and 53% respectively correlations with splenomegaly indicating a major role of the liver in schistosomiasis.

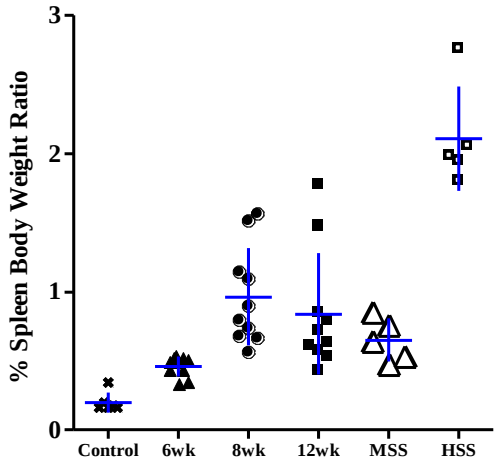

FIGURE 4.2 Percent spleen to body weight ratio comparisons between seven study groups from experimental design 2, $p \leq 0.001$ when HSS mice compared to control, 6-week, 8-week, 12-week infected mice and MSS mice, $p \leq 0.01$ when 12-week, 8-week infected mice compared to control, 6-week mice. Blue lines represent the mean ± SEM.

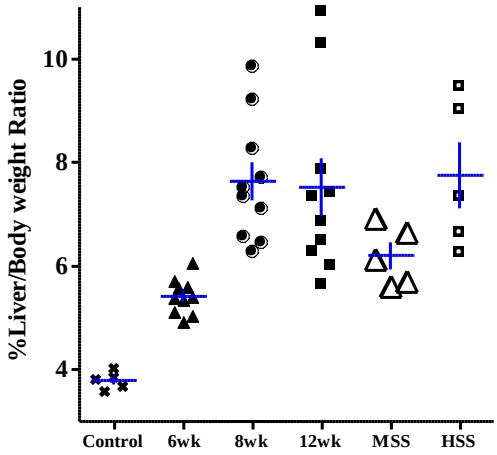

FIGURE 4.3 Percent liver to body weight ratio comparisons between six study groups from experimental design 2, $p \leq 0.001$ when 8-week, 12-week, HSS mice compared to control mice and 6-week infected mice, $p \leq 0.01$ when MSS compared to HSS and

control mice, $p \leq 0.05$ when 6-week infected mice compared to control mice. Blue lines represent the mean ± SEM.

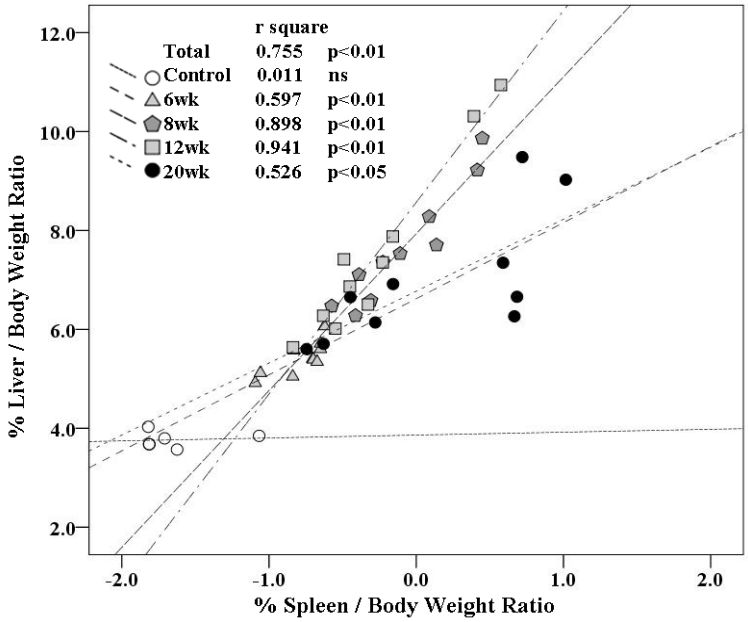

FIGURE 4.4 Scatter plot and linear regression analysis for percent liver to body weight ratio and %SBW between 6-week, 8-week, 12-week and 20-week infected mice (MSS and HSS). The linear regression r square shows the contribution of the liver and spleen with respect to the progress of the schistosomiasis disease.

4.2.3 Liver protein abundance at time post- infection

Liver lysate was used to determine the total protein, which gives a measure of the soluble protein fraction, but not necessarily the membrane bound proteins in the liver. It is also a gross measure to estimate protein synthesis in the liver. In order to assess if schistosomal infection induces impairment of protein synthesis, we measured the total protein in the liver of control, 6-week, 8-week, 12-week, MSS and HSS infected mice. We found that MSS and HSS mice had significantly lower levels ($p \leq 0.001$) when compared to the

control mice, 6-week, 8-week, 12-week infected mice (Figure 4.5). Decreased total protein abundance may be due to decreased ability of the wounded liver to synthesise proteins during schistosome infection.

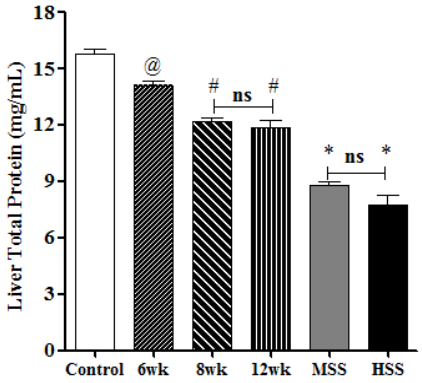

FIGURE 4.5 Mouse liver total protein levels (mg protein per mL of liver lysate) in liver lysate for control, 6-week, 8-week, 12-week, MSS and HSS mice. Shown are mean ± SEM, 1-ANOVA $p \leq 0.01$. *$p \leq 0.001$ HSS and MSS compared to control, 6-week, 8-week, 12-week infected mice; #$p \leq 0.001$ 12-week and 8-week infected mice compared to 6-week infected mice and control; $^{@}p \leq 0.05$ 6-week infected mice compared to control mice; comparison between 8-week and 12-week infected mice, HSS and MSS was statistically not significant (ns) as indicated, comparison tests by Newman-Keuls Multiple Comparison Test.

A total of 2523 and 2422 protein spots were detected in the pI ranges 4-7 and 6-11 respectively. The resolved protein spots were 299 and 136 for the two pI ranges respectively. The abundance of 63 and 13 protein spots between the six study groups changed significantly with 1- ANOVA ≤ 0.01, 2-fold change in average volume ratio and application of FDR using the DeCyder software. MALDI-TOF mass finger printing was

used to identify 44 protein spots which are listed in Table 4.1. An overview of the identified protein spots for experimental design 2 is illustrated in Figure 4.6. The protein spots that changed significantly post infection among the five study groups when compared to control mice are summarised in Table 4.2. Additional information on the identified protein spots is listed in Appendix C.

At 12-week infection, 59 spots in pI 4-7 range and 69 spots in pI 6-11 range had greater than 2-fold change with ANOVA ≤ 0.01 and FDR. A total of 94 spots together, for pI range 4-7 and 6-11 decreased in abundance (almost 73 %), while 34 protein spots increased in abundance (Table 4.2). The maximum number of protein spots that changed compared to control was for 12-week infected mice and a total of 58 protein spots were identified using MALDI-TOF. Table 4.3 lists 23 identified protein spots decreased in abundance, exceptionally and distinctly during 12-week infection. The identified protein spots that changed for 12-week infection were assessed according to Gene Ontology function categories which showed increased protein abundance for immune response proteins and structural proteins and decreased abundance for proteins related to amino acid metabolism, one carbon metabolism, redox reaction proteins and xenobiotic metabolism proteins (Figure 4.7). These results suggest that this time point may be important in the down-regulation of the egg-induced pathology.

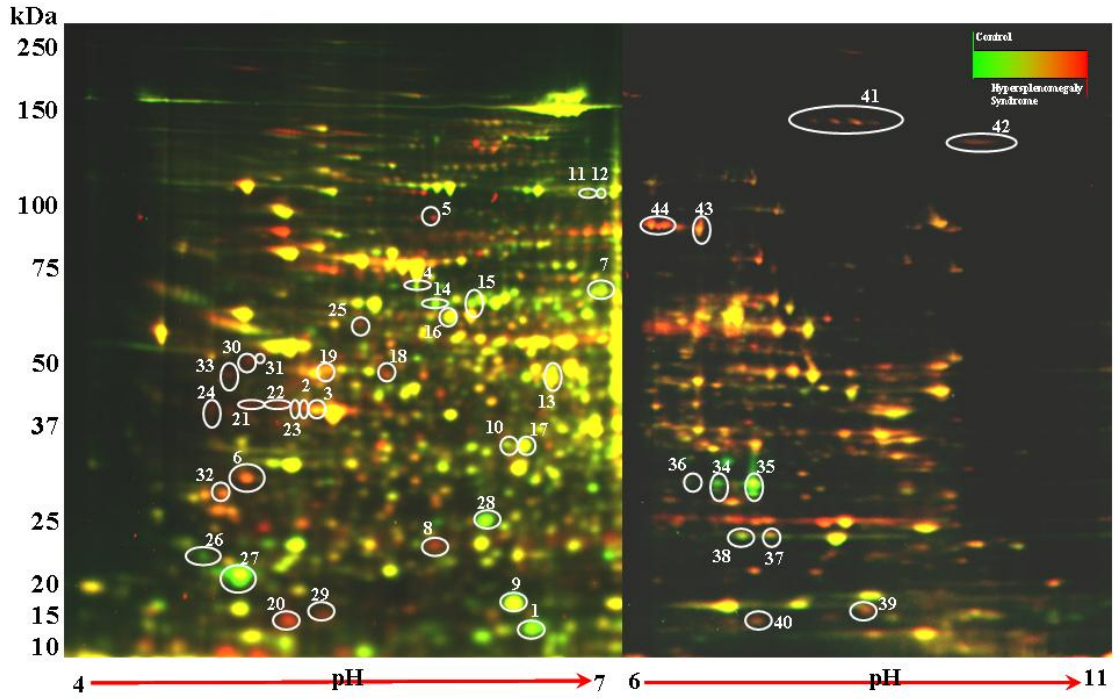

FIGURE 4.6 A pseudocolour map of 44 liver proteins from uninfected and HSS mice separated by 2D-DIGE for the experimental design 2. Liver lysate from control/uninfected liver was labelled with Cy5 (green), lysates from 20-week infected HSS liver was labelled with Cy3 (red) and a pooled internal standard of liver lysates from control, MSS and HSS mice in the study (n=15) was labelled with Cy2 (blue; not shown). Isoelectric focusing was performed on 7 cm IPG strips, pI 4-7 and pI 6-11, and proteins were then separated using SDS-PAGE. The image overlays of Cy5- and Cy3-labeled proteins appear yellow. The numbers correspond to the numbers (No.) of protein spots in Table 4.2. Note that the MUP (protein spots 26, 27) are green showing high abundance in control mice and transferrins (protein spots 43, 44) are red showing high abundance in HSS mice. (NOTE: Transferrin has pI 7.0 and therefore it can be visualised in both pI ranges 4-7 and 6-11 as seen in Chapter 3.)

TABLE 4.1 Experiment design 2: Identified protein spot comparisons between control mice, 6-week, 8-week, 12-week and 20-week (MSS and HSS) infected mice for the pI ranges 4-7 and 6-11 with 2-fold change, 1-ANOVA ≤ 0.01 and FDR.

Spot No.	***Protein Name (pI 4-7)***	***gi Number***	***AVR H/C[1]***	***AVR H/M[1]***	***AVR H/8[1]***	***AVR H/12[1]***	***AVR M/C[1]***	***AVR 12/C[1]***	***AVR 8/C[1]***	***AVR 6/C[1]***
1	60S ribosomal protein	12846804	-2.12	+1.07	+1.57	-1.38	-2.27	-1.54	-3.34	-2.17
2	Actin	49868	+3.80	+1.92	+2.16	+2.26	+1.98	+1.68	+1.75	+1.63
3	Actin	809561	+2.54	+2.95	+2.80	+1.60	-1.16	+1.58	-1.10	-1.81
4	Albumin	26341396	-2.69	-2.38	-1.42	+1.06	-1.13	-2.85	-1.90	-1.21
5	Albumin1	26341396	+3.32	+1.26	-1.02	+1.56	+2.64	+2.12	+3.40	+1.21
6	Annexin5	6753060	+3.07	+2.01	+1.77	+1.46	+1.53	+2.10	+1.73	-1.34
7	BA-DHAK[1]	81879195	-2.52	-2.01	-1.62	+1.03	-1.25	-2.61	-1.56	-1.05
8	BRE[1]	38173925	+2.74	+1.21	+1.38	+1.37	+2.26	+2.01	+1.98	+1.05
9	Cu/Zn superoxide dismutase	226471	-2.15	-1.62	-1.25	-1.47	-1.33	-1.46	-1.72	+1.48
10	Dihydrodiol dehydrogenase	21618806	-2.05	-1.70	-1.27	+1.18	-1.20	-2.41	-1.61	-1.21
11	Dimethylglycine dehydrogenase (DMDH)	59808083	-2.37	-1.54	-1.18	+1.41	-1.54	-3.34	-2.00	-1.49
12	DMDH	59808083	-2.30	-1.52	-1.13	+1.60	-1.51	-3.68	-2.03	-1.64
13	Eno1 protein	54114937	-2.07	-1.96	-1.46	+1.17	-1.05	-2.43	-1.41	+1.10
14	Epoxide hydrolase	15929294	-2.35	-1.72	-1.31	+1.13	-1.36	-2.66	-1.80	-1.03
15	Epoxide hydrolase	15929294	-2.57	-1.75	-1.42	+1.23	-1.46	-3.14	-1.80	-1.01
16	FTCD[1]	18252784	-2.22	-1.74	-1.09	+1.38	-1.28	-3.08	-2.03	-1.05
17	FBPase[1]	14547989	-2.10	-1.95	-1.56	-1.03	-1.08	-2.04	-1.35	-1.02
18	Glutathione synthetase	6680117	+3.53	+1.76	1.12	-1.17	+2.00	+4.14	+3.15	+2.22
19	Heat shock 70kD	31981722	+3.29	+1.08	-1.18	+1.30	+3.05	+2.53	+3.89	+1.69

	protein									
20	Interleukin-2	1504135	+2.86	+1.17	-1.20	-1.14	+2.44	+3.25	+3.42	+1.24
21	Keratin D	293682	+4.99	+3.53	+4.55	+1.90	+1.41	+2.63	+1.09	-1.18
22	Keratin D	293682	+4.93	+3.23	+3.00	+1.43	+1.52	+3.46	+1.64	+1.08
23	Keratin D	293682	+2.75	+2.22	+2.16	+1.66	+1.24	+1.66	+1.27	+1.04
24	Laminin receptor1 (40S ribosomal protein SA)	62024907	+2.87	+1.40	+1.04	-1.04	+2.05	+3.00	+2.75	+1.21
25	Lymphocyte cytosolic protein 1	26326929	+2.48	+1.67	+1.26	-1.11	+1.48	+2.75	+1.97	-1.14
26	MUP[1]	12851568	-8.14	-4.11	-2.85	-4.62	-1.98	-1.76	-2.86	-1.83
27	MUP 3[1]	494384	-2.98	-2.18	-1.42	-1.99	-1.37	-1.49	-2.10	-1.21
28	Peroxiredoxin6	6671549	-3.72	-2.32	-1.15	+1.24	-1.60	-4.62	-3.23	+1.09
29	Retinol Binding Protein1	21730472	+3.32	+1.47	+1.22	-1.02	+2.26	+3.38	+2.71	+1.07
30	RAI1[1]	31981748	+5.22	+3.00	+2.54	+1.65	+1.74	+3.16	+2.06	+1.08
31	RAI1[1]	14577933	+4.27	+3.04	+2.49	+1.27	+1.40	+3.36	+1.72	-1.23
32	Tropomyosin	26341416	+2.30	+1.51	+1.43	+1.15	+1.53	+2.00	+1.61	+1.16
33	Vimentin	31982755	+2.03	+1.66	+1.35	-1.34	+1.22	+2.72	+1.51	-1.14
No.	***Protein Name (pI 6-11)***	***gi Number***	***AVR H/C[1]***	***AVR H/M[1]***	***AVR H/8[1]***	***AVR H/12[1]***	***AVR M/C[1]***	***AVR 12/C[1]***	***AVR 8/C[1]***	***AVR 6/C[1]***
34	Carbonic Anhydrase III	226778	-3.98	-2.17	-1.48	-1.30	-1.84	-3.06	-2.69	-1.14
35	Carbonic Anhydrase III	226778	-3.62	-1.88	-1.49	-1.11	-1.92	-3.26	-2.44	-1.16
36	Carbonic Anhydrase III	226778	-3.86	-1.96	-1.43	-1.33	-1.97	-2.90	-2.69	-1.26
37	GST Pi	2624496	-2.25	-1.49	-1.09	-1.25	-1.51	-1.80	-2.06	-1.56
38	GST Pi	2624496	-2.53	-1.35	+1.05	-1.31	-1.88	-1.93	-2.67	-1.15
39	Hemoglobin	12846939	-2.62	-2.00	-2.33	-1.88	-1.31	-1.40	-1.13	-1.20
40	Hemoglobin	12846939	-2.26	-2.21	-2.49	-1.94	-1.02	-1.17	+1.10	+1.11
41	MHC Class1 HLA	51770518	+5.42	+1.73	+1.03	-1.59	+3.14	+8.63	+5.25	-1.86

42	*Sm*-PEPCK	56753812	+5.11	+1.79	+1.78	+1.04	+2.85	+4.89	+2.88	-2.17
43	Transferrin	62027488	+2.74	+1.94	+1.73	+4.92	+1.41	-1.80	+1.58	+1.53
44	Transferrin	62027488	+4.42	+3.04	+3.43	+9.52	+1.45	-2.15	+1.29	+2.20

[1]**AVR**: average volume ratio between study groups (C, control; 6, 6-week infected; 8, 8-week infected; 12, 12-week infected; M, MSS; and H, HSS);

BA-DHAK**=** Bifunctional ATP-dependent dihydroxyacetone kinase, BRE = Brain and reproductive organ-expressed protein, FBPase = Fructose-1,6-bisphosphatase 1, FTCD = Formimino transferase cyclodeaminase, MUP = Major urinary protein, RAI1= Ribonuclease/angiogenin inhibitor 1. (NOTE: Transferrin has pI 7.0 and therefore the DeCyder data generated in both pI ranges 4-7 and 6-11 as seen in Chapter 3).

TABLE 4.2 Summary of number of protein spots for the five study groups compared to the control mice for the pI ranges 4-7 and 6-11 with 2-fold change, 1-ANOVA ≤ 0.01 and FDR. ↓ represents decreased abundance and ↑ represents increased abundance.

pI range	**4-7**	**6-11**
Study groups	**Protein spots with 1-ANOVA ≤ 0.01, 2-fold change, FDR**	
6-week infection	4 ↓, 2 ↑	1 ↓,1 ↑
8-week infection	16 ↓,19 ↑	7 ↓,2 ↑
12-week infection	27 ↓, 32 ↑	67 ↓, 2 ↑
MSS	3 ↓, 12 ↑	2 ↑
HSS	32 ↓, 31 ↑	8 ↓, 5 ↑

TABLE 4.3 Experiment design 2: Listed below are 58 protein spots specifically for 12-week infected mice with 2-fold change, 1-ANOVA ≤ 0.01, FDR for pI range 4-7 and 6-11 when compared to control mice, 6-week, 8-week and 20-week infected mice (MSS and HSS).

Sr. No.	*Protein Name pI 4-7*	*gi Number*	*AVR H/C[1]*	*AVR M/C[1]*	*AVR 6/C[1]*	*AVR 8/C[1]*	*AVR 12/C[1]*
1	Albumin	26341396	-2.69	-1.13	-1.21	-1.9	**-2.85**
2	Albumin 1	26341396	+3.32	+2.64	+1.21	+3.4	**+2.12**
3	Annexin 5	6753060	+3.07	+1.53	-1.34	+1.73	**+2.10**
4	Bifunctional ATP-dependent dihydroxyacetone kinase/FAD-AMP lyase	81879195	-2.52	-1.25	-1.05	-1.56	**-2.61**
5	Brain and reproductive organ-expressed protein	38173925	+2.74	+2.26	+1.05	+1.98	**+2.01**
6	Carbamoyl Phosphate Synthetase	73918911	-1.63	-1.04	+1.17	-1.73	**-3.33**
7	Dihydrodiol dehydrogenase	21618806	-2.05	-1.20	-1.21	-1.61	**-2.41**
8	Dimethylglycine dehydrogenase	59808083	-2.37	-1.54	-1.49	-2.00	**-3.34**
9	Dimethylglycine dehydrogenase	59808083	-2.3	-1.51	-1.64	-2.03	**-3.68**
10	Eno1 protein	54114937	-2.07	-1.05	+1.1	-1.41	**-2.43**
11	Epoxide Hydrolase	15929294	-2.35	-1.36	-1.03	-1.80	**-2.66**
12	Epoxide Hydrolase	15929294	-2.57	-1.46	-1.01	-1.80	**-3.14**
13	Formiminotransferase cyclodeaminase	18252784	-2.22	-1.28	-1.05	-2.03	**-3.08**
14	Fructose-1; 6-bisphosphatase 1	14547989	-2.1	-1.08	-1.02	-1.35	**-2.04**
15	Glutathione synthetase	6680117	+3.53	+2.00	+2.22	+3.15	**+4.14**

16	Heat shock 70kD protein 5	31981722	+3.29	+3.05	+1.69	+3.89	**+2.53**
17	Interleukin-2	1504135	+2.86	+2.44	+1.24	+3.42	**+3.25**
18	Keratin D	293682	+4.99	+1.41	-1.18	+1.09	**+2.63**
19	Keratin D	293682	+4.93	+1.52	+1.08	+1.64	**3.46**
20	Laminin receptor 1 (ribosomal protein SA)	62024907	+2.87	+2.05	+1.21	+2.75	**+3.00**
21	Lymphocyte cytosolic protein 1	26326929	+2.48	+1.48	-1.14	+1.97	**+2.75**
22	Peroxiredoxin 6	6671549	-3.72	-1.60	+1.09	-3.23	**-4.62**
23	Protein Disulfide Isomerase	74203945	+1.07	-1.05	-1.10	1.42	**+2.17**
24	Protein Disulfide Isomerase	74203945	+1.37	+1.03	+1.03	+1.72	**+2.81**
25	Retinol Binding Protein	21730472	+3.32	+2.26	+1.07	+2.71	**+3.38**
26	Ribonuclease/angiogenin inhibitor 1	31981748	+5.22	+1.74	+1.08	+2.06	**+3.16**
27	Ribonuclease/angiogenin inhibitor 1	14577933	+4.27	+1.40	-1.23	+1.72	**+3.36**
28	Sarcosine Dehydrogenase	26352359	-2.42	-1.52	-1.05	-1.67	**-2.85**
29	Tropomyosin	26341416	+2.30	+1.53	+1.16	+1.61	**+2.00**
30	Vimentin	31982755	+1.95	+1.59	+1.26	+2.11	**+2.53**
31	Vimentin	31982755	+2.03	+1.22	-1.14	+1.51	**+2.72**
Sr. No.	***Protein Name pI 6-11***	***gi Number***	***AVR H/C[1]***	***AVR M/C[1]***	***AVR 6/C[1]***	***AVR 8/C[1]***	***AVR 12/C[1]***
32	acetyl-Coenzyme A acetyltransferase 2	20810027	+1.13	+1.38	+1.53	+1.12	**-2.24**
33	Aldh1a1 protein	32484332	-1.24	+1.10	+1.24	-1.21	**-2.08**
34	Aldolase 2, B isoform	21707669	+1.61	+1.37	+1.95	+1.30	**-2.36**
35	argininosuccinate synthetase	6996911	-1.15	+1.09	+1.21	-1.10	**-2.81**
36	argininosuccinate synthetase	6996911	-1.02	+1.26	+1.29	-1.39	**-2.57**
37	Betaine-homocysteine	62533211	-1.07	1.15	1.42	-1.21	**-2.62**

	methyltransferase						
38	Carbonic Anhydrase III	226778	-3.62	-1.92	-1.14	-2.44	**-3.26**
39	Carbonic Anhydrase III	226778	-3.98	-1.84	-1.16	-2.69	**-3.06**
40	Carbonic Anhydrase III	226778	-3.86	-1.97	-1.26	-2.69	**-2.9**
41	Catalase	15004258	-1.41	-1.11	1.15	-1.41	**-2.63**
42	catalase	26344712	-1.33	1	1.17	-1.34	**-2.5**
43	Electron transfer flavoprotein beta-subunit	21759114	-1.40	-1.00	-1.04	-1.52	**-2.64**
44	Enoyl Coenzyme A hydratase, short chain, 1, mitochondrial	12805413	-1.09	+1.21	+1.08	-1.28	**-2.92**
45	glutamate dehydrogenase	26354278	+1.08	+1.28	+1.31	-1.03	**-2.02**
46	Glutathione S-Transferase Class Pi	2624496	-1.81	-1.30	+1.06	-1.95	**-2.47**
47	Glutathione S-Transferase Class Pi	2624496	-1.64	-1.27	+1.21	-1.55	**-2.09**
48	homogentisate 1, 2-dioxygenase	7549763	-1.3	-1.07	+1.17	-1.35	**-2.85**
49	homogentisate 1, 2-dioxygenase	7549763	+1.10	-1.01	+1.25	-1.04	**-2.72**
50	homogentisate 1, 2-dioxygenase	7549763	-1.06	-1.01	+1.43	-1.12	**-2.26**
51	hydroxyacid oxidase 1, liver	6754156	-1.40	+1.11	+1.17	-1.27	**-2.58**
52	isocitrate dehydrogenase 2	6647554	-1.11	+1.15	+1.24	-1.17	**-2.77**
53	MHC Class 1 HLA	51770518	+5.42	+3.14	-1.86	+5.25	**+8.63**
54	PEPCK	56753812	+5.11	+2.85	-2.17	+2.88	**+4.89**
55	phosphoglycerate kinase	202423	-1.01	+1.13	+1.44	-1.15	**-2.56**
56	solute carrier family 25	16741519	+1.33	+1.28	+1.52	+1.10	**-2.44**
57	Transferrin	62027488	+4.42	+1.45	+1.61	+1.29	**-2.15**
58	urate oxidase	6678509	+1.14	+1.15	+1.32	-1.10	**-2.00**

[1]**AVR**: average volume ratio between study groups (C, control; 6, 6-week infected; 8, 8-week infected; 12, 12-week infected; M, MSS; H, HSS mice). Sr. No. = serial number

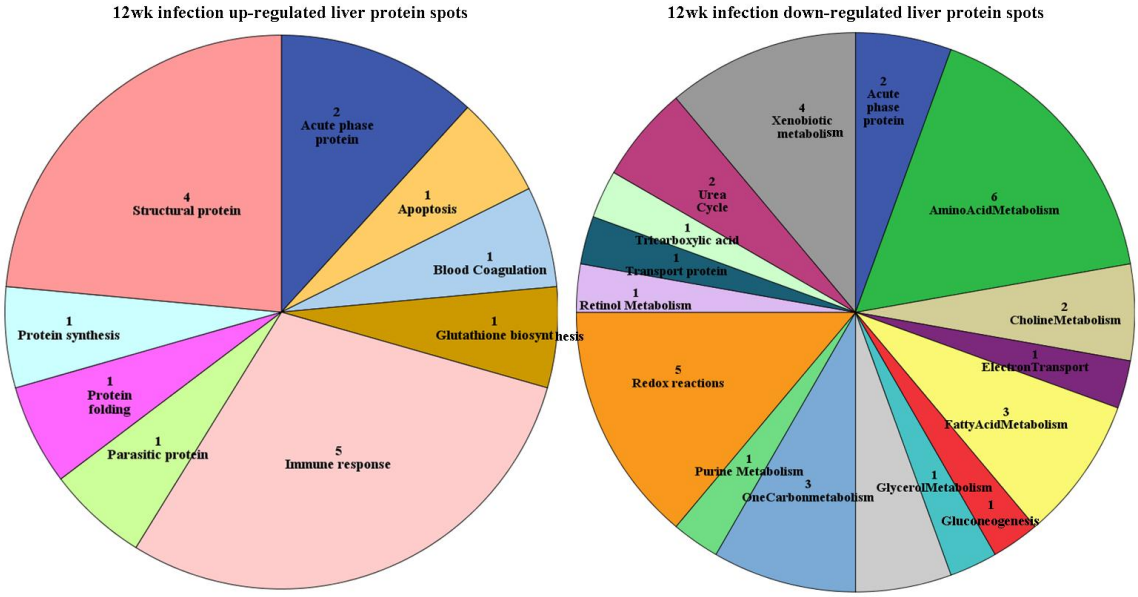

FIGURE 4.7 Liver proteins during 12-week infection: 20 protein spots increased (up-regulated) in abundance and 38 protein spots decreased (down-regulated) in abundance. Numbers represent the number of protein spots in each category. The protein spots were identified using MALDI-TOF mass spectrometry and plotted according to their Gene Ontology function.

4.2.4 Multivariate analysis

The multivariate analysis using the principle component analysis (PCA) showed good separation of the study groups for pI range 4-7 and 6-11 (Figure 4.8 and 4.9) along with the grouping of the 8-week infected and 12-week infected mice with, MSS and/or HSS mice in the 2D-DIGE spot maps. The pI 4-7 PCA plot distinguished the six study groups: 6-week, 8-week, 12-week MSS and HSS mice and control mice. The 6-week infected mice were clustered very close to the control mice. The MSS and HSS mice showed

distinct clustering. In contrast, while most 8-week and 12-week infected mice were clustered into distinct groups, some 8-week and 12-week mice clustered with the 20-week infected mice (Figure 4.8). For the pI 6-11 range PCA plot, control and 6-week infected mice again clustered together whereas the 8-week, 12-week, MSS and HSS mice together formed less distinct clusters. These results may be because the proteins in the pI range 6-11 are difficult to resolve on gels even with the most standardised conditions (Figure 4.9). For both the pI ranges, the protein spots within the ellipse showed 95% significance level. The protein spots within the ellipse in the light blue circle were increased in abundance in disease groups (6-week infected, 8-week infected, 12-week infected, MSS and HSS mice) when compared to control mice. The protein spots within the ellipse in the dark blue circle showed decreased protein spot abundance in disease groups when compared to control mice. The PCA plot for the pI range 4-7 showed one protein outlier (outside the ellipse) in the dark blue circle, which is a MUP isoform very strongly differentially expressed protein during schistosomiasis.

The unsupervised, hierarchical cluster analysis segregated the protein spots and study groups according to the individual disease status in each mouse for pI range 4-7 and 6-11 (Figure 4.10 and 4.11). The heat map showed a distinct protein pattern for MSS and HSS mice for pI 4-7 range (Figure 4.10). The mice numbers wk0805, wk0809, wk1203 and wk1205, had relatively high %SBW ratio when compared within the 8-week and 12-week infected mice groups but had similar %SBW when compared to the %SBW of HSS mice. The %SBW ratios for the above mice numbers were 19.32, 17.65, 27.80 and 23.30 respectively. These mice in the pI 4-7 dendrogram were clustered (flanked) by MSS mice on the left and HSS mice on the right with the heat map colour pattern showing similar

protein patterns between these mice and confirming the fate of these mice leading towards severe disease. Thus, the HCA dendrogram and heat map for pI 4-7 showed clustering of mice from HSS group with mice from other study groups having similar %SBW (wk0805, wk0809, wk1203 and wk1205). However, the dendrogram and heat map for pI range 6-11 showed clustering of wk0809, wk1203 and wk1205 mice together with 12-week infected mice, while one mouse wk0805 clustered with MSS and HSS mice (Figure 4.11). The reason for the inconclusive result for pI 6-11 protein spots may be that the proteins are difficult to resolve, and/or co-migration of different protein spots being another possibility, and therefore the heat map for pI 6-11 is not as consistent as the result for pI 4-7.

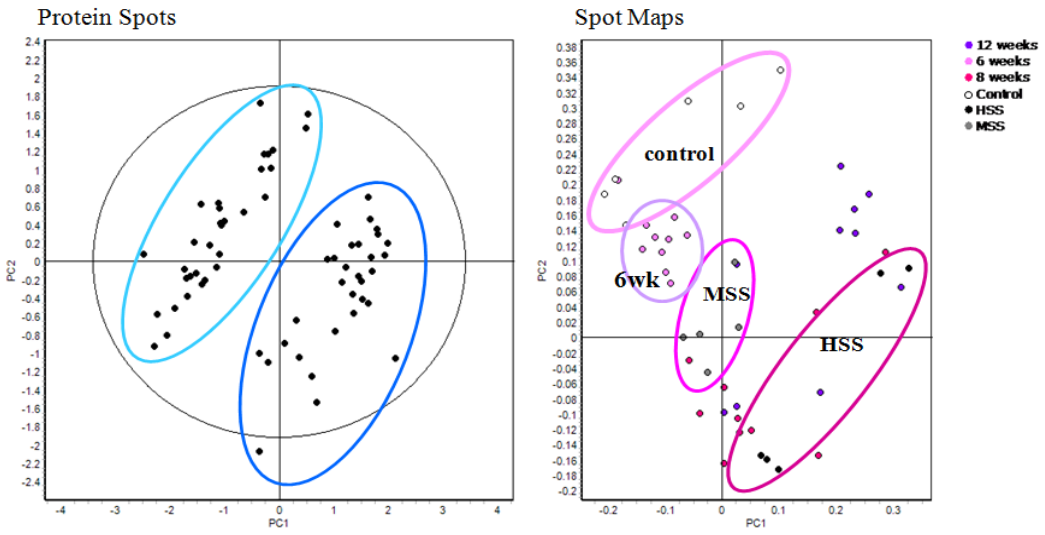

FIGURE 4.8 Principle component analysis plot for the pI range 4-7 protein spots with 2-fold change and 1-ANOVA ≤ 0.01, FDR for the five time point experiment with 63 protein spots. Protein spots within the ellipse show highly abundant (light blue circle, infected mice compared to control mice) and lowly abundant (dark blue circle, infected mice compared to control mice) protein spots. Spot maps (2D-DIGE images) show the best separation of the control and 6-week, MSS and HSS infected mice with 8-week

infected and 12-week infected mice showing grouping with the above 20-week infected mice (MSS and HSS).

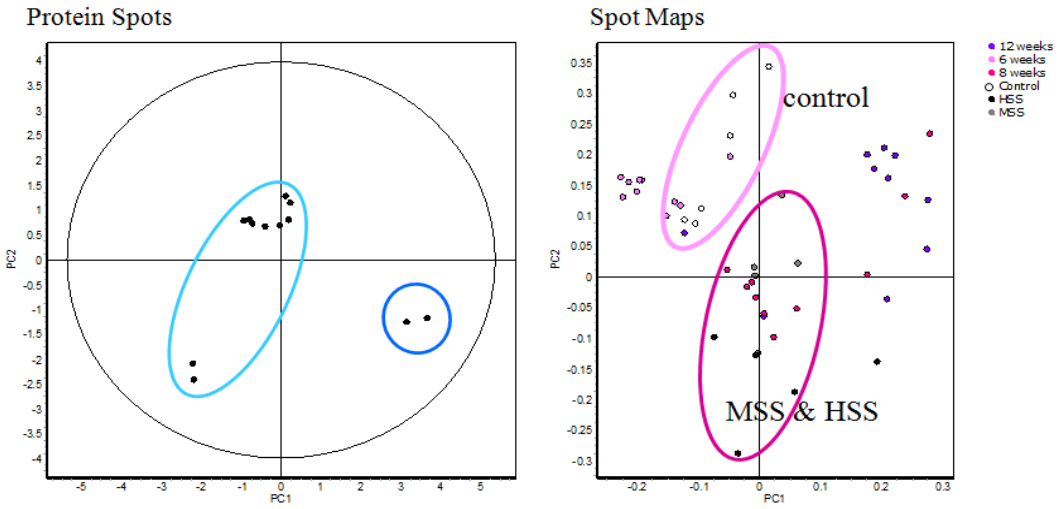

FIGURE 4.9 Principle component analysis plot for the pI range 6-11 protein spots with 2-fold change and 1-ANOVA ≤ 0.01, FDR for the five time point experiment with 13 protein spots. Protein spots within the ellipse show highly abundant (light blue circle, infected mice compared to control mice) and lowly abundant (dark blue circle, infected mice compared to control mice) protein spots. Spot maps (2D-DIGE images) show the best separation of the control and MSS, HSS mice together with 6-week infected, 8-week infected, 12-week infected mice showing grouping with the above three study groups.

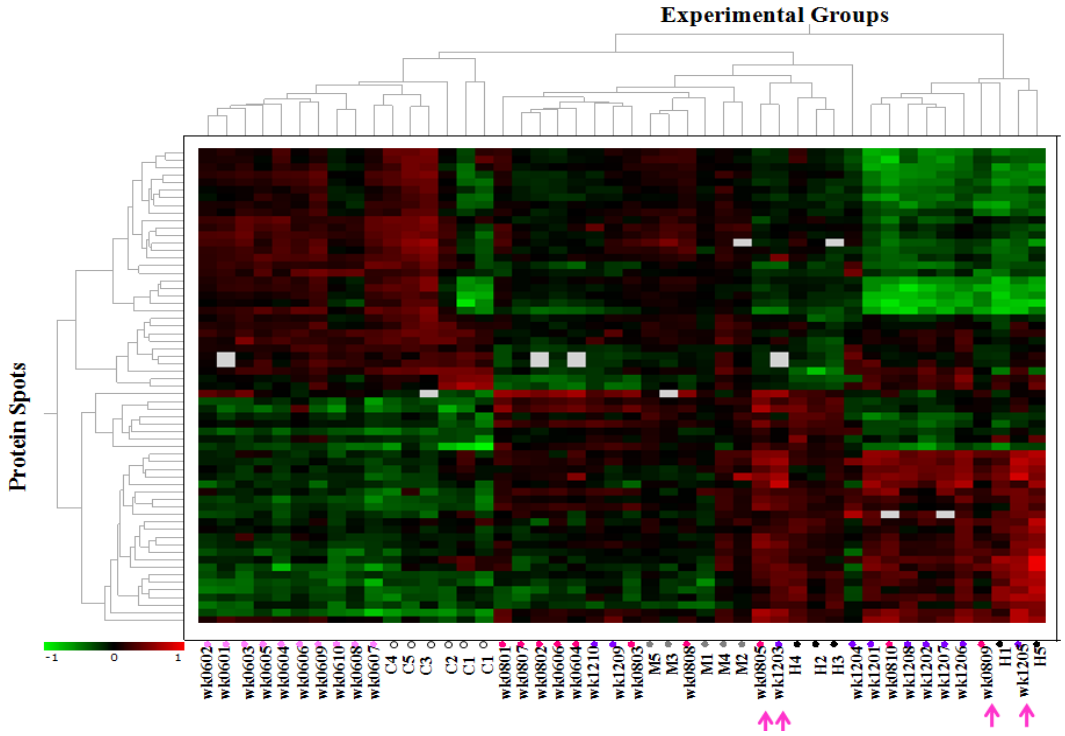

FIGURE 4.10 Hierarchical cluster analysis dendrogram and heat map for five time point experiment for the pI range 4-7 with 63 protein spots in the 2-fold change and 1-ANOVA<0.01, FDR criteria. The dendrogram and heat map illustrates distinct protein pattern between the six study groups with the segregation and alignment of the protein spots with similar functional groups and clustering of experimental groups with similar disease pathology. The colour scale goes from green (more abundant protein spots) to black (no change in protein abundance) to red (less abundant protein spots) with a heat map interval of of 1 representing 10-fold increased abundance and -1 representing 10-fold decreased abundance. (C=control, wk0601-10= 6-week infected, wk0801-10=8-week infected, wk1201-10=12-week infected, M=MSS, H=HSS). Pink arrows indicate mice with high %SBW.

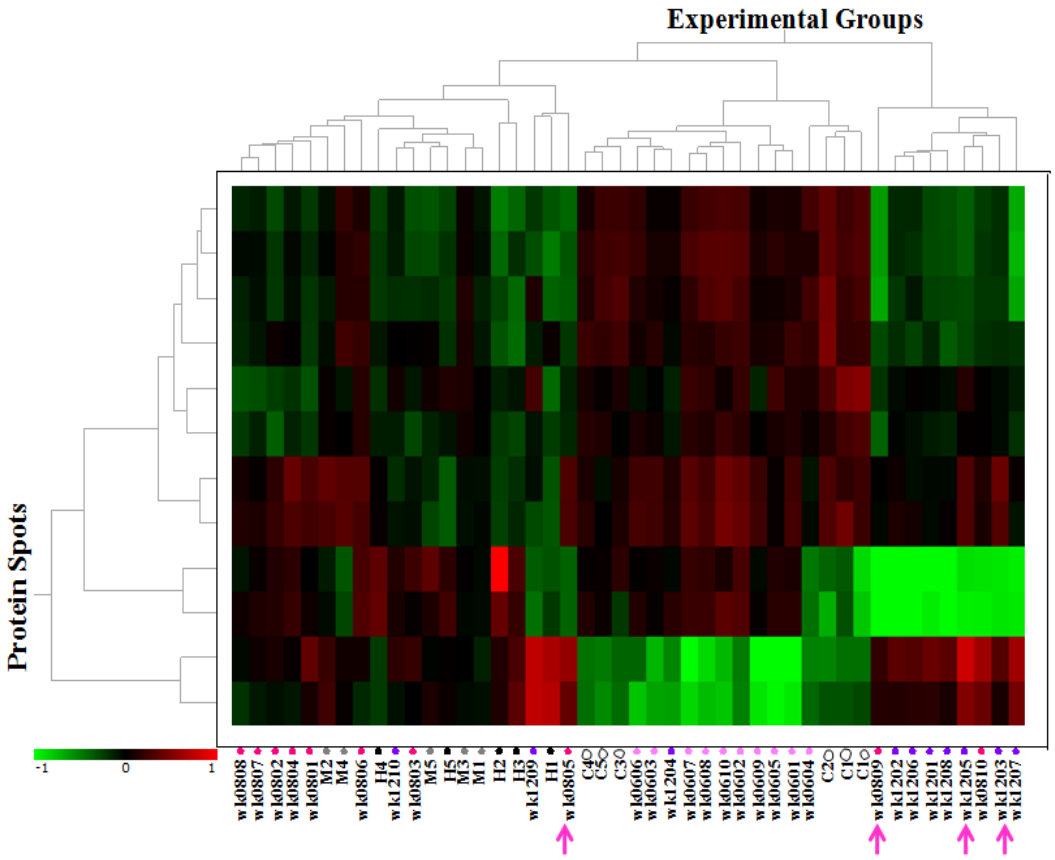

FIGURE 4.11 Hierarchical cluster analysis dendrogram and heat map for five time point experiment for the pI range 6-11 with 13 protein spots in the 2-fold change and 1-ANOVA ≤ 0.01, FDR criteria. The dendrogram and heat map illustrates distinct protein pattern between the six study groups with the segregation and alignment of the protein spots with similar functional groups and clustering of experimental groups with similar disease pathology. The colour scale goes from green (more abundant protein spots) to black (no change in protein abundance) to red (less abundant protein spots) with a heat map interval of 1 representing 10-fold increased abundance and -1 representing 10-fold decreased abundance. (C=control, wk0601-10= 6-week infected, wk0801-10=8-week infected, wk1201-10=12-week infected, M=MSS, H=HSS). Pink arrows indicate mice with high %SBW.

4.2.5 Linear regression correlations

To understand if changes in protein abundance correlated to the severity of pathology, protein spot volumes from each mouse were plotted against %SBW and simple linear regression correlations were performed. This approach helped analyse the effect of each protein on development of splenomegaly. Since 20-week classification of the mice into MSS or HSS was based on the %SBW and gross pathological changes in the liver, a clear distinction in the %SBW for these mice can be seen. However, with the 8-week and 12-week a range of %SBWs can be observed. The relationship between %SBW and spot volume was investigated for several protein spots including transferrin, retinol binding protein1, keratin D, hydroxyproline, MUP, *Sm*-PEPCK, peroxiredoxin 6 and epoxide hydrolase which are addressed below according to their GO function categories and their relation to the disease pathology. In the graph representing linear regression analyses: pink line = 8-week infected, purple line = 12-week infected and black line = 20-week infected mice. Only statistically significant linear regression line data has been shown in subsequent figures.

4.2.5.1 Acute phase proteins

Acute phase proteins like retinol binding protein 1 and transferrin are known to decrease during inflammation as a result of infection and disease. Retinol binding protein-1 is abundant in liver cells, particularly in hepatic stellate cells. We reported increased abundance of this protein in HSS mice in Chapter 3. Similarly, we found retinol binding protein 1 was significantly higher in HSS mice compared to other five study groups. In 12-week infected mice, the spot volumes were higher compared to control and 6-week infected mice (Figure 4.12). Although linear regression analysis did not show a correlation

within individual study groups, when all values are analysed together (r square=0.6046, p < 0.0001) the increased abundance of the protein strongly correlated to splenomegaly, independent of the time of infection. At 20-week infection the slope for the linear regression analysis showed r square=0.7284, p = 0.0017 relating to increased abundance of retinol binding protein 1 during HSS, indicating requirement of this protein possibly for tissue repair (Figure 4.13)

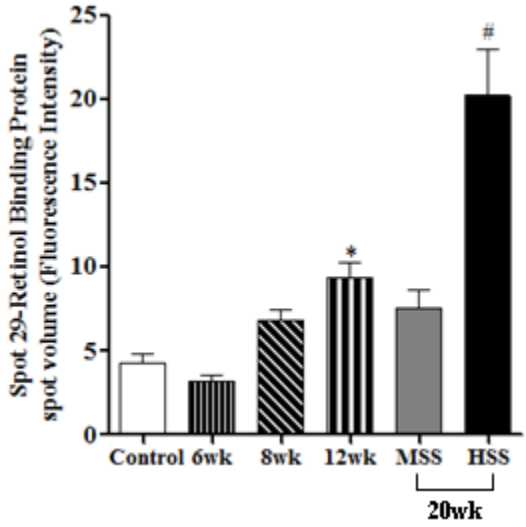

FIGURE 4.12 Mouse retinol binding protein 1 spot volumes were significantly high in HSS mice when compared to control, 6-week, 8-week, 12-week infected mice and MSS mice. Shown are mean ± SEM with 1-ANOVA $p \leq 0.01$ for all. *$p \leq 0.05$ when 12-week infected mice compared to control, 6-week infected mice, #$p \leq 0.001$ when HSS compared to control and 6-week, 8-week, 12-week infected mice and MSS mice by Newman-Keuls Multiple Comparison Test. (20wk = MSS + HSS.)

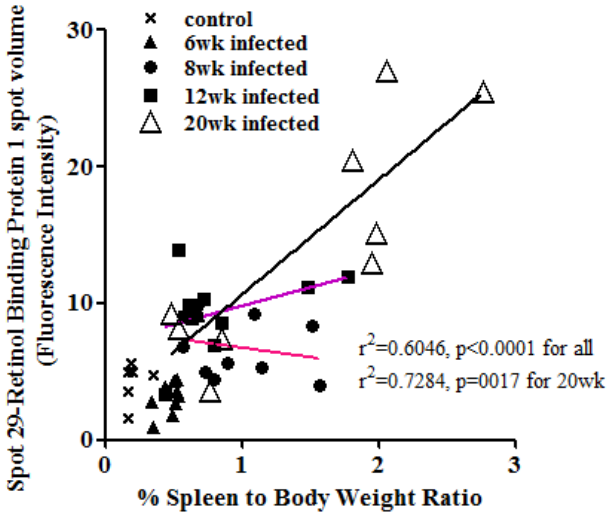

FIGURE 4.13 Comparison of spot volume fluorescence intensity of liver retinol binding protein 1-spot 29 with percent spleen to body weight ratio from control, 6-week infected, 8-week infected, 12-week infected and 20-week infected mice. (Linear regression line: pink = 8-week infected, purple = 12-week infected and black = 20-week infected mice).

The spot volumes for liver **transferrin** (two spots together, spot 43 and 44) increased for 6-week, 8-week, 12-week, MSS and HSS infected mice when compared to control mice (Figure 4.15). These findings were similar to the results in Chapter 3 for 20-week infected mice. The linear regression analysis for spot 43-liver transferrin showed significantly strong relationship with %SBW for all groups independent of time post-infection (r square=0.6637, p=0.0001), in particular, liver transferrin at 12-week infection (r square=0.7538, p<0.0001) correlated strongly with disease severity (%SBW). The linear regression for 20-week infected mice showed that increased transferrin abundance correlated with 92% splenomegaly in schistosomiasis (Figure 4.16). In particular, at 8-week and 12-week infections, there were two mice in each of the group that had increased transferrin abundance suggesting that these mice are likely to develop the disease similar to HSS mice.

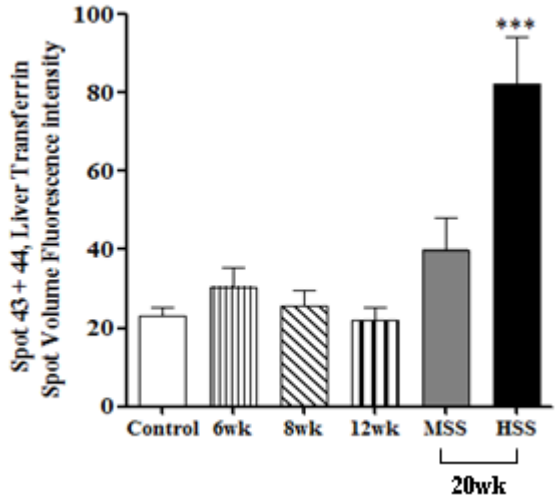

FIGURE 4.14 Comparison of spot volume fluorescence intensity of spot 43 and 44 together for liver transferrin from control, 6-week infected, 8-week infected, 12-week infected, MSS and HSS mice. Shown are mean ± SEM with 1-ANOVA $p \leq 0.01$ for all. ***$p \leq 0.001$ when HSS mice were compared to control and 6-week, 8-week, 12-week infected mice and MSS mice by Newman-Keuls Multiple Comparison Test. (20wk = MSS + HSS.)

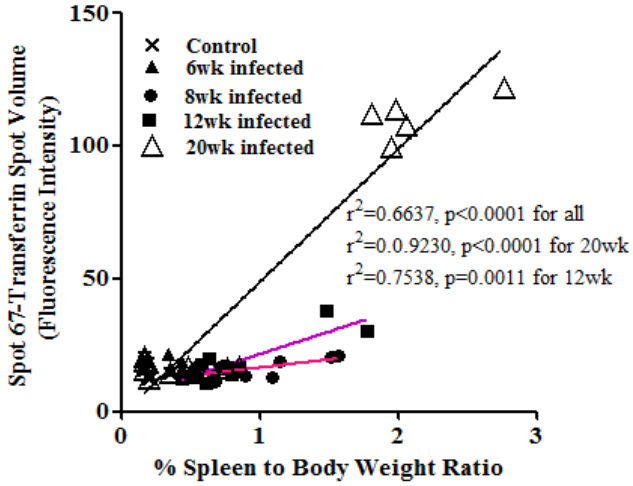

FIGURE 4.15 Comparison of spot volume fluorescence intensity of liver transferrin spot 43 with percent spleen to body weight ratio from control, 6-week infected, 8-week

infected, 12-week infected and 20-week infected mice. (Linear regression line: pink = 8-week infected, purple = 12-week infected and black = 20-week infected mice).

4.2.5.2 Structural proteins

Structural proteins provide structural stability to the cell/tissue/organ. We found increased abundance of collagen isoforms although the increase was not statistically significant. Keratin D is an intermediate filament protein and is thought to be hepatoprotective. In Chapter 3, we found a single spot of liver keratin D with increased abundance for HSS mice alone. Similarly, we found three spots of **liver keratin D** with increased abundance in HSS mice compared to five study groups (Table 4.1, Figure 4.6). Taken together all the spot volumes for the three liver keratin D spots (Table 4.2, spot 21, 22, 23, Figure 4.6), there was almost 13-fold increased abundance for HSS mice, 4-fold increase for MSS mice and 12-week infected mice had almost 8-fold increase in the average volume ratio when compared to control mice (Figure 4.16). In particular, the spot volume for spot-21 showed HSS mice had significantly higher levels ($p \leq 0.05$) compared to other five study groups (Figure 4.16). The linear regression analysis for spot 21-**keratin D** for the six study groups compared with the %SBW gave an r square value of 0.3537, $p<0.0001$ for all spots independent of the time of infection (Figure 4.17) confirming its relation to disease severity. The linear regression lines for 8-week and 12-week infection are indicative of the mice from these groups inclining towards the severe form of the disease (HSS). The increased abundance of liver keratin D correlated with 42% splenomegaly at 20-week infection. The increased abundance of this protein indicates the responses of the liver to chronic infection.

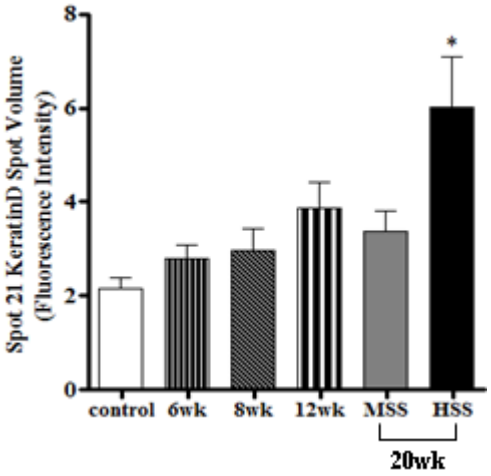

FIGURE 4.16 Mouse keratin D spot volumes were high in HSS mice when compared to control, 6-week, 8-week, 12-week infected mice and MSS mice. Shown are mean ± SEM with 1-ANOVA $p \leq 0.01$ for all. *$p \leq 0.05$ when HSS compared to control and 6-week, 8-week, 12-week infected mice and MSS mice by Newman-Keuls Multiple Comparison Test. (20wk = MSS + HSS.)

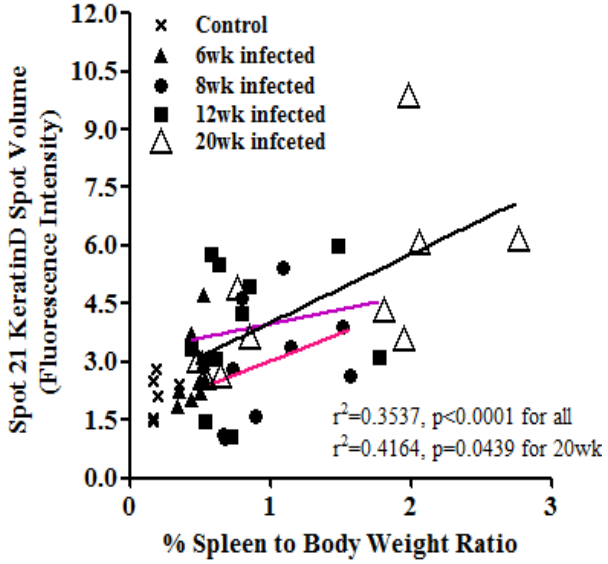

FIGURE 4.17 Comparison of spot volume fluorescence intensity of liver keratin D-spot 21 with percent spleen to body weight ratio from control, 6-week, 8-week, 12-week

infected mice and 20-week infected mice. (Linear regression line: pink = 8-week infected, purple =12-week infected and black = 20-week infected mice).

Collagen contains the amino acid hydroxyproline that is formed by hydroxylation of proline in preformed collagen and therefore can be used as a measure of collagen-associated fibrosis. Liver hydroxyproline was measured using liver tissue from control and infected mice but was not a consequence of the 2D-DIGE analysis. The **liver hydroxyproline** content per g of liver tissue (μg/g of liver tissue) for the six study groups showed high levels in HSS mice than the MSS, 8-week and 12-week infected mice compared to control mice (Figure 4.18). The linear regression analysis for the liver hydroxyproline content per g of liver tissue, increased significantly in HSS mice indicating increased fibrosis in severe disease and the r square value of 0.6833 confirming statistically significant strong relationship, which was independent of time of infection (Figure 4.19). However, the linear regression r square=0.4710, $p = 0.0280$ for 8-week infected mice (pink line) and r square=0.8666, $p < 0.0001$ for 12-week infected mice (purple line) showed a strong influence of hydroxyproline on %SBW during the early infection pathogenesis in schistosomiasis and suggesting that mice from these study groups definitely separate into severe disease form (Figure 4.19). Additionally, at 20-week infection, hydroxyproline showed almost 72% correlation with disease pathology (%SBW) (Figure 4.19). These results for the 8-week, 12-week and 20-week infected mice suggest a strong association of hydroxyproline with the pathogenesis of the schistosomiasis.

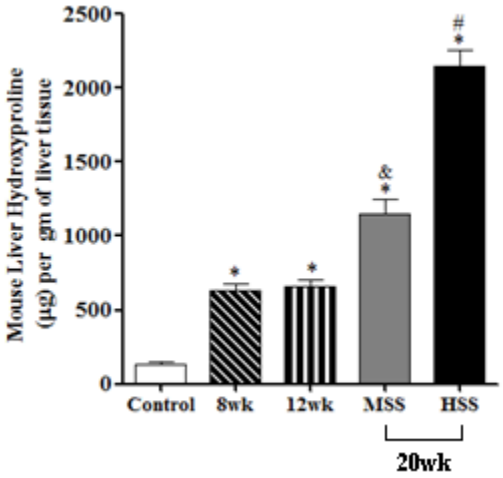

FIGURE 4.18 Mouse liver hydroxyproline levels per g of liver tissue were high in HSS mice when compared to control, 8-week, 12-week and MSS infected mice. Shown are mean ± SEM with 1-ANOVA $p \leq 0.01$ for all. *$p \leq 0.001$ when 8-week, 12-week, MSS and HSS infected mice compared to control mice, #$p \leq 0.001$ when HSS compared to 8-week, 12-week infected mice and MSS, $^{\&}p \leq 0.001$ when MSS compared to 8-week, 12-week by Newman-Keuls Multiple Comparison Test. (20wk = MSS + HSS.)

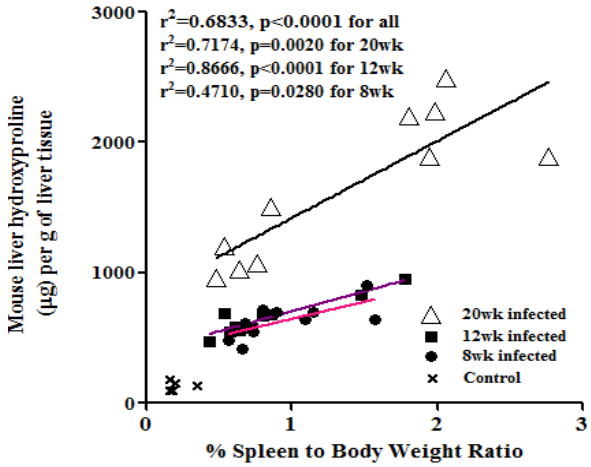

FIGURE 4.19 Linear regression correlations of mouse liver hydroxyproline per g of liver tissue with percent spleen to body weight ratio for five study groups: control mice, 6-week, 8-week, 12-week and 20-week infected mice. The r square value of 0.6833 is

indicative of the strong effect of the progression of disease and fibrosis. (Linear regression line: pink = 8-week infected, purple = 12-week infected and black = 20-week infected mice).

4.2.5.3 Immune related proteins

Immune responses to eggs embedded in the liver are a marked feature of schistosomiasis. Proteins in the immune system that protect the host from the disease mediate these immune responses. We studied two proteins related to immune responses among the five study groups in detail, they include **MHC class I histocompatibility antigen H2 Q4 alpha chain precursor** (MHC class 1 H2Q4 like protein) and interleukin 2. Similar results were observed for MHC class 1 H2Q4 like protein as in Chapter 3. The results obtained in Chapter 3, for interleukin 2 showed increased abundance of the protein in MSS and HSS mice compared to control mice but were not statistically significant because the protein spot was not satisfactorily resolved on the gel.

The MHC class 1 H2Q4 like protein spot volume comparison between six study groups showed that 12-week infected mice had significantly higher protein abundance when compared to other study groups (Figure 4.20). These results suggest that at 12-week infection there is imbalance in immune responses. Linear regression analysis for MHC class 1 H2Q4 like protein demonstrated a strong correlation between protein spot volume intensity for MSS and %SBW (r square=0.9785) (Figure 4.21). The r square for 20-week infected mice (r square=0.7408) suggests that MHC class 1 H2Q4 like protein may be involved in immunomodulation of host response to the eggs embedded in the liver.

The mean values for the cytokine **interleukin 2** were significantly higher for 8-week, 12-week, MSS and HSS mice form the control and 6-week mice (Figure 4.22). The linear regression analysis showed (r square=0.2542, p=0.0004) that interleukin 2 does play an important role in contributing towards splenomegaly (Figure 4.23). Moreover, the inclination of the linear regression line for 20-week infected mice when compared to 8-week and 12-week infection suggests down-modulation of interleukin 2 during chronic disease stage (Figure 4.23). Finally, the linear regression scatter plot for both the immune related proteins at 8-week and 12-week infection showed spot volumes spread out inconsistently (Figure 4.21 and 4.23) this may be due to individual variability in the mice during pathogenesis of schistosomiasis.

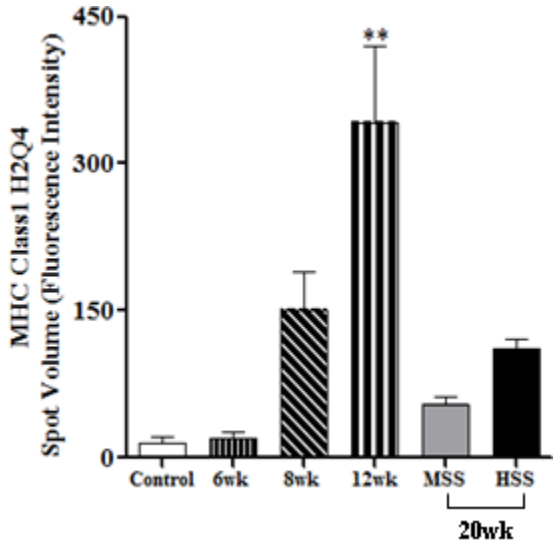

FIGURE 4.20 Comparison of spot volume fluorescence intensity of MHC class I histocompatibility antigen H2 Q4 alpha chain precursor-spot 61 from control, 6-week infected, 8-week infected, 12-week infected, MSS and HSS mice. Shown are mean ± SEM with 1-ANOVA $p \leq 0.01$ for all. **$p \leq 0.05$ when 12-week infected compared to other study groups by Newman-Keuls Multiple Comparison Test. (20wk = MSS + HSS.)

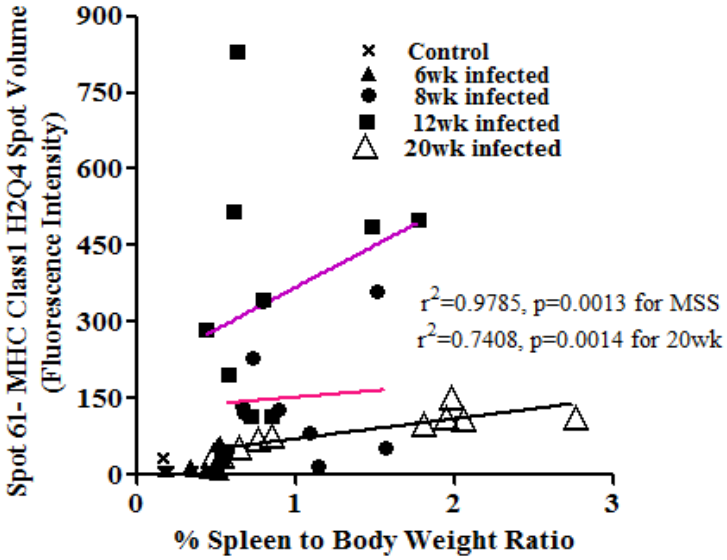

FIGURE 4.21 Comparison of spot volume fluorescence intensity of MHC class I histocompatibility antigen H2 Q4 alpha chain precursor -spot 61 with percent spleen to body weight ratio from control, 6-week infected, 8-week infected, 12-week infected and 20-week infected mice. (Linear regression line: pink = 8-week infected, purple = 12-week infected and black = 20-week infected mice).

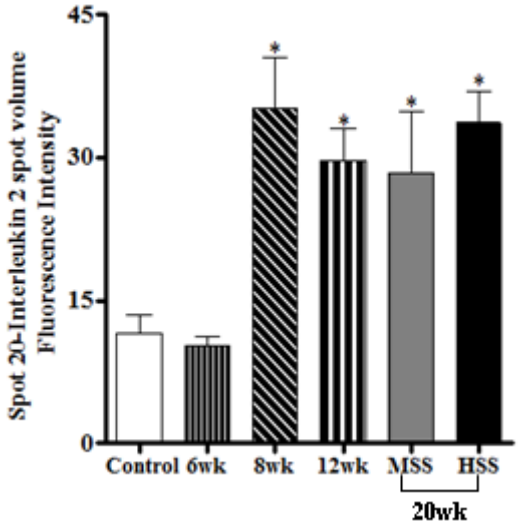

FIGURE 4.22 Comparison of spot volume fluorescence intensity of interleukin 2-spot 20 from control, 6-week infected, 8-week infected, 12-week infected, MSS and HSS mice.

Shown are mean ± SEM with 1-ANOVA $p \leq 0.01$ for all. *$p \leq 0.05$ when 8-week, 12-week, MSS and HSS infected mice compared to control and 6-week infected mice by Newman-Keuls Multiple Comparison Test. (20wk = MSS + HSS.)

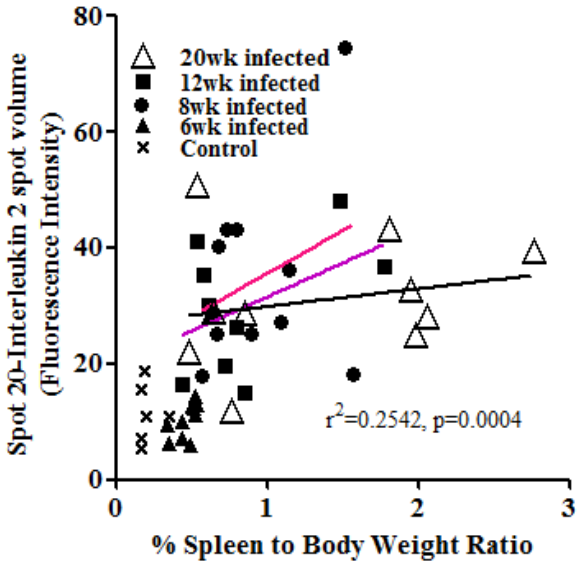

FIGURE 4.23 Comparison of spot volume fluorescence intensity for interleukin-2-spot 20 with percent spleen to body weight ratio from control, 6-week infected, 8-week infected, 12-week infected and 20-week infected mice. (Linear regression line: pink = 8-week infected, purple = 12-week infected and black = 20-week infected mice).

4.2.5.4 Xenobiotic metabolism proteins

During disease, xenobiotic metabolising proteins help removal of toxic molecules. We found two proteins with xenobiotic removal function very interesting these were peroxiredoxin 6 and epoxide hydrolase. The Chapter 3 results of peroxiredoxin 6 showed decreased abundance by 2-fold for HSS mice only however the results were not significant after the application of FDR. In Chapter 3 there were three spots with decreased epoxide activity in MSS mice (6-fold) and HSS mice (8-fold).

The spot volumes for peroxiredoxin 6 significantly decreased for 6-week, 8-week, 12-week, MSS and HSS infected mice when compared to control mice (Figure 4.24) consistent with the findings in Chapter 3. At 8-week and 12-week infections the abundance decreased significantly indicated by the linear regression lines, however at 20-week the levels coming close to levels at 6-week infections. The protein abundance at 20-week infection showed 46% influence on the disease (Figure 4.25). These results indicate that active disease pathology at 8-week and 12-week infection may have impaired the synthesis or functioning of peroxiredoxin 6.

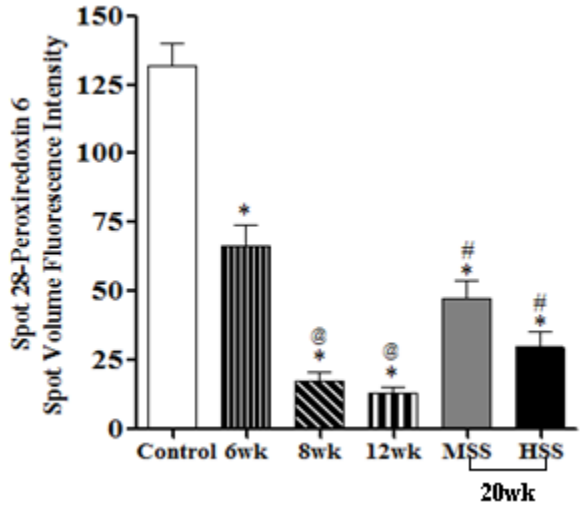

FIGURE 4.24 Comparison of spot volume fluorescence intensity for Spot 28-Peroxiredoxin 6 from control, 6-week infected, 8-week infected, 12-week infected, MSS and HSS mice. Shown are mean ± SEM with 1-ANOVA $p \leq 0.01$ for all. *$p \leq 0.05$ when 6-week, 8-week, 12-week, MSS and HSS mice compared to control, $^{@}p \leq 0.05$ when 8-week and 12-week compared to MSS mice, #$p \leq 0.05$ when MSS and HSS compared to 6-week mice by Newman-Keuls Multiple Comparison Test. (20wk = MSS + HSS.)

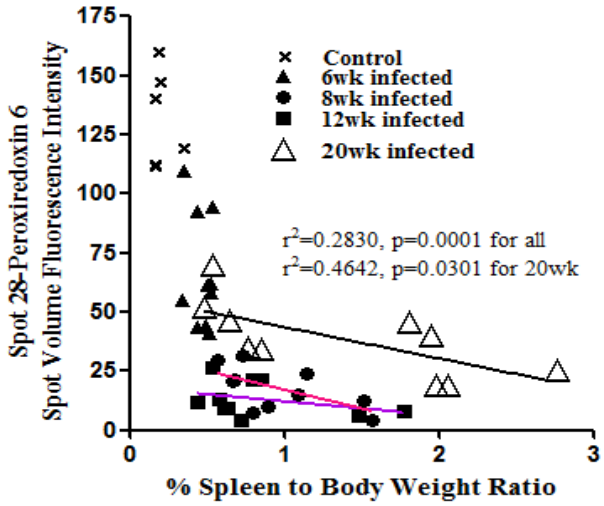

FIGURE 4.25 Comparison of spot volume fluorescence intensity for Spot 28-Peroxiredoxin 6 with percent spleen to body weight ratio from control, 6-week infected, 8-week infected, 12-week infected and 20-week infected mice. (Linear regression line: pink = 8-week infected, purple = 12-week infected and black = 20-week infected mice).

Epoxide hydrolase is located in the peroxisomes and play a significant role in the metabolism of reactive oxygen species produced in response to stress conditions. Similar to the results in Chapter 3, we found one spot with decreased abundance at 8-week, 12-week and HSS infected mice. The epoxide hydrolase spot volume fluorescence intensity for MSS was slightly higher than HSS mice indicating the resolved liver pathology during MSS. The protein abundance decreased at 8-week and 12-week infection and was similar to that of HSS mice (Figure 4.26). The epoxide hydrolase-spot-14 correlated with 28% splenomegaly as analysed by linear regression irrespective of the time of infection. However, at 20-week infection the linear regression for the protein abundance showed r square 0.7732 indicating the strong association with the disease (Figure 4.27). Taken together these results indicate that epoxide hydrolase plays a significant role during chronic schistosomiasis.

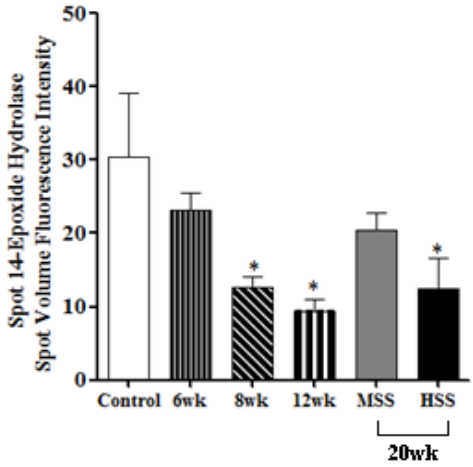

FIGURE 4.26 Comparison of spot volume fluorescence intensity for Spot 14-Epoxide hydrolase from control, 6-week infected, 8-week infected, 12-week infected, MSS and HSS mice. Shown are mean ± SEM with 1-ANOVA $p \leq 0.01$ for all. *$p \leq 0.05$ when 8-week, 12-week, HSS mice compared to control mice by Newman-Keuls Multiple Comparison Test. (20wk = MSS + HSS.)

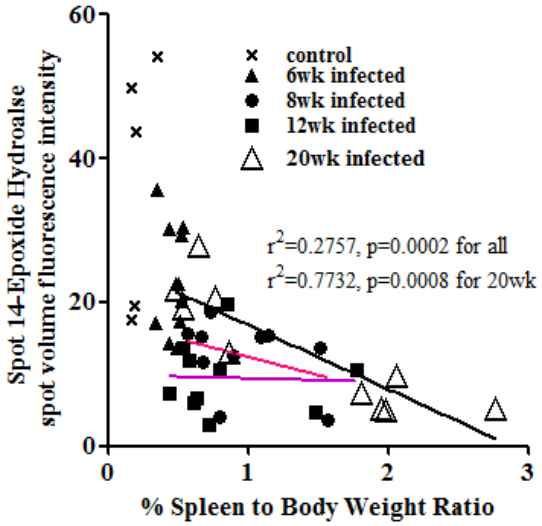

FIGURE 4.27 Linear regression analysis for spot 14-epoxide hydrolase with percent spleen to body weight ratio from control, 6-week infected, 8-week infected, 12-week

infected and 20-week infected mice. (Linear regression line: pink = 8-week infected, purple = 12-week infected and black = 20-week infected mice).

4.2.5.5 MUP and *Sm*-PEPCK

MUP is a pheromone protein and its decreased abundance is related to infection and disease. We found two spots with decreased MUP activity in HSS mice. These findings were similar to the results in Chapter 3. The mean MUP spot volumes showed significantly decreased levels in HSS mice compared to other five study groups (Figure 4.28). The r square value for MUP spot volume linear regression was 0.395, $p<0.0001$ independent of the time of infection. Although the linear regression for 8-week and 12-week infected mice was not statistically significant the regression line inclined towards the 20-week infected mice linear regression line indicating that some mice display protein patterns similar to severe disease (Figure 4.29) and may follow the same path as for the chronic disease.

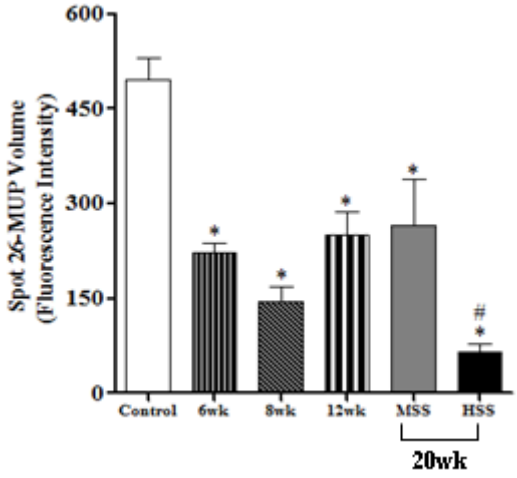

FIGURE 4.28 Comparison of spot volume fluorescence intensity of liver MUP-spot 26 from control, 6-week infected, 8-week infected, 12-week infected, MSS and HSS mice.

Shown are mean ± SEM with 1-ANOVA $p \leq 0.01$ for all. *$p \leq 0.001$ when 6-week, 8-week, 12-week, MSS and HSS infected mice compared to control mice, #$p \leq 0.05$ when HSS compared to 6-week, 12-week and MSS mice by Newman-Keuls Multiple Comparison Test. (20wk = MSS + HSS.)

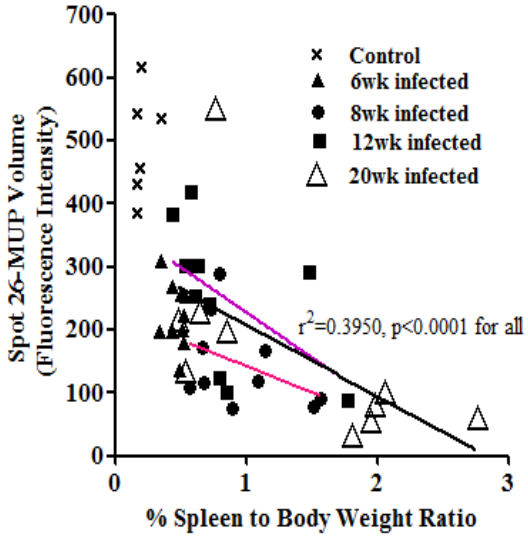

FIGURE 4.29 Comparison of spot volume fluorescence intensity of liver MUP-spot 26 with percent spleen to body weight ratio from control, 6-week infected, 8-week infected, 12-week infected and 20-week infected mice. (Linear regression line: pink = 8-week infected, purple = 12-week infected and black = 20-week infected mice).

***Sm*-PEPCK,** a parasite protein showed increased abundance during disease progression confirming the results in Chapter 3. In particular, the protein abundance increased for 12-week and HSS mice indicating the role of this protein at these time points post-infection (Figure 4.30). The r square value of 0.3971 showed a significant association of the protein on splenomegaly during schistosomiasis. Two mice each from 8-week and 12-week infected mice display protein patterns similar to 20-week infected mice (HSS mice)

confirmed by the linear regression lines for 8-week and 12-week infection (Figure 4.31). The r square 0.8732 showed the increased abundance of this protein during chronic stage of the disease (Figure 4.31). We believe our results for *Sm*-PEPCK suggest that increased abundance may indicate the orientation of the disease towards severity.

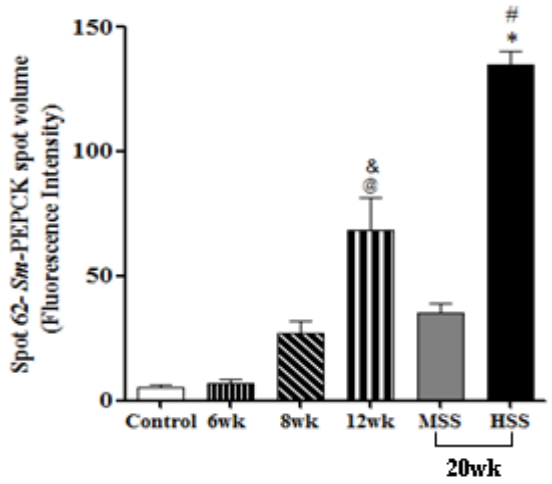

FIGURE 4.30 Comparison of spot volume fluorescence intensity of *S. mansoni*-phosphoenolpyruvate carboxykinase-spot 62 from control, 6-week infected, 8-week infected, 12-week infected, MSS and HSS mice. Shown are mean ± SEM, 1-ANOVA $p \leq 0.01$ for all. *$p \leq 0.001$ when HSS mice compared to control mice, 6-week, 8-week and MSS mice, #$p \leq 0.01$ when HSS compared to 12-week mice, $^{@}p \leq 0.001$ when 12-week mice compared to control and 6-week mice, $^{\&}p \leq 0.01$ when 12-week mice compared to MSS mice by Newman-Keuls Multiple Comparison Test. (20wk = MSS + HSS.)

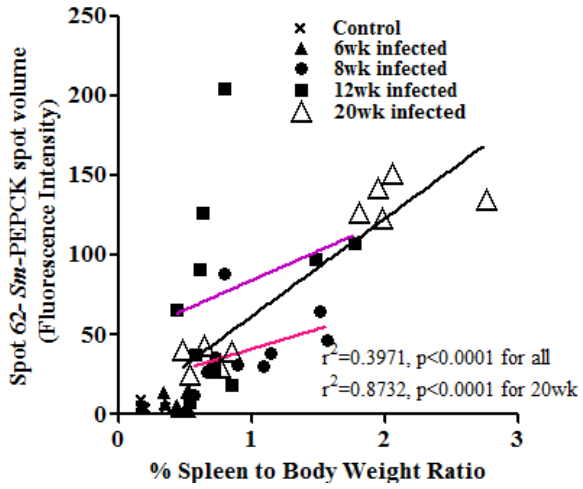

FIGURE 4.31 Comparison of spot volume fluorescence intensity of *Schistosoma mansoni* phosphoenolpyruvate carboxykinase-spot 62 with percent spleen to body weight ratio from control, 6-week infected, 8-week infected, 12-week infected, and 20-week infected mice. (Linear regression line: pink = 8-week infected, purple = 12-week infected and black = 20-week infected mice).

4.2.6 Multiple regression analysis

We used multiple regression analysis to test the multiple protein spot volumes (independent variables) simultaneously and investigate the concurrent effects of different proteins on disease pathology represented by %SBW (splenomegaly) or %LBW (hepatomegaly) in our study. In this analysis, the standardised β value indicates the extent of effect of the independent variable on the dependent variable in the presence of other independent variables and the coefficient of determination (r square) shows the linear relationship between the two variables (dependent and independent). The protein spot volumes were logarithmically ($\log_e$) transformed to normalise the data. All the protein spot volumes, on univariate analysis significantly related to the disease progression, were

entered by the forward stepwise method into a multiple regression analysis to identify the determinants of splenomegaly and hepatomegaly (dependent variables).

We found that liver hydroxyproline was the strongest predictor of splenomegaly (r square = 0.757, standardised β = 0.870, p=0.000) and hepatomegaly (r square = 0.455, standardised β = 0.674, p = 0.000) indicating it major role in disease pathology. As hydroxyproline was such a strong predictor of splenomegaly and hepatomegaly, in order to identify other protein predictors, the data was analysed independent of hydroxyproline in a similar way as described above. We found that MUP, *Sm*-PEPCK, keratin D and IL-2 together, predicted 81% of splenomegaly with MUP being the dominant predictor and related inversely to the development of the disease. In a separate analysis, we found that MUP, *Sm*-PEPCK and IL-2 together, correlated with 58% hepatomegaly, with MUP and IL-2 levels related inversely to hepatomegaly. (The negative value for standardised beta means that the independent variable is inversely proportional to dependent variable). Importantly, keratin D was the distinct predictor of splenomegaly (Table 4.4).

TABLE 4.4 Predictors of splenomegaly and hepatomegaly.

	r square	**Standardised β Coefficient**	**p value**
Predictors of splenomegaly			
MUP	0.604	-0.612	0.000
Keratin D	0.129	+0.287	0.000
***Sm*-PEPCK**	0.054	+0.169	0.043
IL-2	0.019	+0.175	0.050
Predictors of hepatomegaly			
MUP	0.373	-0.451	0.000

***Sm*-PEPCK**	0.161	+0.296	0.015
IL-2	0.042	-0.256	0.048

With the aim of identifying the predictors of splenomegaly and hepatomegaly at each time post-infection, a stepwise multiple regression analysis was done using liver hydroxyproline, transferrin, peroxiredoxin 6, MUP, keratin D, *Sm*-PEPCK, carbonic anhydrase III, interleukin 2, GSTPi as independent variables. At 8-week, 12-week and 20-week infections, liver hydroxyproline was the strongest predictor of splenomegaly (Table 4.5). Our data suggest that splenomegaly at 8-week infections was suppressed by transferrin (standardised β = -0.705). Hepatomegaly was predicted strongly by liver hydroxyproline except at 8-week infections, where transferrin was the strongest variable that negatively correlated to 61% (standardised β = -0.772) hepatomegaly (Table 4.6). Additionally, peroxiredoxin 6 had significant effects on hepatomegaly at 8-week and 20-week infections. Peroxiredoxin 6 change was negatively associated with 55% hepatomegaly at 20-week infection (standardised β = -0.556) (Table 4.6). The results from multiple regression analyses suggest that hydroxyproline has an important role in aggravated disease pathology with a simultaneous effect of acute phase protein transferrin to diminish the effects of pathology on the scarred liver.

Taken together, the results for protein abundance data, the linear regression and multiple regression analyses and the %SBW for all study groups indicate that, at 8-week and 12-week infection there emerges a distinct pattern of protein abundance which suggests of certain specific mechanisms and impact of unknown molecules that contribute towards the

segregation of these disease groups into moderate and severe pathology in schistosomiasis disease (Figure 4.32).

TABLE 4.5 Predictors of splenomegaly at time post-infection.

Time post-infection	Predictors of splenomegaly	r square	Standardised β Coefficient	p value
8-week (n=10)	Hydroxyproline	0.514	+0.717	0.020
	Transferrin	0.497	-0.705	0.023
12-week (n=10)	Hydroxyproline	0.825	+0.908	0.000
20-week (n=10)	Hydroxyproline	0.834	+0.913	0.000

TABLE 4.6 Predictors of hepatomegaly at time post-infection.

Time post-infection	Predictors of hepatomegaly	r square	Standardised β Coefficient	p value
8-week (n=10)	Transferrin	0.610	-0.772	0.001
	Hydroxyproline	0.177	+0.484	0.006
	Peroxiredoxin 6	0.145	+0.442	0.012
12-week (n=10)	Hydroxyproline	0.822	+0.878	0.000
	Sm-PEPCK	0.081	0.287	0.046
20-week (n=10)	Hydroxyproline	0.463	+0.714	0.000
	Peroxiredoxin 6	0.308	-0.556	0.018

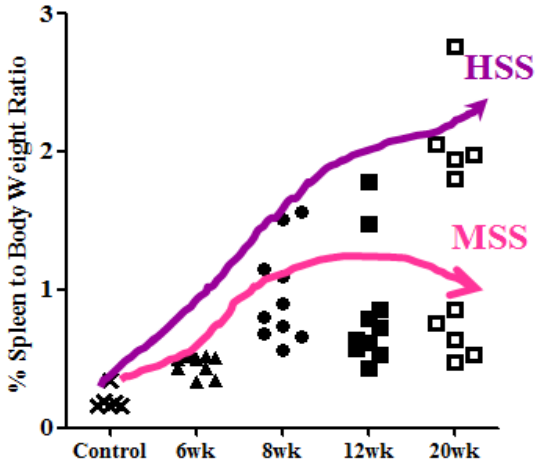

FIGURE 4.32 Specific mechanisms contribute towards segregation of the mice at 8-week and 12-week infections either towards moderate (MSS) or severe (HSS) disease progression.

4.3 Discussion

The %SBW comparison between the five study groups (Figure 4.2) suggests aggravated splenomegaly is a marked feature of the severe schistosomiasis as previously indicated (Henderson *et al.*, 1993) and similar to the findings in Chapter 3. The significant increase in hepatomegaly in the five study groups (Figure 4.3). These results were similar to the findings in hepatomegaly associated with ethanol consumption (Roede *et al.*, 2008). The linear regression analysis between percent liver to body weight ratio and %SBW showed the important role of the liver during the schistosomiasis. These findings are unique to this study and suggest an interplay between liver and spleen during pathogenesis of schistosomiasis as the disease progresses towards severity (Figure 4.4).

4.3.1 Liver protein abundance at time post infection

Liver total protein comparison between the five study groups showed decreased abundance when compared to control mice (Figure 4.5). These results support the findings from *S. mansoni* infected mice studies which demonstrated a significant decrease in liver total protein abundance at 8 week infection (Aly and Aly, 2006) suggesting that during schistosomiasis infection, the scarred liver is unable to synthesise proteins normally.

The differential protein abundance among the six study groups gave a total of 44 protein spots (Figure 4.6, Table 4.1). Importantly, the data suggests that transferrin isoforms, retinol binding protein1, MUP isoforms, peroxiredoxin 6, keratin D isoforms, epoxide hydrolase isoforms, MHC Class 1 H2Q4 like protein and *Sm*-PEPCK play a role in disease progression. While most differences for comparison with control mice were for 128 protein spots in 12-week infected mice we found greatest difference in level of change for 76 protein spots in HSS mice indicating greatest changes for 12-week infected mice but greatest magnitude of changes for 20-week infected mice.

Interestingly, the protein spot abundance data for 12-week infection reflects the extent of liver dysfunction and the severity of liver damage due to schistosome worms and eggs (Table 4.1 and 4.2, Figure 4.7). In particular, proteins related to amino acid metabolism (homogentisate 1, 2-dioxygenase), fatty acid metabolism (acetyl-Coenzyme A acetyltransferase 2), xenobiotic metabolism (catalase, carbonic anhydrase III, GST Pi), energy metabolism (aldolase 2, electron transfer flavoprotein beta-subunit, glutamate dehydrogenase, isocitrate dehydrogenase 2), urea cycle (argininosuccinate synthetase) were decreased significantly. Moreover, the data at 12-week infection showed increased

apoptotic and blood coagulation proteins (Figure 4.7). These results are supported by a human intestinal schistosomiasis study that demonstrated an important role of apoptosis in schistosomiasis (Carneiro-Santos *et al.*, 2000) and another study which suggests an important role for blood coagulation in modulating the cytokine and antigenic mediated immune responses in hepatosplenic schistosomiasis (El-Bassiouni *et al.*, 1998). Additionally, El-Meneza *et al*. demonstrated maximal hepatic fibrosis occurs at 12-week infection (El-Meneza *et al.*, 1989) supporting the findings in our study whereby suggesting that the increased abundance of cytoskeletal and extracellular matrix proteins (structural proteins) are a marked feature of 12-week infection (Figure 4.7). Previous work has shown that spontaneous and prominent immunomodulation of chronic schistosomiasis pathology at 12-week infection (Pelley *et al.*, 1976). The results in our study support the findings of Pelley *et al*. and suggest that immunomodulatory mechanisms contribute to the pathology at 12-week infection.

The linear regression scatter plots for all the protein spots examined at 8-week and 12-week infection (retinol binding protein 1, transferrin, keratin D, MHC class 1 H2Q4 like protein, interleukin 2, peroxiredoxin 6 and epoxide hydrolase) showed two spot volumes as outliers indicating that distinct changes occur at 12-week infection and even at 8-week infection. A study in 8-week *S. mansoni* infected mice analysed metabolic profiles and reported reduced levels of the tricarboxylic acid cycle intermediates, increased pyruvate levels, impairment in amino acid metabolism and fatty acid metabolism (Wang *et al.*, 2004) similar to the findings in our study. Moreover, another study also reported liver dysfunction at 8-week infection (Harvie *et al.*, 2007). While these studies found significant differences at 8-week infection similar to our findings, our results suggest

profound differences at 12-week infection. Our report on liver proteins in CBA/J mice is exclusive as it compared the protein abundance at 6-week, 8-week, 12-week and 20-week infections and showed that the response is varied at different times post infection. Together the protein spot abundance data for 6-week, 8-week 12-week, MSS and HSS infections suggests that the liver dysfunction was elevated in 12-week infected CBA/J mice.

4.3.2 Multivariate analysis

The PCA plot successfully distinguished the study groups according to the disease pattern (Figure 4.8) and protein abundance for pI range 4-7 and these results were confirmed by HCA (Figure 4.10). In contrast, the multivariate analysis of the protein spots for pI range 6-11 was unable to identify discrete clusters consistent with the separate groups. The possible reasons for the lack of discrete clusters may be the lower resolution of the gels in the 6-11 pI range. The HCA dendrogram and heat map for pI range 4-7 showed clustering of mice with similar %SBW. This provides evidence that mice with high %SBW ratio may follow the hepatosplenic disease path irrespective of the week of infection. Finally, PCA and HCA performed on the 44 protein spots (33 protein spots for pI range 4-7 and 11 protein spots for pI range 6-11) showed that some mice at 8-week and 12-week infection cluster with the chronic (MSS and HSS) mice with similar protein abundance pattern suggesting that these time points post-infection harbour crucial events that separate the mice into MSS and HSS disease forms.

4.3.3 Linear regression correlations

Chapter 3 discussed the acute phase proteins (transferrin isoforms, retinol binding protein 1), structural proteins (collagen isoforms, keratin D) and immune response proteins (MHC Class 1 H2Q4 like protein) in relation to 20-week schistosome infection. In this chapter we have investigated the relation of protein abundance at 6-week, 8-week, 12-week infections with control mice and 20-week infections and especially with splenomegaly representative of the disease pathology. The average volume ratios between the study groups (Table 4.1) demonstrate the impact of the disease on the protein abundance or vice versa. The following sections discuss the proteins according to their Gene Ontology function and the reasons and mechanisms that may affect the abundance of some interesting proteins shown in Figure 4.6. Additionally, our study assessed the amino acid hydroxyproline, which is discussed in the structural proteins section.

4.3.3.1 Acute phase proteins

Retinol binding protein 1, a negative acute phase protein, levels for HSS mice showed increased abundance during severe disease while no significant association was found for 8-week, 12-week and MSS infected mice (Figure 4.12). The linear regression analysis for retinol binding protein 1 at 20-week infection with %SBW showed r square=0.7284, p=0.0017 (Figure 4.13). These findings support the previous results for 20-week infection comparisons (Chapter 3) and previous studies have demonstrated increased levels of retinol binding protein 1 during myofibroblastic differentiation in rat fibrosis (Uchio *et al.*, 2002) and in human liver fibrosis and cirrhosis diseases during wound healing (Lepreux *et al.*, 2004). As retinol binding protein 1 is mainly expressed in the liver, the increased

protein abundance in our study indicates a possible role for retinol binding protein 1 in hepatic tissue repair.

We found increased **transferrin** abundance especially in HSS mice (Table 4.2, Figure 4.14) these results not only support the findings form Chapter 3, but also implies a greater role of liver transferrin at 12-week infection (r square= 0.7538, p=0.0011, Figure 4.15) and 20-week infection (r square= 0.9230, $p < 0.0001$, Figure 4.15) during schistosomiasis pathology. Since transferrin is a iron containing protein it acts an important source of iron for the developing schistosomulae or schistosome worms (Clemens and Basch, 1989) indicating the reason for the increased abundance during 12-week and 20-week infection. Interestingly, the multiple regression analysis showed that transferrin abundance at 8-week infection was inversely proportional to the progressive pathology in schistosomiasis (Table 4.5, Table 4.6). In support of this finding, a previous study suggests that the decreased abundance of transferrin is temporary is due to reduced rate of synthesis during infectious and toxic diseases of the liver (Jarnum and Lassen, 1961). Together, these findings warrant further investigation with the fact that retinol binding protein 1 and transferrin are negative acute reactants and showed increased abundance during schistosomiasis disease.

4.3.3.2 Structural proteins

We found significantly increased abundance of **keratin D** in HSS mice compared to other study groups (Figure 4.16) similar to the findings in Chapter 3. The linear regression analysis showed significant correlations at 20-week infection. When all the keratin D spot volumes were assessed together the linear regression remained significant independent of

the time of infection (Figure 4.17). Increased abundance of keratin D has been reported in alcoholic liver fibrosis (Salmhofer *et al.*, 1994) and chronic HCV infection (Strnad *et al.*, 2006) supporting the findings in our study and indicating that similar mechanisms may be involved in schistosomiasis fibrosis. Additionally, Salmhofer *et al.* demonstrated more acidic forms of keratin D during liver injury, possibly similar to the results shown in Figure 4.6 (spots 21, 22, 23) suggesting that spot 21 and 22 may be the acidic forms, although this requires further investigation. Zatloukal and co-workers demonstrated that alterations of the hepatocytic keratin cytoskeleton are due to increased oxidative stress and reactive oxygen species during liver disease. The authors indicate that keratin D is necessary for hepatocyte structural stability and is a modulator of toxic stress and apoptosis (Zatloukal *et al.*, 2004). In schistosomiasis also, reactive oxygen species play an important role in granuloma formation and disease progression (Elsammak *et al.*, 2008), thus our results indicate that keratin D may be involved in stress modulation in the scarred liver during schistosomiasis. Additionally, Bastos and co-workers have confirmed the role of keratin D in liver regeneration (Bastos *et al.*, 1992). We believe that increased keratin D abundance in our study may indicate its hepatoprotective role during liver disease and definitely these results may possibly be useful in assessing liver pathology in schistosomiasis.

Hydroxyproline is an amino acid found in collagen and formed by hydroxylation of proline in preformed collagen. Hydroxyproline makes up 10% of the weight of the collagen and therefore used as an as a measure of tissue collagen content. During collagen synthesis, free hydroxyproline or hydroxyproline containing peptides appear as by-products or due to improper incorporation of the amino acid in the collagen protein

(Robertson, 1964). During fibrosis, accumulation of collagen due to imbalance in collagen synthesis and degradation (Takahashi *et al.*, 1980) may lead to increased hydroxyproline. In Chapter 3 we found increased abundance of collagen isoforms during 20-week murine schistosomiasis and therefore we assessed liver hydroxyproline as it indicates the degree of fibrosis. We found increased abundance of liver hydroxyproline in HSS mice compared to 8-week, 12-week and MSS infected mice (Figure 4.18). Studies have demonstrated high liver hydroxyproline at 8-week *S. mansoni* infection (Cheever and Barral-Netto, 1985, Hoffmann *et al.*, 2001), 12-week infection, 18-week infection (El-Meneza *et al.*, 1989) and 20-week infection (Montesano *et al.*, 2002) which is in line with the findings in our study (Figure 4.18). The linear regression correlations for liver hydroxyproline per g of liver tissue showed a strong role of hydroxyproline in the pathogenesis of splenomegaly, which is independent of the time of infection (Figure 4.19). The r square values for 8-week, 12-week and 20-week infected mice showed the prominent effect of hydroxyproline (90%) on %SBW especially at 12-week infection supporting previous findings (El-Meneza *et al.*, 1989). Ours is the only study that compares together the liver hydroxyproline levels in CBA/J mouse model during schistosome-mediated liver pathology from 8-week, 12-week and 20-week infections together. Measuring the levels of this amino acid in murine and human sera will assess severe fibrosis in the disease and affect treatment strategies in humans.

4.3.3.3 Immune related proteins

The **MHC Class 1 H2Q4 like protein** mean spot volume for 12-week infected mice was 3 times the value for HSS mice. The spot volume for MSS mice was half the value for HSS mice. The spot volume for 8-week infected mice was 3 times the value for MSS mice

(Table 4.2, Figure 4.24). These results suggest that the egg induced inflammation is ongoing in 8-week and 12-week infected mice while it is resolved in MSS mice. The values for 8-week and 12-week infections are indicative of active parasitism and increase in hepatomegaly and splenomegaly, proposing a definitive role of non-classical MHC Class 1 like molecules in schistosomiasis pathology. The linear regression correlation (r square=0.9785) for MSS (Figure 4.25) mice suggest the definitive role of immune responses in resolving the egg inflammation in MSS mice as is seen in intestinal schistosomiasis (Santos *et al.*, 1992). In addition, the non-classical MHC class I molecules are also involved in non-immune functions like interactions with pheromone receptors (receptors involved with MUP like molecules) present on the cell surfaces of the mice vomeronasal organ (Ohtsuka *et al.*, 2008), thus suggesting a complex role of this protein not only during disease but also in health.

The liver **interleukin 2** (IL-2) spot volume data showed increased abundance for 8-week, 12-week, MSS and HSS infected mice (Table 4.2, Figure 4.26). When the all the spot volumes for IL-2 were analysed for linear regression the results independent of the time of infection indicate that IL-2 abundance correlated with 25% of splenomegaly during murine schistosomiasis (Figure 4.27). During schistosomiasis the Th1 cells secrete this cytokine as an immune response to the parasite eggs logged in the liver (Brunet *et al.*, 1998). Previous studies have shown decreased abundance of IL-2 mRNA in granulomatous livers (Henderson *et al.*, 1991) in contrast to the findings in our study. Conversely some studies indicate increased abundance of IL-2 during granulomatous inflammation in murine schistosomiasis (Yamashita and Boros, 1992) and human hepatosplenic schistosomiasis (Talaat *et al.*, 2007) consistent with the results in our study.

The present study in murine schistosomiasis showed increased abundance of MHC Class 1 H2Q4 like protein and IL-2 during pathogenesis of the disease further studies are required to define the role of these proteins during human schistosomiasis disease.

4.3.3.4 Xenobiotic metabolism proteins

Peroxiredoxin 6 belongs to the family of the thiol specific antioxidant proteins. Peroxiredoxin 6 is a bifunctional 25 kDa protein with both glutathione peroxidase and phospholipase A_2 activities and uses glutathione and ascorbate as electron donors. It is the only member of the peroxiredoxin family that has the ability to remove hydrogen peroxide and phospholipid hydroperoxide and therefore, able to reduce the accumulation of phospholipid hydroperoxides in plasma membranes. Our study showed decreased abundance of peroxiredoxin 6 for 6-week, 8-week, 12-week, MSS and HSS infected mice compared to control mice (Table 4.2, Figure 4.28) and consistent with the findings in alcoholic liver disease in mice that suggested excessive oxidation of the protein during liver injury (Roede *et al.*, 2008). Our results thus indicate that schistosome-mediated liver disease may be involved in oxidation of peroxiredoxin 6. Alternatively, recent studies suggest that over oxidized peroxiredoxin after oxidative stress can be reduced back to the active form during recovery from stress-related to inflammation and disease and importantly there is very slow regeneration of peroxiredoxin 6 (Chevallet *et al.*, 2003). We believe that the over oxidized peroxiredoxin 6 may be the reason for decreased protein abundance at 8-week and 12-week infection and possibly also the cause for slow regeneration of active form of peroxiredoxin 6 in HSS mice (spot volume 29.76) compared to MSS mice (spot volume 47.32) (Figure 4.28, Figure 4.29). The linear and multiple regression analysis for 20-week infected mice showed that peroxiredoxin 6

(Figure 4.29, Table 4.6) plays an important role in pathogenesis of hepatosplenomegaly during schistosomiasis. Oxidation of peroxiredoxin leads to acidic isoforms and disulphide bonded dimers. As low abundance of peroxiredoxin 6 was detected in our study, it is possible that this change reflects oxidation of peroxiredoxin 6 because of oxidative stress.

Epoxide hydrolases are a group of enzymes that catalyse the conversion of epoxides to less toxic and readily excretable dihydrodiols, hence an important component of the peroxisomes. Epoxide hydrolases are found in all mammalian tissues with the highest levels in liver and kidney. During hepatocellular cancer there is increased epoxide hydrolase activity (Murray *et al.*, 1993) and during mutagen and carcinogen-induced liver injury activity of liver epoxide hydrolase mRNA increases by 3-fold (Pickett and Lu, 1981) which is in contrast to the results in our study. Our results indicate decreased synthesis of this scavenging enzyme during schistosome infection (Table 4.2, Figure 4.32). The linear regression analysis showed that decreased abundance of epoxide hydrolase correlated with 77% of splenomegaly at 20-week infection (Figure 4.33). Taken together the results for the xenobiotic metabolising enzymes the decreased abundance can be a unique combination for assessing hepatosplenic disease.

4.3.3.5 MUP and *Sm*-PEPCK

MUP is a potent pheromone mouse protein synthesised in the liver. We found decreased abundance of MUP with disease progression indicating a strong impact of the hepatosplenic disease on the pathophysiology of the protein (Figure 4.20). MUP decreased by almost 7-fold in HSS mice and is a marked feature of our study (Table 4.2, Figure 4.20)

and similar to the previous findings discussed in Chapter 3. Studies have demonstrated multi-hormonal regulation of liver MUP in healthy mice (Knopf *et al.*, 1983) which may be impaired during diseased conditions. In murine schistosomiasis whether MUP regulation is due to the host's response to parasitism and/or the impact of the parasite infection on the MUP metabolism merits investigation. Decreased abundance of MUP in hepatocellular carcinoma (Elchuri *et al.*, 2007) is similar to the findings in our study. The linear regression analysis showed the impact of MUP on splenomegaly during schistosomiasis (Figure 4.21). The results from our study indicate that MUP may be involved in pro-cancerous mechanisms in schistosomiasis. The similarity of MUP protein to human epididymal-specific lipocalin-9 (Virtanen and Kinnunen, 2008) is promising because it may help assess the human hepatosplenic disease but whether lipocalin-9 has similar consequences in human schistosomiasis merits investigation.

High abundance of parasite protein ***Sm*-PEPCK** at 12-week and HSS infections (Table 4.2, Figure 4.22) suggests increased gluconeogenesis for the energy needs of the parasite indicating the active infection during these time points post-infection. When all the *Sm*-PEPCK spot volumes were combined, the linear regression analysis supported the role of the protein in schistosomiasis disease pathology irrespective of the time of infection (Figure 4.23). The linear regression analysis for 20-week infected mice showed that *Sm*-PEPCK predicted 87% of splenomegaly (Figure 4.23). Furthermore, a recent study reported that during host-schistosome interactions, glyceroneogenesis a phosphoenolpyruvate carboxykinase (PEPCK)-dependent pathway is active and uses glutamine as a precursor (Yang *et al.*, 2009). Indeed this indicates that during murine-schistosome interactions this pathway is active and acts as an alternative source of energy

for the parasite in the liver portal area. Another study demonstrated *Sm*-PEPCK as a novel egg antigen with a T-cell epitope (Asahi *et al.,* 2000) this information, in combination with the results in our study suggest that *Sm*-PEPCK can possibly be an infection specific marker for human schistosomiasis however merits elucidation and investigation.

4.3.4 Multiple regression analysis

A forward stepwise multiple regression analysis identified determinants of hepatomegaly and splenomegaly. Liver hydroxyproline proved to be the strongest predictor of splenomegaly using multiple regression analysis. MUP, keratin D and *Sm*-PEPCK together correlated with 78% splenomegaly while MUP inversely related to disease development. Similarly, the strongest predictor for hepatomegaly was liver hydroxyproline with a 46% effect. MUP and *Sm*-PEPCK together correlated with 53% hepatomegaly. The multivariate analysis at time post-infection revealed valuable information regarding the effect of hydroxyproline, transferrin, MUP, keratin D, peroxiredoxin 6 protein abundance on hepatomegaly and splenomegaly in schistosomiasis. These results are suggestive of the importance of these proteins during disease progress and may be useful as diagnostic markers. Also, if used in a battery of tests may assist in distinguishing human hepatosplenic schistosomiasis. Finally, together the protein abundance patterns identified using 2D-DIGE and predictors of splenomegaly determined using multiple regression analysis the results from our study warrant investigation in mouse and human sera that will help assess the intestinal and hepatosplenic disease in humans.

4.4 Conclusion

Proteomic analysis of the liver at different stages of the S*chistosomiasis mansoni* revealed complex and compact differences between the six study groups. The splenomegaly and hepatomegaly data reflect the gravity of the schistosome infection. The Gene Ontology protein function data showed that at 12-week infection with decreased protein functionality confirming the only pathological stage in disease progression with severe liver dysfunction as measured by number of changes, while HSS mice showed greatest magnitude of changes. The present data also supports the theory of segregation of 8-week and 12-week infected mice into MSS and HSS most probably due to some unknown molecular factors during disease progression. Liver and serum hydroxyproline levels related strongly with the severe pathology which is indicative of a liver candidate protein fibrosis marker. Nonetheless, the multiple regression analysis showed transferrin, MUP, keratin D and peroxiredoxin 6 are important in disease pathology demanding attention. Remarkably, two spots related to epoxide hydrolase activity had decreased abundance in HSS and 12-week infected mice which is contradictory to the findings of other studies, if thoroughly investigated could help assess severe hepatosplenic disease. High abundance of *Sm*-PEPCK through the progression of the disease not only indicates the potential of the protein as a candidate marker for schistosome infection but also signifying its strong relation to the severity of the disease. Finally, the estimation of these proteins in serum will be of great value in assessing hepatosplenic schistosomiasis.

CHAPTER 5: SERUM ANALYSIS

5.1 Introduction

Serum analysis was performed to test the strength and efficacy of the candidate protein marker/s identified in the CBA/J mouse liver study. To test whether the differences in the mouse candidate liver protein markers are reflected in the mouse serum we performed the 2D-DIGE serum analysis. Mouse sera were labelled with CyDyes, analysed for differential protein spot patterns and protein spots were identified using mass spectrometry. The experimental design 3 for the serum 2D-DIGE is listed in Appendix A. Using targeted assays the candidate liver protein markers were then verified in five sera each for control, MSS and HSS mice. The candidate liver protein markers assessed in the mouse liver and serum analysis were detected in human serum samples at the Division of Parasitic Diseases, Centers for Disease Control and Prevention, Atlanta, USA. Targeted biochemical assays were used to analyse 23 INT (intestinal schistosomiasis) sera, 14 HS (hepatosplenic schistosomiasis) sera and 13 normal human sera. Details for human sera are in the Table 5.2.

The proteins that were tested as candidate liver markers were based on the results obtained from the liver and serum 2D-DIGE experiments and linear and multiple regression analyses. The following candidate liver markers were selected as putative diagnostic markers for human hepatosplenic schistosomiasis that include connective tissue growth factor (CTGF), transferrin, keratin D and hydroxyproline. The reasons for the selection of the putative diagnostic markers are discussed below.

CTGF plays a vital role in fibrogenesis by triggering collagen synthesis in fibrotic diseases (Kovalenko *et al.*, 2009) and an important predictor for schistosomiasis fibrosis (Dessein *et al.*, 2009). In Chapter 3, Figure 3.6 demonstrates an increased abundance of Collagen 6a1 isoforms in animals with severe disease. Thus, CTGF was selected as one of the candidate liver protein markers. Transferrin and keratin D (Figure 4.15 and 4.17) were included in the study for detection in human serum samples due to the results obtained in the mouse liver and serum 2D-DIGE data that suggested an association with severe pathology (Chapter 4). Hydroxyproline is a biochemical indicator of collagen synthesis and a measure of fibrosis in schistosomiasis (Cheever and Barral-Netto, 1985) and high serum hydroxyproline levels have been demonstrated in hepatic fibrosis (George and Chandrakasan, 2000). Hydroxyproline was selected as the candidate liver protein marker due to the increased abundance of hydroxyproline in the liver (Chapter 4, Figure 4.19).

Proteins like major urinary protein (MUP) and *Sm*-PEPCK were possible candidate protein markers, but MUP is a male pheromone, hence only useful for infected males. *Sm*-PEPCK is a parasite protein but at present has no available detection antibody. In addition, the protein is more indicative of schistosomiasis infection, rather than a marker of severe disease. As a result, these proteins were not included in the current mouse and human sera studies. Finally, to assess the status of liver function during schistosomiasis, we detected the serum total protein for mice and human sera. The detection of serum total protein reflects the changes in protein synthesis during disease. Serum total protein is a measure of the total protein in the serum and therefore detection of individual protein patterns using targeted assays is recommended.

5.2 Results

5.2.1 Mouse serum 2D-DIGE analysis

The DeCyder software analysed the differences between the control, MSS and HSS mouse sera for the pI range 3-10. A total of 60 protein spots changed with infection, of which 21 protein spots showed 2-fold change in the average volume ratio with 1-ANOVA $p \leq 0.01$ in the pI range 3-10. Eighteen of these were identified using MALDI-TOF mass spectrometry and are listed in Table 5.1 (Figure 5.1). The aim of the mouse serum 2D-DIGE was to explore the basic differences in the MSS and HSS sera and therefore the FDR feature was not applied to the analysis. Depletion of highly abundant proteins like albumin, transferrin, haptoglobin and immunoglobulins that represent >90% of all serum proteins improves the detection sensitivity of protein spots in the 2D-DIGE analysis. However, serum depletion of highly abundant proteins was not performed to understand the genuine protein patterns for all protein isoforms associated with MSS and HSS sera. Additional information of the identified protein spots is listed in Appendix C.

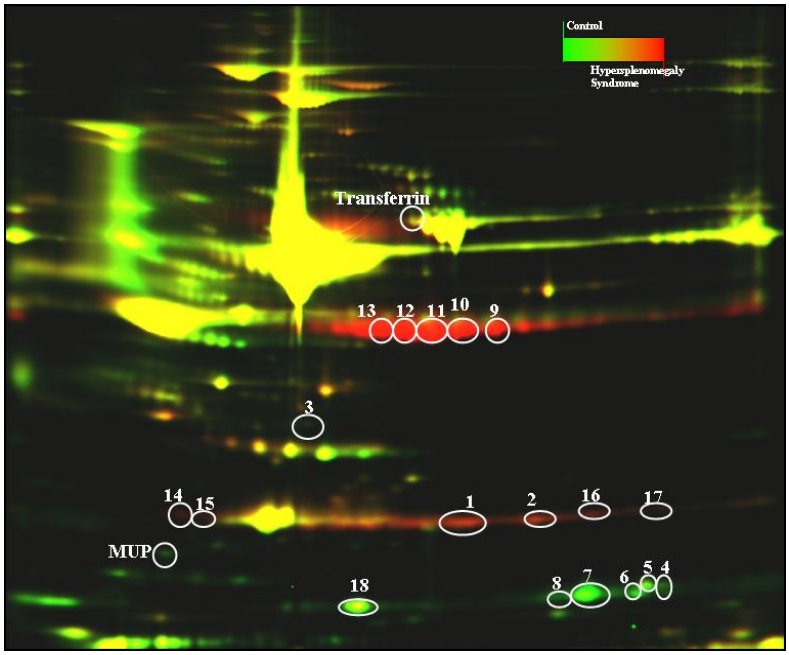

FIGURE 5.1 Pseudocolour 2D-DIGE map for 10 μg protein per serum sample for control and HSS mice. Serum from control/uninfected mice (pooled sera, n=5) was labelled with Cy5 (green), serum from 20-week infected HSS mice (pooled sera, n=5) was labelled with Cy3 (red) and a pooled internal standard of sera from all mice in the study (n=15) was labelled with Cy2 (blue; not shown). Isoelectric focusing was performed on 7 cm IPG strips pI 3-10, and proteins were separated using SDS-PAGE. MUP (green) and transferrin (yellow) are shown. The image overlays of Cy5- and Cy3-labeled proteins appear yellow.

The mouse serum 2D-DIGE showed some apparent immune-related differences related to immunoglobulin light and heavy chains in the MSS and HSS mice. There was decreased abundance in the haemoglobin chains (spot 4-8, Figure 5.1, Table 5.1), and increased abundance in complement C3 (spot 3) and decreased abundance in transthyretin (spot 18) indicating the effect of schistosome infection.

The serum MUP and the transferrin spots were not statistically significant using the criteria of 2-fold change, 1-ANOVA $p \leq 0.01$ (Table 5.2). Therefore, to detect whether MUP and transferrin showed the same differential pattern as in the liver 2D-DIGE analysis, we extracted the spot volume data from serum 2D-DIGE maps for serum MUP and transferrin spots (Figure 5.1). There was a significant difference between control, MSS and HSS mouse serum MUP and transferrin (Figure 5.2). These results support the liver lysate 2D-DIGE (Chapter 3 and Chapter 4) and western blot (Chapter 4) data. Finally, our mouse serum 2D-DIGE study has revealed that the isoforms for highly abundant proteins (immunoglobulins, transferrin) showed specific differential patterns distinct for MSS and HSS mice.

TABLE 5.1 Experimental design 3: Identified protein spot comparisons for control, MSS and HSS sera for the pI range 3-10, 2-fold change, 1-ANOVA $p \leq 0.01$.

Spot No.	***Protein Name***	***AVR H/C[1]***	***AVR M/C[1]***	***AVR H/M[1]***	***gi number***	***pI[1]***	***Mw[1] (kDa)***	***Fun.[2]***	***Ref.[1]***
1	Chain L; Crystal Structure Of The Fab Fragment (Light Chain)	+10.4	+5.97	+1.74	18655521	5.8	15.87	IMM	(Pearce and MacDonald, 2002)
2	Light Chain	+7.31	+3.52	+2.08	18655521	5.8	15.87	IMM	(Pearce and MacDonald, 2002)
3	Complement component 3	+2.72	+2.67	+1.02	28175786	6.3	188.0	IMM	(La Flamme *et al.*, 2003a)
4	Haemoglobin beta-1 chain	-7.28	-2.92	-2.49	1183932	7.1	15.94	OXT	(Brindley *et al.*, 1997, Nagi *et al.*, 1999)
5	Haemoglobin beta-1 chain	-9.59	-2.60	-3.69	1183932	7.1	15.94	OXT	(Brindley *et al.*, 1997, Nagi *et al.*, 1999)
6	Haemoglobin beta-1 chain	-14.1	-5.81	-2.42	1183932	7.1	15.94	OXT	(Brindley *et al.*, 1997, Nagi *et al.*,

									1999)
7	Haemoglobin beta-1 chain	-19.4	-7.59	-2.55	1183932	7.1	15.94	OXT	(Brindley *et al.*, 1997, Nagi *et al.*, 1999)
8	Haemoglobin beta-1 chain	-9.24	-6.03	-1.53	1183932	7.1	15.94	OXT	(Brindley *et al.*, 1997, Nagi *et al.*, 1999)
9	Immunoglobulin heavy chain	+13.3	+8.92	+1.49	13097381	6.6	51.67	IMM	(Pearce and MacDonald, 2002)
10	Immunoglobulin gamma1 heavy chain (IGHC)	+23.3	+20.1	+1.16	21304450	6.0	56.08	IMM	(Pearce and MacDonald, 2002)
11	IGHC	+21.8	+17.7	+1.23	21304450	6.0	56.08	IMM	(Pearce and MacDonald, 2002)
12	IGHC	+23.0	+15.9	+1.44	21304450	6.0	56.08	IMM	(Pearce and MacDonald, 2002)
13	IGHC	+17.2	+12.3	+1.39	21304450	6.0	56.08	IMM	(Pearce and MacDonald, 2002)
14	Immunoglobulin kappa chain (IKC)	+6.90	+1.90	+1.65	20269237	8.0	24.43	IMM	(Pearce and MacDonald, 2002)
15	IKC	+3.95	+4.06	+1.99	20269237	8.0	24.43	IMM	(Pearce and MacDonald, 2002)
16	IKC	+8.07	+3.71	+1.86	20269237	8.0	24.43	IMM	(Pearce and MacDonald, 2002)
17	IKC	+8.32	+2.34	+1.70	20269237	8.0	24.43	IMM	(Pearce and MacDonald, 2002)
18	Transthyretin	-2.60	-2.23	-1.15	19354093	5.8	15.87	TRT	(Camacho-Lobato and Borges, 1998, Strauss, 2002)

[1]***AVR*:** average volume ratio between study groups (***C***, control; ***M***, MSS; and ***H***, HSS); ***pI*:** isoelectric pH; ***Mw*:** molecular weight; ***Ref*:** references refer to association of protein with various diseases. [2]***Func.*:** Function (IMM, immune response; OXT, oxygen transporter; TRT, thyroxine retinol tranporter).

TABLE 5.2 Serum MUP and transferrin average volume ratio (AVR) comparison between control (C), MSS (M) and HSS (H) mice sera for pI range 3-10.

Protein name	***AVR H/C***	***AVR M/C***	***AVR H/M***	***gi Number***	***1-ANOVA***
MUP	-7.94	-2.51	-3.17	13276755	0.013
Transferrin	+1.95	-1.11	+2.17	62027488	0.019

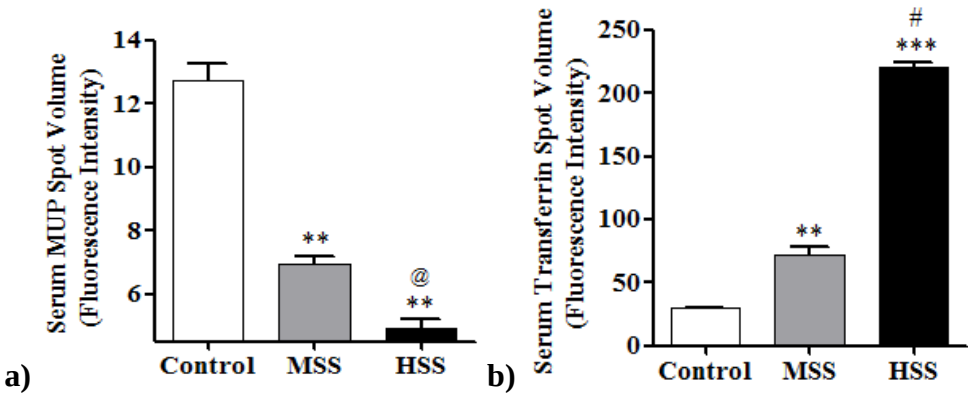

FIGURE 5.2 Mouse serum (a) MUP and (b) transferrin spot volume data from serum 2D-DIGE maps, 1-ANOVA $p \leq 0.01$ for all spot volumes. *** $p \leq 0.001$ HSS mice compared to control mice, # $p \leq 0.001$ HSS mice compared to MSS mice, **$p \leq 0.01$ MSS mice compared to control mice, $^{@}p \leq 0.05$ HSS mice compared to MSS mice by Newman-Keuls Multiple Comparison Test.

5.2.2 Mouse serum analysis using targeted assays

We tested the candidate liver protein markers in mouse sera to verify the changes seen in mouse liver and serum 2D-DIGE analysis. Estimation of the mouse serum for total protein

(BCA assay, Chapter 2, section 2.15), hydroxyproline (Hydroxyproline assay, Chapter 2, section 2.12), keratin D (Western Blot, Chapter 2, section 2.10), CTGF (CTGF ELISA, Chapter 2, section 2.11) and transferrin (Transferrin ELISA, Chapter 2, section 2.15) revealed interesting results and are summarised in Table 5.3.

TABLE 5.3 Summary of results for mouse serum analysis. Shown are mean ± SEM.

No.	Mouse serum test	Control	MSS	HSS
1.	**Total protein (mg/mL)[@]**	29.0 ± 1.2	29.2 ±1.9	27.8 ±1.4
2.	**Hydroxyproline (μg/mL) [@]**	5.3 ± 1.3	9.2 ± 2.6	19.4 ± 3.9*
3.	**Keratin D (Band volume)**	$6.8 \times 10^6 \pm 0.5 \times 10^6$	$6.2 \times 10^6 \pm 0.3 \times 10^6$	$10.8 \times 10^6 \pm 0.5 \times 10^6$ ***
4.	**CTGF (ng/mL) [@]**	20.1 ± 0.4	37.2 ± 7.9	108.1 ± 23.7 **
5.	**Transferrin (Band volume)**	$1.0 \times 10^6 \pm 0.1 \times 10^6$	$0.9 \times 10^6 \pm 0.1 \times 10^6$	$1.8 \times 10^6 \pm 0.2 \times 10^6$*

***$p \leq 0.001$, **$p \leq 0.01$, *$p \leq 0.05$ when HSS mice compared to control and MSS mice

[@]Unit indicates level per mL of serum.

Serum total protein is a commonly used liver function test and measures the total amount of protein in the serum. The mouse serum total protein concentration was similar among the study groups (control, 8-week, 12-week, MSS and HSS mice, Figure 5.3). The mouse serum total protein results were in contrast to the results obtained for mouse liver total protein that showed decreased liver total protein for diseased (6-week, 8-week, 12-week and 20-week infected) mice (Figure 4.5, Chapter 4). The serum results indicate that measurement of specific proteins like immunoglobulin patterns, as seen in serum 2D-

DIGE analysis (Table 5.1), may help to identify changes and differentiate between the two disease syndromes.

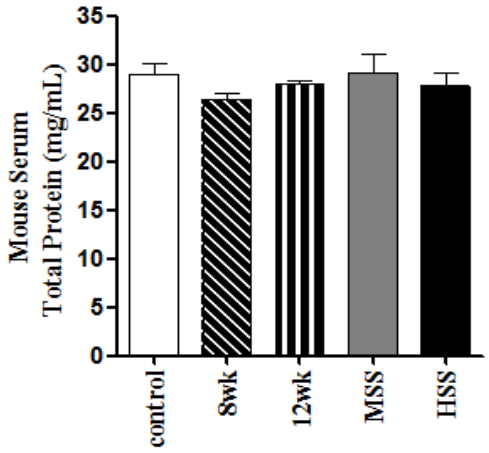

FIGURE 5.3 Mouse serum total protein. The mean concentrations ± SEM were similar among the study groups (control, n=5; 8-week, n=10; 12-week, n=10; MSS, n=5; HSS, n=5).

Hydroxyproline is an amino acid found in collagen and therefore a measure of imbalance in collagen synthesis and degradation. We found that serum hydroxyproline levels for mice with HSS disease were significantly higher than MSS and control mice (Figure 5.4). The increased levels of serum hydroxyproline probably reflect the leakage of the amino acid into the circulatory system from the damaged and fibrotic liver during severe disease. In line with the findings of liver hydroxyproline in Chapter 3, this amino acid has been for the first time studied in schistosomiasis sera and definitely be worth investigating in human hepatosplenic disease.

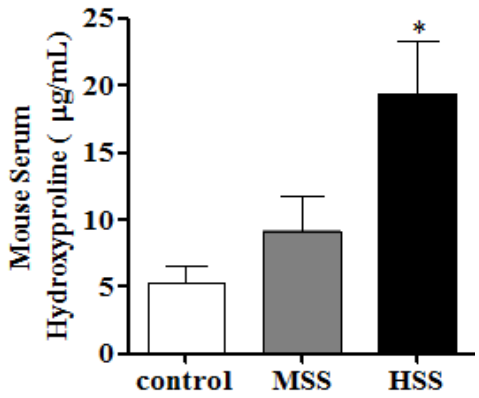

FIGURE 5.4 Mouse serum hydroxyproline levels were higher in HSS mice compared to control and MSS mice. Shown are the means ± SEM (control, n=5; MSS, n=5; HSS, n=5), 1-ANOVA $p \leq 0.05$ for all, *$p \leq 0.05$ when HSS compared to control or MSS mouse groups by Newman-Keuls Multiple Comparison Test.

Keratin D is an intermediate filament protein and increased abundance in HSS mice compared to MSS and control mice was demonstrated in Chapter 3 and Chapter 4. The levels of mouse serum keratin D detected by western blot results were higher in animals with HSS compared to serum from animals with MSS and control mice (Figure 5.5). These results support the mouse liver 2D-DIGE data and emphasise the importance of this protein as a good candidate liver protein marker for hepatosplenic schistosomiasis.

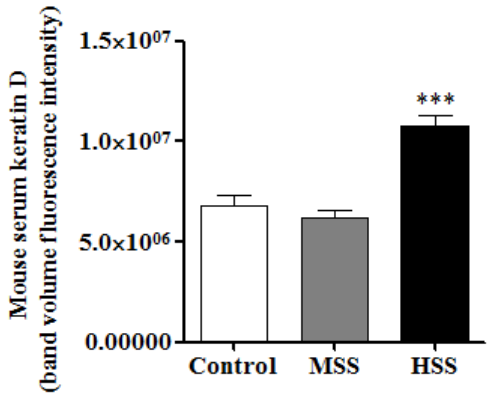

FIGURE 5.5 Western blot analysis of mouse serum keratin D, means ± SEM (control, n=5; MSS, n=5; HSS, n=5), with an overall 1-ANOVA $p \leq 0.01$, ***$p \leq 0.001$ when HSS mice were compared to control and MSS mice by Newman-Keuls Multiple Comparison Test. Mouse serum keratin D western blot images are in Appendix G.

CTGF represents the increased collagen synthesis during fibrosis and therefore assessment of this protein was important. The detection of mouse serum CTGF using ELISA demonstrated significantly increased levels in HSS mice compared to MSS and control mice (Figure 5.6). The serum CTGF results were in line with the increased collagen isoforms observed in Chapter 3 and if assessed in human sera can be used as an indicator of liver fibrosis in human schistosomiasis.

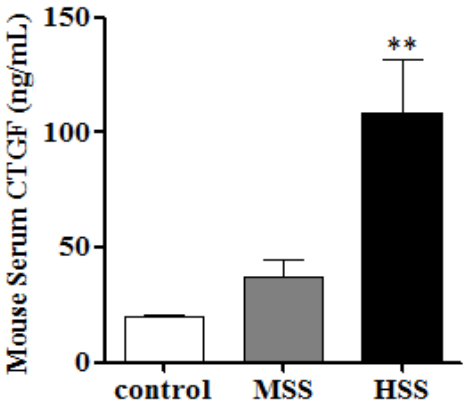

FIGURE 5.6 Mouse serum CTGF was analysed by ELISA, means ± SEM (control, n=5; MSS, n=5; HSS, n=5), 1-ANOVA $p \leq 0.01$, **$p \leq 0.01$ when HSS mice were compared to MSS and control mice by Newman-Keuls Multiple Comparison Test. (The serum control CTGF values are referred to from Cheng *et al.* (Cheng *et al.*, 2006)).

The mouse serum transferrin band volume fluorescence intensity analysed using western blot for each control mice and 8-week, 12-week, MSS and HSS infected mice showed HSS mice had significantly higher transferrin abundance compared to other study groups (Figure 5.7). These findings are in line with the results for liver transferrin abundance (Chapter 3) and serum transferrin 2D-DIGE data (Figure 5.2b) that indicated HSS mice had increased transferrin abundance. The transferrin results in our study contrast its function of "negative acute phase protein" and therefore estimation of transferrin in human sera will possibly help reflect more on mechanisms of action of this acute phase protein during schistosomiasis.

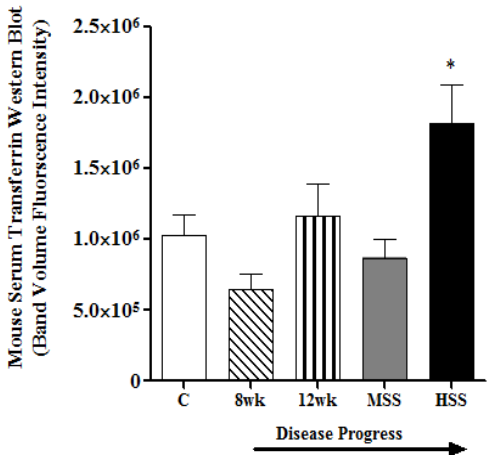

FIGURE 5.7 Mouse serum transferrin western blot analysis for control (C; n=5), 8-week infected (n=10), 12-week infected (n=10) and MSS (n=5), and HSS (n=5) groups. The means ± SEM of protein band fluorescence intensity are shown. Levels of HSS mice were significantly higher (* $p \leq 0.05$ by Newman-Keuls Multiple Comparison Test) than those in control mice, 8-week, 12-week and MSS infected mice.

5.2.3 Human serum analysis using targeted assays

The human serum analysis was planned to extend the mouse serum experiments and detect whether similar changes occur in human sera. The candidate liver protein markers: total protein (BCA assay, Chapter 2, section 2.15), hydroxyproline (Hydroxyproline assay, Chapter 2, section 2.12), keratin D (Western Blot, Chapter 2, section 2.10), CTGF (CTGF ELISA, Chapter 2, section 2.11) and transferrin (Transferrin ELISA, Chapter 2, section 2.15) were tested in human sera to determine their specificity for any of the INT and HS disease forms. The effect of possible confounding factors like HIV-1 infection status and ultrasound detected fibrosis were also tested. The human serum data was compared in four ways: normal, INT and HS groups, HIV-1 co-infection serostatus among INT and HS patients, then based on image patterns IPA, IPC and IPD/E and finally HIV-1 co-infection

serostatus among image patterns. Table 5.4 shows the characteristics for the human sera, analysed in our study. The INT and HS patients were male carwashers from Kisumu, Kenya and the normal human sera were from the Centers for Disease and Prevention, Atlanta, USA. The results for normal, INT and HS human serum analysis are tabulated in Table 5.5.

TABLE 5.4 Characteristics for human serum samples based on ultrasound image patterns and HIV-1 infection status.

Subjects	**Normal**	**INT[1]**		**HS[1]**			
n (total)	13	23		14			
Ultrasound Image Pattern (IP)	-	IPA[1]		IPC[1]		IPD/E[1]	
n (according to image pattern)	-	23		10		4	
HIV-1 infection status	-	**-ve**	**+ve**	**-ve**	**+ve**	**-ve**	**+ve**
n (according to HIV-1 status)	-	11	12	6	4	4	-

[1]INT: intestinal schistosomiasis, HS: hepatosplenic schistosomiasis, IPA: image pattern "A", IPC: image pattern "C", IPD/E: image pattern "D/E". n = number of subjects.

TABLE 5.5 Summary of results for human serum analysis. Shown are mean ± SEM.

No.	**Human serum test**	**Normal**	**INT**	**HS**
1.	**Total protein (mg/mL)** $^{@}$	92.1 ± 2.4	$159.7 \pm 1.7^{***}$	$162.3 \pm 3.1^{***}$
2.	**Hydroxyproline (μg/mL)** $^{@}$	5.8 ± 1.1	$16.7 \pm 2.6^{**}$	$17.2 \pm 2.5^{**}$
3.	**Keratin D (Band volume)**	$8.5\times10^{6} \pm 0.5\times10^{6}$	$10.2\times10^{6} \pm 0.7\times10^{6}$	$15.8\times10^{6} \pm 0.1\times10^{6}$ $^{@\,\#\#}$
4.	**CTGF (ng/mL)** $^{@}$	5.6 ± 0.7	$13.4 \pm 2.7^{\&}$	5.1 ± 1.4
5.	**Transferrin (mg/mL)** $^{@}$	-	3.8 ± 0.3	3.9 ± 0.2

***p ≤ 0.001, **p ≤ 0.01 when INT and HS sera compared to normal human sera, [@]p ≤ 0.05 when HS compared to normal human sera, ##p ≤ 0.01 when HS compared to INT sera, [&] p ≤ 0.05 when INT compared to HS and normal human sera

[@]Unit indicates level per mL of serum.

The mean human serum total protein was significantly higher (p ≤ 0.001) in the INT and HS when compared to normal sera. The serum total protein results for INT and HS groups were in contrast to the mouse serum total protein data. Because the serum total protein is a gross measure of liver function, these results suggest excessive liver cell damage during human schistosomiasis cause leakage of the proteins into the circulation. Thus, human serum total protein assessed the extent of liver dysfunction in schistosomiasis. When serum total protein for INT and HS was categorised into HIV-1 seropositive and seronegative groups, no statistical difference was found.

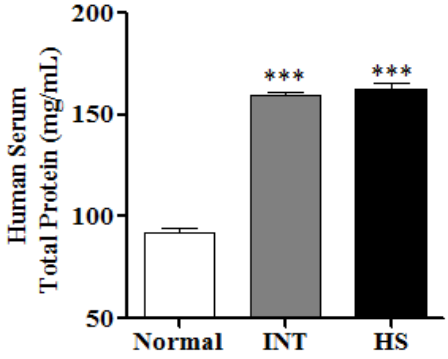

FIGURE 5.8 Human serum total protein, means ± SEM, 1-ANOVA p ≤ 0.01, ***p ≤ 0.001 when compared to normal human sera by Newman-Keuls Multiple Comparison Test.

The serum hydroxyproline levels were higher in the HSS mice alone while the human sera analysis showed high levels in both chronic human disease forms. The mean serum hydroxyproline was high in persons with INT and HS disease forms than the mean values of sera from normal individuals (Figure 5.9). In human disease, the serum hydroxyproline levels may be due to the successive or continuous re-infections and therefore a constant initiation of collagen synthesis during schistosomiasis disease. When the serum hydroxyproline concentrations were analysed based on the HIV-1 serostatus, lower levels were found in HIV-1 seropositive patients than in HIV-1 seronegative patients, although this difference was not statistically significant. But HS HIV-1 seropositive patients had significantly ($p \leq 0.05$) lower levels compared to HS HIV-1 seronegative patients (Figure 5.10). Definitely, these results indicate that HIV-1 co-infection may lead to reduced fibrosis in schistosomiasis.

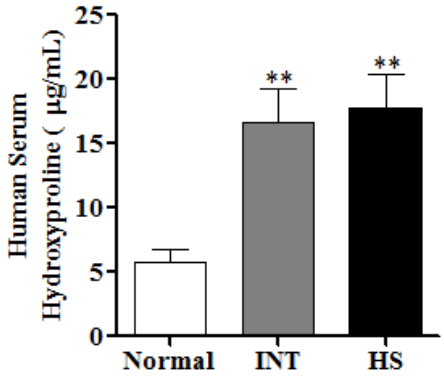

FIGURE 5.9 Human serum hydroxyproline levels among study subjects. Shown are means ± SEM, 1-ANOVA $p \leq 0.01$, **$p \leq 0.01$ when INT and HS sera were compared to normal human sera by Newman-Keuls Multiple Comparison Test.

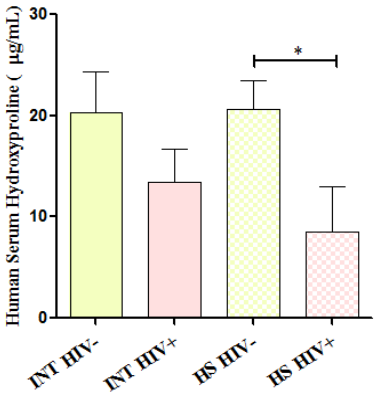

FIGURE 5.10 Human serum hydroxyproline comparison within INT and HS groups separated by HIV-1 co-infection status, means ± SEM. *p ≤ 0.05 when HS HIV-1 seronegative patients were compared to HS HIV-1 seropositive individuals (n=4) by Newman-Keuls Multiple Comparison Test.

The mouse serum keratin D (cytokeratin 18) western blot showed higher values in HSS mice compared to MSS and control mice. Consistent with the findings in mouse sera, the serum cytokeratin 18 was significantly higher in HS sera compared to INT and normal human sera (Figure 5.11). This relationship remained statistically significant (*p ≤ 0.05) even when INT and HS HIV-1 seronegative groups were compared (Figure 5.12) whereas INT and HS HIV-1 seropositive keratin D levels were similar. These results indicate that during severe disease there is a significant effect of the infection on the levels of cytokeratin 18 suggestive of a strong marker for hepatosplenic schistosomiasis.

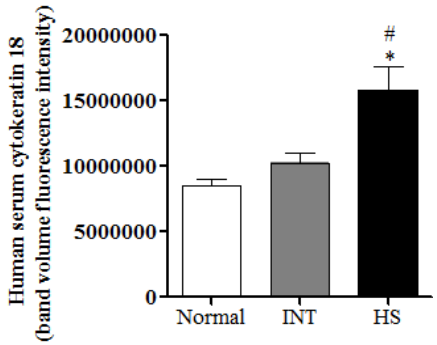

FIGURE 5.11 Human serum cytokeratin 18 using western blot analysis, means ± SEM, 1-ANOVA $p \leq 0.01$, *$p \leq 0.05$ when HS compared to normal human sera, #$p \leq 0.01$ when HS compared to INT sera by Newman-Keuls Multiple Comparison Test. Human serum western blot cytokeratin 18 images are in Appendix G.

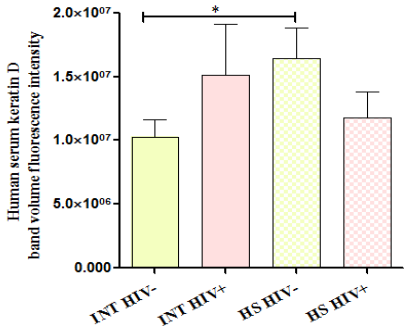

FIGURE 5.12 Human serum cytokeratin 18 levels within INT and HS groups separated by HIV-1 co-infection status. Shown are means ± SEM, 1-ANOVA $p \leq 0.01$, *$p \leq 0.05$ when INT HIV-1 seronegative was compared with HS HIV-1 seronegative sera by Newman-Keuls Multiple Comparison Test.

The human serum CTGF results contrasted with the mouse sera results that demonstrated higher values in sera from HSS mice than MSS animals. In the humans, INT sera showed significantly higher values compared to HS and normal human sera (Figure 5.13). When CTGF levels were categorised into HIV-1 seronegative and seropositive groups, patients

with HS irrespective of the HIV-1 serostatus had lower levels compared to INT patients irrespective of the HIV-1 serostatus (Figure 5.14). These results suggest that contrary to the findings in mouse studies, CTGF levels are positively associated with moderate not severe disease. Protein CTGF may still prove a valuable biomarker although its pathology is unclear.

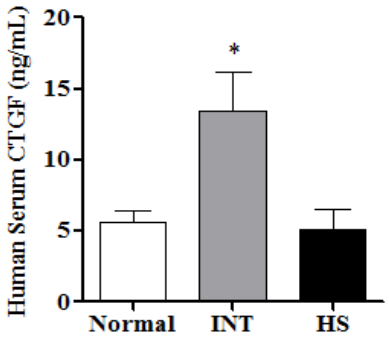

FIGURE 5.13 Human serum CTGF, means ± SEM, 1-ANOVA $p \leq 0.05$, *$p \leq 0.05$ when INT compared to HS and normal human sera by Newman-Keuls Multiple Comparison Test.

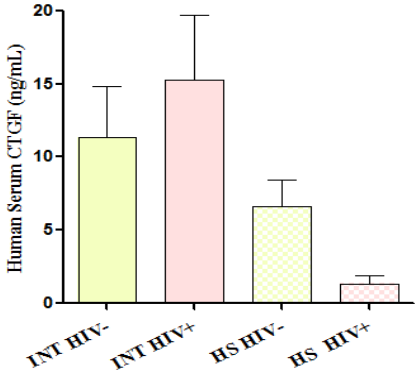

FIGURE 5.14 Human serum CTGF levels within INT and HS groups separated by HIV-1 co-infection status. Differences between the groups were not significant by Newman-Keuls Multiple Comparison Test.

Based on the results from the mouse liver and serum analyses, transferrin was one of the best candidate markers that showed significantly high abundance in HSS mice compared to MSS and control mice. In contrast, the human serum transferrin quantified using ELISA demonstrated similar levels for INT and HS (Figure 5.15) both within the normal human sera reference range (3.0 to 5.2 mg/ml, Serum transferrin assay kit, Alpha Diagnostic Intl., Inc., USA). When INT and HS serum transferrin was tested for patient groups divided into HIV-1 seronegative and seropositive categories, the HIV-1 seropositive groups showed lower transferrin levels. However, only sera from the INT HIV-1 seropositive patient group had significantly ($p \leq 0.05$) lower transferrin compared to its counterpart (Figure 5.16). The results from the HIV-1 co-infection serostatus may relate to the decreased abundance of transferrin a negative acute phase protein during infection.

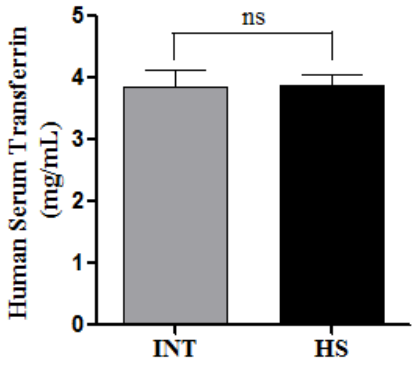

FIGURE 5.15 Human serum transferrin ELISA results. Shown are the means ± SEM. Levels in INT and HS groups were similar (ns, not significant).

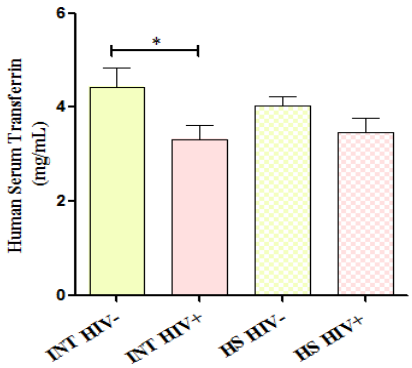

FIGURE 5.16 Human serum transferrin comparison within INT and HS groups separated by HIV-1 co-infection status, means ± SEM. *p ≤ 0.05 when INT HIV-1 negative compared to INT HIV-1 positive by Newman-Keuls Multiple Comparison Test.

During schistosomiasis granuloma formation and the resulting pathology depends on and is mediated by CD4 cells. Therefore, the CD4 count was evaluated which showed that persons with severe hepatosplenic disease displayed strikingly reduced peripheral blood T cells. The CD4 count was lower in HS patients than INT patients, although the comparison was not statistically significant (Figure 5.17). When divided into HIV-1 seronegative and seropositive categories, INT HIV-1 seropositive patients had significantly lower ($p \leq 0.01$) CD4 counts than their INT seronegative counterparts. HS HIV-1 seronegative and HS HIV-1 seropositive groups had similar CD4 counts but were significantly lower ($p \leq 0.05$) in comparison to INT HIV-1 seronegative patients (Figure 5.18). These results suggest that severe disease with HIV-1 coinfection results in reduced CD4 counts and may aggravate the disease.

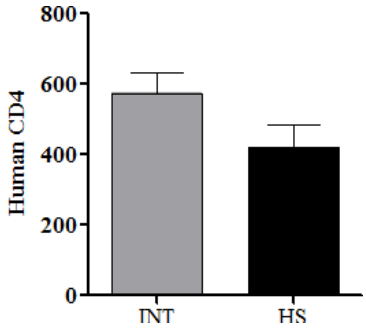

FIGURE 5.17 Human CD4 count comparison between INT and HS groups was not significant by Newman-Keuls Multiple Comparison Test.

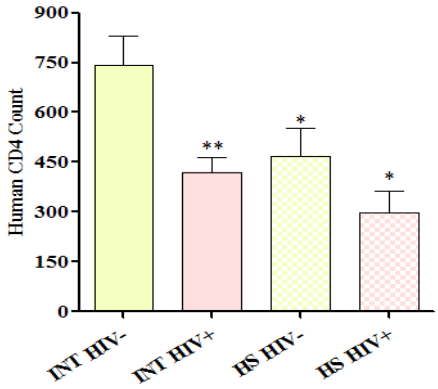

FIGURE 5.18 Human CD4 count comparison within INT and HS groups separated by HIV-1 co-infection status. The means ± SEM differed by 1-ANOVA ≤ 0.01 for all groups. *p ≤ 0.05 when HS HIV-1 seronegative and HS HIV-1 seropositive were compared to INT HIV-1 seronegative, ** p ≤ 0.01 when INT HIV-1 seropositive was compared to INT HIV-1 seronegative by Newman-Keuls Multiple Comparison Test.

When all the candidate protein markers were reviewed according to the image patterns as described by Mwinzi *et al.* (Mwinzi *et al.*, 2004) and the HIV-1 infection status none of the protein levels were statistically significant among the: IPA, IPC and IPD/E groups

except for serum hydroxyproline and CD4 counts. There were no HIV-1 seropositive patients in the IPD/E group.

Serum hydroxyproline was significantly higher in the IPD/E group than IPA and IPC. This correlates with the higher degree of fibrosis detected by ultrasound that is associated with the severe form of hepatosplenic disease (Figure 5.19). Categorising the serum hydroxyproline image patterns according to the HIV-1 seronegative and seropositive groups showed no statistical significance, however the hydroxyproline levels were lower in HIV-1 seropositive patients than the HIV-1 seronegative patients (Figure 5.20).

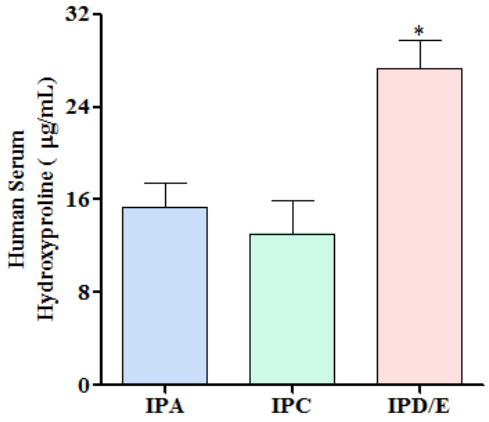

FIGURE 5.19 Human serum hydroxyproline compared according to ultrasound image patterns (fibrosis in IPA<IPC< IP/E). The means ± SEM differed in 1-ANOVA ≤ 0.05 for all groups, *p ≤ 0.05 when IPD/E was compared to IPA and IPC by Newman-Keuls Multiple Comparison Test.

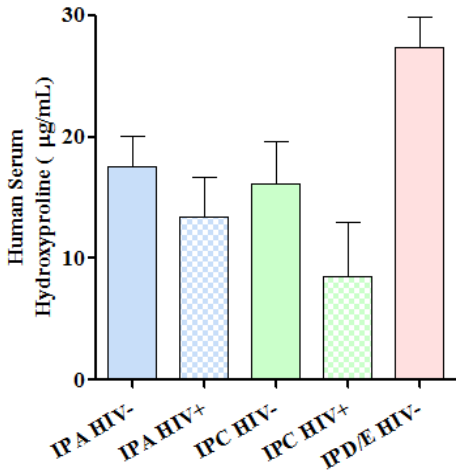

FIGURE 5.20 Human serum hydroxyproline levels according to ultrasound image patterns (fibrosis in IPA<IPC< IP/E) separated by HIV co-infection status, shown are the mean ± SEM, the group comparison was not statistically significant.

When the CD4 counts were evaluated according to the image patterns the differences were not statistically significant although IPD/E patients had low counts when compared to IPA and IPC (Figure 5.21). However, the HIV-1 co-infection status in the CD4 count subjects showed that HIV-1 seropositive patients had lower CD4 counts moreover severe hepatosplenic disease patients (IPD/E) had much lower CD4 counts when compared to moderate disease (IPA) and hepatosplenic (IPC) patients (Figure 5.22). Thus, interplay of the T cells between schistosomiasis and HIV-1 infection may possibly lead to the depletion of these cells and ultimately decreased immunity making the subject vulnerable to more infections.

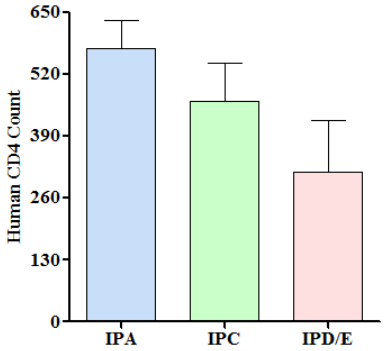

FIGURE 5.21 Human CD4 count according to ultrasound image patterns (fibrosis in IPA<IPC< IP/E), shown are the mean ± SEM, the group comparisons were not statistically significant.

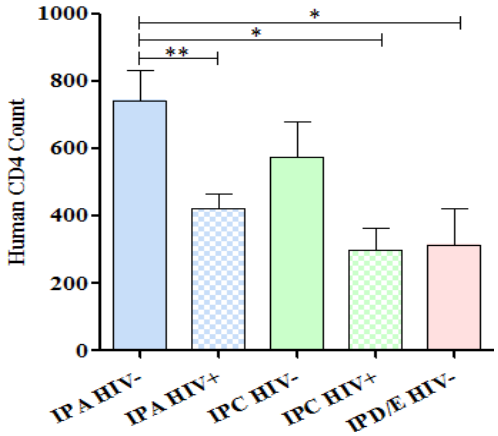

FIGURE 5.22 Human CD4 count comparison according to ultrasound image patterns (fibrosis in IPA<IPC< IP/E) separated by HIV co-infection status. The means ± SEM differed by 1-ANOVA ≤ 0.01 for all groups. ** p ≤ 0.01 when IPA HIV-1 seronegative were compared with IPA HIV-1 seropositive, *p ≤ 0.05 when IPA HIV-1 seronegative was compared with IPC HIV-1 seropositive and IPD/E HIV-1 seronegative by Newman-Keuls Multiple Comparison Test.

5.2.4 Multiple regression analysis

The candidate protein markers were normalised logarithmically (log_e) and entered into stepwise multivariate regression analysis to generate strong determinants of ultrasound detected fibrosis in human schistosomiasis. When all the ultrasound image patterns were combined together, cytokeratin 18 with r square=0.142, standardised β=0.377, p=0.031 was the only predictor of fibrosis in humans irrespective of the grading of the image pattern. These results indicate a possible role of this protein in the pathogenesis of human schistosomiasis and therefore might be a useful biomarker for the disease.

5.3 Discussion

5.3.1 Mouse serum analysis using 2D-DIGE

The results from the mouse serum 2D-DIGE experiments showed changes in many immune related proteins, consistent with previous findings (Jassim *et al.*, 1987, Pearce and MacDonald, 2002). The mouse serum 2D-DIGE analysis identified protein spots corresponding to **light immunoglobulin chains** (Figure 5.1, spots 1, 2, 14-17, Table 5.1) and **heavy immunoglobulin chains** (Figure 5.1, spots 9-13,Table 5.1). There was increased abundance of different isoforms of light and heavy immunoglobulins for MSS and HSS mice compared to control mice. In particular, the abundance of immunoglobulin gamma 1 heavy chain increased by almost 85-fold for HSS mice and 66-fold for MSS mice. The abundance of immunoglobulin kappa chain increased by almost 27-fold for HSS mice and 12-fold for MSS mice.

Complement C3 is a positive acute phase protein and it enhances Th2 responses during *S. mansoni* infection (La Flamme *et al.*, 2003a) and this may be a possible reason for the

increased abundance by 2-fold in MSS and HSS mice, thereby providing protection during parasitic infections.

We found five **haemoglobin** spots (Figure 5.1, spots 4-8, Table 5.1) decreased by 7 to 19 fold for HSS mice and 2 to 7 fold for MSS mice. The prevalence of anaemia is almost 66% in schistosome-infected women (Ajanga *et al.*, 2006) and highly prevalent in schistosome-infected children (Sturrock *et al.*, 1996). Studies ascribe the consumption of red blood cells by adult schistosomes as a possibility for the cause of anaemia. The reason that the adult *S. mansoni* pairs reside in the host blood vessels for lifetime and derive iron from haemoglobin from red blood cells required for their growth, development and reproduction (Brindley *et al.*, 1997) supporting the findings in our study and indicating severe anaemia in diseased mice.

We found **transthyretin** abundance decreased by 2-fold in MSS and HSS mice compared to control mice. Tansthyretin is a negative acute phase protein and serum and cerebrospinal fluid carrier of the thyroid hormone thyroxine and retinol. Decreased levels of transthyretin in human hepatosplenic schistosomiasis have been reported previously (Camacho-Lobato and Borges, 1998, Strauss, 2002) indicating liver dysfunction.

Importantly, the spot volume for serum **MUP** showed decreased abundance and serum **transferrin** spot volume showed increased abundance in HSS mice compared to MSS and control mice (Figure 5.2). These results were consistent with findings for the liver lysate 2D-DIGE and western blot analysis in Chapter 3. Estimation of these proteins in human sera may possibly generate biomarkers for hepatosplenic disease. Additionally, future

work will utilise methods to delete the high abundance proteins (albumin, immunoglobulins, haptoglobin and transferrin) as they represent >90% of all the serum proteins. This approach will allow a better analysis of the low abundance proteins that have significant changes during infection.

5.3.2 Mouse and human serum analysis using targeted assays

Comparison of proteomic patterns in livers and sera of mice with MSS and HSS led to the discovery of the candidate proteins as pathology markers in mouse and human sera. The candidates we identified for further analysis include the amino acid hydroxyproline, serum keratin D (cytokeratin 18), serum connective tissue growth factor and serum transferrin are discussed sequentially in relation to schistosomiasis pathology. To measure the changes in protein synthesis during schistosomiasis we assessed serum total protein.

The **serum total protein** was assessed to determine whether liver inflammation during disease is reflected in the circulating blood. Although serum total protein is a measure of protein turnover during disease state especially with nutritional problems, kidney disease or liver disease and assesses liver function, the mouse serum total protein profile in our study was similar between the five study groups (Figure 5.3). Our results in mice sera are consistent with the studies in *Schistosomiasis mansoni* mice (Rutkowski and Bruce, 1971), in schistosomiasis patients (Mousa *et al.,* 1976) and in Egyptian children with schistosomiasis, hepatitis B and C virus-related liver diseases which demonstrated similar serum total protein levels (Mahdy *et al.*, 2007). However, human schistosomiasis-HCV co-infection studies showed a 33% reduction in serum total protein concentrations (Fahim *et al.,* 2000). In contrast, a previous study demonstrated that mice with progressive *S.*

mansoni infection showed increase in serum total proteins (Evans and Stirewalt, 1957), similar to a serological study in rhesus monkeys infected with *S. mansoni* (Smithers and Walker, 1961). These studies support the results in our human sera study (Figure 5.8) where both INT and HS patients had increased protein. Further studies of specific proteins separately would be advantageous to assess the disease pathology.

Changes in mouse liver **hydroxyproline** levels were reflected in serum analysis. Mouse serum hydroxyproline was higher in HSS mice compared to MSS and control mice (Figure 5.4) consistent with the high results for liver hydroxyproline in HSS mice (Chapter 3). Our results are similar to the findings in toxicity induced hepatic fibrosis (George and Chandrakasan, 2000) and in *Schistosomiasis mansoni* at 10-week infection (Dunn *et al.*, 1977). The serum hydroxyproline levels in INT and HS patients were similar and higher than normal human sera (Figure 5.9). The results from the human sera support the findings from gingival fibroblasts (Heng *et al.*, 2006) and in patients with liver fibrosis (Attallah *et al.*, 2007). Our human sera data differed from the mouse serum data in that it failed to differentiate between the moderate and severe disease. However, when serum hydroxyproline levels were analysed according to the ultrasound image pattern categories (Figure 5.19), patients with IPD/E had significantly higher levels than person with IPA and IPC, consistent with the findings in ultrasound detected fibrosis (Mwinzi *et al.*, 2004) suggesting that serum hydroxyproline levels reflect the degree of fibrosis in human schistosomiasis. Additionally, sera from persons with HIV-1 seropositive category showed lower hydroxyproline levels than HIV-1 seronegative category, although this was only statistically significant ($p \leq 0.05$) among groups with the HS disease form (Figure 5.10). Serum hydroxyproline in other viral infection studies showed increased levels of the

protein due to increased collagen synthesis and degradation (Attallah *et al.*, 2007, Kucharz, 1984) indicating altered collagen synthesis and degradation in schistosomiasis and HIV-1 co-infections. Previous HIV-1 infection studies show similar ultrasound detectable fibrosis in HIV-1 seronegative and HIV-1 seropositive patients with schistosome infection (Secor, 2006). The results in our study indicate that HIV-1 co-infection during schistosomiasis reduces the fibrosis or the HIV-1 infection in itself creates immune deficiency that alleviates the impact of schistosome infection on the liver (Figure 5.20), thus indicating the limitations of ultrasound for detection of fibrosis in schistosomiasis and the importance of serum hydroxyproline detection in these subjects. In addition, if the IPD/E patients were HIV-1 seropositive, this could mean that these patients may have decreased fibrosis or if the HIV-1 co-infection is severe it may lead to death.

The serum **keratin D** (cytokeratin 18) western blot confirmed the liver 2D-DIGE results and showed a strong relationship between HSS mice and serum keratin D levels (Figure 5.5). Supporting the mouse serum data, the human serum western blot showed significantly increased keratin D levels in HS patients when compared to INT and normal subjects (Figure 5.11). Studies in non-alcoholic liver disease have recorded high levels of serum keratin D similar to our study (Aoyama and Tanaka, 2009, Vos *et al.*, 2008). Keratin D is similar to human cytokeratin 18 and acidic forms of this protein have been demonstrated in alcoholic hepatitis and hepatic steatosis (Salmhofer *et al.*, 1994). Furthermore, analysis of the modification pattern of keratin D associated with schistosomiasis might identify a specific pattern, which relates to the severity of disease. HIV-1 co-infection showed there was no significant difference between seronegative and seropositive patients, but the INT seronegative patients had lower keratin D levels

compared to HS seronegative patients (Figure 5.12). Together, the data suggests that HIV-1 co-infection does not affect keratin D levels. Additionally, keratin D emerged as a possible predictor of ultrasound detected fibrosis in human schistosomiasis supporting the findings in chronic HCV infection associated fibrosis (Strnad *et al.*, 2006). Our study showed increased levels of keratin D in mouse and human serum studies, verifying these results on a larger number of human serum samples may generate a clearer picture of the relevance of this protein to the disease state.

Connective tissue growth factor is triggered by TGF-β during hepatic fibrosis and is highly expressed in fibrotic tissues. As a result, CTGF can be used as a measure of collagen synthesis. In our study, CTGF levels were significantly elevated in HSS compared to control and MSS mice, reflecting extensive fibrosis in the severe form of the disease (Figure 5.6). A study in transgenic livers *in vivo* demonstrated elevated levels of CTGF mRNA and CTGF protein (Tong *et al.*, 2009). Another study showed high serum CTGF levels are a useful non-invasive biomarker for assessment of liver fibrosis (Kovalenko *et al.*, 2009). These studies are in line with our findings and support CTGF as a candidate marker for human hepatosplenic schistosomiasis. However, in our study, human serum CTGF levels were higher in INT patients than in individuals with HS patients ($p \leq 0.01$, Figure 5.13). This contrasts a recent study conducted in schistosome-infected Chinese, Sudanese, and Brazilians subjects that reported two single nucleotide polymorphisms (rs9402373 and rs12526196) located close to the CTGF gene as valuable markers for disease progression in schistosomiasis hepatic fibrosis (Dessein *et al.*, 2009). The HS CTGF levels were lower than the INT patients irrespective of the HIV-1 serostatus, the comparisons were not statistically significant (Figure 5.14). Our results

indicate that CTGF is potential marker for INT although further investigation using larger sample size as well as other co-infected (other helminth) serum samples may help in the validation.

The results for mouse **serum transferrin** western blot data showed high abundance in HSS mice (Figure 5.7) comparable to data from 8-week *S. mansoni* infections in C57BL/6 mice (Harvie *et al.*, 2007) and in Nigerian woman with urinary schistosomiasis (Salawu and Arinola, 2004). In contrast, previously it has been reported that reduced serum transferrin levels are a manifestation of hepatosplenomegaly in Egyptian schistosomiasis patients (Saif *et al.*, 1977), analogous to the study in *S. mansoni* 8-week infected mice (El-Rigel and Hetta, 2006). The human serum transferrin analysis in our study showed similar levels in INT and HS patients (Figure 5.15) which were in the normal reference range for humans (3.0 - 5.2 mg/mL). HIV-1 co-infection resulted in decreased levels of transferrin compared to seronegative subjects; this difference was statistically significant within the INT patient groups ($p \leq 0.05$, Figure 5.16). The decreased levels of serum transferrin in HIV-1 co-infection reflect the role of transferrin as an acute phase protein that decreases with inflammation during HIV-infection.

The CD4 count showed results consistent with previous observations that persons with severe hepatosplenic disease present with reduced amounts of blood T cells (Figure 5.17). The CD4 counts in INT and HS seronegative and seropositive patients were discussed previously (Mwinzi *et al*., 2004) and showed reduced CD4 counts in HIV-1 seropositive individuals (Figure 5.18). In addition, the authors found an effect of ultrasound-detectable fibrosis leading to lower CD4 counts in IPD/E patients compared to IPA and IPC (Figure

5.21). HIV-1 co-infection status showed seronegative schistosomiasis patients had high CD4 count than seropositive patients (Figure 5.22) (Mwinzi *et al.*, 2004).

5.4 Conclusion

The serum 2D-DIGE maps showed distinctive serum protein patterns between MSS and HSS mice, in particular the heavy and light immunoglobulin protein spot patterns were also distinct and different. MUP and transferrin emerged as protein markers for HSS mice and complement component 3, transthyretin being infection specific. Importantly, the serum CyDye labelling saturated the high abundant proteins with the CyDyes and reduced the sensitivity for low abundant proteins. Therefore, selective immunodepletion of serum for high abundant proteins (albumin, immunoglobulins, transferrin, and haptoglobin) may allow detection of the serum for low abundant proteins that will aid in detecting diagnostic markers for schistosome-mediated liver disease. The present investigation demonstrated a strong correlation between the mouse serum data and the mouse liver data. However, the human serum data did not produce the same results for all the candidate protein markers. In particular, human serum total protein, CTGF and transferrin results were not consistent with the findings in the mouse serum data. Human CTGF levels were high in INT patients. The human serum hydroxyproline and keratin D had comparable results to the mouse serum data. Human hydroxyproline and keratin D proved to be useful for assessing severe schistosomiasis. However, future studies should include MUP and *Sm*-PEPCK as markers for pathology in human schistosomiasis. Because some of the serum samples came from HIV-1 seropositive subjects, we tested what effect this co-infection may have on the serum results. Only hydroxyproline and transferrin were affected by HIV-1 co-infections, with both markers being decreased in seropositive patients. Further studies with larger

patient populations would help to validate the candidate protein markers as predictors of schistosomiasis pathology. Taken together the results indicate the importance of hydroxyproline, keratin D and CTGF as promising candidates for elaborate sero-epidemiological studies, which may help in differentiating the intestinal and hepatosplenic schistosomiasis.

CHAPTER 6: DISCUSSION

6.1 Summary of this research

The primary aim of this project was to identify candidate liver protein markers in mice, which could serve as diagnostic markers for human hepatosplenic schistosomiasis. A secondary aim was to assess differential protein abundance during moderate splenomegaly and hypersplenomegaly syndromes in CBA/J mice, to understand the underlying pathological mechanisms that direct the development of these 2 disease forms found in human schistosomiasis. Using a proteomic approach to compare the liver and serum protein profiles, the global impact of schistosome infection on the liver could be determined at various times post infection. Together these experiments using the mouse model identified several candidate markers including transferrin, MUP, keratin D, CTGF, and hydroxyproline. However, analysis of the serum samples from infected subjects revealed that of these candidates only keratin D and hydroxyproline served as robust markers of HS. Overall, these studies have identified and validated unique candidate markers for future development and have revealed distinct and specific changes in liver protein expression during infection that may help elucidate the molecular mechanisms of disease pathology during schistosomiasis.

6.1.1 Candidate markers of fibrosis

The two marked pathological features of chronic schistosomiasis, granulomatous lesions (Stadecker, 1999) and fibrosis (Boros, 1989), differ among the intestinal and hepatosplenic forms. Our study identified and examined the expression of extracellular matrix associated proteins that are essential to these two processes including collagen,

hydroxyproline, and connective tissue growth factor (CTGF). Collagen isoforms 6a1 and IVX were the major collagen isoforms identified and have been previously associated with fibrotic transformation in alcoholic liver (Stickel *et al.*, 2001). While collagen isoforms did not reach significance in our time point experiment, two collagen-associated proteins/products, hydroxyproline and CTGF were significantly correlated with hepatosplenic disease. Hydroxyproline, an amino acid found in collagen, increased in severe disease in mice and human sera and reflected fibrosis in severe hepatosplenic disease. Our study is the first to measure hydroxyproline in the serum of subjects with schistosomiasis and to demonstrate a significant correlation between serum levels and fibrosis.

CTGF induces collagen synthesis during liver fibrogenesis (Paradis *et al.*, 1999) but its role in schistosome-mediated liver fibrosis is unknown. CTGF may also induce collagen synthesis and fibrosis in schistosome infection, or alternatively, the fibrosis may result from impaired collagen degradation and be independent of CTGF. Indeed, a study by Andrade *et al*. demonstrated that collagen synthesis and degradation occur at the same time (Andrade, 1992). Our results showed that while mouse serum CTGF levels were high in HSS mice, the human serum CTGF levels were specifically increased in INT patients. These contradictory results suggest that there is differential regulation of the fibrotic process in our experimental model and in human schistosomiasis. However, CTGF may still prove a useful inverse correlate of fibrosis in human schistosomiasis, and further studies into the involvement of CTFG in human schistosomiasis are merited.

6.1.2 Candidate markers of inflammation

The 2D-DIGE study revealed that the negative acute phase proteins: transferrin, albumin, group specific component and retinol binding protein increased during severe disease, which is in contrast to their expected function during inflammation. This association of negative acute phase reactants with schistosome infection is unique to our study. Increased transferrin has been described by (Potter *et al.*, 1985) in alcoholic liver disease and increased retinol binding protein has been described by (Uchio *et al.*, 2002) in hepatic fibrogenesis similar to the findings in our study indicating that evaluation of these protein in mouse and human sera may be useful. However, evaluation of transferrin levels in human subjects indicated that the levels were within the normal range. Whether this lack of correlation to disease is due to fundamental differences between human disease and our mouse model or some unknown confounding disease interaction is unclear. Nevertheless, these results indicate that transferrin, despite its promising results, is not a useful biomarker

Xenobiotic metabolising proteins, which should increase in parasitic infections for removal of reactive oxygen species and toxic products generated due to infection, were decreased in abundance at 8-weeks, 12-weeks, and 20-weeks post infection, which is another major finding from our study. Most significantly, three spots with epoxide hydrolase activity were decreased with severe schistosome infection contradictory to the report by Murray *et al.* (1993) and one spot with peroxiredoxin 6 activity decreased in abundance in HSS mice similar to the study by Roede *et al.* (2008). While these proteins were not assessed in the serum by targeted assays, given their strong and unique

associations with disease, they have potential as markers and thus warrant further investigation.

6.1.3 Other candidate markers

Two novel proteins that were identified as potential markers of diagnostic value were MUP and *Sm*-PEPCK. MUP, a pheromone protein with similarity to human epididymal-specific lipocalin-9, decreased in HSS mice when compared to 6-week, 8-week, and 12-week and MSS infected mice. The decreased abundance of MUP was confirmed by western blot technique in liver and serum and consistent with the report in murine hepatocarcinogenesis (Dragani *et al.*, 1989) suggesting that assessment of this protein in human sera may help identify hepatosplenic schistosomiasis. One drawback to the use of this protein is that it is considered to be male-specific, thus the usefullness as a disease form biomarker for all schistosomiasis patients is unclear.

Sm-PEPCK a parasite protein showed increased abundance in MSS and HSS mice. Although using Western blot we found that murine PEPCK was also increased in the livers of MSS and HSS mice, we confirmed that the PEPCK identified by 2D-DIGE was parasite-derived by soluble egg antigen electrophoresis and mass spectrometry. We believe that *Sm*-PEPCK may be useful as an infection specific marker or possibly a therapeutic target. A previous study has described it as a novel egg antigen for schistosome infection (Asahi *et al.*, 2000) and indicated the role for this protein in the pathogenesis of schistosomiasis.

6.1.4 Disease kinetics

The 2D-DIGE map comparison for 6-week, 8-week, 12-week, 20-week infection with control CBA/J mice identified 34 protein spots that showed increased abundance and 94 protein spots that showed decreased abundance during 12-week infection alone, verifying the fact that 12-week mice have severe liver dysfunction compared to any other study groups. In particular, at 12-week infection proteins associated with amino acid metabolism, fatty acid metabolism, one carbon metabolism, redox reactions and xenobiotic metabolism were decreased and specifically there was decreased abundance of basic proteins (pI range 6-11) at 12-week infection. Although, 12-week infected mice showed profound changes in greatest number of protein spots, 8-week infected mice also showed significant changes and 20-week infected mice showed greatest magnitude of changes indicating that all the three time points post-infection are critical during the pathogenesis of schistosomiasis.

6.1.5 Statistical analyses for identification of candidates

The multivariate cluster analysis using PCA and HCA, aided in confirming the differentially expressed protein patterns distinct for HSS and MSS mice and 8-week and 12-week infected mice with especially high %SBW. These results indicate that certain mechanisms or molecules in mice and/or the parasite contribute towards the segregation of these infected groups into MSS and HSS mice. Multiple regression analysis of the various proteins related to disease progression identified liver hydroxyproline, a measure of collagen synthesis and damage, as the strongest predictor of splenomegaly and hepatomegaly. Once hydroxyproline was removed, the next strongest indicator of splenomegaly was keratin D. Moreover, our analysis of mouse and human serum samples for hydroxyproline and keratin D, confirmed these results. Finally, our multiple regression

analysis identified MUP, *Sm*-PEPCK, transferrin and peroxiredoxin 6 as liver proteins that appear to act synergistically during the pathogenesis of murine schistosomiasis. Together these analyses have revealed not only potential biomarkers for hepatosplenomegaly but also possible molecular interactions that may be involved in the pathogenesis of severe disease.

6.1.6 Validation of candidate protein markers

Using targeted assays, we investigated the usefulness of the candidates identified from the mouse liver and serum 2D-DIGE studies. Contrary to our expectations, the human serum analysis showed diverse results compared to mouse serum data. The human CTGF was significantly high in INT patients than HS patients. The keratin D results were similar to the mouse serum analysis and showed significantly higher levels in HS patients than INT patients. Human serum hydroxyproline were similar in INT and HS patients although higher than normal subjects. However, when stratified for ultrasound-assessed fibrosis, hydroxyproline did correlate with severe fibrosis suggesting that it may only serve as a late and not an early marker of fibrosis. Ultimately, our study was successful in identifying candidate liver protein markers for human hepatosplenic schistosomiasis. We believe that keratin D may serve as a marker for HS and CTGF as a marker for INT patients, while serum hydroxyproline may reflect late stage fibrosis.

6.2 Future directions

CBA/J mouse model is an excellent model for future experiments related to schistosomiasis disease forms and hepatic fibrosis. Using the CBA/J mouse model at early infections, as early as 1, 2, 3, 4, 5, 6 week and applying the 2D-DIGE approach and

depletion of highly abundant proteins, low abundance proteins can be targeted. The present study was successful in identifying candidate liver protein markers; however, 2D-DIGE experiments using narrow range IPG Dry strips might be useful in targeting proteins that have co-migrated due to similar pI or molecular weight. One important fact that cannot be ignored is that disease in the mice is a result of the single exposure to the parasite while in the human disease is a consequence of successive re-infections and therefore it would be worth investigating the protein abundance in mouse re-infections. This approach will identify proteins expressed during re-infections.

Using high-throughput mass spectrometry like tandem mass spectrometry and liquid chromatography-mass spectrometry (LC/MS/MS) systems may identify post-translational modifications (e.g. glycosylation, phosphorylation, hydroxylation) of proteins that are unique during schistosomiasis disease. Although, two-dimensional electrophoresis coupled to mass spectrometry is the most versatile technique in proteomic analysis (Penque, 2009), a review by (Lambert *et al.*, 2005) enumerates the importance of gel-free techniques coupled with Surface-Enhanced Laser Desorption/Ionization Time-of-Flight Mass Spectrometry (SELDI-TOF MS), liquid chromatography (LC/MS) and Capillary Electrophoresis (CE)-MS to identify novel biomarkers. The above techniques together with multiple reaction monitoring assays could help separate and identify individual liver derived protein and peptide constituents in plasma (McKay *et al.*, 2007), from either host or parasite with potentials of a biomarker. Furthermore, quantitative differences among control and diseased samples can be analysed using label based methods such as ICAT (isotype-coded affinity tag) or $^{16}O/^{18}O$ labelling or iTRAQ (isobaric tag for relative and absolute quantification) (Shen *et al.*, 2006). Label free methods such as mass spectral peak

intensities of peptide ions (ratios of ion intensities for peptides) and spectral counting (number of spectra per protein) (Old *et al.,* 2005) are promising methods to measure differential changes in protein abundance during disease. Using these approaches will solve certain problems in 2D-DIGE techniques like streaky protein migration and inconsistent resolving of protein spots on the gel, which makes biomarker discovery difficult.

Immunohistochemical localisation of identified proteins related to disease in non-infected and infected liver tissue using confocal microscopy can explain the possible reasons for the increased or decreased abundance of proteins during the progression of the disease. This experiment could also help understand whether the proteins are increased as a result of immune cell activity of liver granuloma or hepatocyte interactions with the liver granuloma. Conversely, immunoprecipitation can be used to validate the identified protein spots by using targeted antibodies.

Two important proteins identified by this study were MUP and *Sm*-PEPCK as predictors of splenomegaly. MUP has similarity to human epididymal-specific lipocalin-9 and *Sm*-PEPCK is a parasitic protein makes further research more interesting. Detection antibody is available for human epididymal-specific lipocalin-9 and could be used to monitor the protein pattern in early and late stages of human schistosomiasis. *Sm*-PEPCK antibody engineering and designing is a complex process, therefore alternatively, high-throughput mass spectrometry coupled with information from schistosome database (Berriman *et al.*, 2009) could help quantify the *Sm*-PEPCK protein in mouse serum, liver and human serum samples as well as detect whether the protein is post-translationally modified during

schistosome infection. This strategy might identify a potential drug target for treatment of schistosomiasis disease. The peculiar abundance pattern of peroxiredoxin6 in MSS and HSS mice requires more in-depth study to determine whether this pattern is due to over oxidation of the protein or decreased synthesis of the protein during schistosome infection.

Because 2D-DIGE requires very small sample volume, using the finger prick method to collect human serum samples, and a similar experiment based on the mouse serum 2D-DIGE in our study with depletion techniques can allow identification of low abundant protein patterns in human intestinal and hepatosplenic schistosomiasis. Moreover, human serological studies require large number of serum samples for candidate protein markers to be established as "biomarkers" (Schulz and Grimes, 2005) therefore detection of the candidate protein markers: CTGF, hydroxyproline and keratin D in a large sample size can help establish a reference range for these proteins.

Finally, because schistosome infection does not occur in isolation, studying how the expression of our candidate protein markers is altered during other parasitic infections that invade the liver like *Fasciola hepatica* and *P. falciparum* would determine the specificity of the protein candidates for *S. mansoni* infections. Additionally, examination of the candidate protein markers in human serum samples from liver fibrosis, liver cirrhosis, hepatocellular carcinoma, hepatitis, alcoholic liver disease and non-alcoholic liver disease will confirm or refute whether the disease-specific protein abundance patterns we observed in our candidates are unique to schistosomiasis-induced fibrosis or reflect a more general inflammation-mediated fibrotic process.

REFERENCES

Abdel-Wahab, M. F., G. Esmat, A. Farrag, Y. A. El-Boraey, and G. T. Strickland. 1992. Grading of hepatic schistosomiasis by the use of ultrasonography. American Journal of Tropical Medicine and Hygiene 46:403-408.

Abdella Eltoum, I., H. W. Ghalib, A. F. A. Gadir, S. M. Suliaman, and M. M. A. Homeida. 1991. Lack of association between schistosomiasis and hepatitis B virus infection in Gezira-Managil area, Sudan. Transactions of the Royal Society of Tropical Medicine and Hygiene 85:81-82.

Agaton, C., J. Galli, I. H. Guthenberg, L. Janzon, M. Hansson, A. Asplund, E. Brundell, S. Lindberg, I. Ruthberg, K. Wester, D. Wurtz, C. Höög, J. Lundeberg, S. Ståhl, F. Pontén, and M. Uhlén. 2003. Affinity proteomics for systematic protein profiling of chromosome 21 gene products in human tissues. Molecular and Cellular Proteomics 2:405-414.

Ajanga, A., N. J. S. Lwambo, L. Blair, U. Nyandindi, A. Fenwick, and S. Brooker. 2006. Schistosoma mansoni in pregnancy and associations with anaemia in northwest Tanzania. Transactions of the Royal Society of Tropical Medicine and Hygiene 100:59-63.

Al-Sherbiny, M., A. Osman, K. Hancock, A. Deelder, and V. Tsang. 1999. Application of immunodiagnostic assays: detection of antibodies and circulating antigens in human schistosomiasis and correlation with clinical findings. American Journal of Tropical Medicine and Hygiene 60:960-966.

Altmann, F. 2007. The role of protein glycosylation in allergy. International Archives of Allergy Immunology 142:99-115.

Aly, H. F., and S. A. Aly. 2006. Essential role of Citrus reticulata and mirazid in treatment of Schistosoma mansoni infected mice: biochemical and parasitological studies. Polish Journal of Food and Nutrition Sciences 15/56:461-467.

Ancelin, M. L., G. Torpier, H. J. Vial, and A. Capron. 1987. Choline incorporation by Schistosoma mansoni: distribution of choline metabolites during development and after sexual differentiation. Journal of Parasitology 73:530-535.

Andrade, Z. A. 1992. Morphological features of collagen degradation in advanced hepatic schistosomiasis of man. Memorias do Instituto Oswaldo Cruz 87 Suppl 4:129-138.

Andrade, Z. A., and W. N. Abreu. 1971. Follicular lymphoma of the spleen in patients with hepatosplenic schistosomiasis mansoni. American Journal of Tropical Medicine and Hygiene 20:237-243.

Andrade, Z. A., E. Peixoto, S. Guerret, and J. Grimaud. 1992. Hepatic connective tissue changes in hepatosplenic schistosomiasis. Human Pathology 23:566-573.

Aoyama, T., and N. Tanaka. 2009. Serum cytokeratin 18 levels are useful biomarkers for estimating the histological activity score of nonalcoholic fatty liver disease. Chemistry and Physics of Lipids 160:S43-S43.

Araujo, M. I., and E. M. De Carvalho. 2006. Human schistosomiasis decreases immune responses to allergens and clinical manifestations of asthma. Chemical Immunology and Allergy 90:29-44.

Arinola, O. G. 2004. Metal binding acute phase proteins and trace elements in Nigerian children with urinary schistosomiasis. Biokemistri 16:23-27.

Asahi, H., A. Osman, R. M. Cook, P. T. LoVerde, and M. J. Stadecker. 2000. Schistosoma mansoni phosphoenolpyruvate carboxykinase, a novel egg antigen: immunological properties of the recombinant protein and identification of a T-cell epitope. Infection and Immunity 68:3385-3393.

Asamoto, M., and S. M. Cohen. 1994. Prohibitin gene is overexpressed but not mutated in rat bladder carcinomas and cell lines. Cancer Letters 83:201-207.

Attallah, A. M., E. A. Toson, G. E. Shiha, M. M. Omran, M. M. Abdel-Aziz, and I. El-Dosoky. 2007. Evaluation of serum procollagen aminoterminal propeptide III, laminin, and hydroxyproline as predictors of severe fibrosis in patients with chronic Hepatitis C. Journal of Immunoassay and Immunochemistry 28:199 - 211.

Badawi, A. F., D. P. Cooper, M. H. Mostafa, M. J. Doenhoff, A. Probert, P. Fallon, R. Cooper, and P. J. O'Connor. 1993. Promutagenic methylation damage in liver DNA of mice infected with Schistosoma mansoni. Carcinogenesis 14:653-657.

Basile, D., G. Bon, E. Lecuyer, M. Gosset, and Y. Douadi. 2007. Co-infection Schistosoma mansoni and Mycobacterium tuberculosis, about a case and literature review. Travel medicine and infectious disease 5:412-413.

Bastos, R., P. Engel, C. Pujades, R. Falchetto, R. Aligue, and O. Bachs. 1992. Increase of cytokeratin D during liver regeneration: Association with the nuclear matrix. Hepatology 16:1434-1446.

Battista, S., F. Bar, G. Mengozzi, E. Zanon, M. Grosso, and G. Molino. 1997. Hyperdynamic circulation in patients with cirrhosis: direct measurement of nitric oxide levels in hepatic and portal veins. Journal of Hepatology 26:75-80.

Beddek, A. J., P. Rawson, L. Peng, R. Snell, K. Lehnert, H. E. Ward, and T. W. Jordan. 2008. Profiling the metabolic proteome of bovine mammary tissue. Proteomics 8:1502-1515.

Bedwani, R., E. Renganathan, F. El Kwhsky, C. Braga, H. H. Abu Seif, T. Abul Azm, A. Zaki, S. Franceschi, P. Boffetta, and C. La Vecchia. 1998. Schistosomiasis and the risk of bladder cancer in Alexandria, Egypt. British Journal of Cancer 77:1186-1189.

Berhe, N., B. Myrvang, and S. G. Gundersen. 2007. Intensity of Schistosoma mansoni, Hepatitis B, age, and sex predict levels of hepatic periportal thickening/fibrosis (PPT/F): A large-scale community-based study in Ethiopia. American Journal of Tropical Medicine and Hygiene 77:1079-1086.

Berriman, M., B. J. Haas, P. T. LoVerde, R. A. Wilson, G. P. Dillon, G. C. Cerqueira, S. T. Mashiyama, B. Al-Lazikani, L. F. Andrade, P. D. Ashton, M. A. Aslett, D. C. Bartholomeu, G. Blandin, C. R. Caffrey, A. Coghlan, R. Coulson, T. A. Day, A. Delcher, R. DeMarco, A. Djikeng, T. Eyre, J. A. Gamble, E. Ghedin, Y. Gu, C. Hertz-Fowler, H. Hirai, Y. Hirai, R. Houston, A. Ivens, D. A. Johnston, D. Lacerda, C. D. Macedo, P. McVeigh, Z. Ning, G. Oliveira, J. P. Overington, J. Parkhill, M. Pertea, R. J. Pierce, A. V. Protasio, M. A. Quail, M.-A. Rajandream, J. Rogers, M. Sajid, S. L. Salzberg, M. Stanke, A. R. Tivey, O. White, D. L. Williams, J. Wortman, W. Wu, M. Zamanian, A. Zerlotini, C. M. Fraser-Liggett, B. G. Barrell, and N. M. El-Sayed. 2009. The genome of the blood fluke Schistosoma mansoni. Nature 460:352-358.

Biempica, L., M. A. Dunn, I. A. Kamel, R. Kamel, P. K. Hait, C. Fleischner, S. L. Biempica, C. H. Wu, and M. Rojkind. 1983. Liver collagen-type characterization in human schistosomiasis: A histological, ultrastructural, and immunocytochemical correlation. American Journal of Tropical Medicine and Hygiene 32:316-325.

Blanc, J., C. Lalanne, C. Plomion, J. Schmitter, K. Bathany, J. Gion, P. Bioulac-Sage, C. Balabaud, M. Bonneu, and J. Rosenbaum. 2005. Proteomic analysis of

differentially expressed proteins in hepatocellular carcinoma developed in patients with chronic viral hepatitis C. Proteomics 5:3778-3789.

Boehme, M. W. J., P. K. Kataaha, and E. J. Holborow. 1989. Autoantibodies to intermediate filaments in sera of patients with Schistosoma mansoni infection. Clinical and Experimental Immunology 77:230-233.

Bolarin, D. M., K. Barker, and G. C. Fuller. 1985. Serum and liver enzymes of collagen synthesis in hepatic murine schistosomiasis mansoni. Transactions of the Royal Society of Tropical Medicine and Hygiene 79:826-830.

Booth, M., J. K. Mwatha, S. Joseph, F. M. Jones, H. Kadzo, E. Ireri, F. Kazibwe, J. Kemijumbi, C. Kariuki, G. Kimani, J. H. Ouma, N. B. Kabatereine, B. J. Vennervald, and D. W. Dunne. 2004. Periportal fibrosis in human Schistosoma mansoni infection is associated with low IL-10, low IFN-gamma, high TNF-alpha, or low RANTES, depending on age and gender. Journal of Immunology 172:1295-1303.

Boros, D. L. 1989. Immunopathology of Schistosoma mansoni infection. Clinical Microbiology Reviews 2:250-269.

Brindley, P. J., B. H. Kalinna, J. P. Dalton, S. R. Day, J. Y. M. Wong, M. L. Smythe, and D. P. McManus. 1997. Proteolytic degradation of host hemoglobin by schistosomes. Molecular and Biochemical Parasitology 89:1-9.

Brito, E., F. Santoro, and H. Rocha. 1979. Immune complexes in schistosomiasis. VI. Circulating IC levels in patients with and without nephropathy. Revista do Instituto de Medicina Tropical de Sao Paulo 21:119-124.

Brouwer, K. C., P. D. Ndhlovu, Y. Wagatsuma, A. Munatsi, and C. J. Shiff. 2003. Epidemiological assessment of Schistosoma haematobium induced kidney and bladder pathology in rural Zimbabwe. Acta Tropica 85:339-347.

Brown, M., G. Miiro, P. Nkurunziza, C. Watera, M. A. Quigley, D. W. Dunne, J. A. Whitworth, and A. M. Elliott. 2006. Schistosoma mansoni, nematode infections, and progression to active tuberculosis among HIV-1-infected Ugandans. The American Society of Tropical Medicine and Hygiene 74:819-825.

Brunet, L. R., D. W. Dunne, and E. J. Pearce. 1998. Cytokine interaction and immune responses during schistosoma mansoni Infection. Parasitology Today 14:422-427.

Caldas, I. R., A. C. Campi-Azevedo, L. F. A. Oliveira, A. M. S. Silveira, R. C. Oliveira, and G. Gazzinelli. 2008. Human schistosomiasis mansoni: Immune responses during acute and chronic phases of the infection. Acta Tropica 108:109-117.

Camacho-Lobato, L., and D. R. Borges. 1998. Early liver dysfunction in schistosomiasis. Journal of Hepatology 29:233-240.

Capuano, F., F. Guerrieri, and S. Papa. 1997. Oxidative phosphorylation enzymes in normal and neoplastic cell growth. Journal of Bioenergetics and Biomembranes 29:379-384.

Carneiro-Santos, P., O. Martins-Filho, L. F. Alves-Oliveira, A. M. S. Silveira, P. Coura-Filho, I. R. C. Viana, R. A. Wilson, and R. Correa-Oliveira. 2000. Apoptosis: a mechanism of immunoregulation during human schistosomiasis mansoni. Parasite Immunology 22:267-277.

Cetre-Sossahc. C. B. , M. A. M., G. L. Freeman Jr., M. T. Willard, D. G. Colley, and W. E. Secor. 2007. Early responses associated with chronic pathology in murine schistosomiasis. Parasite Immunology 29:241-249.

Cheever, A. W., and M. Barral-Netto. 1985. Fibroblast stimulating activity of extracts of hepatic granulomata of Schistosoma mansoni-infected rodents with marked or slight hepatic fibrosis. Transactions of the Royal Society of Tropical Medicine and Hygiene 79:319-321.

Cheever, A. W., J. A. Lenzi, H. L. Lenzi, and Z. A. Andrade. 2002. Experimental models of Schistosoma mansoni infection. Memorias do Instituto Oswaldo Cruz 97:917-940.

Cheever, A. W., Y. Xu, J. G. Macedonia, T. Cox, S. Hieny, and A. Sher. 1992. The role of cytokines in the pathogenesis of hepatic granulomatous disease in Schistosoma mansoni infected mice. Memorias do Instituto Oswaldo Cruz 87 Suppl 4:81-85.

Chen, H. B., K. Pan, M. K. Tang, Y. L. Chui, L. Chen, Z. J. Su, Z. Y. Shen, E. M. Li, W. Xie, and K. K. H. Lee. 2008. Comparative proteomic analysis reveals differentially expressed proteins regulated by a potential tumor promoter, BRE, in human esophageal carcinoma cells. Biochemistry and Cell Biology 86:302-311.

Cheng, O., R. Thuillier, E. Sampson, G. Schultz, P. Ruiz, X. Zhang, P. S. T. Yuen, and R. B. Mannon. 2006. Connective tissue growth factor is a biomarker and mediator of kidney allograft fibrosis. American Journal of Transplantation 6:2292-2306.

Chevallet, M., E. Wagner, S. Luche, A. van Dorsselaer, E. Leize-Wagner, and T. Rabilloud. 2003. Regeneration of peroxiredoxins during recovery after oxidative stress. Journal of Biological Chemistry 278:37146-37153.

Chiarini, L., C. Takiya, R. Borojevic, and A. Monteiro. 2006. Long-term culture of cholangiocytes from liver fibro-granulomatous lesions. BMC Gastroenterology 6:13.

Chiavaroli, R., and P. Grima. 2008. Detection of early liver fibrosis in patients with intestinal schistosomiasis: Sonographic and histologic findings in Schistosoma mansoni Infection. Infection 36:585-589.

Chich, J.-F., O. David, F. Villers, B. Schaeffer, D. Lutomski, and S. Huet. 2007. Statistics for proteomics: Experimental design and 2-DE differential analysis. Journal of Chromatography B 849:261-272.

Chitsulo, L., D. Engels, A. Montresor, and L. Savioli. 2000. The global status of schistosomiasis and its control. Acta Tropica 77:41-51.

Chu, P., J. Pardo, H. Zhao, C. C. Li, E. Pali, M. M. Shen, K. Qu, S. X. Yu, B. C. B. Huang, P. Yu, E. S. Masuda, S. M. Molineaux, F. Kolbinger, G. Aversa, J. De Vries, D. G. Payan, and X. C. Liao. 2003. Systematic identification of regulatory proteins critical for T-cell activation. Journal of Biology 2:211-2116.

Clemens, L. E., and P. F. Basch. 1989. Schistosoma mansoni: Effect of transferrin and growth factors on development of schistosomula in vitro. Journal of Parasitology 75:417-421.

Colley, D. G., and G. L. Freeman Jr. 1980. Differences in adult Schistosoma mansoni worm burden requirements for the establishment of resistance to reinfection in inbred mice: I. CBA/J and C57BL/6 mice. American Journal of Tropical Medicine and Hygiene 29:1279-1285.

Conceição, M. J., C. A. Argento, V. L. A. Chagas, C. M. Takiya, D. C. Moura, and S. C. Silva. 1998. Prognosis of schistosomiasis mansoni patients infected with hepatitis B virus. Memorias do Instituto Oswaldo Cruz 93:255-258.

Cooke, A., P. Tonks, F. M. Jones, H. O'Shea, P. Hutchings, A. J. C. Fulford, and Dunne. 1999. Infection with Schistosoma mansoni prevents insulin dependent diabetes mellitus in non-obese diabetic mice. Parasite Immunology 21:169-176.

Corachan, M. 2002. Schistosomiasis and international travel. Clinical Infectious Diseases 35:446-450.

Correale, J., and M. Farez. 2007. Association between parasite infection and immune responses in multiple sclerosis. Annals of Neurology 61:97-108.

Crompton, D. W. T. 1999. How much human helminthiasis is there in the world? Journal of Parasitology 85:397-403.

Cummings, R., and A. Nyame. 1996. Glycobiology of schistosomiasis. FASEB J. 10:838-848.

Dahl, B., P. M. G. F.V. Schiødt, and T. K. J. Ramlau. 2001. Gc-globulin is an acute phase reactant and an indicator of muscle injury after spinal surgery. Inflammation Research 50:39-43.

Dam, G. J. v., B. J. Bogitsh, R. J. M. v. Zeyl, J. P. Rotmans, and A. M. Deelder. 1996. Schistosoma mansoni: In vitro and In vivo excretion of CAA and CCA by developing schistosomula and adult worms. The Journal of Parasitology 82:557-564.

De Morais, C. N. L., J. R. De Souza, W. G. Melo, M. L. Aroucha, P. Miranda, A. L. C. Domingues, F. G. C. Abath, and S. M. L. Montenegro. 2008. Cytokine profile associated with chronic and acute human schistosomiasis mansoni. Memorias do Instituto Oswaldo Cruz 103:561-568.

Deelder, A. M. 1992. Diagnostic markers in schistosomiasis. Memorias do Instituto Oswaldo Cruz 87:125-127.

Dessein, A., C. Chevillard, V. Arnaud, X. Hou, A. A. Hamdoun, H. Dessein, H. He, S. A. Abdelmaboud, X. Luo, J. Li, A. Varoquaux, A. Mergani, M. Abdelwahed, J. Zhou, A. Monis, M. G. R. Pitta, N. Gasmelseed, S. Cabantous, Y. Zhao, A. Prata, C. Brandt, N. E. Elwali, L. Argiro, and Y. Li. 2009. Variants of CTGF are associated with hepatic fibrosis in Chinese, Sudanese, and Brazilians infected with schistosomes. Journal of Experimental Medicine 206:2321-2328.

Diallo, T. O., F. Remoue, A. M. Schacht, N. Charrier, J.-P. Dompnier, S. Pillet, O. Garraud, A. A. N'Diaye, A. Capron, M. Capron, and G. Riveau. 2004. Schistosomiasis co-infection in humans influences inflammatory markers in uncomplicated Plasmodium falciparum malaria. Parasite Immunology 26:365-369.

Doughty, B. L., E. A. Ottesen, T. E. Nash, and S. M. Phillips. 1984. Delayed hypersensitivity granuloma formation around Schistosoma mansoni eggs in vitro. III. Granuloma formation and modulation in human schistosomiasis mansoni. Journal of Immunology 133:993-997.

Dragani, T. A., F. S. Falvella, G. Manenti, M. A. Pierotti, and R. A. Gambetta. 1996. Downexpression of aldehyde dehydrogenase 1 in murine lung tumors. Molecular Carcinogenesis 16:123-125.

Dragani, T. A., G. Manenti, M. R. M. Sacchi, B. M. Colombo, and G. Della Porta. 1989. Major urinary protein as a negative tumor marker in mouse hepatocarcinogenesis. Molecular Carcinogenesis 2:355-360.

Drummond, S. C., L. C. D. S. Silva, R. S. Do Amaral, S. R. Sousa-Pereira, C. M. Antunes, and J. R. Lambertucci. 2006. Morbidity of schistosomiasis mansoni in the state of Minas Gerais, Brazil. Memorias do Instituto Oswaldo Cruz 101:37-44.

Dunn, M. A., M. Rojkind, and K. S. Warren. 1977. Liver collagen synthesis in murine schistosomiasis. Journal of Clinical Investigation 59:666-674.

El-Bassiouni, N. E., A. E. El Bassiouny, N. A. Hussein, H. H. El-Sayed, I. M. Ibrahim, M. G. Lotfy, and S. A. Omran. 1998. The coagulation profile in hepatosplenic schistosomiasis. Blood Coagulation and Fibrinolysis 9:189-194.

el-Kady, I. M., S. A. el-Masry, G. Badra, and K. A. Halafawy. 2004. Different cytokine patterns in patients coinfected with hepatitis C virus and Schistosoma mansoni. Egyptian Journal of Immunology 11:23-29.

El-Koraie, A. F., N. M. Baddour, A. G. Adam, E. H. El-Kashef, and A. M. El Nahas. 2002. Cytoskeletal protein expression and regenerative markers in schistosomal nephropathy. Nephrology Dialysis Transplantation 17:803-812.

El-Meneza, S., G. R. Olds, T. F. Kresina, and A. A. F. Mahmoud. 1989. Dynamics of hepatic connective tissue matrix constituents during murine Schistosoma mansoni infection. Hepatology 9:50-56.

El-Rigel, N., and M. H. Hetta. 2006. Effect of Citrus reticulata on serum protein fractions of mice after Schistosoma mansoni infcetion. Journal of Applied Sciences 6:1447-1455.

Elchuri, S., M. Naeemuddin, O. Sharpe, W. H. Robinson, and T. T. Huang. 2007. Identification of biomarkers associated with the development of hepatocellular carcinoma in CuZn superoxide dismutase deficient mice. Proteomics 7:2121-2129.

Elsammak, M. Y., R. M. Al-Sharkaweey, M. S. Ragab, G. A. Amin, and M. H. Kandil. 2008. IL-4 and reactive oxygen species are elevated in Egyptian patients affected with schistosomal liver disease. Parasite Immunology 30:603-609.

Evans, A. S., and M. A. Stirewalt. 1957. Serologic reactions in Schistosoma mansoni infections: III. Ionographic fractionation of sera of mice with progressive disease. Experimental Parasitology 6:8-17.

Fahim, F. A., A. Y. Esmat, G. K. Hassan, and A. Abdel-Bary. 2000. Biochemical changes in patients with combined chronic schistosomiasis and viral hepatitis C infections. Disease Markers 16:111-118.

Feldmeier, H., R. C. Daccal, M. J. Martins, V. Soares, and R. Martins. 1998. Genital manifestations of schistosomiasis mansoni in women: important but neglected. Memorias do Instituto Oswaldo Cruz 93:127-133.

Feldmeier, H., P. Leutscher, G. Poggensee, and G. Harms. 1999. Male genital schistosomiasis and haemospermia. Tropical Medicine and International Health 4:791-793.

Forestier, M., R. Bänninger, J. Reichen, and M. Solioz. 2003. Betaine homocysteine methyltransferase: Gene cloning and expression analysis in rat liver cirrhosis. Biochimica et Biophysica Acta - Molecular Basis of Disease 1638:29-34.

Freeman Jr, G. L., M. A. Montesano, W. E. Secor, D. G. Colley, M. J. Howard, and S. C. Bosshardt. 1996. Immunopathogenesis and immunoregulation in schistosomiasis. Distinct chronic pathologic syndromes in CBA/J mice. Annals of the New York Academy of Sciences 797:151-165.

George, J., and G. Chandrakasan. 2000. Biochemical abnormalities during the progression of hepatic fibrosis induced by dimethylnitrosamine. Clinical Biochemistry 33:563-570.

Gharib, B., O. M. S. Abdallahi, H. Dessein, and M. D. Reggi. 1999. Development of eosinophil peroxidase activity and concomitant alteration of the antioxidant defenses in the liver of mice infected with Schistosoma mansoni. Journal of Hepatology 30:594-602.

Giometti, C. S., X. Liang, S. L. Tollaksen, D. B. Wall, D. M. Lubman, V. Subbarao, and M. S. Rao. 2000. Mouse liver selenium-binding protein decreased in abundance by peroxisome proliferators. Electrophoresis 21:2162-2169.

Githeko, A. 2009. Changing climate and isotherms shifts diseases to new heights in East African highlands P.^Pp. Tropical Diseases Research to Foster Innovation & Knowledge Application (TropIKA.net).

Grillo, M. A., and S. Colombatto. 2008. S-adenosylmethionine and its products. Amino Acids 34:187-193.

Grzych, J. M., E. Pearce, A. Cheever, Z. A. Caulada, P. Caspar, S. Heiny, F. Lewis, and A. Sher. 1991. Egg deposition is the major stimulus for the production of Th2 cytokines in murine schistomiasis mansoni. Journal of Immunology 146:1322-1327.

Guo, W., H. Xu, J. Chen, Y. Yang, J. W. Jin, R. Fu, H. M. Liu, X. L. Zha, Z. G. Zhang, and W. Y. Huang. 2007. Prohibitin suppresses renal interstitial fibroblasts proliferation and phenotypic change induced by transforming growth factor-β1. Molecular and Cellular Biochemistry 295:167-177.

Hammond, K. D., and D. Balinsky. 1978. Activities of key gluconeogenic enzymes and glycogen synthase in rat and human livers, hepatomas, and hepatoma cell cultures. Cancer Research 38:1317-1322.

Harvie, M., T. W. Jordan, and A. C. LaFlamme. 2007. Differential liver protein expression during schistosomiasis. Infection and Immunity 75:736-744.

Hayes, P. C., L. May, J. D. Hayes, and D. J. Harrison. 1991. Glutathione S-transferases in human liver cancer. Gut 32:1546-1549.

Helmby, H. 2007. Schistosomiasis and malaria: another piece of the crossreactivity puzzle. Trends in Parasitology 23:88-90.

Henderson, G. S., J. T. Conary, M. Summar, T. L. McCurley, and D. G. Colley. 1991. In vivo molecular analysis of lymphokines involved in the murine immune response during Schistosoma mansoni infection. I. IL-4 mRNA, not IL-2 mRNA, is abundant in the granulomatous livers, mesenteric lymph nodes, and spleens of infected mice. Journal of Immunology 147:992-997.

Henderson, G. S., N. A. Nix, M. A. Montesano, D. Gold, G. L. Freeman Jr, T. L. McCurley, and D. G. Colley. 1993. Two distinct pathological syndromes in male

CBA/J inbred mice with chronic Schistosoma mansoni infections. American Journal of Pathology 142:703-714.

Heng, E. C. K., Y. Huang, S. A. Black Jr, and P. C. Trackman. 2006. CCN2, connective tissue growth factor, stimulates collagen deposition by gingival fibroblasts via module 3 and alpha6- and beta1 integrins. Journal of Cellular Biochemistry 98:409-420.

Henkel, C., M. Roderfeld, R. Weiskirchen, M. L. Berres, S. Hillebrandt, F. Lammert, H. E. Meyer, K. Stühler, J. Graf, and E. Roeb. 2006. Changes of the hepatic proteome in murine models for toxically induced fibrogenesis and sclerosing cholangitis. Proteomics 6:6538-6548.

Herbert, D. R., T. Orekov, C. Perkins, and F. D. Finkelman. 2008. IL-10 and TGF-beta redundantly protect against severe liver injury and mortality during acute schistosomiasis. Journal of immunology (Baltimore, Md. : 1950) 181:7214-7220.

Hernandez, H. J., Y. Wang, N. Tzellas, and M. J. Stadecker. 1997. Expression of class II, but not class I, major histocompatibility complex molecules is required for granuloma formation in infection with Schistosoma mansoni. European Journal of Immunology 27:1170-1176.

Hirata, M., M. Kage, M. Takushima, and T. Fukuma. 1993. Different courses of granulomatous reactions around Schistosoma japonicum eggs in three strains of mice. The Journal of Parasitology 79:266-273.

Hoffmann, K. F., T. C. McCarty, D. H. Segal, M. Chiaramonte, M. Hesse, E. M. Davis, A. W. Cheever, P. S. Meltzer, H. C. Morse III, and T. A. Wynn. 2001. Disease fingerprinting with cDNA microarrays reveals distinct gene expression profiles in lethal type-1 and type-2 cytokine-mediated inflammatory reactions. FASEB J.:01-0306fje.

Israelsson, C., H. Bengtsson, A. Kylberg, K. Kullander, A. Lewén, L. Hillered, and T. Ebendal. 2008. Distinct cellular patterns of upregulated chemokine expression supporting a prominent inflammatory role in traumatic brain injury. Journal of Neurotrauma 25:959-974.

Jankovic, D., A. W. Cheever, M. C. Kullberg, T. A. Wynn, G. Yap, P. Caspar, F. A. Lewis, R. Clynes, J. V. Ravetch, and A. Sher. 1998. CD4+ T cell-mediated granulomatous pathology in schistosomiasis is downregulated by a B cell-

dependent mechanism requiring Fc receptor signaling. Journal of Experimental Medicine 187:619-629.

Jarnum, S., and N. A. Lassen. 1961. Albumin and transferrin metabolism in infectious and toxic diseases Scandinavian Journal of Clinical and Laboratory Investigation 13:357-368.

Jassim, A., D. Catty, and K. Hassan. 1987. Antibody isotypes of immune complexes in schistosomiasis mansoni in Sudan. Parasite Immunology 9:651-665.

Kamal, S., M. Madwar, L. Bianchi, A. E. L. Tawil, R. Fawzy, T. Peters, and J. W. F. Rasenack. 2000. Clinical, virological and histopathological features: long-term follow-up in patients with chronic hepatitis C co-infected with S. mansoni. Liver 20:281-289.

Kamal, S. M., L. Bianchi, A. A. Tawil, M. Koziel, K. E. S. Khalifa, T. Peter, and J. W. Rasenack. 2001. Specific cellular immune response and cytokine patterns in patients coinfected with Hepatitis C virus and Schistosoma mansoni. The Journal of Infectious Diseases 184:972-982.

Kanyugo, M. S., H. S. Ozwara, W. T. Mutahi, and D. S. Yole. 2009. Parasitological and immunopathological responses Balb/C mice with concomitant Schistosoma Mansoni and Plasmodium Berghei infections. The Internet Journal of Tropical Medicine 5.

Karanja, D. M. S., A. W. Hightower, D. G. Colley, P. N. M. Mwinzi, K. Galil, J. Andove, and W. E. Secor. 2002. Resistance to reinfection with Schistosoma mansoni in occupationally exposed adults and effect of HIV-1 co-infection on susceptibility to schistosomiasis: a longitudinal study. The Lancet 360:592-596.

Kardorff, R., C. Mugashe, R. M. Gabone, C. Mahlert, and E. Doehring. 1999. Diagnostic value of connective tissue metabolites in Schistosoma mansoni related liver disease. Acta Tropica 73:153-164.

Karp, N. A., and K. S. Lilley. 2005. Maximising sensitivity for detecting changes in protein expression: Experimental design using minimal CyDyes. Proteomics 5:3105-3115.

Karp, N. A., M. Spencer, H. Lindsay, K. O'Dell, and K. S. Lilley. 2005. Impact of replicate types on proteomic expression analysis. Journal of Proteome Research 4:1867-1871.

Kaviratne, M., M. Hesse, M. Leusink, A. W. Cheever, S. J. Davies, J. H. McKerrow, L. M. Wakefield, J. J. Letterio, and T. A. Wynn. 2004. IL-13 activates a mechanism of tissue fibrosis that is completely TGF-beta independent. Journal of Immunology 173:4020-4029.

King, C. H., and M. Dangerfield-Cha. 2008. The unacknowledged impact of chronic schistosomiasis. Chronic Illness 4:65-79.

Knopf, J. L., J. F. Gallagher, and W. A. Held. 1983. Differential, multihormonal regulation of the mouse major urinary protein gene family in the liver. Molecular and Cellular Biology 3:2232-2240.

Kogulan, P., and D. R. Lucey. 2007. Schistosomiasis. P.^Pp., W. W. Emmons, F. Talavera, J. F. John Jr, E. Mylonakis and B. A. Cunha, eds. Medscape.

Kojiro, M., S. Kakizoe, and H. Yano. 1986. Hepatocellular carcinoma and Schistosomiasis japonica. A clinicopathologic study of 59 autopsy cases of hepatocellular carcinoma associated with chronic Schistosomiasis japonica. Acta Pathologica Japonica 36:525-532.

Kovalenko, E., F. Tacke, O. A. Gressner, H. W. Zimmermann, B. Lahme, A. Janetzko, T. Wiederholt, T. Berg, T. Mller, C. Trautwein, A. M. Gressner, and R. Weiskirchen. 2009. Validation of connective tissue growth factor (CTGF/CCN2) and its gene polymorphisms as noninvasive biomarkers for the assessment of liver fibrosis. Journal of Viral Hepatitis 16:612-620.

Krupenko, S. A., and N. V. Oleinik. 2002. 10-formyltetrahydrofolate dehydrogenase, one of the major folate enzymes, is down-regulated in tumor tissues and possesses suppressor effects on cancer cells. Cell Growth Differentiation 13:227-236.

Ku, N., J. M. Darling, S. M. Krams, C. O. Esquivel, E. B. Keeffe, R. K. Sibley, Y. M. Lee, T. L. Wright, and M. B. Omary. 2003. Keratin 8 and 18 mutations are risk factors for developing liver disease of multiple etiologies. Proceedings of the National Academy of Sciences of the United States of America 100:6063-6068.

Kucharz, E. 1984. Clinical and experimental studies on collagen metabolism in hepatic disorders. Medecine interne 22:129-140.

La Flamme, A. C., A. S. MacDonald, C. R. Huxtable, M. Carroll, and E. J. Pearce. 2003a. Lack of C3 affects Th2 response development and the sequelae of chemotherapy in schistosomiasis. Journal of Immunology 170:470-476.

La Flamme, A. C., E. A. Patton, B. Bauman, and E. J. Pearce. 2001. IL-4 plays a crucial role in regulating oxidative damage in the liver during schistosomiasis. Journal of Immunology 166:1903-1911.

La Flamme, A. C., K. Ruddenklau, and B. T. Backstrom. 2003b. Schistosomiasis decreases central nervous system inflammation and alters the progression of experimental autoimmune encephalomyelitis. Infection and Immunity 71:4996-5004.

Lambert, J.-P., M. Ethier, J. C. Smith, and D. Figeys. 2005. Proteomics: from gel based to gel free. Analytical Chemistry 77:3771-3788.

Lardans, V., and C. Dissous. 1998. Snail Control Strategies for Reduction of Schistosomiasis Transmission. Parasitology Today 14:413-417.

Lawley, T. J., E. A. Ottesen, R. A. Hiatt, and L. A. Gazze. 1979. Circulating immune complexes in acute schistosomiasis. Clinical and Experimental Immunology 37:221-227.

Leal, J. F., I. Ferrer, C. Blanco-Aparicio, J. Hernandez-Losa, C. S. Ramony, A. Carnero, and M. E. Lleonart. 2008. S-adenosylhomocysteine hydrolase downregulation contributes to tumorigenesis. Carcinogenesis 29:2089-2095.

Lee, H., C. Shun, L. Chiou, C. Chen, G. Huang, and J. Sheu. 2005. Hydroxyproline content of needle biopsies as an objective measure of liver fibrosis: Emphasis on sampling variability. Journal of Gastroenterology and Hepatology 20:1109-1114.

Lepreux, S., P. Bioulac-Sage, G. Gabbiani, V. Sapin, C. Housset, J. Rosenbaum, C. Balabaud, and A. Desmoulière. 2004. Cellular retinol-binding protein-1 expression in normal and fibrotic/cirrhotic human liver: different patterns of expression in hepatic stellate cells and (myo)fibroblast subpopulations. Journal of Hepatology 40:774-780.

Li, Q., A. K. Ching, B. C. Chan, S. K. Chow, P. Lim, T. C. Ho, W. Ip, C. Wong, C. W. Lam, K. K. Lee, J. Y. Chan, and Y. Chui. 2004. A death receptor-associated anti-apoptotic protein, BRE, inhibits mitochondrial apoptotic pathway. Journal of Biological Chemistry 279:52106-52116.

Lim, S. O., S. Park, W. Kim, S. G. Park, H. Kim, Y. Kim, T. Sohn, J. Noh, and G. Jung. 2002. Proteome analysis of hepatocellular carcinoma. Biochemical and Biophysical Research Communications 291:1031-1037.

Lopes de Faria, J. 1954. Cor Pulmonale in Manson's Schistosomiasis I. Frequency in Necropsy Material; Pulmonary Vascular Changes Caused by Schistosome Ova. American Journal of Pathology 30:167-193.

Lopes, R. I., R. N. Lopes, K. R. Leite, and D. Prando. 2003. Testicular schistosomiasis simulating malignancy. The Lancet Infectious Diseases 3:556-556.

Lyra, L. G., G. Rebouças, and Z. A. Andrade. 1976. Hepatitis B surface antigen carrier state in hepatosplenic schistosomiasis. Gastroenterology 71:641-645.

Madbouly, K., A. Senagore, A. Mukerjee, A. Hussien, M. Shehata, P. Navine, C. Delaney, and V. Fazio. 2007. Colorectal cancer in a population with endemic Schistosoma mansoni : Is this an at-risk population? International Journal of Colorectal Disease 22:175-181.

Magnussen, P. 2003. Treatment and re-treatment strategies for schistosomiasis control in different epidemiological settings: a review of 10 years' experiences. Acta Tropica 86:243-254.

Mahdy, K. A., H. H. Ahmed, F. Mannaa, and A. Abdel-Shaheed. 2007. Clinical benefits of biochemical markers of bone turnover in Egyptian children with chronic liver diseases. World Journal of Gastroenterology 13:785-790.

Martinelli, R., A. C. B. Noblat, E. Brito, and H. Rocha. 1989. Schistosoma mansoni-induced mesangiocapillary glomerulonephritis: Influence of therapy. Kidney International 35:1227-1233.

Mayer, D. A., and B. Fried. 2007. The role of helminth infections in carcinogenesis. P.^Pp. 239-296 in Advances in Parasitology, R. Muller, D. Rollinson and S. I. Hay, eds.

McKay, M. J., J. Sherman, M. T. Laver, M. S. Baker, S. J. Clarke, and M. P. Molloy. 2007. The development of multiple reaction monitoring assays for liver-derived plasma proteins. Proteomics - Clinical Applications 1:1570-1581.

Mehlhorn, H. 2009. Energy metabolism P.^Pp. in Parasitology Research & Encyclopedic Reference of Parasitology H. Mehlhorn, ed. Springer-Verlag Heidelberg.

Meier, U., O. Gressner, F. Lammert, and A. M. Gressner. 2006. Gc-Globulin: roles in response to injury. Clinical Chemistry 52:1247-1253.

Mishra, S., L. C. Murphy, B. L. Gregoire Nyomba, and L. J. Murphy. 2005. Prohibitin: a potential target for new therapeutics. Trends in Molecular Medicine 11:192-197.

Mohamed-Ali, Q., N.-E. M. A. Elwali, A. A. Abdelhameed, A. Mergani, S. Rahoud, K. E. Elagib, O. K. Saeed, L. Abel, M. M. A. Magzoub, and A. J. Dessein. 1999. Susceptibility to periportal (Symmers) fibrosis in human Schistosoma mansoni infections: Evidence that intensity and duration of infection, gender, and inherited factors are critical in disease progression. The Journal of Infectious Diseases 180:1298-1306.

Montesano, M. A., D. G. Colley, G. L. Freeman Jr., and W. E. Secor. 1999. Neonatal exposure to idiotype induces Schistosoma mansoni egg antigen-specific cellular and humoral immune responses. Journal of Immunology 163:898-905.

Montesano, M. A., D. G. Colley, M. T. Willard, G. L. Freeman Jr., and W. E. Secor. 2002. Idiotypes expressed early in experimental Schistosoma mansoni infections predict clinical outcomes of chronic disease. Journal of Experimental Medicine 195:1223-1228.

Morais, C. N., B. M. Carvalho, W. G. Melo, E. P. Lopes, A. L. C. Domingues, N. T. Jucá, W. Souza, F. G. Abath, and S. M. Montenegro. 2006. Preliminar evaluation of cytokines in the hepatitis C-schistosomiasis co-infection. Memorias do Instituto Oswaldo Cruz 101:353-354.

Morand, J. F., J. Macri, and K. Adeli. 2005. Proteomic profiling of hepatic endoplasmic reticulum-associated proteins in an animal model of insulin resistance and metabolic dyslipidemia. Journal of Biological Chemistry 280:17626-17633.

Morikawa, H., A. Tamori, S. Nishiguchi, M. Enomoto, D. Habu, N. Kawada, and S. Shiomi. 2007. Expression of connective tissue growth factor in the human liver with idiopathic portal hypertension. Molecular medicine 13:240-245.

Mortati Neto, N., J. P. S. Grando, and H. A. Moreira. 2004. Testicular schistosomiasis mimicking tumour. International Brazilian Journal of Urology 30:502-503.

Mostafa, M. H., S. A. Sheweita, and P. J. O'Connor. 1999. Relationship between schistosomiasis and bladder cancer. Clinical Microbiology Reviews 12:97-111.

Mouk, E. M. O., P. N. M. Mwinzi, C. L. Black, J. M. Carter, Z. W. Ng'ang'a, M. M. Gicheru, W. E. Secor, D. M. S. Karanja, and D. G. Colley. 2009. Childhood coinfections with Plasmodium falciparum and Schistosoma mansoni result in lower percentages of activated T cells and T regulatory memory cells than

schistosomiasis only. American Journal of Tropical Medicine and Hygiene 80:475-478.

Mousa, W., C. I. Waslien, and M. M. Mansour. 1976. Serum glycoproteins in schistosomiasis. American Journal of Tropical Medicine and Hygiene 25:709-713.

Mulla, A., H. C. Christian, E. Solito, N. Mendoza, J. F. Morris, and J. C. Buckingham. 2004. Expression, subcellular localization and phosphorylation status of annexins 1 and 5 in human pituitary adenomas and a growth hormone-secreting carcinoma. Clinical Endocrinology 60:107-119.

Murray, G. I., P. J. Paterson, R. J. Weaver, S. W. B. Ewen, W. T. Melvin, and M. D. Burke. 1993. The expression of cytochrome P-450, epoxide hydrolase, and glutathione s-transferase in hepatocellular carcinoma. Cancer 71:36-43.

Mwinzi, P. N. M., D. M. S. Karanja, I. Kareko, P. W. Magak, A. S. S. Orago, D. G. Colley, and W. E. Secor. 2004. Short Report: Evaluation of hepatic fibrosis in persons co-infected with Schistosoma mansoni and human immunodefiency virus 1. American Journal of Tropical Medicine and Hygiene 71:783-786.

Nagi, M. A. M., A. Kumar, J. S. Mubarak, and S. A. Bamashmoos. 1999. Epidemiological, clinical and haematological profile of schistosomiasis in Yemen. Eastern Mediterranean Health Journal 5:177-181.

Nicolls, D. J., L. H. Weld, E. Schwartz, C. Reed, F. von Sonnenburg, D. O. Freedman, P. E. Kozarsky, and for the GeoSentinel Surveillance Network. 2008. Characteristics of schistosomiasis in travelers reported to the GeoSentinel Surveillance Network 1997-2008. American Journal of Tropical Medicine and Hygiene 79:729-734.

Nyame, A. K., F. A. Lewis, B. L. Doughty, R. Correa-Oliveira, and R. D. Cummings. 2003. Immunity to schistosomiasis: glycans are potential antigenic targets for immune intervention. Experimental Parasitology 104:1-13.

Ohtsuka, M., H. Inoko, J. Kulski, and S. Yoshimura. 2008. Major histocompatibility complex (MHC) class Ib gene duplications, organization and expression patterns in mouse strain C57BL/6. BMC Genomics 9:178.

Old, W. M., K. Meyer-Arendt, L. Aveline-Wolf, K. G. Pierce, A. Mendoza, J. R. Sevinsky, K. A. Resing, and N. G. Ahn. 2005. Comparison of label-free methods for quantifying human proteins by shotgun proteomics. Molecular and Cellular Proteomics 4:1487-1502.

Olds, G., and S. Dasarathy. 2001. Recent advances in schistosomiasis. Current Infectious Disease Reports 3:59-67.

Otegbayo, J. A., O. G. Arinola, A. Aje, O. A. Oluwasola, O. H. Okiwelu, and L. S. Salimonu. 2005. Usefulness of acute phase proteins for monitoring development of hepatocellular carcinoma in hepatitis B virus carriers. West African Journal of Medicine 24:124-127.

Otogawa, K., T. Ogawa, R. Shiga, K. Ikeda, and N. Kawada. 2009. Induction of tropomyosin during hepatic stellate cell activation and the progression of liver fibrosis. Hepatology International 3:378-383.

Ouma, J. H., B. J. Vennervald, H. C. Kariuki, and A. E. Butterworth. 2001. Morbidity in schistosomiasis: an update. Trends in Parasitology 17:117-118.

Paradis, V., D. Dargere, M. Vidaud, A.-C. d. Gouville, S. Huet, V. Martinez, J.-M. Gauthier, N. Ba, R. Sobesky, V. Ratziu, and P. Bedossa. 1999. Expression of connective tissue growth factor in experimental rat and human liver fibrosis. Hepatology 30:968-976.

Parise, E. R., and H. Rosa. 1992. Serum laminin in hepatic schistosomiasis. Transactions of the Royal Society of Tropical Medicine and Hygiene 86:179-181.

Pearce, E. J. 2005. Priming of the immune response by schistosome eggs. Parasite Immunology 27:265-270.

Pearce, E. J., and A. S. MacDonald. 2002. The immunology of schistosomiasis. Nature Reviews Immunology 2:499-511.

Pelley, R. P., J. J. Ruffier, and K. S. Warren. 1976. Suppressive effect of a chronic helminth infection, Schistosomiasis mansoni, on the in vitro responses of spleen and lymph node cells to the T cell mitogens phytohemagglutinin and concanavalin A. Infection and Immunity 13:1176-1183.

Penque, D. 2009. Two-dimensional gel electrophoresis and mass spectrometry for biomarker discovery. Proteomics - Clinical Applications 3:155-172.

Pereira, L. M. M. B., A. L. C. Domingues, V. Spinelli, and I. G. McFarlane. 1998. Ultrasonography of the liver and spleen in Brazilian patients with hepatosplenic schistosomiasis and cirrhosis. Transactions of the Royal Society of Tropical Medicine and Hygiene 92:639-642.

Petrak, J., D. Myslivcova, P. Halada, R. Cmejla, J. Cmejlova, D. Vyoral, and C. D. Vulpe. 2007. Iron-independent specific protein expression pattern in the liver of HFE-deficient mice. The International Journal of Biochemistry & Cell Biology 39:1006-1015.

Pickett, C. B., and A. Y. Lu. 1981. Effect of phenobarbital on the level of translatable rat liver epoxide hydrolase mRNA. Proceedings of the National Academy of Sciences of the United States of America 78:893-897.

Poggensee, G., I. Kiwelu, V. Weger, D. GÃ¶ppner, T. Diedrich, I. Krantz, and H. Feldmeier. 2000. Female genital schistosomiasis of the lower genital tract: Prevalence and disease associated morbidity in Northern Tanzania. The Journal of Infectious Diseases 181:1210-1213.

Pontes, L. A., E. Dias-Neto, and A. Rabello. 2002. Detection by polymerase chain reaction of Schistosoma mansoni DNA in human serum and feces. American Journal of Tropical Medicine and Hygiene 66:157-162.

Potter, B. J., R. W. G. Chapman, R. M. Nunes, D. Sorrentino, and S. Sherlock. 1985. Transferrin metabolism in alcoholic liver disease. Hepatology 5:714-721.

Qi, Y., X. Chen, C. Chan, D. Li, C. Yuan, F. Yu, M. C. Lin, D. T. Yew, H. Kung, and L. Lai. 2008. Two-dimensional differential gel electrophoresis/analysis of diethylnitrosamine induced rat hepatocellular carcinoma. International Journal of Cancer 122:2682-2688.

Rachfal, A. W., and D. R. Brigstock. 2003. Connective tissue growth factor (CTGF/CCN2) in hepatic fibrosis. Hepatology Research 26:1-9.

Rezende, S. A., V. R. Oliveira, A. M. Silva, J. B. Alves, A. M. Goes, and L. F. L. Reis. 1997. Mice lacking the gamma interferon receptor have an impaired granulomatous reaction to Schistosoma mansoni infection. Infection and Immunity 65:3457-3461.

Richter, J., C. Hatz, G. Campagne, N. R. Bergquist, and J. M. Jenkins. 2000. Ultrasound in Schistosomiasis: A Practical Guide to the Standardized Use of Ultrasonography for the Assessment of Schistosomiasis- Related Morbidity. Geneva: World Health Organization.55.

Richter, J., K. Zwingenberger, Q. M. Ali, W. d. M. Lima, A. R. Dacal, G. V. de Siqueira, E. Doehring-Schwerdtfeger, and H. Feldmeier. 1992. Hepatosplenic

schistosomiasis: comparison of sonographic findings in Brazilian and Sudanese patients--correlation of sonographic findings with clinical symptoms. Radiology 184:711-716.

Robertson, W., van B. 1964. Metabolism of collagen in mammalian tissues. Biophysical Journal 4:93-106.

Roede, J. R., B. J. Stewart, and D. R. Petersen. 2008. Decreased expression of peroxiredoxin 6 in a mouse model of ethanol consumption. Free Radical Biology and Medicine 45:1551-1558.

Rowland, H. A. K. 1971. Intestinal schistosomiasis. Gut 12:663-667.

Rudd, P. M., T. Elliott, P. Cresswell, I. A. Wilson, and R. A. Dwek. 2001. Glycosylation and the immune system. Science 291:2370-2376.

Rumbley, C. A., S. A. Zekavat, H. Sugaya, P. J. Perrin, M. A. Ramadan, and S. M. Phillips. 1998. The schistosome granuloma: Characterization of lymphocyte migration, activation, and cytokine production. Journal of Immunology 161:4129-4137.

Rutitzky, L. I., H. J. Hernandez, and M. J. Stadecker. 2001. Th1-polarizing immunization with egg antigens correlates with severe exacerbation of immunopathology and death in schistosome infection. Proceedings of the National Academy of Sciences of the United States of America 98:13243-13248.

Rutkowski, R. B., and J. I. Bruce. 1971. Serum enzyme alteration of mice exposed to schistosomiasis mansoni. International Journal of Biochemistry 2:137-145.

Saber, M. A., D. A. Shafritz, and M. A. Zern. 1983. Changes in collagen and albumin mRNA in liver tissue of mice infected with Schistosoma mansoni as determined by in situ hybridization. Journal of Cell Biology 97:986-992.

Saif, M., J. Tawfik, M. A. Ali, S. F. El-Mahrouky, N. Galil, and M. N. Galal. 1977. Serum transferrin, albumin and IgG levels in hepatosplenic bilharziasis in Egypt. The Journal of the Egyptian Medical Association 60:731-743.

Salawu, L., and O. G. Arinola. 2004. Acute phase proteins in pregnant women with urinary schistosomiasis in live villages, Osun State, Nigeria. African Journal of Biomedical Research 7:103-106.

Salmhofer, H., I. Rainer, K. Zatloukal, and H. Denk. 1994. Posttranslational events involved in griseofulvin-induced keratin cytoskeleton alterations. Hepatology 20:731-740.

Sandoval, N., M. Siles-Lucas, J. L. Aban, J. L. Pérez-Arellano, T. Gárate, and A. Muro. 2006. Schistosoma mansoni: A diagnostic approach to detect acute schistosomiasis infection in a murine model by PCR. Experimental Parasitology 114:84-88.

Santos, F. L. N., E. J. L. Cerqueira, and N. M. Soares. 2005. Comparison of the thick smear and Kato-Katz techniques for diagnosis of intestinal helminth infections. Revista da Sociedade Brasileira de Medicina Tropical 38:196-198.

Santos, R. d. O., A. A. Barbosa Júnior, and Z. A. Andrade. 1992. Dynamics of fibrosis production and resorption in intestinal schistosomiasis of mice. Memorias do Instituto Oswaldo Cruz 87:25-31.

Santos, S. G., E. C. Campbell, S. Lynch, V. Wong, A. N. Antoniou, and S. J. Powis. 2007. Major histocompatibility complex class I-ERp57-Tapasin interactions within the peptide-loading complex. Journal of Biological Chemistry 282:17587-17593.

Schiødt, F. V. 2008. Gc - globulin in liver disease. Danish Medical Bulletin 55:131-146.

Schulz, K. F., and D. A. Grimes. 2005. Sample size calculations in randomised trials: mandatory and mystical. The Lancet 365:1348-1353.

Scrimgeour, E. M., and D. C. Gajdusek. 1985. Involvement of the central nervous system in Schistosoma mansoni and S. haematobium infection. A review. Brain 108:1023-1038.

Secor, W. E. 2005. Immunology of human schistosomiasis: off the beaten path. Parasite Immunology 27:309-316.

Secor, W. E. 2006. Interactions between schistosomiasis and infection with HIV-1. Parasite Immunology 28:597-603.

Secor, W. E., D. M. Karanja, and D. G. Colley. 2004. Interactions between schistosomiasis and human immunodeficiency virus in Western Kenya. Memorias do Instituto Oswaldo Cruz 99:93-95.

Secor, W. E., A. Shah, P. M. N. Mwinzi, B. A. Ndenga, C. O. Watta, and D. M. S. Karanja. 2003. Increased density of human immunodeficiency virus type 1 coreceptors CCR5 and CXCR4 on the surfaces of CD4 T cells and monocytes of

patients with Schistosoma mansoni infection. Infection and Immunity 71:6668-6671.

Sewell, D., Z. Qing, E. Reinke, D. Elliot, J. Weinstock, M. Sandor, and Z. Fabry. 2003. Immunomodulation of experimental autoimmune encephalomyelitis by helminth ova immunization. International Immunology 15:59-69.

Shahin, M., D. Schuppan, R. Waldherr, J. Risteli, L. Risteli, E. R. Savolainen, C. Oesterling, H. M. A. Rahman, A. M. El Sahly, S. M. A. Razek, O. E. Ruby, A. Koch, and H. K. Seitz. 1992. Serum procollagen peptides and collagen type VI for the assessment of activity and degree of hepatic fibrosis in schistosomiasis and alcoholic liver disease. Hepatology 15:637-644.

Shen, Z., M.-w. Wang, and S. P. Briggs. 2006. Use of high-throughput LC-MS/MS proteomics technologies in drug discovery. Drug Discovery Today: Technologies 3:301-306.

Silva, L. M., S. A. Oliveira, R. Ribeiro-dos-Santos, Z. A. Andrade, and M. B. P. Soares. 2004. Comparison of immune responses of Schistosoma mansoni-infected mice with distinct chronic forms of the disease. Acta Tropica 91:189-196.

Smithers, S. R., and P. J. Walker. 1961. Serum protein changes in monkeys infected with Schistosoma mansoni, with special reference to the metabolism of albumin. Experimental Parasitology 11:39-49.

Stadecker, M. J. 1999. The development of granulomas in schistosomiasis: Genetic backgrounds, regulatory pathways, and specific egg antigen responses that influence the magnitude of disease. Microbes and Infection 1:505-510.

Stadecker, M. J., H. Asahi, E. Finger, H. J. Hernandez, L. I. Rutitzky, and J. Sun. 2004. The immunobiology of Th1 polarization in high-pathology schistosomiasis. Immunological Reviews 201:168-179.

Stickel, F., R. Urbaschek, D. Schuppan, G. Poeschl, C. Oesterling, C. Conradt, R. S. McCuskey, U. A. Simanowski, and H. K. Seitz. 2001. Serum collagen type VI and XIV and hyaluronic acid as early indicators for altered connective tissue turnover in alcoholic liver disease. Digestive Diseases and Sciences 46:2025-2032.

Strathmann, J., K. Paal, C. Ittrich, E. Krause, K. E. Appel, H. P. Glauert, A. Buchmann, and M. Schwarz. 2007. Proteome analysis of chemically induced mouse liver tumors with different genotype. Proteomics 7:3318-3331.

Strauss, E. 2002. Hepatosplenic schistosomiasis: a model for the study of portal hypertension. Annals of Hepatology 1:6-11.

Strnad, P., T. C. Lienau, G. Tao, L. C. Lazzeroni, F. Stickel, D. Schuppan, and M. Bishr Omary. 2006. Keratin variants associate with progression of fibrosis during chronic hepatitis C infection. Hepatology 43:1354-1363.

Strnad, P., C. Stumptner, K. Zatloukal, and H. Denk. 2008. Intermediate filament cytoskeleton of the liver in health and disease. Histochemistry and Cell Biology 129:735-749.

Sturrock, R. F., H. C. Kariuki, F. W. Thiongo, J. W. Gachare, B. G. O. Omondi, J. H. Ouma, G. Mbugua, and A. E. Butterworth. 1996. Schistosomiasis mansoni in Kenya: relationship between infection and anaemia in schoolchildren at the community level. Transactions of the Royal Society of Tropical Medicine and Hygiene 90:48-54.

Sun, W., B. Xing, Y. Sun, X. Du, M. Lu, C. Hao, Z. Lu, W. Mi, S. Wu, H. Wei, X. Gao, Y. Zhu, Y. Jiang, a. X. Qian, and F. He. 2007. Proteome analysis of hepatocellular carcinoma by two-dimensional difference gel electrophoresis: Novel protein markers in hepatocellular carcinoma tissues. Molecular and Cellular Proteomics 6:1798-1808.

Takahashi, S., M. A. Dunn, and S. Seifter. 1980. Liver collagenase in murine schistosomiasis. Gastroenterology 78:1425-1431.

Takougang, I., P. Kamtchouing, J. Meli, N. Nkele, J. Keuzeta, S. Fotso, S. Fokoua, and M. Wamba Temgoua. 2008. Female genital urinary schistosomiasis: Is there an association with infertility? Tropical Medicine and Health 36:149-154.

Talaat, R. M., A. I. El-Bassiouny, A. M. Osman, M. Yossif, R. Charmy, and M. M. Al-Sherbiny. 2007. Cytokine secretion profile associated with periportal fibrosis in S. mansoni-infected Egyptian patients. Parasitology Research 101:289-299.

Tarrab-Hazdai, R., T. Hanoch, S. Jeon, H. Pauli, D. Gold, R. Arnon, and R. Seger. 2005. Ecto- and exo-protein kinases in Schistosoma mansoni: regulation of surface phosphorylation by acetylcholine and identification of the alpha subunit of CKII as a major secreted protein kinase. The Journal of Parasitology 91:756-763.

Thome-Kromer, B., I. Bonk, M. Klatt, G. Nebrich, M. Taufmann, S. Bryant, U. Wacker, and A. Köpke. 2003. Towards the identification of liver toxicity markers: A proteome study in human cell culture and rats. Proteomics 3:1835-1862.

Tong, Z., R. Chen, D. S. Alt, S. Kemper, B. Perbal, and D. R. Brigstock. 2009. Susceptibility to liver fibrosis in mice expressing a connective tissue growth factor transgene in hepatocytes. Hepatology 50:939-947.

Uchio, K., B. Tuchweber, N. Manabe, G. Gabbiani, J. Rosenbaum, and A. Desmouliere. 2002. Cellular retinol-binding protein-1 expression and modulation during in vivo and in vitro myofibroblastic differentation of rat hepatic stellate cells and portal fibroblasts. Laboratory Investigation 82:619-628.

Uji, Y., A. Karmen, H. Okabe, K. Hata, M. Miura, K. Ozaki, M. Minamizaki, T. Shibata, and S. Inayama. 1994. Measurement of free and total hydroxyproline by automated flow injection of serum or urine samples from maintenance hemodialysis patients with renal osteodystrophy. Journal of Clinical Laboratory Analysis 8:267-272.

Utzinger, J., E. K. N'goran, A. N'dri, C. Lengeler, and M. Tanner. 2000. Efficacy of praziquantel against Schistosoma mansoni with particular consideration for intensity of infection. Tropical Medicine and International Health 5:771-778.

Van der Werf, M. J., S. J. De Vlas, S. Brooker, C. W. N. Looman, N. J. D. Nagelkerke, J. D. F. Habbema, and D. Engels. 2003. Quantification of clinical morbidity associated with schistosome infection in sub-Saharan Africa. Acta Tropica 86:125-139.

Van Waes, L., and C. S. Lieber. 1977. Glutamate dehydrogenase: a reliable marker of liver cell necrosis in the alcoholic. British Medical Journal 2:1508-1510.

Vasiliou, V., A. Pappa, and D. R. Petersen. 2000. Role of aldehyde dehydrogenases in endogenous and xenobiotic metabolism. Chemico-Biological Interactions 129:1-19.

Vennervald, B. J., and K. Polman. 2009. Helminths and malignancy. Parasite Immunology 31:686-696.

Virtanen, T., and T. Kinnunen. 2008. Clinical allergy and immunology Series. P.^Pp. 576 in Allergens and Allergen Immunotherapy, R. F. Lockey, and D. K. Ledford, ed. Informa Health Care.

Viswanathan, S., M. Unlu, and J. S. Minden. 2006. Two-dimensional difference gel electrophoresis. Nature Protocols 1:1351-1358.

Vos, M., S. Barve, S. Joshi-Barve, J. Carew, P. Whitington, and C. McClain. 2008. Cytokeratin 18, a marker of cell death, is increased in children with suspected nonalcoholic fatty liver disease. Journal of pediatric gastroenterology and nutrition 47:481-485.

Wang, Y., E. Holmes, J. K. Nicholson, O. Cloarec, J. Chollet, M. Tanner, B. H. Singer, and J. r. Utzinger. 2004. Metabonomic investigations in mice infected with Schistosoma mansoni: An approach for biomarker identification. Proceedings of the National Academy of Sciences of the United States of America 101:12676-12681.

Ward, W. O., D. A. Delker, S. D. Hester, S. Thai, D. C. Wolf, J. W. Allen, and S. Nesnow. 2006. Transcriptional profiles in liver from mice treated with hepatotumorigenic and nonhepatotumorigenic triazole conazole fungicides: Propiconazole, Triadimefon, and Myclobutanil. Toxicologic Pathology 34:863-878.

Wegrzyn, P., J. Jura, T. Kupiec, W. Piekoszewski, B. Wladyka, A. Zarebski, and A. Koj. 2006. A search for genes modulated by interleukin-6 alone or with interleukin-1beta in HepG2 cells using differential display analysis. Biochimica et Biophysica Acta (BBA) - Molecular Basis of Disease 1762:319-328.

Wynn, T. A., R. W. Thompson, A. W. Cheever, and M. M. Mentink-Kane. 2004. Immunopathogenesis of schistosomiasis. Immunological Reviews 201:156-167.

Xu, C., and Z. Wang. 2008. Comparative proteomic analysis of livers from ketotic cows. Veterinary Research Communications 32:263-273.

Xu, W., L. W. Wang, J. Z. Shi, and Z. J. Gong. 2009. Effects of RNA interference targeting transforming growth factor-beta 1 on immune hepatic fibrosis induced by Concanavalin A in mice. Hepatobiliary and Pancreatic Diseases International 8:300-308.

Yamamoto, S., Y. Tomita, S. Nakamori, Y. Hoshida, H. Nagano, K. Dono, K. Umeshita, M. Sakon, M. Monden, and K. Aozasa. 2003. Elevated expression of valosin-containing protein (p97) in hepatocellular carcinoma is correlated with increased incidence of tumor recurrence. Journal of Clinical Oncology 21:447-452.

Yamashita, T., and D. L. Boros. 1992. IL-4 influences IL-2 production and granulomatous inflammation in murine schistosomiasis mansoni. The Journal of Immunology 149:3659-3664.

Yang, J., S. C. Kalhan, and R. W. Hanson. 2009. What Is the Metabolic Role of Phosphoenolpyruvate Carboxykinase? Journal of Biological Chemistry 284:27025-27029.

Yap, G., A. Cheever, P. Caspar, D. Jankovic, and A. Sher. 1997. Unimpaired down-modulation of the hepatic granulomatous response in CD8 T-cell- and gamma interferon-deficient mice chronically infected with Schistosoma mansoni. Infection and Immunity 65:2583-2586.

Yilmaz, Y. 2009. "Defragmenting" the noninvasive diagnosis of nonalcoholic steatohepatitis: hopes from cytokeratin-18. Hepatology 50:990-991.

Zatloukal, K., C. Stumptner, A. Fuchsbichler, P. Fickert, C. Lackner, M. Trauner, and H. Denk. 2004. The keratin cytoskeleton in liver diseases. The Journal of Pathology 204:367-376.

Zwingenberger, K., H. Feldmeier, J. A. Nogueira Queiroz, J. G. V. Vergetti Siquieia, H. Farias Auto, J. E. Alencar, and U. Bienzle. 1988. Liver involvement in human schistosomiasis mansoni. Assessment by immunological and biochemical markers. Parasitology Research 74:448-455.

APPENDICES

APPENDIX A

EXPERIMENTAL DESIGN 1: 8 gels for pI 4-7 and 8 gels for pI 6-11

(Samples labelled with CyDyes were randomised across the gels.)

Gel No.	Cy2 Internal Standard	Cy3 Sample	Cy5 Sample
1	10 μg pooled sample[1]	10 μg sample 1C[2]	10 μg sample 1M[2]
2	10 μg pooled sample[1]	10 μg sample 2H[2]	10 μg sample 2C[2]
3	10 μg pooled sample[1]	10 μg sample 3C[2]	10 μg sample 3M[2]
4	10 μg pooled sample[1]	10 μg sample 4H[2]	10 μg sample 4C[2]
5	10 μg pooled sample[1]	10 μg sample 5C[2]	10 μg sample 5M[2]
6	10 μg pooled sample[1]	10 μg sample 2M[2]	10 μg sample 3H[2]
7	10 μg pooled sample[1]	10 μg sample 4M[2]	10 μg sample 1H[2]
8	10 μg pooled sample[1]	10 μg sample 5H[2]	10 μg sample 1C[2]

[1]10 μg protein each of the liver lysates from 5 C, 5 M and 5 H

[2]C, control (uninfected /normal); M, MSS; H, HSS

EXPERIMENTAL DESIGN 2: 23 gels for pI 4-7 and 23 gels for pI 6-11

(Samples labelled with CyDyes were randomised across the gels.)

Gel No.	Cy2 Internal Standard	Cy3 Sample	Cy5 Sample
1	10 μg pooled sample[1]	10 μg sample 1C[2]	10 μg sample 1M[2]
2	10 μg pooled sample[1]	10 μg sample 2H[2]	10 μg sample 2C[2]
3	10 μg pooled sample[1]	10 μg sample 3C[2]	10 μg sample 3M[2]
4	10 μg pooled sample[1]	10 μg sample 4H[2]	10 μg sample 4C[2]
5	10 μg pooled sample[1]	10 μg sample 5C[2]	10 μg sample 5M[2]
6	10 μg pooled sample[1]	10 μg sample 2M[2]	10 μg sample 3H[2]
7	10 μg pooled sample[1]	10 μg sample 4M[2]	10 μg sample 1H[2]
8	10 μg pooled sample[1]	10 μg sample 5H[2]	10 μg sample 1C[2]
9	10 μg pooled sample[1]	10 μg sample 6-week-01	10 μg sample 8-week-02
10	10 μg pooled sample[1]	10 μg sample 8-week-03	10 μg sample 6-week-02
11	10 μg pooled sample[1]	10 μg sample 6-week-03	10 μg sample 8-week-06
12	10 μg pooled sample[1]	10 μg sample 12-week-09	10 μg sample 6-week-04
13	10 μg pooled sample[1]	10 μg sample 6-week-05	10 μg sample 12-week-10
14	10 μg pooled sample[1]	10 μg sample 8-week-09	10 μg sample 6-week-06
15	10 μg pooled sample[1]	10 μg sample 6-week-07	10 μg sample 12-week-02
16	10 μg pooled sample[1]	10 μg sample 12-week-05	10 μg sample 6-week-08
17	10 μg pooled sample[1]	10 μg sample 6-week-09	10 μg sample 8-week-08
18	10 μg pooled sample[1]	10 μg sample 12-week-01	10 μg sample 6-week-10
19	10 μg pooled sample[1]	10 μg sample 8-week-01	10 μg sample 12-week-08
20	10 μg pooled sample[1]	10 μg sample 12-week-03	10 μg sample 8-week-04
21	10 μg pooled sample[1]	10 μg sample 8-week-05	10 μg sample 12-week-06
22	10 μg pooled sample[1]	10 μg sample 12-week-04	10 μg sample 8-week-07
23	10 μg pooled sample[1]	10 μg sample 8-week-10	10 μg sample 12-week-07

[1]10 μg protein each of the liver lysates from 5 C, 5 M and 5 H

[2](C, control (uninfected /normal); M, MSS; H, HSS)

6-week, 6-week infected liver lysate (10 samples); 8-week, 8-week infected liver lysate (10 samples); 12-week, 12-week infected liver lysate (10 samples).

EXPERIMENTAL DESIGN 3: 3 gels for pI 3-10.

(Samples labelled with CyDyes were randomised across the gels.)

Gel No.	Cy2 Internal Standard	Cy3 Sample	Cy5 Sample
1	Pool of 15 serum samples[1]	Pooled C serum[2]	Pooled M serum[3]
2	Pool of 15 serum samples[1]	Pooled H serum[4]	Pooled C serum[2]
3	Pool of 15 serum samples[1]	Pooled M serum[3]	Pooled H serum[4]

[1]Pool of (5C +5M + 5H) sera, 10 μg protein each;

[2] Pool of 5 C sera; [3] Pool of 5 M sera; [4] Pool of 5 H sera

(C, control (uninfected /normal); M, MSS; H, HSS).

APPENDIX B

2D-DIGE GEL IMAGE ANALYSIS USING DECYDER SOFTWARE 6.5

In the DeCyder Software 6.5 control panel, load gel images using “Image Loader”. Load Cy2, Cy3, Cy5 images one at a time.

Using “Batch Processor” for the Differential In-gel Analysis and Biological Variation Analysis for all the gel images together will create Workspaces respectively.

In the “Spot Table” Biological Variation Analysis (BVA) module segregate the gel images according to the experimental groups and name them accordingly.

In the “Match Table” BVA module match the protein spots using the “Internal Standard”.

The “Protein Table” BVA module allows the viewing of the differential pattern analysis. It allows selecting and comparing the experimental groups. It calculates the average fold ratio between groups with the choice for “False Discovery Rate” selection criteria.

The BVA saved data can be used in the Extended Data Analysis (EDA) module to analyse the Differential Expression Analysis (DEA), Principle Component Analysis (PCA), Hierarchical Cluster Analysis (HCA) and Discriminant Analysis for Marker Selection (DAMS). The EDA is a module for multivariate analysis.

The DEA graphically illustrates the increase and decrease in protein spots in the experimental groups with ANOVA, Student T-Test and Multiple Comparison Tests.

PCA is supervised clustering which reduces the multidimensionality of the huge data sets and makes comparison between data sets (protein spots and DIGE proteomic images) easier.

HCA is unsupervised clustering making compassion between protein spots on gel images, experimental groups and protein spot volumes feasible. The dendrogram and heat map

together give a lot of information about the similarities in functional groups in protein spots and similarities between study groups.

Based on the resolution of the gel images and protein spots the DAMS feature allows the protein spot data to be analysed for biomarker selection.

Shown below is the sequential analysis for pI 4-7 for Experimental Design 1 and 2 with illustrations form the DeCyder software.

FIGURE B1

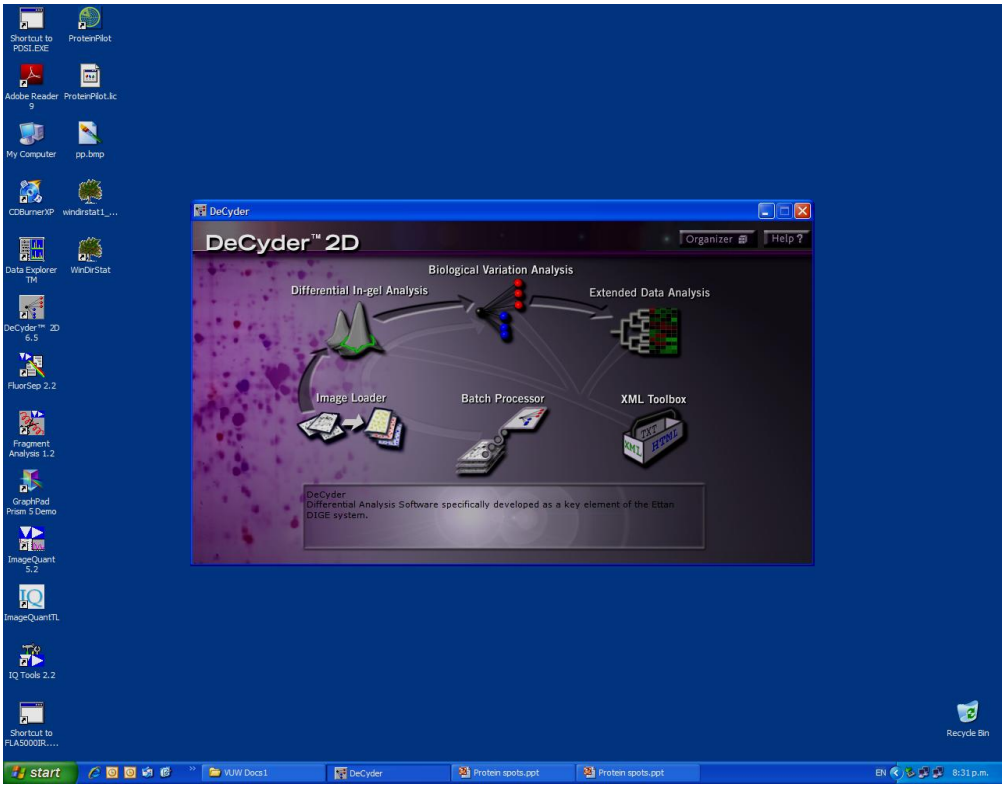

FIGURE B2

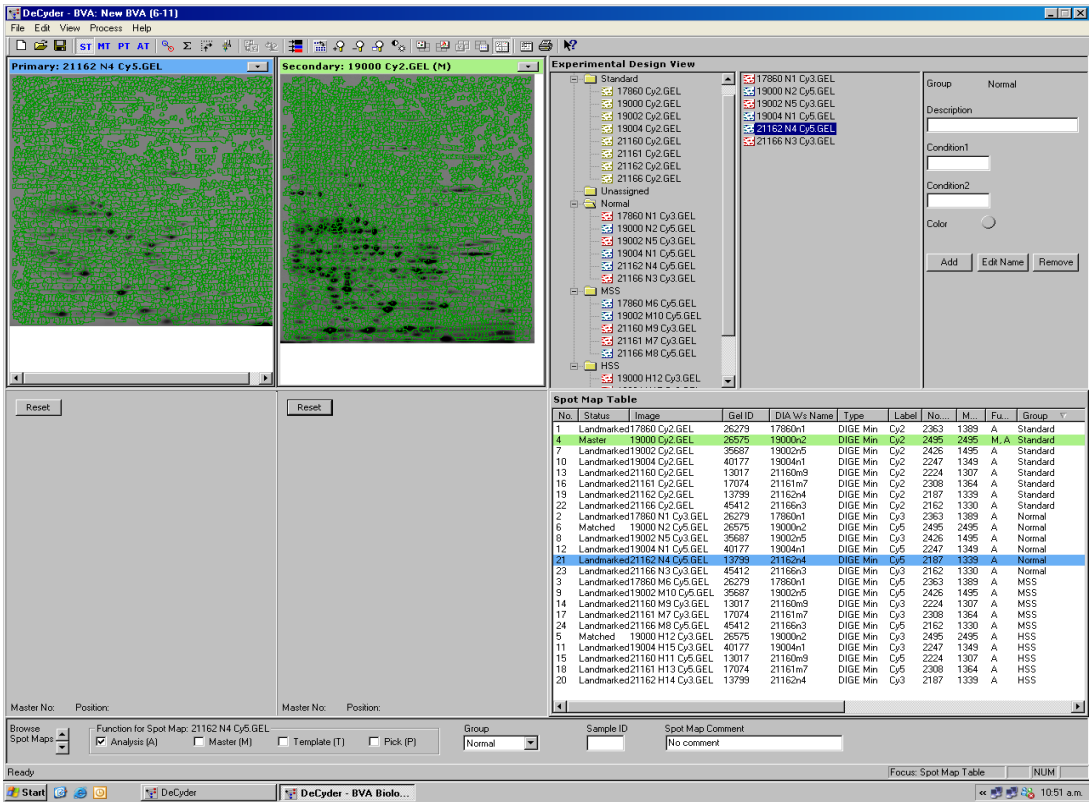

FIGURE B3

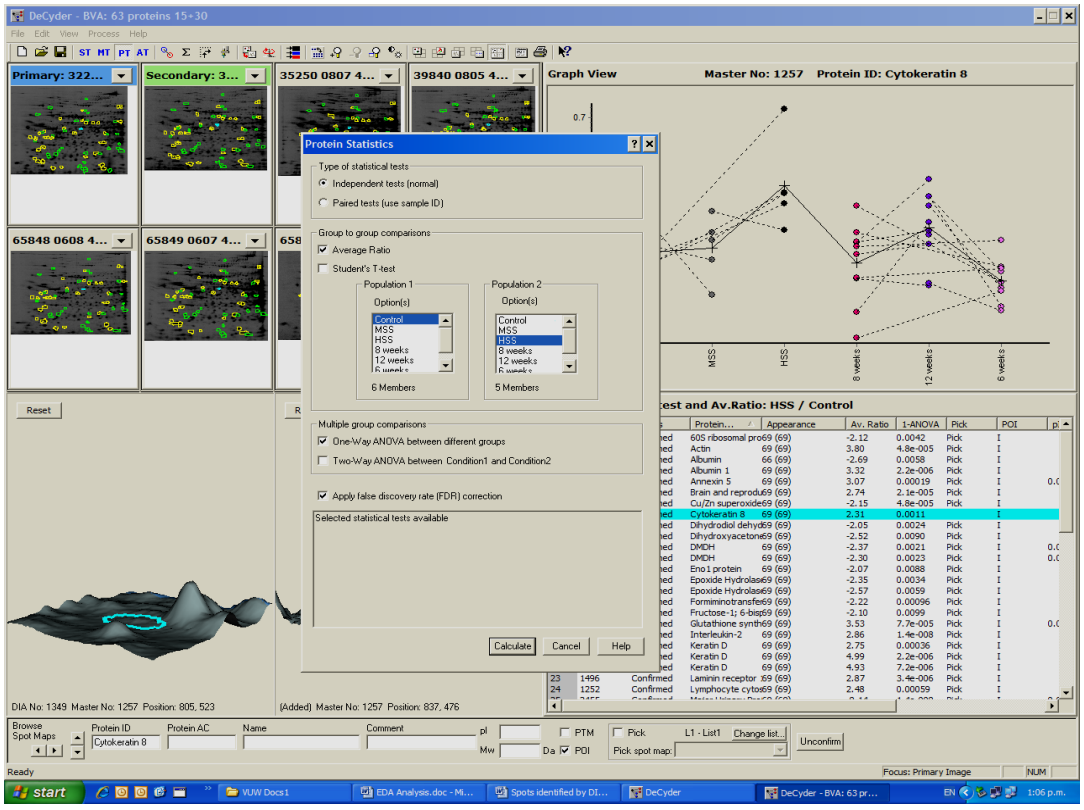

FIGURE B4

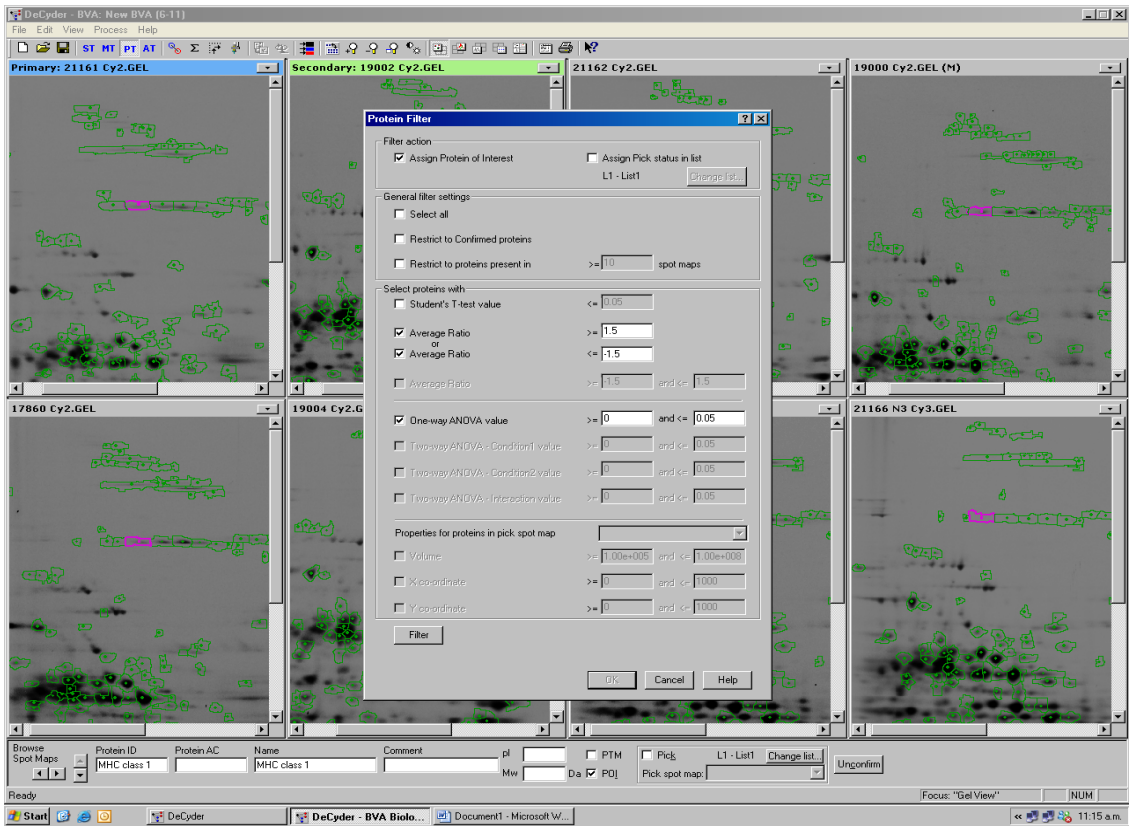

FIGURE B5

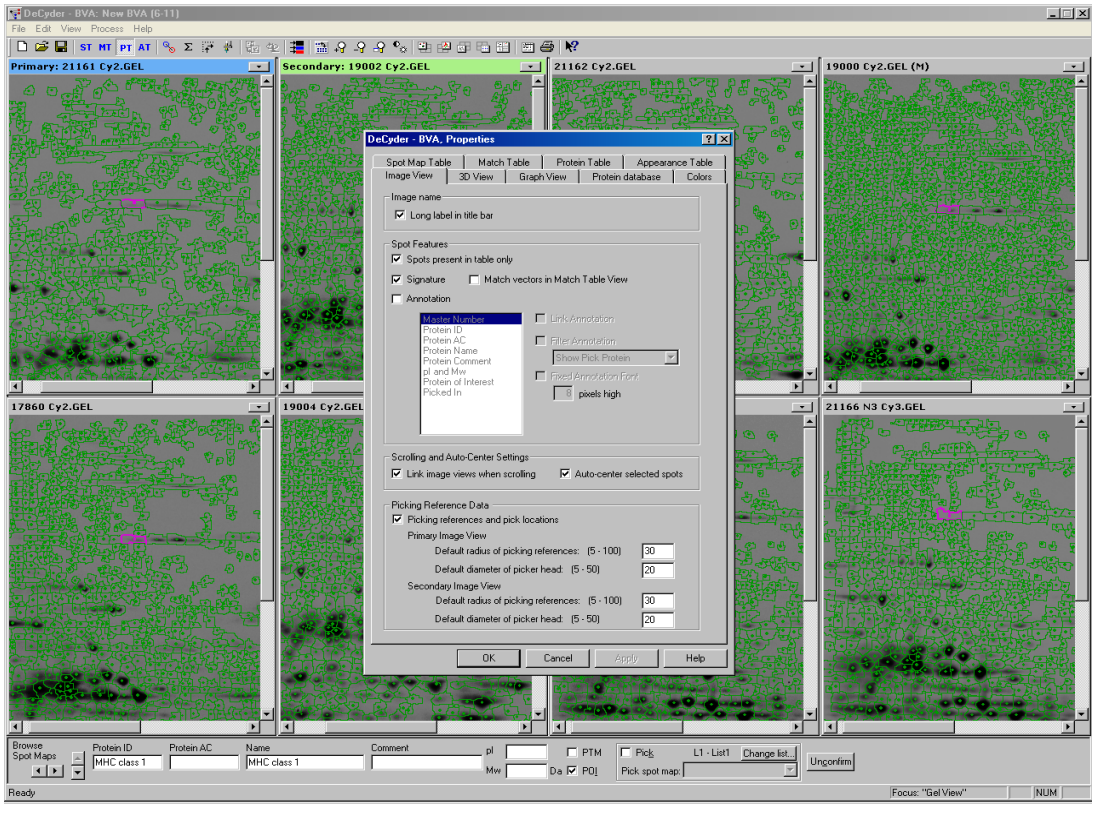

FIGURE B6 Analysis for Experiment Design 1

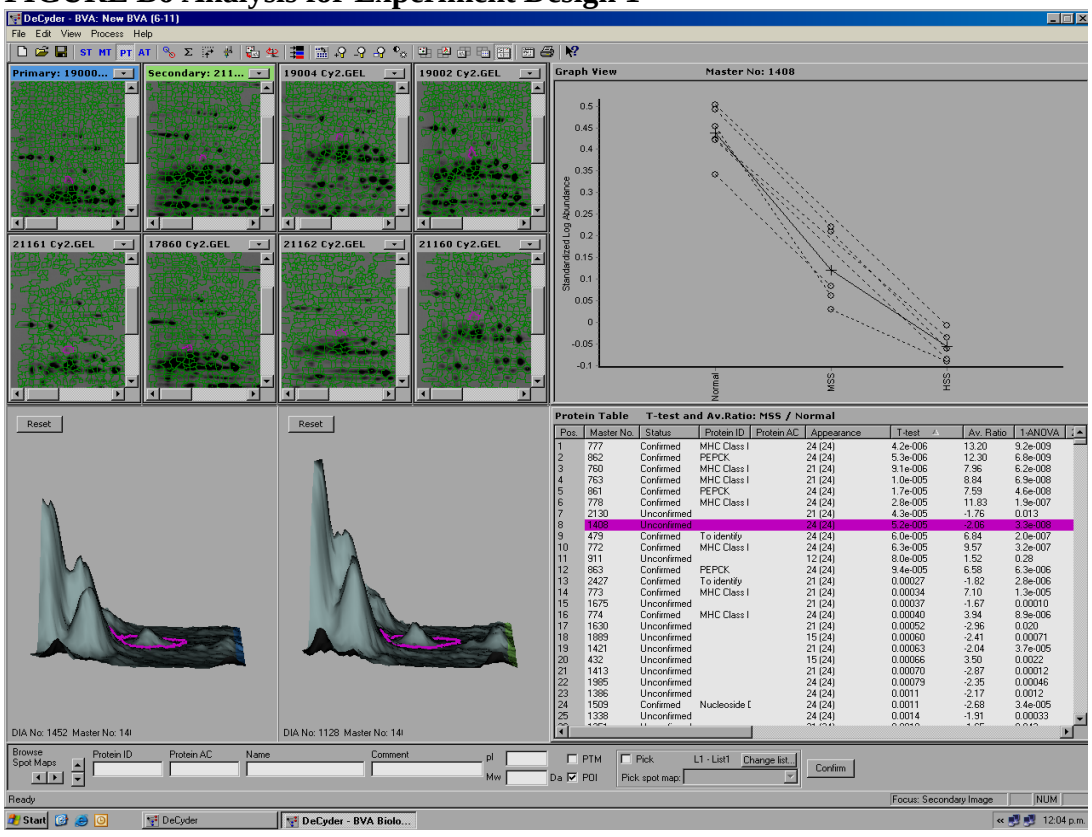

FIGURE B7

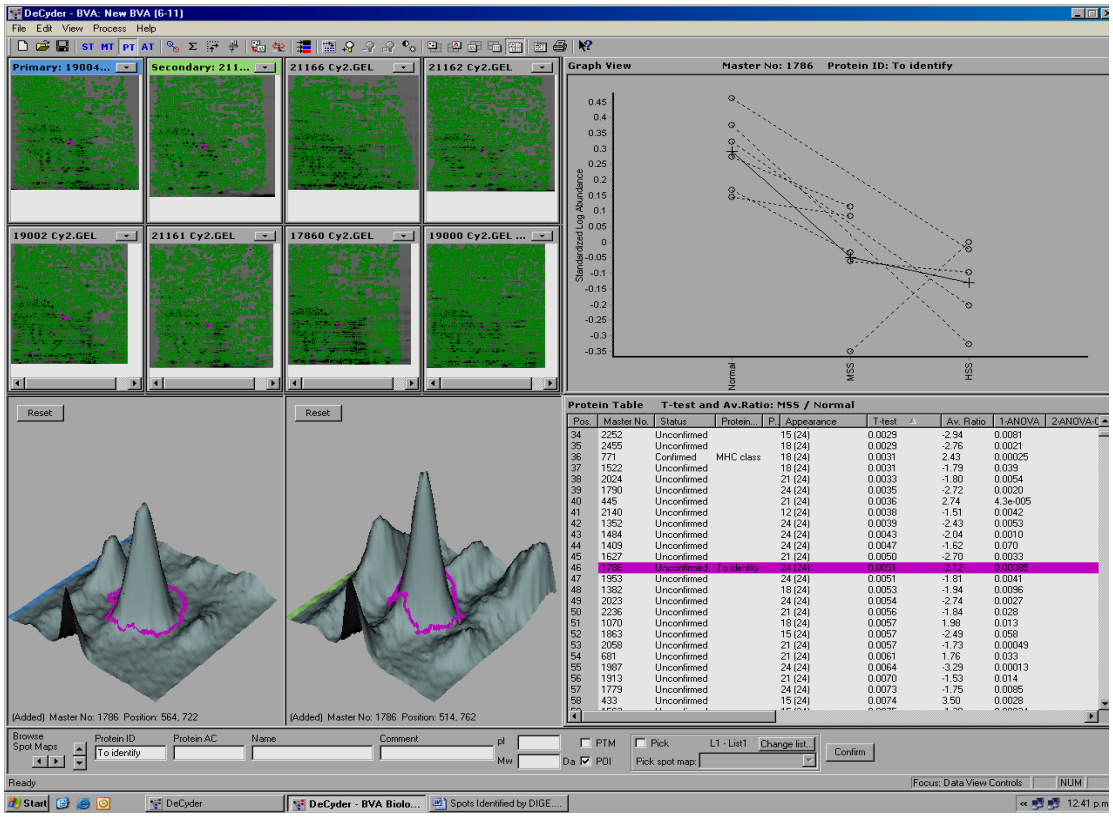

FIGURE B8

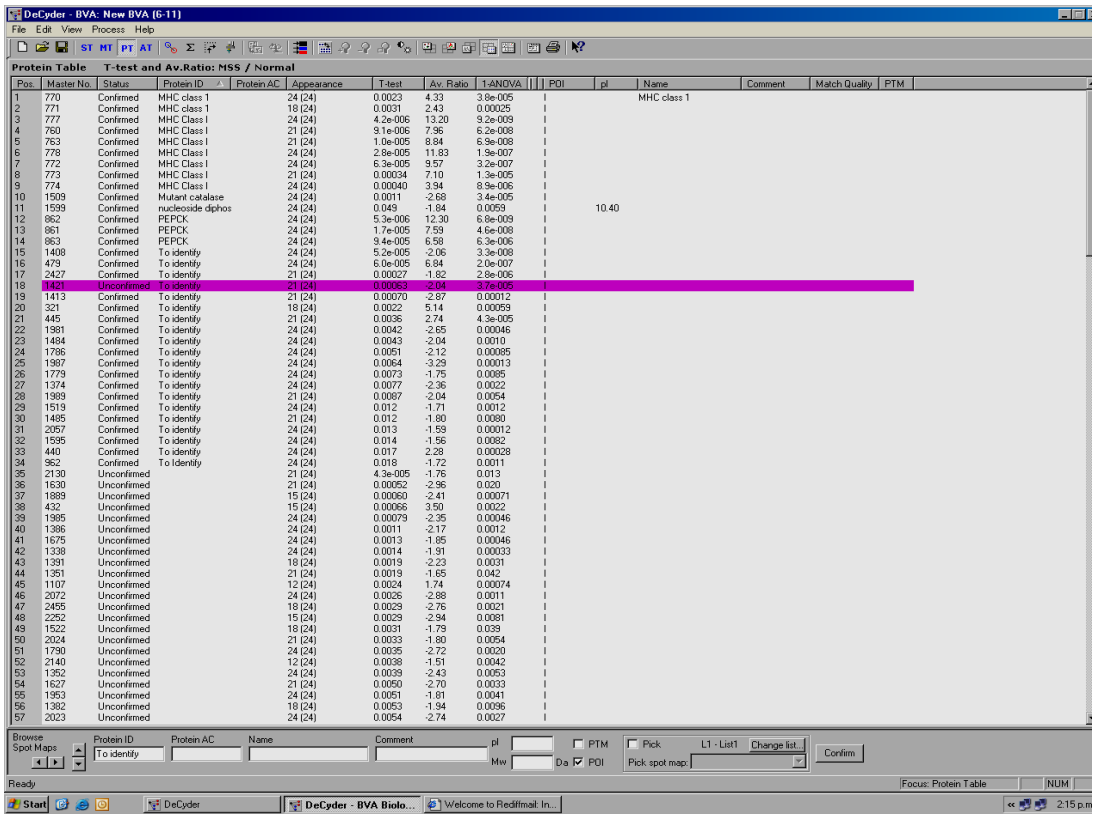

FIGURE B9

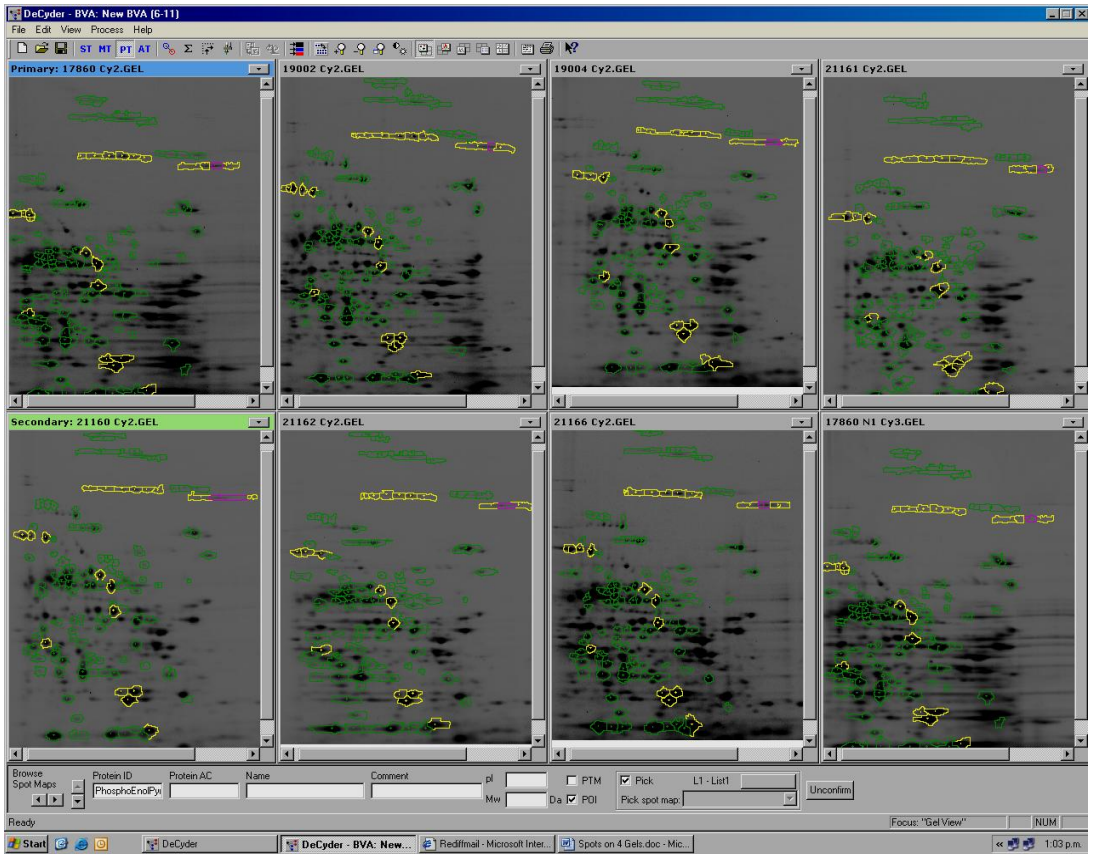

FIGURE B10 Analysis for Experiment Design 2
HSS/Control, ANOVA 0.01, 2-fold, with FDR

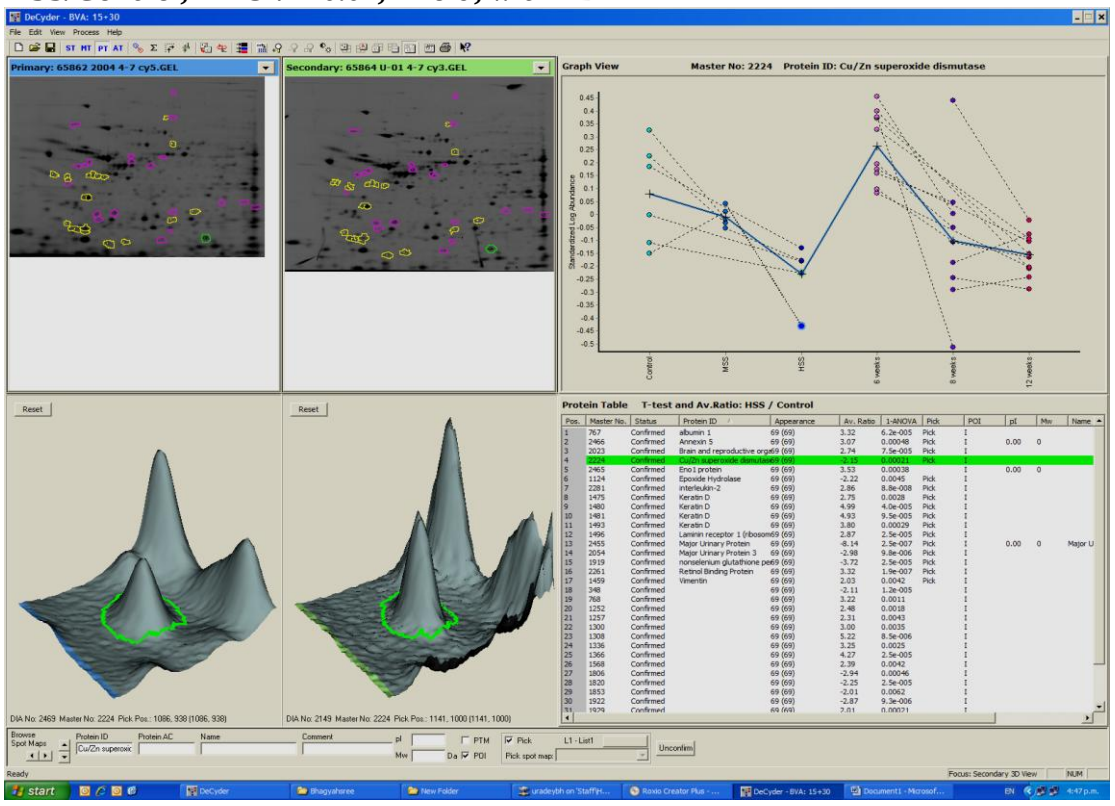

FIGURE B11 HSS/Control, ANOVA 0.01, 2-fold, with FDR

DeCyder - BVA: 15+30

File Edit View Process Help

Protein Table T-test and Av.Ratio: HSS / Control

Pos.	Master No.	Status	Protein ID	Appearance	Av. Ratio	1-ANOVA	Pick	POI	pI	Mw	Name	Comment
1	767	Confirmed	albumin 1	69 (69)	3.32	6.2e-005	Pick	I				
2	2466	Confirmed	Annexin 5	69 (69)	3.07	0.00048	Pick	I	0.00	0		
3	2023	Confirmed	Brain and reproductive orga	69 (69)	2.74	7.5e-005	Pick	I				
4	2224	Confirmed	Cu/Zn superoxide dismutase	69 (69)	-2.15	0.00021	Pick	I				
5	2465	Confirmed	Eno1 protein	69 (69)	3.53	0.00038		I	0.00	0		
6	1124	Confirmed	Epoxide Hydrolase	69 (69)	-2.22	0.0045	Pick	I				
7	2281	Confirmed	interleukin-2	69 (69)	2.86	8.8e-008	Pick	I				
8	1475	Confirmed	Keratin D	69 (69)	2.75	0.0028	Pick	I				
9	1480	Confirmed	Keratin D	69 (69)	4.99	4.0e-005	Pick	I				
10	1481	Confirmed	Keratin D	69 (69)	4.93	9.5e-005	Pick	I				
11	1493	Confirmed	Keratin D	69 (69)	3.80	0.00029	Pick	I				
12	1496	Confirmed	Laminin receptor 1 (ribosom	69 (69)	2.87	2.5e-005	Pick	I				
13	2455	Confirmed	Major Urinary Protein	69 (69)	-8.14	2.5e-007	Pick	I	0.00	0	Major Urinary Protein	
14	2054	Confirmed	Major Urinary Protein 3	69 (69)	-2.98	9.8e-006	Pick	I				
15	1919	Confirmed	nonselenium glutathione pe	69 (69)	-3.72	2.5e-005	Pick	I				
16	2261	Confirmed	Retinol Binding Protein	69 (69)	3.32	1.9e-007	Pick	I				
17	1459	Confirmed	Vimentin	69 (69)	2.03	0.0042	Pick	I				
18	348	Confirmed		69 (69)	-2.11	1.2e-005		I				
19	768	Confirmed		69 (69)	3.22	0.0011		I				
20	1252	Confirmed		69 (69)	2.48	0.0018		I				
21	1257	Confirmed		69 (69)	2.31	0.0043		I				
22	1300	Confirmed		69 (69)	3.00	0.0035		I				
23	1308	Confirmed		69 (69)	5.22	8.5e-006		I				
24	1336	Confirmed		69 (69)	3.25	0.0025		I				
25	1366	Confirmed		69 (69)	4.27	2.5e-005		I				
26	1568	Confirmed		69 (69)	2.39	0.0042		I				
27	1806	Confirmed		69 (69)	-2.94	0.00046		I				
28	1820	Confirmed		69 (69)	-2.25	2.5e-005		I				
29	1853	Confirmed		69 (69)	-2.01	0.0062		I				
30	1922	Confirmed		69 (69)	-2.87	9.3e-006		I				
31	1929	Confirmed		69 (69)	2.01	0.00021		I				
32	1944	Confirmed		69 (69)	6.13	8.8e-008		I				
33	2007	Confirmed		69 (69)	-2.05	0.00028		I				
34	2154	Confirmed		66 (69)	2.41	0.0030		I				
35	2251	Confirmed		69 (69)	2.17	2.5e-005		I				
36	2467	Confirmed		69 (69)	3.13	0.0024		I	0.00	0		

FIGURE B12 Extended Data Analysis

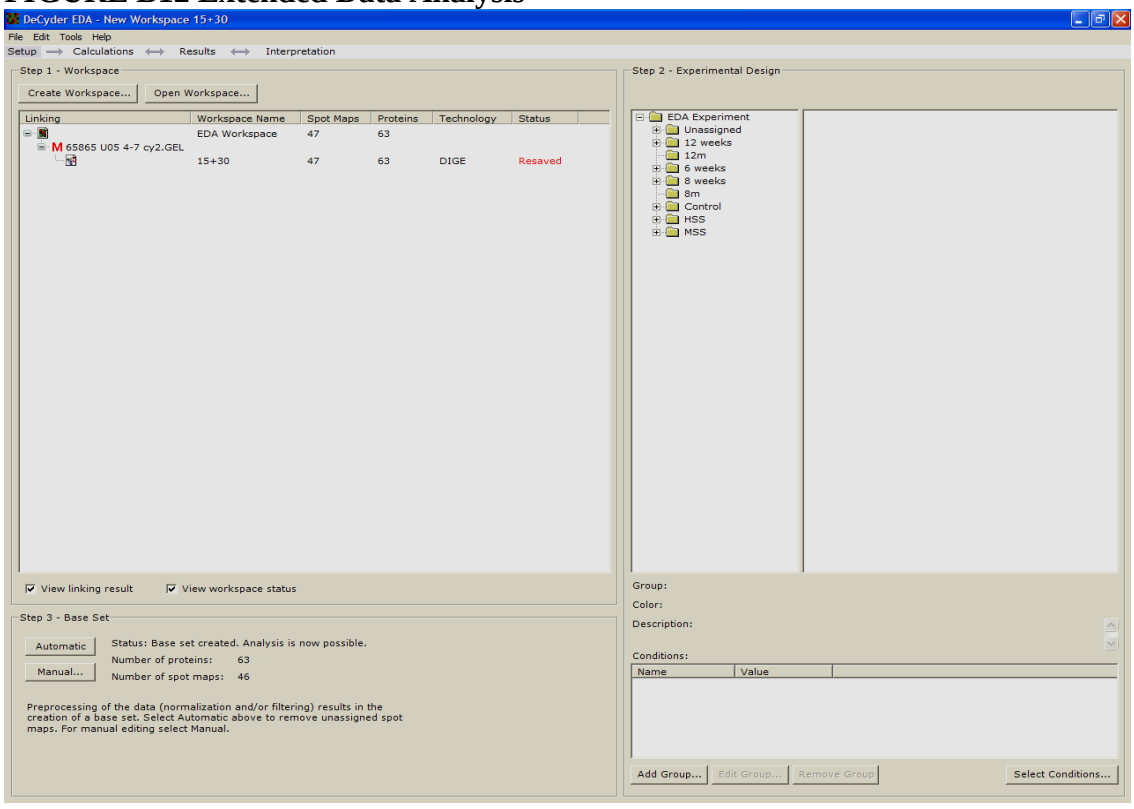

FIGURE B13

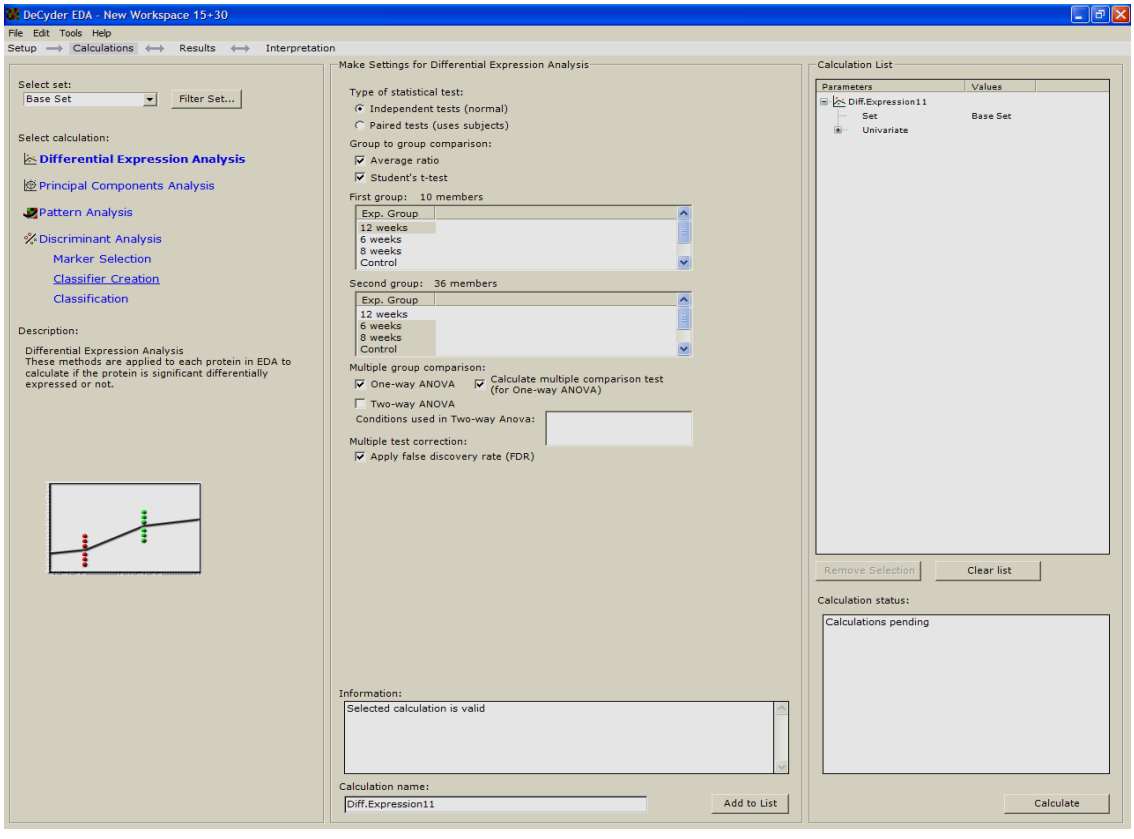

FIGURE B14

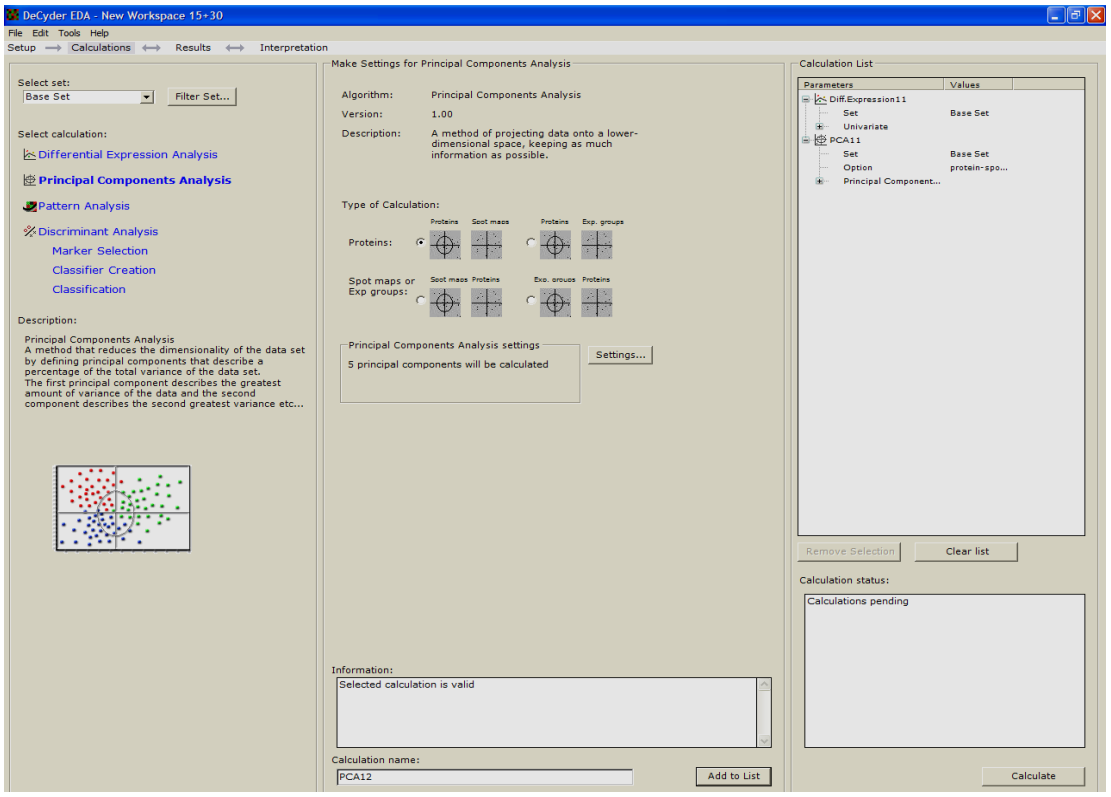

FIGURE B15

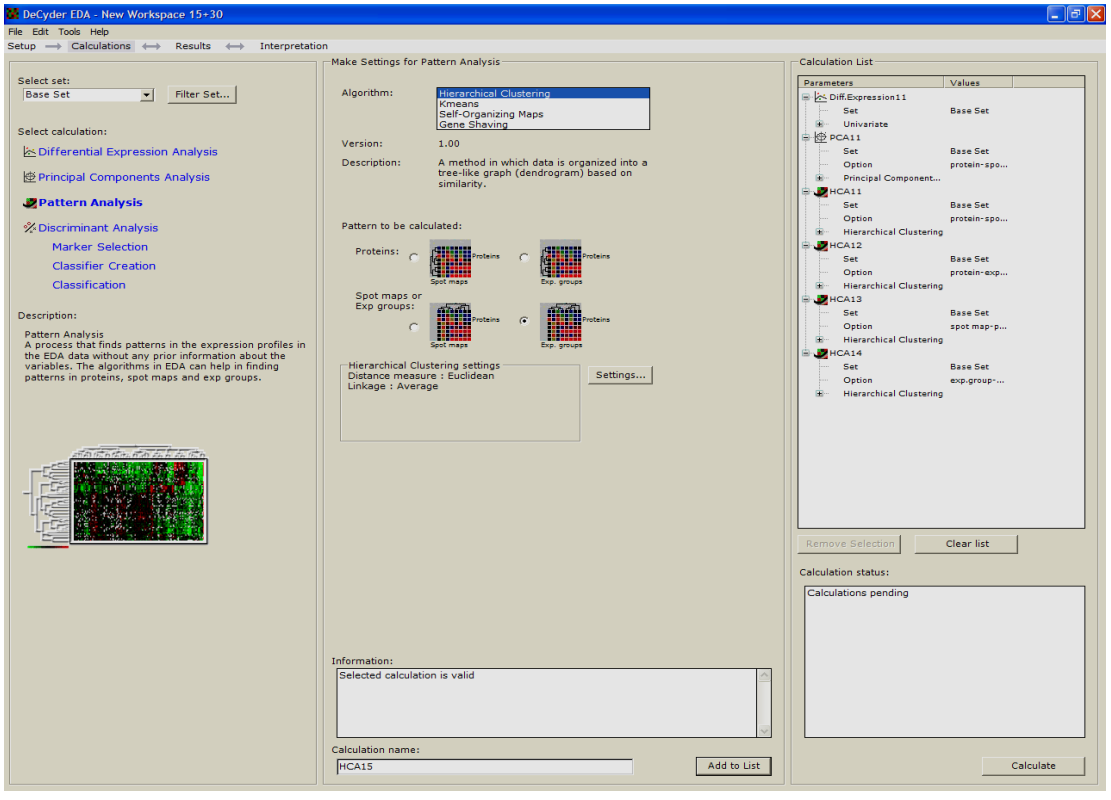

FIGURE B16

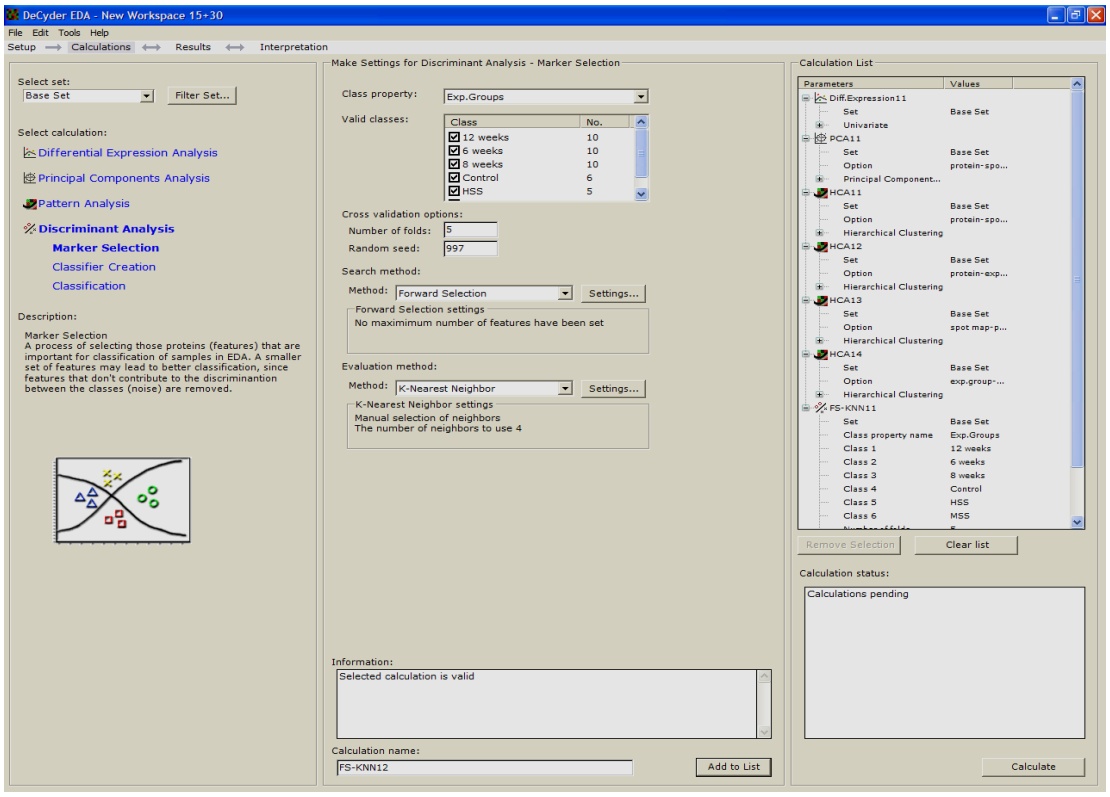

FIGURE B17 Differential Expression Analysis (DEA)

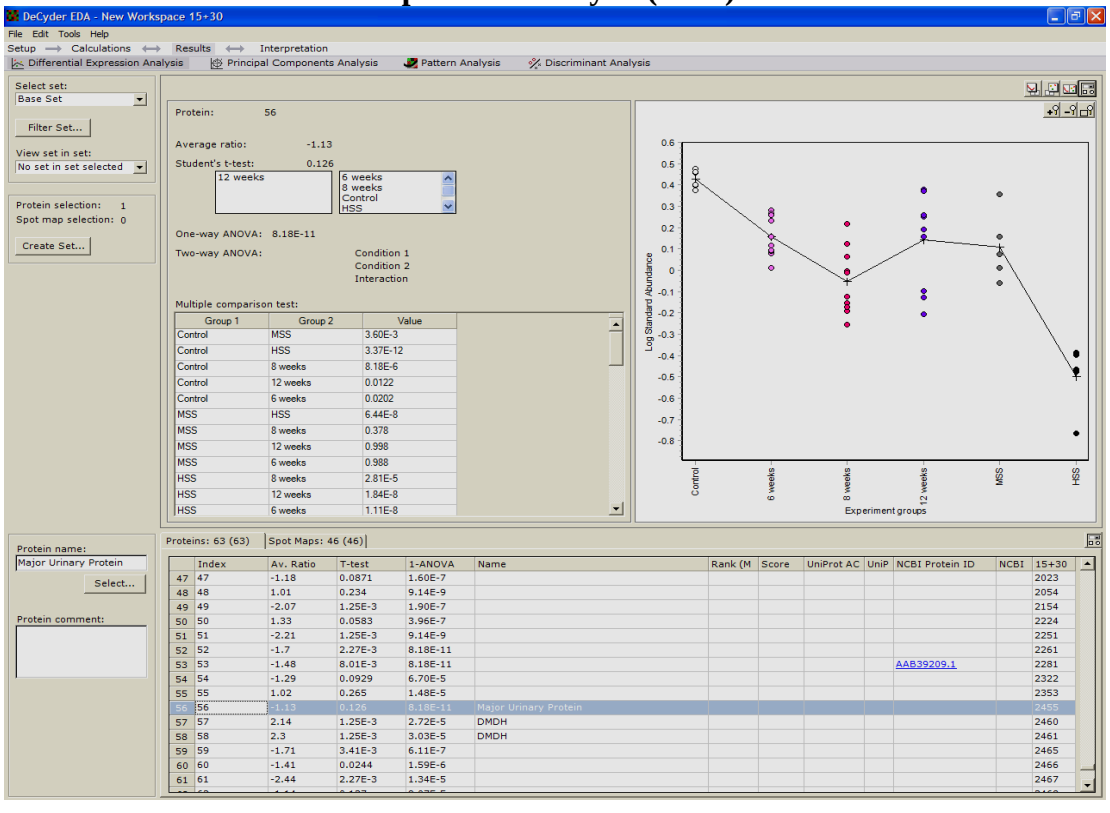

FIGURE B18 Principle Component Analysis (PCA)

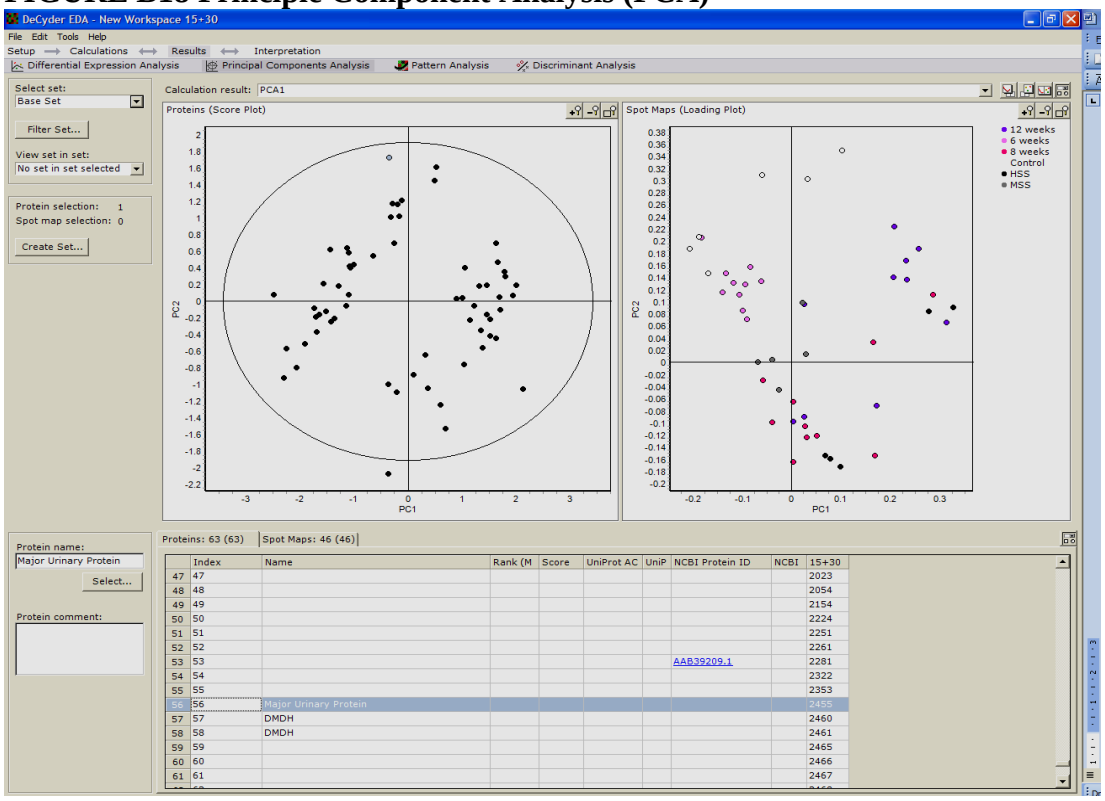

FIGURE B19 Hierarchical Cluster Analysis (HCA)

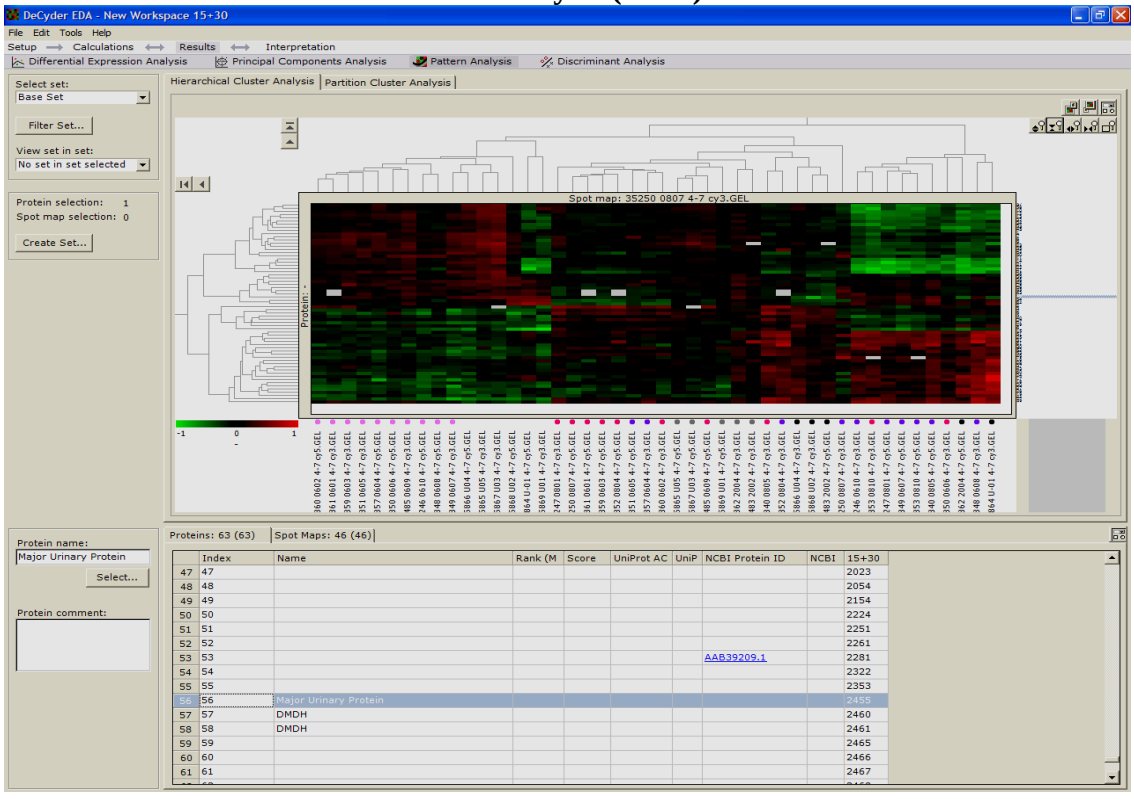

FIGURE B20 Discriminant Analysis for Marker Selection (DAMS)

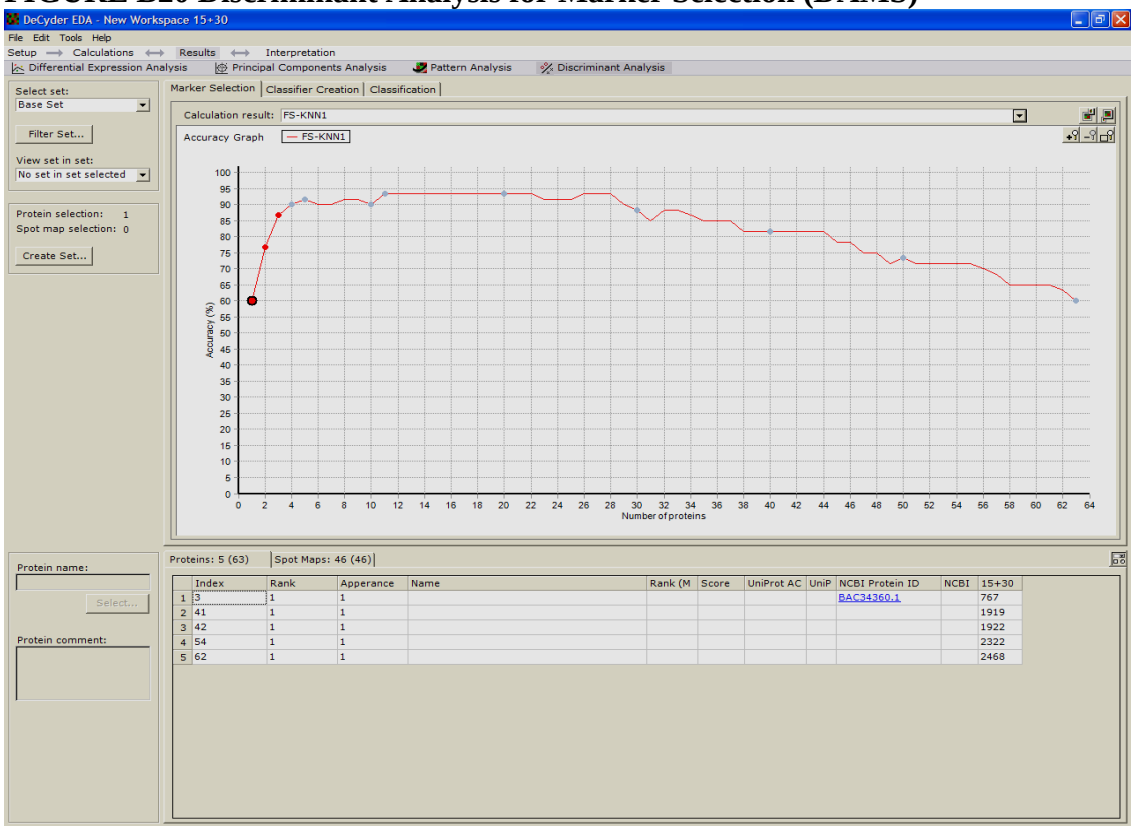

APPENDIX C

Protein spot identifications using preparative gel

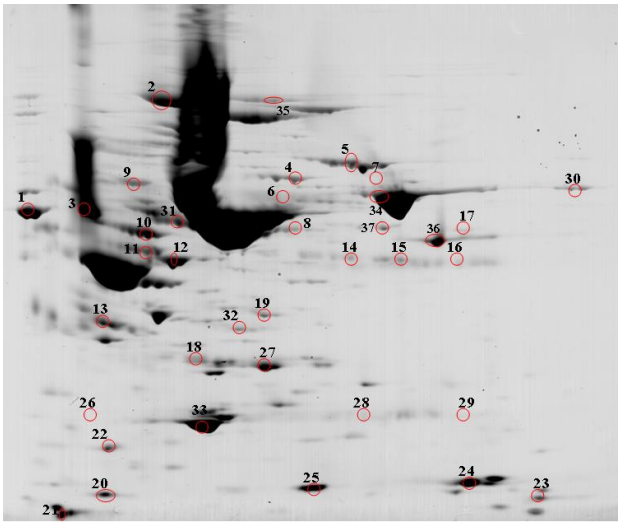

FIGURE C1 Preparative gel pI 3-10 with 75 µg protein from HSS serum. Numbers 1 to 33 are proteins identified by peptide mass finger printing using MALDI-TOF mass spectrometry. Below is the list of proteins.

TABLE C1 List of protein spots for Figure C1.

Spot No.	Expectation	Protein Description	Seq. Cov.%	pI	kDa	Peptides matched
1	3.7×10^{-11}	gi|19353306|gb|AAH24643.1| Albumin 1 [Mus musculus]	47	5.8	70.73	27
2	8.2×10^{-3}	gi|31982171|ref|NP_032671.2| murinoglobulin 1 [Mus musculus]	17	6.0	166.71	17
3	8.8×10^{-3}	gi|16741103|gb|AAH16407.1| Serine (or cysteine) proteinase inhibitor, clade A, member 3K [Mus musculus]	33	5.0	47.05	10
4	7.5×10^{-5}	gi|28916693|ref|NP_666232.2| gelsolin [Mus musculus]	19	5.8	86.32	13
5	2.6×10^{-5}	gi|31982113|ref|NP_032903.2| plasminogen [Mus musculus]	19	6.2	93.50	18
6	6.3×10^{-4}	gi|70049|pir||MHMSM Ig mu chain C region, membrane-bound form - mouse	20	5.9	53.27	11
7	3.0×10^{-3}	gi|60359986|dbj|BAD90212.1| mKIAA4106 protein [Mus musculus]	22	6.5	87.85	10
8	4.0×10^{-3}	gi|23956086|ref|NP_059067.1| hemopexin [Mus musculus]	28	8.4	52.06	11

9	8.9×10^{-4}	gi|72679472|gb|AAI00598.1| Unknown (protein for MGC:118711) (afamin)[Mus musculus]	29	5.5	71.33	20
10	6.0×10^{-6}	gi|63694077|ref|XP_622665.1| PREDICTED: similar to HMW kininogen-I variant [Mus musculus]	44	5.0	54.27	25
11	8.6×10^{-3}	gi|6650539|gb|AAF21895.1| epsilon-sarcoglycan [Mus musculus]	19	6.4	50.86	7
12	4.7×10^{-4}	gi|51172612|ref|NP_032122.1| group specific component (vitamin D-binding protein)[Mus musculus]	40	5.4	55.18	11
13	4.5×10^{-4}	gi|122120|sp|P01898|HA10_MOUSE H-2 class I histocompatibility antigen, Q10 alpha chain precursor	25	5.2	37.18	7
14	2.5×10^{-3}	gi|21304450|emb|CAD32498.1| immunoglobulin gamma1 heavy chain [Mus musculus]	6	6.0	56.08	9
15	6.7×10^{-3}	gi|26665404|dbj|BAC44885.1| immunoglobulin gamma-1 heavy chain [Mus musculus]	10	6.8	52.09	5
16	7.3×10^{-3}	gi|13097381|gb|AAH03435.1| Igh-4 protein [Mus musculus]	6	6.6	51.67	6
17	8.0×10^{-3}	gi|387437|gb|AAA39549.1| MHC factor B	29	9.1	54.56	16
18	7.4×10^{-6}	gi|34785996|gb|AAH57983.1| Pzp protein [Mus musculus] (Alpha-2-macroglobulin precursor (Pregnancy zone protein)) or **Sm 20.8 (*S. mansoni*)**	10	6.2	167.23	19
19	4.3×10^{-3}	gi|28175786|gb|AAH43338.1| Complement component 3 [Mus musculus]	10	6.3	188.01	14
20	8.3×10^{-3}	gi|16741595|gb|AAH16602.1| Galactokinase 1 [Mus musculus]	16	5.2	42.68	5
21	8.2×10^{-3}	gi|13096928|gb|AAH03261.1| Aurora kinase B (protein kinase)[Mus musculus]	26	9.6	39.53	5
22	3.8×10^{-3}	gi|13276755|emb|CAC34259.1| Major Urinary Protein [Mus musculus]	36	4.9	20.93	9
23	1.2×10^{-3}	gi|63561993|ref|XP_112440.3| PREDICTED: heparan sulfate D-glucosaminyl 3-O-sulfotransferase 2 [Mus musculus]	18	10.0	38.06	5
24	9.1×10^{-3}	gi|1183932|emb|CAA32224.1| haemoglobin beta-1 chain [Mus	56	7.1	15.94	9

		musculus]				
25	3.9×10^{-5}	gi|19354093|gb|AAH24702.1| Transthyretin [Mus musculus]	61	5.8	15.87	8
26	4.8×10^{-3}	gi|18655521|pdb|1IQW|L Chain L, Crystal Structure Of The Fab Fragment Of The Mouse Anti-Human Fas Antibody Hfe7a	36	5.0	24.16	6
27	7.7×10^{-5}	gi|34785996|gb|AAH57983.1| Pzp protein [Mus musculus] (Alpha-2-macroglobulin precursor (Pregnancy zone protein))	9	6.2	167.23	16
28	2.3×10^{-3}	gi|7024437|emb|CAB75889.1| immunoglobulin light chain [Mus musculus]	20	5.4	24.27	6
29	8.4×10^{-3}	gi|20269237|dbj|BAB90990.1| immunoglobulin kappa chain [Mus musculus]	40	8.0	24.43	8
31	1.0×10^{-3}	gi|23956086|ref|NP_059067.1| hemopexin [Mus musculus]	26	8.4	52.06	11
32	5.5×10^{-4}	gi|28175786|gb|AAH43338.1| Complement component 3 [Mus musculus] or **Glutathione Peroxidase(*S. mansoni*)**	10	6.3	188.01	23
33	1.4×10^{-9}	gi|2145139|gb|AAB58426.1| apolipoprotein A-I [Mus musculus]	51	5.5	30.35	18
34	2.4×10^{-5}	gi|62027488|gb|AAH92046.1| Transferrin [Mus musculus]	36	7.0	78.87	21
35	3.8×10^{-3}	gi|41946979|gb|AAH66092.1| Complement component factor h [Mus musculus]	9	6.7	143.80	12
36	2.1×10^{-5}	gi|28172876 protein 4.1G [Mus musculus]	15	6.2	77.24	11
37	5.4×10^{-3}	gi|18381134|gb|AAH22129.1| C8b protein [Mus musculus] (Complement component 8 subunit beta)	24	6.5	57.06	10

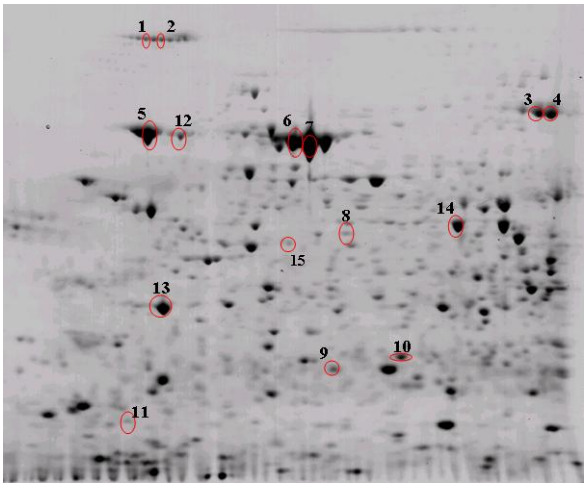

FIGURE C2: Preparative gel pI 4-7 with 400 µg protein from HSS liver lysate. Numbers 1 to 14 are proteins identified by peptide mass finger printing using MALDI-TOF mass spectrometry. Below is the list of proteins.

TABLE C2 List of protein spots for Figure C2.

Spot No.	Expectation	Protein Description	Seq. Cov. %	pI	kDa	Peptides matched
1	4.4×10^{-4}	gi|27817830|dbj|BAC55524.2| connectin/titin N2A-PEVK [Mus musculus]	8	5.6	130.71	20
3	8.4×10^{-3}	gi|62027488|gb|AAH92046.1| Transferrin [Mus musculus]	20	7.0	78.87	19
4	6.7×10^{-3}	gi|62027488|gb|AAH92046.1| Transferrin [Mus musculus]	11	7.0	78.87	16
5	1.1×10^{-3}	gi|31981722|ref|NP_071705.2| heat shock 70kD protein 5 (glucose-regulated protein) [Mus musculus]	34	5.0	72.52	19
6	6.0×10^{-5}	gi|26341396|dbj|BAC34360.1| unnamed protein product [Mus musculus] (Albumin 1)	28	5.5	67.04	14
7	5.3×10^{-5}	gi|26341396|dbj|BAC34360.1| Albumin [Mus musculus]	31	5.5	67.04	14
8	9.6×10^{-3}	gi|2612795|emb|CAA05364.1| annexin VIII [Mus musculus]	25	5.6	37.05	14
9	3.6×10^{-3}	gi|38173925|gb|AAH61000.1| Brain and reproductive organ-expressed protein [Mus musculus]	14	5.7	43.95	9
10	9.8×10^{-3}	gi|59889574|ref|NP_038943.3| zinc finger protein 238 isoform 2 [Mus musculus]	14	5.4	59.45	9

11	5.5×10^{-4}	gi|1504135|gb|AAB39209.1| interleukin-2 [Mus musculus]	19	4.9	18.68	5
12	6.8×10^{-3}	gi|31981722|ref|NP_071705.2| heat shock 70kD protein 5 (glucose-regulated protein) [Mus musculus]	31	5.0	72.52	16
13	5.1×10^{-3}	gi|47117852|sp|P46718|PDCD2_MOUSE Programmed cell death protein 2 (Zinc finger protein Rp-8)	10	5.2	39.41	7
14	6.9×10^{-4}	gi|13278412|gb|AAH04017.1| Eno1 protein [Mus musculus]	31	5.6	38.62	12
15	6.8×10^{-4}	gi|6680117|ref|NP_032206.1| glutathione synthetase [Mus musculus]	31	5.6	52.46	15

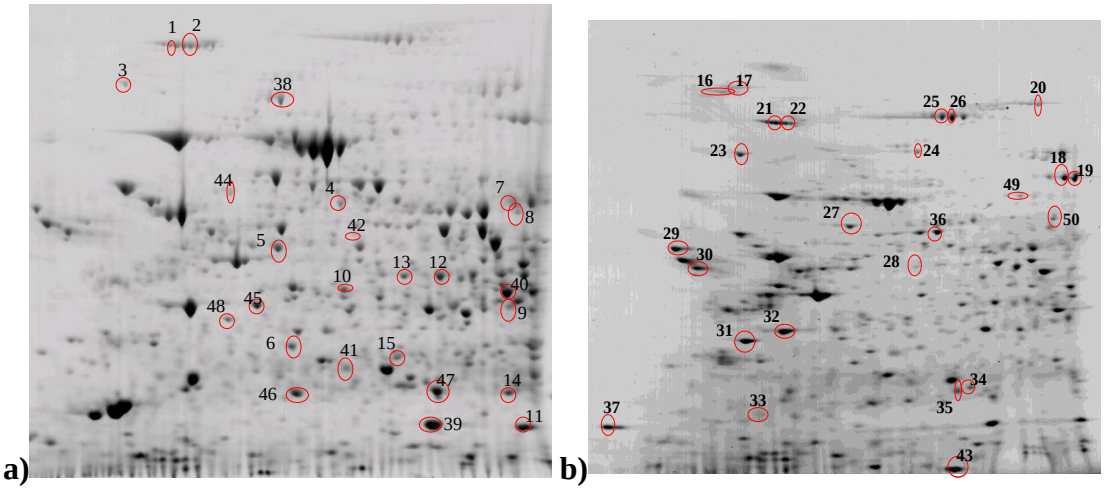

FIGURE C3 a) Preparative gel pI 4-7 with 400 µg protein from MSS liver lysate. **b)** Preparative gel pI 4-7with 75 µg protein from HSS liver lysate. Numbers 1 to 50 are proteins identified by peptide mass finger printing using MALDI-TOF mass spectrometry. Below is the list of proteins.

TABLE C3 List of protein spots for Figure C3 (a, b).

Spot No.	Expectation	Protein Description	Seq. Cov.%	pI	kDa	Peptides matched
1	9.1×10^{-3}	gi|12805443|gb|AAH02194.1| Col6a1 protein [Mus musculus]	19	5.8	44.76	9
2	7.7×10^{-3}	gi|12805443|gb|AAH02194.1| Col6a1 protein [Mus musculus]	19	5.8	44.76	9
3	1.3×10^{-4}	gi|14714615|gb|AAH10445.1| Tumor rejection antigen gp96 [Mus musculus]	15	4.7	92.76	9
4	9.9×10^{-4}	gi|285016|pir||S27878 selenium-binding	21	6.0	52.90	12

		protein, hepatic - mouse				
5	1.8×10^{-4}	gi|19353306|gb|AAH24643.1| Albumin 1 [Mus musculus]	26	5.8	70.73	13
6	6.6×10^{-3}	gi|13384778|ref|NP_079672.1| 6-phosphogluconolactonase [Mus musculus]	32	5.6	27.46	20
7	7.4×10^{-3}	gi|9910128|ref|NP_064377.1| aldehyde dehydrogenase 9, subfamily A1 [Mus musculus]	29	6.6	54.47	13
9	7.4×10^{-3}	gi|63517253|ref|XP_144057.3| PREDICTED: similar to elastase 3B, pancreatic [Mus musculus]	9	6.4	38.02	6
10	5.9×10^{-3}	gi|20380027|gb|AAH28817.1| Fthfd protein [Mus musculus]	10	5.6	99.55	10
	-	gi|23271467|gb|AAH24055.1| Fthfd protein [Mus musculus]	10	5.7	99.57	10
11	8.8×10^{-4}	gi|56800495|emb|CAI35365.1| expressed in non-metastatic cells 1 protein [Mus musculus]	45	9.1	14.13	7
12	3.4×10^{-4}	gi|5834643|emb|CAB55352.1| N-acetylgalactosaminyltransferase T-6 [Mus musculus]	7	9.5	72.23	5
13	3.5×10^{-7}	gi|7106255|ref|NP_031508.1| arginase 1, liver [Mus musculus]	64	6.5	34.96	20
14	3.4×10^{-3}	gi|26986064|emb|CAC81903.1| albumin [Mus musculus]	37	5.5	24.23	18
15	9.8×10^{-3}	gi|59889574|ref|NP_038943.3| zinc finger protein 238 isoform 2 [Mus musculus]	14	5.4	59.45	11
16	9.2×10^{-3}	gi|30420885|gb|AAO64442.1| collagen type XIV [Mus musculus]	11	5.0	194.30	6
17	4.8×10^{-3}	gi|30420885|gb|AAO64442.1| collagen type XIV [Mus musculus]	18	5.0	194.30	8
18	5.2×10^{-6}	gi|62027488|gb|AAH92046.1| Transferrin [Mus musculus]	23	7.0	78.87	19
19	9.2×10^{-7}	gi|62027488|gb|AAH92046.1| Transferrin [Mus musculus]	30	7.0	78.87	20
20	7.0×10^{-6}	gi|73918911|sp|Q8C196|CPSM_MOUSE Carbamoyl-phosphate synthase [ammonia], mitochondrial precursor (Carbamoyl-phosphate synthetase I) (CPSase I)	20	6.5	165.80	24
21	8.1×10^{-3}	gi|12805443|gb|AAH02194.1| Col6a1 protein [Mus musculus]	24	5.8	44.76	11
22	8.6×10^{-3}	gi|12805443|gb|AAH02194.1| Col6a1 protein [Mus musculus]	14	5.8	44.76	8
23	3.9×10^{-7}	gi|14714615|gb|AAH10445.1| Tumor rejection antigen gp96 [Mus musculus]	24	4.7	92.76	12
24	9.6×10^{-4}	gi|20380027|gb|AAH28817.1| Fthfd protein	22	5.6	99.55	18

		[Mus musculus]				
25	4.9×10^{-3}	gi|73918911|sp|Q8C196|CPSM_MOUSE Carbamoyl-phosphate synthase [ammonia], mitochondrial precursor (CPSase I)	25	6.5	165.80	22
26	5.0×10^{-4}	gi|73918911|sp|Q8C196|CPSM_MOUSE Carbamoyl-phosphate synthase [ammonia], mitochondrial precursor (CPSase I)	25	6.5	165.80	22
27	1.9×10^{-3}	gi|31981679|ref|NP_034607.2| heat shock protein 1 (chaperonin) [Mus musculus]	28	5.7	61.11	15
29, 30	4.4×10^{-3}	gi|28913521|gb|AAH48688.1| Similar to zinc finger protein (C2H2 type) 276 [Mus musculus]	36	5.7	11.62	5
31	4.4×10^{-4}	gi|13277612|gb|AAH03716.1| Anxa5 protein [Mus musculus]	45	4.8	35.78	19
32	8.3×10^{-3}	gi|6677739|ref|NP_033086.1| regucalcin [Mus musculus]	25	5.2	33.90	17
34	4.4×10^{-4}	gi|27753960|ref|NP_083907.2| hypothetical protein LOC76491 [Mus musculus] (alpha/beta hydrolase domain containing 14b)	16	5.8	22.55	7
36	4.1×10^{-4}	gi|26353794|dbj|BAC40527.1| unnamed protein product [Mus musculus] (protein disulfide-isomerase (EC 5.3.4.1) ERp61)	38	5.8	57.12	12
37	9.2×10^{-4}	gi|26338069|dbj|BAC32720.1| unnamed protein product [Mus musculus]	28	4.2	12.43	3
38	7.0×10^{-3}	gi|26326751|dbj|BAC27119.1| unnamed protein product [Mus musculus] (valosin containing protein)	22	5.1	90.04	7
39	3.8×10^{-4}	gi|226471|prf||1513495A Cu/Zn superoxide dismutase	45	6.0	15.91	7
40	8.2×10^{-5}	gi|7106255|ref|NP_031508.1| arginase 1, liver [Mus musculus]	58	6.5	34.96	15
42	1.8×10^{-4}	gi|13542782|gb|AAH05595.1| Anxa6 protein [Mus musculus]	8	5.3	75.70	6
43	4.0×10^{-3}	gi|12849189|dbj|BAB28242.1| unnamed protein product [Mus musculus](Ubiquitin B)	25	6.9	34.38	10
44	8.5×10^{-3}	gi|51172612|ref|NP_032122.1| group specific component [Mus musculus]	15	5.4	55.18	7
48	6.4×10^{-4}	gi|13385584|ref|NP_080361.1| MAWD binding protein homolog 2 [Mus musculus]	47	5.2	32.19	14
50	8.6×10^{-3}	gi|31980726|ref|NP_082408.2| phosphoglucomutase 2 [Mus musculus]	32	6.3	61.78	15

a) 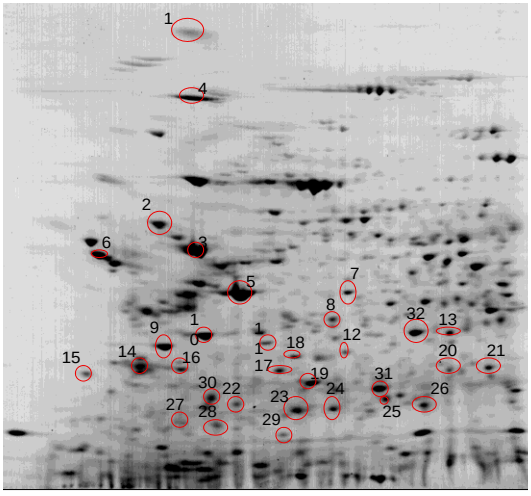 b) 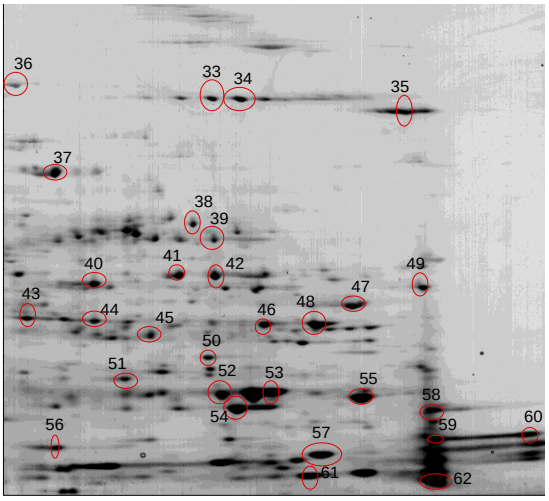

FIGURE C4 a) Preparative gel pI 4-7 with 60 µg protein from HSS liver lysate. **b)** Preparative gel pI 6-11 with 60 µg protein from HSS liver **l**ysate. Numbers 1 to 62 are proteins identified by peptide mass finger printing using MALDI-TOF mass spectrometry.

TABLE C4 List of protein spots for FigureC4 (a,b).

Spot No.	Expectation	Protein Description	Seq. Cov. %	pI	kDa	Peptides matched
1	4.4×10^{-3}	gi|28373538|pdb|1LB3|A Chain A, Structure Of Recombinant Mouse L Chain Ferritin At 1.2 A Resolution	38	5.6	20.68	11
3	5.9×10^{-4}	gi|23272966|gb|AAH37127.1| Atp5b protein [Mus musculus]	27	5.2	56.65	24
4	4.5×10^{-4}	gi|12805443|gb|AAH02194.1| Col6a1 protein [Mus musculus]	20	5.8	44.76	9
5	2.1×10^{-2}	gi|49868|emb|CAA27396.1| put. beta-actin (aa 27-375) [Mus musculus]	21	5.8	39.45	8
10	4.4×10^{-5}	gi|74191500 unnamed protein product [Mus musculus] Protein Disulfide Isomerase (PDIb) family proteins	28	4.8	57.42	15
11	6.9×10^{-5}	gi|33416530|gb|AAH55871.1| Annexin A4 [Mus musculus]	37	5.4	36.20	16
12	7.7×10^{-4}	gi|388921|gb|AAC37635.1| purine nucleoside phosphorylase	36	5.9	32.54	9
13	8.5×10^{-4}	gi|63712196|ref|XP_354652.3| PREDICTED: 3-hydroxyanthranilate 3,4-dioxygenase [Mus musculus]	33	6.3	25.61	10
18	5.3×10^{-4}	gi|56206786|emb|CAI24278.1| prohibitin [Mus musculus]	34	6.0	23.04	11
19	8.9×10^{-3}	gi|63660253|ref|XP_619203.1|	37	9.6	20.73	8

		PREDICTED: hypothetical protein XP_619203 [Mus musculus]				
22	7.1×10^{-5}	gi|12844989|dbj|BAB26576.1| unnamed protein product [Mus musculus] (phosphoglycerate mutase 1)	55	6.7	28.80	14
23	6.3×10^{-3}	gi|51830637|ref|XP_141626.3| PREDICTED: hypothetical protein XP_141626 [Mus musculus] (PREDICTED: similar to Ubiquitin-conjugating enzyme E2Q (putative) 2 [Mus musculus])	11	4.5	43.56	7
24	1.7×10^{-3}	gi|26338652|dbj|BAC32997.1| unnamed protein product [Mus musculus]	19	6.8	19.39	7
25	1.6×10^{-3}	gi|28373538|pdb|1LB3|A Chain A, Structure Of Recombinant Mouse L Chain Ferritin At 1.2 A Resolution	38	5.6	20.68	9
26	5.2×10^{-4}	gi|12846314|dbj|BAB27120.1| unnamed protein product [Mus musculus] (Peroxiredoxin 1)	31	8.6	22.45	11
27	2.6×10^{-3}	gi|13385268|ref|NP_080073.1| cytochrome b-5 [Mus musculus]	49	4.9	15.22	6
28	1.6×10^{-4}	gi|33585469|gb|AAH55479.1| Pik4ca protein [Mus musculus] / unknown [Schistosoma japonicum]	17	6.2	35.86	8
29	3.9×10^{-3}	gi|46401561|dbj|BAD16627.1| peptidylarginine deiminase, type IV [Mus musculus]/ ubiquitin [Schistosoma mansoni]	13	6.6	74.97	14
30	8.5×10^{-5}	gi|51859026|gb|AAH81432.1| Glyoxalase 1 [Mus musculus]	27	5.2	20.96	11
31	8.7×10^{-3}	gi|50510361|dbj|BAD32166.1| nonselenium glutathione peroxidase [Mus musculus] (peroxiredoxin 6)	28	6.0	25.05	7
32	6.3×10^{-7}	gi|56206644|emb|CAI24411.1| malate dehydrogenase, soluble [Mus musculus]	15	6.2	36.66	8
33	3.8×10^{-3}	gi|51770518|ref|XP_489790.1| PREDICTED: similar to MHC class I histocompatibility antigen H-2 Q4 alpha chain precursor - mouse [Mus musculus]	8	7.3	71.74	5
34	2.9×10^{-3}	gi|51770518|ref|XP_489790.1| PREDICTED: similar to MHC class I histocompatibility antigen H-2 Q4 alpha chain precursor - mouse [Mus musculus]	16	7.3	71.74	7
35	1.4×10^{-3}	gi|56753812 SJCHGC06900 protein [Schistosoma japonicum](gi|74828716 *S. mansoni*-Phosphoenolpyruvate carboxykinase (*Sm*-PEPCK))	16	6.4	71.33	6

36	2.2×10^{-6}	gi|62027488|gb|AAH92046.1| Transferrin [Mus musculus]	24	7.0	78.87	16
37	4.6×10^{-4}	gi|73918911|sp|Q8C196|CPSM_MOUSE Carbamoyl-phosphate synthase [ammonia], mitochondrial precursor (Carbamoyl-phosphate synthetase I) (CPSase I)	9	6.5	165.8	8
38	2.5×10^{-3}	gi|15004258|gb|AAK73774.1| mutant catalase [Mus musculus]	18	7.8	60.01	14
39	4.7×10^{-3}	gi|63575386|ref|XP_620669.1| PREDICTED: similar to Nucleoside diphosphate kinase B (NDK B) (NDP kinase B) (P18) [Mus musculus]	22	10.4	14.98	6
40	5.8×10^{-4}	gi|8569275|pdb|1QCO|B Chain B, Crystal Structure Of Fumarylacetoacetate Hydrolase Complexed With Fumarate And Acetoacetate	30	7.0	46.72	15
41	9.4×10^{-4}	gi|202423|gb|AAA70267.1| phosphoglycerate kinase	27	7.7	44.92	14
42	5.2×10^{-3}	gi|26339842|dbj|BAC33584.1| unnamed protein product [Mus musculus] (Sulfatase)	11	9.5	70.61	19
43	8.1×10^{-3}	gi|7106255|ref|NP_031508.1| arginase 1, liver [Mus musculus]	37	6.5	34.96	14
44	3.4×10^{-3}	gi|6679184|ref|NP_032795.1| ornithine transcarbamylase [Mus musculus]	30	8.9	39.86	10
47	2.9×10^{-4}	gi|21450291|ref|NP_659152.1| aldolase 2, B isoform [Mus musculus]	27	9.0	39.95	12
48	8.9×10^{-5}	gi|6678509|ref|NP_033500.1| urate oxidase [Mus musculus]	45	8.7	35.25	19
49	8.4×10^{-6}	gi|2690302|gb|AAB91426.1| aspartate aminotransferase precursor [Mus musculus]	26	9.3	47.79	9
50	2.2×10^{-3}	gi|12846591|dbj|BAB27227.1| Cytochrome b5 reductase [Mus musculus]	37	9.3	33.78	17
52	5.9×10^{-3}	gi|193690|gb|AAA37748.1| glutathione transferase (EC 2.5.1.18)	40	7.8	24.82	11
53	5.4×10^{-3}	gi|10197496|gb|AAG14901.1| CD5.1 [Mus musculus]	9	9.6	55.14	14
54	3.6×10^{-4}	gi|2624496|pdb|1BAY|B Chain B, Glutathione S-Transferase Yfyf Cys 47-Carboxymethylated Class Pi, Free Enzyme	41	8.3	23.52	9
55	9.4×10^{-3}	gi|56752803 Schistosoma japonicum short chain dehydrogenase	23	9.9	24.19	11
56	2.4×10^{-3}	gi|55716028 Rpl13 protein [Mus musculus] (Ribosomal Protein L 13)	17	9.9	24.64	10
57	4.0×10^{-3}	gi|40786428|ref|NP_955398.1| galactose-	24	8.5	47.12	14

		3-O-sulfotransferase 2 [Mus musculus]				
58	1.1×10^{-3}	gi|54607171|ref|NP_032502.3| keratin complex 2, basic, gene 6a [Mus musculus]	22	8.3	59.66	16
60	3.7×10^{-3}	gi|18044023|gb|AAH19638.1| 4632417K18Rik protein [Mus musculus]	10	5.9	45.82	10
61	6.3×10^{-3}	gi|56237900|emb|CAI25914.1| zinc finger protein 287 [Mus musculus]	11	8.8	87.58	19
62	2.7×10^{-3}	gi|45219726|gb|AAH66798.1| RIKEN cDNA 3000003F02 [Mus musculus]	11	8.6	79.91	15

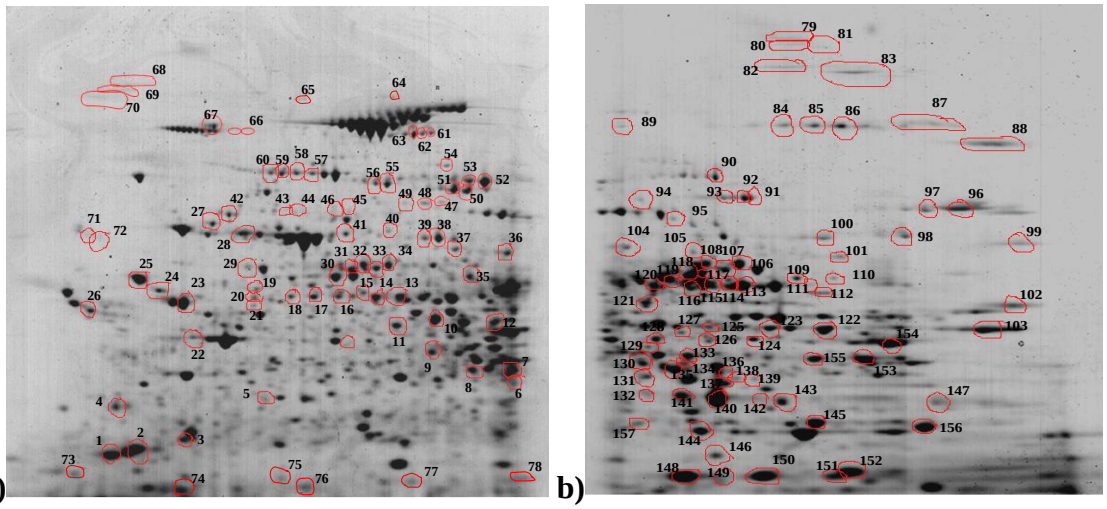

FIGURE C5 a) Preparative gel pI 4-7 with 75 µg protein from HSS liver lysate. **b)** Preparative gel pI 6-11 with 75 µg protein from HSS liver lysate. Numbers 1 to 157 are proteins identified by peptide mass finger printing using MALDI-TOF mass spectrometry.

TABLE C5 List of protein spots for Figure C5 (a, b).

Spot No.	Expectation	Protein Description	Seq. Cov.%	pI	kDa	Peptides matched
1	8.2×10^{-3}	gi|53271|emb|CAA27227.1| MUP [Mus musculus]	70	4.8	17.71	8
2	8.3×10^{-3}	gi|53271|emb|CAA27227.1| MUP [Mus musculus]	70	4.8	17.71	8
3	5.5×10^{-4}	gi|115615 Calpain (Calcium-activated neutral proteinase) (CANP)	14	5.3	87.56	5
4	7.6×10^{-3}	gi|1841387|dbj|BAA11751.1| 14-3-3 zeta [Mus musculus]	31	4.7	27.88	12
5	2.8×10^{-4}	gi|56206786|emb|CAI24278.1| prohibitin [Mus musculus]	29	6.0	23.04	11

6	8.1×10^{-4}	gi|62533211|gb|AAH93510.1| Betaine-homocysteine methyltransferase [Mus musculus]	25	8.4	45.46	16
7	3.5×10^{-3}	gi|62533211|gb|AAH93510.1| Betaine-homocysteine methyltransferase [Mus musculus]	33	8.4	45.46	14
8	9.5×10^{-3}	gi|6166177|sp|P15105|GLNA_MOUSE Glutamine synthetase (Glutamate--ammonia ligase) (GS)	21	6.5	42.81	13
9	1.8×10^{-4}	gi|12584974|ref|NP_075022.1| betaine-homocysteine methyltransferase 2 [Mus musculus]	26	6.0	40.28	15
10	2.7×10^{-3}	gi|63471580|ref|XP_619602.1| PREDICTED: similar to S-adenosylhomocysteine hydrolase [Mus musculus]	28	6.1	48.08	14
11	1.0×10^{-3}	gi|63471580|ref|XP_619602.1| PREDICTED: similar to S-adenosylhomocysteine hydrolase [Mus musculus]	24	6.1	48.08	13
12	5.2×10^{-4}	gi|7549763|ref|NP_038575.1| homogentisate 1, 2-dioxygenase [Mus musculus]	24	6.9	50.77	11
13	5.5×10^{-4}	gi|29244162 hypothetical protein LOC237029 [Mus musculus]	19	5.1	54.68	10
16	9.6×10^{-3}	gi|285016|pir||S27878 selenium-binding protein, hepatic - mouse	35	6.0	52.90	17
17	4.0×10^{-5}	gi|18848341|gb|AAH24106.1| Selenium binding protein 2 [Mus musculus]	31	5.8	53.16	12
18	2.3×10^{-3}	gi|18848341|gb|AAH24106.1| Selenium binding protein 2 [Mus musculus]	21	5.8	53.16	10
21	2.7×10^{-3}	gi|50510861|dbj|BAD32416.1| mKIAA1258 protein (guanine deaminase)[Mus musculus]	27	5.4	55.11	14
22	4.9×10^{-3}	gi|809561|emb|CAA31455.1| gamma-actin [Mus musculus]	21	5.6	41.34	7
23	3.7×10^{-4}	gi|23272966|gb|AAH37127.1| Atp5b protein [Mus musculus]	25	5.2	56.65	23
24	4.4×10^{-5}	gi|74203945 Protein Disulfide Isomerase [Mus musculus]	19	4.8	56.97	11
25	5.0×10^{-10}	gi|74203945 prolyl 4-hydroxylase, beta polypeptide [Mus musculus]	36	4.8	56.97	18
27	2.7×10^{-3}	gi|45219865|gb|AAH66857.1| protein disulfide isomerase associated 4 [Mus musculus]	26	5.9	65.41	13
29	2.9×10^{-3}	gi|183396771|ref|NP_034607.3| heat	22	5.7	61.11	12

		shock protein 1 (chaperonin) [Mus musculus]				
30	8.3×10^{-3}	gi|18252784|ref|NP_543121.1| formiminotransferase cyclodeaminase [Mus musculus]	36	5.8	59.55	16
31	9.8×10^{-4}	gi|15929294|gb|AAH15087.1| Epoxide hydrolase 2, cytoplasmic [Mus musculus]	14	5.9	63.07	11
33	2.9×10^{-3}	gi|15929294|gb|AAH15087.1| Epoxide hydrolase 2, cytoplasmic [Mus musculus]	10	5.9	63.07	8
38	3.2×10^{-7}	gi|3851614|gb|AAC72373.1| succinate dehydrogenase Fp subunit [Mus musculus]	27	6.2	59.27	15
39	6.5×10^{-3}	gi|3851614|gb|AAC72373.1| succinate dehydrogenase Fp subunit [Mus musculus]	17	6.2	59.27	12
40	3.6×10^{-3}	gi|26329893|dbj|BAC28685.1| glycerol phosphate dehydrogenase 2, mitochondrial [Mus musculus]	24	6.2	81.38	16
41	5.2×10^{-3}	gi|21704020|ref|NP_663493.1| NADH dehydrogenase (ubiquinone) Fe-S protein 1 [Mus musculus]	25	5.5	80.76	13
42	4.3×10^{-4}	gi|19879234|gb|AAK27416.1| mitochondrial assembly regulatory factor [Mus musculus]	17	6.4	86.85	9
50	4.1×10^{-5}	gi|51705066|ref|XP_129769.5| PREDICTED: carbamoyl-phosphate synthetase 1 [Mus musculus]	14	6.4	166.9	20
51	5.0×10^{-4}	gi|59808083|gb|AAH89599.1| Dimethylglycine dehydrogenase, precursor [Mus musculus]	18	7.8	97.44	11
52	5.3×10^{-4}	gi|73918911|sp|Q8C196|CPSM_MOUSE Carbamoyl-phosphate synthase [ammonia], mitochondrial precursor (Carbamoyl-phosphate synthetase I) (CPSase I)	20	6.5	165.8	23
53	8.6×10^{-3}	gi|73918911|sp|Q8C196|CPSM_MOUSE Carbamoyl-phosphate synthase [ammonia], mitochondrial precursor (Carbamoyl-phosphate synthetase I) (CPSase I)	14	6.5	165.8	20
54	1.4×10^{-3}	gi|33563270|ref|NP_035086.1| oxoglutarate dehydrogenase (lipoamide) [Mus musculus]	12	6.5	117.4	19
55	1.4×10^{-5}	gi|26352359|dbj|BAC39816.1| Sarcosine Dehydrogenase [Mus musculus]	37	6.4	57.84	17
57	1.1×10^{-4}	gi|20380027|gb|AAH28817.1| Fthfd protein [Mus musculus]	34	5.6	99.55	20

58	3.6×10^{-4}	gi|23271467|gb|AAH24055.1| Fthfd protein [Mus musculus]	33	5.7	99.57	19
61	7.4×10^{-3}	gi|200246|gb|AAA39897.1| pyruvate carboxylase	13	6.1	103.1	18
62	8.4×10^{-3}	gi|26346581|dbj|BAC36939.1| pyruvate decarboxylase [Mus musculus]	30	5.8	91.42	25
63	2.5×10^{-3}	gi|200246|gb|AAA39897.1| pyruvate carboxylase	16	6.1	103.8	22
64	4.3×10^{-4}	gi|48976025|ref|NP_598665.1| acetyl-Coenzyme A carboxylase beta [Mus musculus]	14	5.9	278.1	25
65	2.4×10^{-3}	gi|31542333|ref|NP_067370.2| hypoxia up-regulated 1 [Mus musculus]	21	5.2	111.4	20
68	4.8×10^{-3}	gi|30420885|gb|AAO64442.1| collagen type XIV [Mus musculus]	18	5.0	194.3	7
69	9.2×10^{-3}	gi|30420885|gb|AAO64442.1| collagen type XIV [Mus musculus]	11	5.0	194.3	6
71	1.0×10^{-5}	gi|57013837|sp|O08795|GLU2B_MOUSE Glucosidase II beta subunit precursor (Protein kinase C substrate, 60.1 kDa protein, heavy chain) (PKCSH) (80K-H protein)	13	4.4	59.74	9
72	1.3×10^{-3}	gi|57013837|sp|O08795|GLU2B_MOUSE Glucosidase II beta subunit precursor (Protein kinase C substrate, 60.1 kDa protein, heavy chain) (PKCSH) (80K-H protein)	15	4.4	59.74	10
74	4.6×10^{-6}	gi|27369605|ref|NP_766039.1| UDP-N-acetyl-alpha-D-galactosamine:polypeptide N-acetylgalactosaminyltransferase 6 [Mus musculus]	13	9.2	72.25	16
83	3.9×10^{-3}	gi|27464957|gb|AAN64234.1| DNA polymerase theta short isoform [Mus musculus]	9	7.2	252.4	21
84	3.8×10^{-3}	gi|51770518|ref|XP_489790.1| PREDICTED: similar to MHC class I histocompatibility antigen H-2 Q4 alpha chain precursor - mouse [Mus musculus]	8	7.3	71.74	5
85	2.9×10^{-3}	gi|51770518|ref|XP_489790.1| PREDICTED: similar to MHC class I histocompatibility antigen H-2 Q4 alpha chain precursor - mouse [Mus musculus]	16	7.3	71.74	7
86	1.7×10^{-3}	gi|51770518|ref|XP_489790.1| PREDICTED: similar to MHC class I histocompatibility antigen H-2 Q4 alpha chain precursor - mouse [Mus musculus]	10	7.3	71.74	6

88	1.3×10^{-3}	gi|56753812 SJCHGC06900 protein [Schistosoma japonicum](Phosphoenolpyruvate carboxykinase (PEPCK))	16	6.5	71.33	6
91	6.2×10^{-4}	gi|18079339|ref|NP_542364.1| aconitase 2, mitochondrial [Mus musculus]	22	8.4	86.19	13
96	1.3×10^{-6}	gi|54887356|gb|AAH37009.1| Hydroxyacyl-Coenzyme A dehydrogenase/3-ketoacyl-Coenzyme A thiolase/enoyl-Coenzyme A hydratase (trifunctional protein), alpha subunit [Mus musculus]	32	9.5	83.31	18
97	7.0×10^{-3}	gi|1213008|emb|CAA62015.1| 17beta-hydroxysteroid dehydrogenase IV [Mus musculus]	16	9.0	80.02	14
98	1.3×10^{-3}	gi|16741519|gb|AAH16571.1| Slc25a13 protein (solute carrier family 25 (mitochondrial carrier, adenine nucleotide translocator))[Mus musculus]	39	9.5	44.55	15
99	5.3×10^{-3}	gi|54887356|gb|AAH37009.1| Hydroxyacyl-Coenzyme A dehydrogenase/3-ketoacyl-Coenzyme A thiolase/enoyl-Coenzyme A hydratase (trifunctional protein), alpha subunit [Mus musculus]	13	9.5	83.31	11
100	4.4×10^{-4}	gi|6753514|ref|NP_034079.1| carnitine palmitoyltransferase 2 [Mus musculus]	15	8.8	74.54	12
102	7.6×10^{-3}	gi|26350301|dbj|BAC38790.1| trifunctional enzyme, thiolase [Mus musculus]	39	9.6	51.77	13
103	1.2×10^{-6}	gi|2690302|gb|AAB91426.1| aspartate aminotransferase precursor [Mus musculus]	35	9.3	47.79	11
104	8.2×10^{-3}	gi|26344475|dbj|BAC35888.1| electron transferring flavoprotein, dehydrogenase [Mus musculus]	22	7.4	69.06	9
105	7.9×10^{-3}	gi|34328415|ref|NP_780647.2| aldehyde dehydrogenase 4 family, member A1 [Mus musculus]	23	8.9	62.25	10
106	3.1×10^{-4}	gi|45476581|ref|NP_035457.1| sterol carrier protein 2, liver [Mus musculus]	17	7.2	59.74	10
107	7.6×10^{-6}	gi|26344712|dbj|BAC36005.1| mutant catalase [Mus musculus]	30	7.8	60.10	14
108	8.6×10^{-3}	gi|18848352|gb|AAH24133.1| aldehyde dehydrogenase 4 family, member A1 protein [Mus musculus]	19	8.6	60.78	14
112	6.2×10^{-3}	gi|6680748 ATP synthase, H+	30	9.2	59.83	16

		transporting, mitochondrial F1 complex, alpha subunit, isoform 1 [Mus musculus]				
113	8.7×10^{-3}	gi|74146998 ATP synthase, H+ transporting, mitochondrial F1 complex, alpha subunit, isoform 1 [Mus musculus]	28	9.3	56.03	15
114	7.1×10^{-5}	gi|74146998 ATP synthase, H+ transporting, mitochondrial F1 complex, alpha subunit, isoform 1 [Mus musculus]	29	9.3	56.03	15
115	7.9×10^{-3}	gi|74211977 ATP synthase, H+ transporting, mitochondrial F1 complex, alpha subunit, isoform 1 [Mus musculus]	30	9.3	59.86	16
116	3.6×10^{-3}	gi|37542157|gb|AAK72480.1| core 2 beta-1,6-N-acetylglucosaminyltransferase II [Mus musculus]	20	9.0	51.41	11
117	2.3×10^{-3}	gi|26354278|dbj|BAC40767.1| glutamate dehydrogenase [Mus musculus]	25	8.6	61.60	11
118	2.2×10^{-3}	gi|26344712|dbj|BAC36005.1| mutant catalase [Mus musculus]	26	7.8	60.10	13
119	2.4×10^{-3}	gi|26354278|dbj|BAC40767.1| glutamate dehydrogenase [Mus musculus]	27	8.6	61.60	12
120	6.5×10^{-4}	gi|23271115|gb|AAH33440.1| Aldehyde dehydrogenase family 6, subfamily A1 [Mus musculus]	35	8.6	58.46	15
121	6.7×10^{-3}	gi|7549763|ref|NP_038575.1| homogentisate 1, 2-dioxygenase [Mus musculus]	31	6.9	50.77	13
122	8.6×10^{-5}	gi|20810027|gb|AAH28901.1| Acetyl-Coenzyme A acyltransferase 2 (mitochondrial 3-oxoacyl-Coenzyme A thiolase) [Mus musculus]	42	8.8	42.30	21
123	6.7×10^{-5}	gi|20810027|gb|AAH28901.1| Acetyl-Coenzyme A acyltransferase 2 (mitochondrial 3-oxoacyl-Coenzyme A thiolase) [Mus musculus]	31	8.8	42.30	15
124	5.4×10^{-3}	gi|12850542|dbj|BAB28763.1| acetyl-Coenzyme A acetyltransferase 2 [Mus musculus]	16	7.2	38.64	9
125	7.3×10^{-3}	gi|20810027|gb|AAH28901.1| Acetyl-Coenzyme A acyltransferase 2 (mitochondrial 3-oxoacyl-Coenzyme A thiolase) [Mus musculus]	53	8.8	42.30	23
126	2.1×10^{-4}	gi|6754156 hydroxyacid oxidase 1, liver [Mus musculus]	21	7.6	41.26	11
127	4.1×10^{-3}	gi|7709978|ref|NP_057911.1| alanine-glyoxylate aminotransferase [Mus musculus]	27	8.9	46.20	19
129	1.4×10^{-3}	gi|42490808|gb|AAH66164.1|	11	9.1	57.01	9

		interleukin 31RA protein [Mus musculus]				
130	8.1×10^{-3}	gi|62533211|gb|AAH93510.1| Betaine-homocysteine methyltransferase [Mus musculus]	39	8.4	45.46	10
131	5.9×10^{-3}	gi|62533211|gb|AAH93510.1| Betaine-homocysteine methyltransferase [Mus musculus]	19	8.4	45.46	6
133	3.6×10^{-3}	gi|62533211|gb|AAH93510.1| Betaine-homocysteine methyltransferase [Mus musculus]	19	8.4	45.46	13
135	2.9×10^{-3}	gi|55669643|pdb|1R8Y|H Chain H, Crystal Structure Of Mouse Glycine N-Methyltransferase (Monoclinic Form)	27	7.3	32.98	10
137	2.5×10^{-3}	gi|226778|prf||1605130A carbonic anhydrase III	14	8.0	29.61	6
138	9.7×10^{-4}	gi|62533211|gb|AAH93510.1| Betaine-homocysteine methyltransferase [Mus musculus]	28	8.4	45.46	15
139	2.0×10^{-4}	gi|62533211|gb|AAH93510.1| Betaine-homocysteine methyltransferase [Mus musculus]	23	8.4	45.46	12
140	6.2×10^{-3}	gi|226778|prf||1605130A carbonic anhydrase III	29	8.0	29.61	12
141	8.9×10^{-3}	gi|1864018|gb|AAB48543.1| triosephosphate isomerase [Mus musculus]	52	5.6	22.72	13
143	5.1×10^{-5}	gi|21759114|sp|Q9DCW4|ETFB_MOUSE Electron transfer flavoprotein beta-subunit (Beta-ETF)	43	8.9	27.52	16
144	2.9×10^{-3}	gi|2624496|pdb|1BAY|B Chain B, Glutathione S-Transferase Yfyf Cys 47-Carboxymethylated Class Pi, Free Enzyme	45	8.3	23.52	10
145	2.9×10^{-4}	gi|6754084 glutathione S-transferase, mu 1 [Mus musculus]	41	7.7	26.06	11
146	4.0×10^{-3}	gi|12846244|dbj|BAB27089.1| peptidylprolyl isomerase A [Mus musculus]	57	8.7	18.14	12
147	1.8×10^{-3}	gi|48474620|sp|Q99LB2|DHRS4_MOUSE Dehydrogenase/reductase SDR family member 4 (NADPH-dependent carbonyl reductase/NADP-retinol dehydrogenase) (CR) (PHCR)	27	9.6	27.96	15
149	2.8×10^{-3}	gi|4760594|dbj|BAA77357.1| beta-2-globin [Mus musculus]	30	8.2	15.84	6
150	5.5×10^{-3}	gi|4760590|dbj|BAA77355.1| beta-1-globin [Mus musculus]	55	7.3	15.81	7

151	4.0×10^{-3}	gi|4760594|dbj|BAA77357.1| beta-2-globin [Mus musculus]	64	8.2	15.84	8
152	4.1×10^{-5}	gi|12846939|dbj|BAB27370.1| hemoglobin, beta adult major chain [Mus musculus]	28	9.3	15.30	5
153	8.3×10^{-4}	gi|6678509|ref|NP_033500.1| urate oxidase [Mus musculus]	51	8.7	35.2	17
154	3.7×10^{-3}	gi|21707669|gb|AAH34173.1| Aldolase 2, B isoform [Mus musculus]	34	9.0	39.97	16
155	8.1×10^{-3}	gi|6678509|ref|NP_033500.1| urate oxidase [Mus musculus]	40	8.7	35.25	12
156	2.4×10^{-3}	gi|193703|gb|AAA37751.1| glutathione transferase alpha 3	30	8.8	25.40	7
157	4.3×10^{-3}	gi|52139036|gb|AAH82563.1| Angiopoietin-like 1 [Mus musculus]	22	9.1	56.76	10

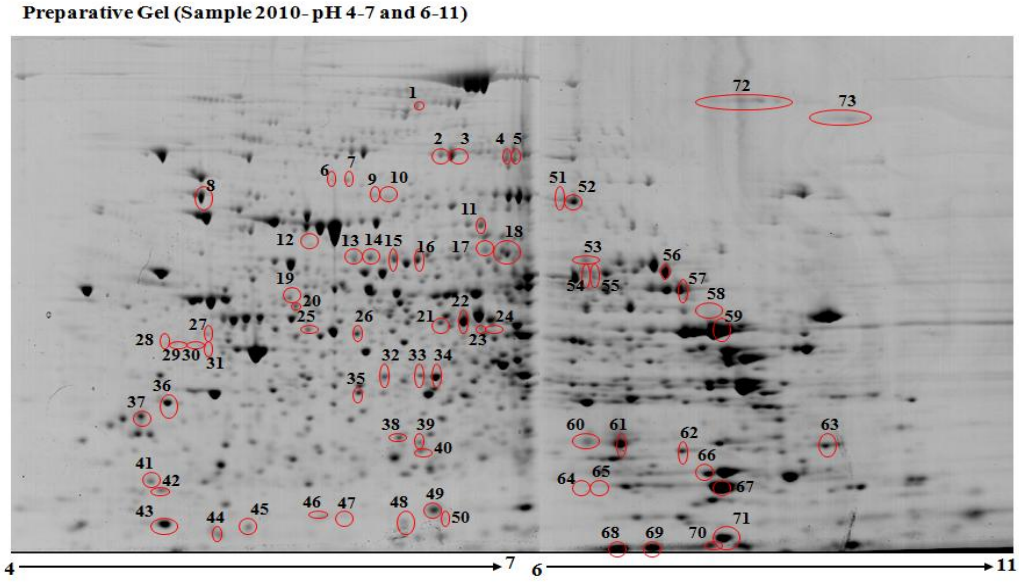

FIGURE C6 Preparative gel pI 4-7 and 6-11 with 75 μg protein from HSS liver lysate. Numbers 1 to 72 were proteins identified by peptide mass finger printing using MALDI-TOF mass spectrometry.

TABLE C6 List of protein spots for Figure C6.

Spot No.	Expectation	Protein Name	Seq. Cov.%	*pI*	kDa	Peptides matched
2	6.6×10^{-4}	gi|26352359|dbj|BAC39816.1| sarcosine dehydrogenase [Mus musculus]	34	6.4	57.84	26
3	3.6×10^{-3}	gi|26352359|dbj|BAC39816.1| sarcosine dehydrogenase [Mus musculus]	42	6.4	57.84	28

4	4.2×10^{-3}	gi|59808083|gb|AAH89599.1| Dimethylglycine dehydrogenase, precursor [Mus musculus]	22	7.8	97.44	12
5	4.3×10^{-3}	gi|59808083|gb|AAH89599.1| Dimethylglycine dehydrogenase, precursor [Mus musculus]	36	7.8	97.44	18
6	8.8×10^{-3}	gi|26341396|dbj|BAC34360.1| unnamed protein product (Albumin 1) [Mus musculus]	14	5.5	67.04	7
7	3.0×10^{-3}	gi|26354755|dbj|BAC41004.1| unnamed protein product (gelsolin) [Mus musculus]	15	5.7	81.07	9
8	1.8×10^{-6}	gi|6678329|ref|NP_033399.1| transglutaminase 2, C polypeptide [Mus musculus]	35	5.0	78.18	19
11	7.4×10^{-3}	gi|15030102|gb|AAH11301.1| succinate dehydrogenase Fp subunit [Mus musculus]	24	7.2	73.39	13
15	4.8×10^{-4}	gi|15929294|gb|AAH15087.1| Epoxide hydrolase 2, cytoplasmic [Mus musculus]	44	5.9	63.07	16
16	7.0×10^{-6}	gi|15929294|gb|AAH15087.1| Epoxide hydrolase 2, cytoplasmic [Mus musculus]	38	5.9	63.07	15
18	2.5×10^{-4}	IPI00310669 Dihydroxyacetone kinase	39	6.4	59.94	10
19	5.6×10^{-3}	gi|60392921|sp|P11369|POL2_MOUSE Retrovirus-related Pol polyprotein LINE-1 (Long interspersed element-1) (L1) [Contains: Reverse transcriptase ; Endonuclease]	18	9.9	150.59	6
22	2.2×10^{-3}	gi|904132|gb|AAA70378.1| S-adenosyl-L-homocysteine hydrolase	30	6.0	48.17	15
23	3.0×10^{-4}	gi|54114937|gb|AAH39179.1| Eno1 protein [Mus musculus]	40	7.8	50.18	15
24	8.4×10^{-5}	gi|12836655|dbj|BAB23751.1| isovaleryl coenzyme A dehydrogenase [Mus musculus]	25	8.7	46.61	13
27	8.6×10^{-3}	gi|293682|gb|AAA39373.1| keratin D	27	5.3	47.47	9
28	2.1×10^{-4}	gi|293682|gb|AAA39373.1| keratin D	16	5.3	47.47	7
29	3.4×10^{-3}	gi|309215|gb|AAA37551.1| EndoA' cytokeratin (5' end put.); putative	35	5.4	53.22	14
33	2.9×10^{-3}	gi|21618806|gb|AAH31710.1| Dhdh protein [Mus musculus]	31	5.9	36.97	9
34	2.0×10^{-6}	IPI00228630 Fructose-1,6-bisphosphatase 1	51	6.2	37.30	14
35	1.4×10^{-3}	gi|31982229|ref|NP_032465.2| ketohexokinase [Mus musculus]	21	5.8	33.29	5
36	1.2×10^{-4}	gi|13277612|gb|AAH03716.1| Anxa5 protein [Mus musculus]	39	4.8	35.78	13
37	5.5×10^{-3}	gi|26341416|dbj|BAC34370.1| unnamed	32	4.7	28.99	16

		protein product (tropomyosin 3, gamma) [Mus musculus]				
38	3.0×10^{-3}	gi|50510361|dbj|BAD32166.1| mKIAA0106 protein (nonselenium glutathione peroxidise) (peroxiredoxin 6) [Mus musculus]	22	6.0	25.17	6
41	4.9×10^{-4}	gi|63545837|ref|XP_620353.1| PREDICTED: similar to tumor protein, translationally-controlled 1 [Mus musculus]	17	6.1	82.14	6
42	5.4×10^{-3}	gi|71051244|gb|AAH99597.1| Major urinary protein 1 [Mus musculus]	56	4.9	21.04	9
43	6.4×10^{-3}	gi|13385268|ref|NP_080073.1| cytochrome b-5 [Mus musculus]	43	4.9	15.22	5
45	3.1×10^{-3}	gi|21730472|pdb|1KGL|A Chain A, Solution Structure Of Cellular Retinol Binding Protein Type- I In Complex With All-Trans-Retinol	56	5.1	15.86	7
49	9.5×10^{-4}	gi|226471|prf||1513495A Cu/Zn superoxide dismutase	52	6.0	15.91	8
50	9.7×10^{-4}	gi|12846804|dbj|BAB27309.1| unnamed protein product [Mus musculus] (60S ribosomal protein)	25	11.6	23.83	7
51	4.0×10^{-5}	gi|20330802|ref|NP_598738.1| transferrin [Mus musculus]	26	7.0	78.87	20
52	1.4×10^{-5}	gi|62027488|gb|AAH92046.1| Transferrin [Mus musculus]	31	7.0	78.87	19
53	5.1×10^{-3}	gi|18848352|gb|AAH24133.1| Aldh4a1 protein [Mus musculus]	31	8.6	60.78	13
54	5.1×10^{-8}	gi|442441|gb|AAA66054.1| catalase [Mus musculus]	42	8.3	60.00	23
56	3.2×10^{-7}	gi|442441|gb|AAA66054.1| catalase [Mus musculus]	34	8.3	60.00	19
57	9.9×10^{-3}	gi|6729934|pdb|1MAB|A Chain A, Rat Liver F1-Atpase (ATP synthase, H+ transporting, mitochondrial F1 complex, alpha subunit, isoform 1)	33	8.4	55.38	17
58	1.9×10^{-4}	gi|62533211|gb|AAH93510.1| Betaine-homocysteine methyltransferase [Mus musculus]	24	8.4	45.46	7
60	9.0×10^{-3}	gi|51243036|ref|NP_001003717.1| oxysterol-binding protein-like protein 8 isoform b [Mus musculus]	23	7.3	97.53	7
62	7.0×10^{-3}	gi|49257190|gb|AAH72658.1| Enoyl Coenzyme A hydratase, short chain, 1, mitochondrial [Mus musculus]	36	9.3	31.95	10
64	7.8×10^{-3}	gi|2624496|pdb|1BAY|B Chain B,	46	8.3	23.52	9

		Glutathione S-Transferase Yfyf Cys 47-Carboxymethylated Class Pi, Free Enzyme				
65	9.6×10^{-3}	gi|2624496|pdb|1BAY|B Chain B, Glutathione S-Transferase Yfyf Cys 47-Carboxymethylated Class Pi, Free Enzyme	37	8.3	23.52	7
66	5.2×10^{-3}	gi|33468899|ref|NP_034489.1| glutathione S-transferase, mu 3 [Mus musculus]	50	7.8	25.91	8
67	2.9×10^{-3}	gi|2624496|pdb|1BAY|B Chain B, Glutathione S-Transferase Yfyf Cys 47-Carboxymethylated Class Pi, Free Enzyme	52	8.3	23.52	9
69	1.7×10^{-4}	gi|4760590|dbj|BAA77355.1| beta-1-globin [Mus musculus]	37	7.3	15.81	5
70	2.3×10^{-4}	IPI00828873 Beta-2-globin	52	7.9	15.85	5
72	3.5×10^{-3}	gi|51770518|ref|XP_489790.1| PREDICTED: similar to MHC class I histocompatibility antigen H-2 Q4 alpha chain precursor - mouse [Mus musculus]	15	7.3	71.74	6

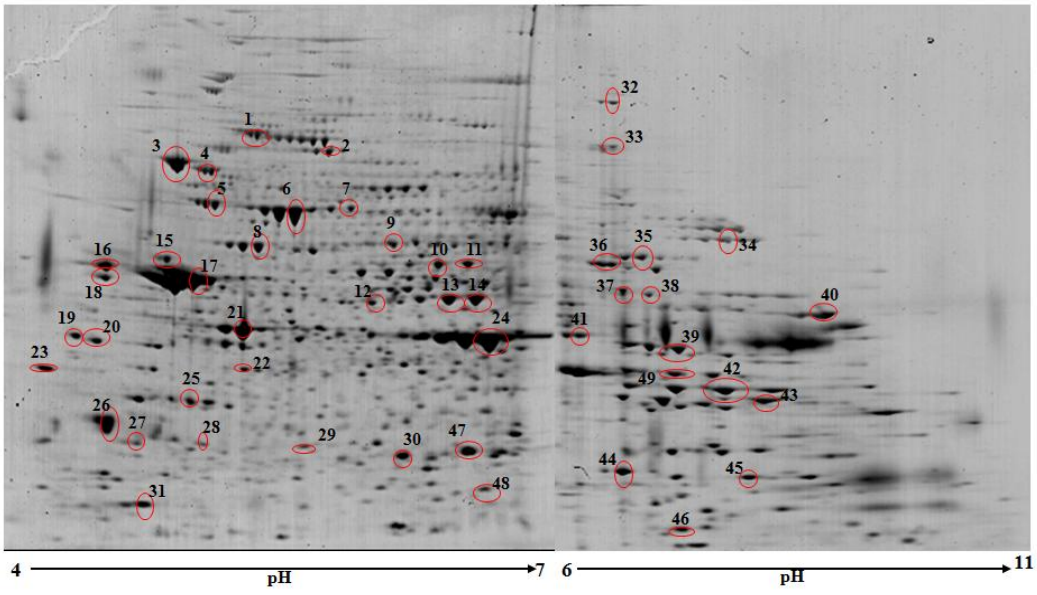

FIGURE C7 Preparative gel pI range 4-7 and 6-11 for **soluble egg antigen** with 75 μg protein. Numbers 1 to 49 are proteins identified by peptide mass finger printing using MALDI-TOF mass spectrometry.

TABLE C7 List of protein spots for Figure C7.

Spot No.	Expectation	Protein Description	Seq. Cov.%	pI	kDa	Peptides matched
1	8.4×10^{-4}	gi|320988|pir||A60608 paramyosin - fluke (Schistosoma mansoni) (fragment)	43	5.1	51.19	14

2	3.9×10^{-3}	gi|56758882|gb|AAW27581.1| unknown [Schistosoma japonicum]	31	5.5	89.55	6
3	5.3×10^{-3}	gi|320985|pir||A45529 heat shock protein 86 - fluke (Schistosoma mansoni) (fragment)	39	5.4	51.43	16
4	8.8×10^{-4}	gi|320985|pir||A45529 heat shock protein 86 - fluke (Schistosoma mansoni) (fragment)	43	5.4	51.43	17
5	4.0×10^{-3}	gi|2829289|gb|AAC00519.1| HSP70 [Schistosoma japonicum]	26	5.1	71.64	15
6	3.8×10^{-4}	gi|10168|emb|CAA28976.1| 70,000 mol wt antigen/hsp70 homologue (619 AA) [Schistosoma mansoni]	12	5.4	68.36	12
7	2.0×10^{-4}	gi|56753427|gb|AAW24917.1| unknown [Schistosoma japonicum]	23	6.3	71.45	13
-	-	gi|2829291|gb|AAC00520.1| HSP70 [Schistosoma japonicum]	23	5.4	56.05	-
8	6.4×10^{-3}	gi|21634531|gb|AAM69406.1| heat shock protein HSP60 [Schistosoma mansoni]	38	5.3	58.76	17
9	1.8×10^{-4}	gi|1314808|gb|AAA99815.1| T-complex polypeptide 1 alpha subunit [Schistosoma mansoni]	26	6.0	60.05	11
10	8.7×10^{-3}	gi|313121|emb|CAA80521.1| ER-luminal cysteine protease ER 60 [Schistosoma mansoni]	37	6.3	54.80	18
11	2.5×10^{-4}	gi|313121|emb|CAA80521.1| ER-luminal cysteine protease ER 60 [Schistosoma mansoni]	36	6.3	54.80	18
12	7.0×10^{-3}	gi|29841421|gb|AAP06453.1| similar to NM_019693 HLA-B associated transcript 1 in Homo sapiens [Schistosoma japonicum]	20	6.5	47.68	8
13	1.1×10^{-3}	gi|3023710|sp|Q27877|ENO_SCHMA Enolase (2-phosphoglycerate dehydratase) (2-phospho-D-glycerate hydro-lyase)	44	6.2	47.43	18
14	1.7×10^{-4}	gi|3023710|sp|Q27877|ENO_SCHMA Enolase (2-phosphoglycerate dehydratase) (2-phospho-D-glycerate hydro-lyase)	45	6.2	47.43	19
15	9.8×10^{-5}	gi|312018|emb|CAA80520.1| protein disulfide isomerase homologue [Schistosoma mansoni]	48	4.9	54.48	20
16	2.6×10^{-3}	gi|1345835|sp|Q06814|CRTC_SCHMA Calreticulin precursor (SM4 protein)	33	4.7	45.55	15
17	8.0×10^{-4}	gi|496495|emb|CAA55978.1| alpha tubulin 2 [Patella vulgata]	32	4.9	50.88	13
18	1.8×10^{-3}	gi|1345835|sp|Q06814|CRTC_SCHMA Calreticulin precursor (SM4 protein)	45	4.7	45.55	18

19	2.1×10^{-3}	gi|1174756|sp|P42638|TPM2_SCHMA Tropomyosin 2 (TMII)	68	4.5	32.68	21
20	2.6×10^{-4}	gi|320989|pir||A60607 tropomyosin - fluke (Schistosoma mansoni)	62	4.6	32.99	20
21	1.2×10^{-3}	gi|189503078 | actin [Schistosoma japonicum]	28	5.4	41.71	7
22	1.8×10^{-3}	gi|67625681|tpe|CAJ00225.1| TPA: gag protein [Schistosoma mansoni]	31	9.5	26.31	6
23	5.4×10^{-4}	gi|76154879 SJCHGC07268 protein [Schistosoma japonicum]	36	8.1	16.33	6
24	1.9×10^{-3}	gi|627088|pir||A54521 40k egg antigen (clone 10F5) - fluke (Schistosoma mansoni)	30	6.2	39.56	11
25	7.5×10^{-3}	gi|6649234|gb|AAF21436.1| 14-3-3 epsilon [Schistosoma mansoni]	38	4.9	28.85	9
26	2.3×10^{-3}	gi|790658|gb|AAC46983.1| 14-3-3 protein	58	4.7	28.47	17
27	2.4×10^{-4}	gi|56757579|gb|AAW26951.1| unknown [Schistosoma japonicum]	42	4.8	22.74	13
28	1.4×10^{-4}	gi|29841012 similar to NM_011967 proteasome (prosome, macropain) subunit, alpha type 5 in Mus musculus [Schistosoma japonicum]	45	5.2	27.47	11
29	2.4×10^{-3}	gi|2529289|gb|AAB95297.1| heat shock protein 70 [Biomphalaria glabrata]	35	5.5	69.92	10
30	1.4×10^{-3}	gi|10281261|gb|AAG15507.1| thioredoxin peroxidase 1 [Schistosoma mansoni]	48	6.1	21.31	9
31	1.5×10^{-3}	gi|1711398|sp|Q07167|SM16_SCHMA 16 kDa calcium-binding protein (Egg antigen SME16)	44	5.0	16.83	6
32	9.4×10^{-4}	gi|4581919|gb|AAD24794.1| phosphoenolpyruvate carboxykinase [Schistosoma mansoni]	12	6.8	71.47	7
33	8.6×10^{-3}	gi|4581919|gb|AAD24794.1| phosphoenolpyruvate carboxykinase [Schistosoma mansoni]	16	6.8	71.47	6
34	6.5×10^{-4}	gi|156118913 creatine kinase [Schistosoma mansoni]	28	7.9	77.42	16
35	6.0×10^{-3}	gi|56755541|gb|AAW25949.1| unknown [Schistosoma japonicum]	27	8.5	72.59	15
36	1.8×10^{-3}	gi|4581919|gb|AAD24794.1| phosphoenolpyruvate carboxykinase [Schistosoma mansoni]	30	6.8	71.47	14
37	9.8×10^{-3}	gi|29841414 similar to GenBank Accession Number AB022159 chaperonin containing TCP-1 zeta-1 subunit in Mus musculus [Schistosoma japonicum]	31	6.8	26.49	7

38	1.5×10^{-3}	gi|60601894|gb|AAX27404.1| unknown [Schistosoma japonicum]	44	6.4	31.41	12
39	2.1×10^{-5}	gi|556413|gb|AAA93516.1| phosphoglycerate kinase	36	6.8	44.89	13
40	2.1×10^{-3}	gi|47551121|ref|NP_999743.1| mitochondrial ATP synthase alpha subunit precursor [Strongylocentrotus purpuratus]	23	8.4	59.82	9
41	5.0×10^{-3}	gi|627088|pir||A54521 40k egg antigen (clone 10F5) - fluke (Schistosoma mansoni)	30	6.2	39.56	11
42	9.5×10^{-3}	gi|84411|pir||JL0121 glyceraldehyde-3-phosphate dehydrogenase (phosphorylating) (EC 1.2.1.12) - fluke (Schistosoma mansoni)	51	8.4	36.64	20
43	1.2×10^{-3}	gi|56758570|gb|AAW27425.1| unknown [Schistosoma japonicum]	22	9.3	36.91	10
44	5.1×10^{-3}	gi|73535312|pdb|1U3I|A Chain A, Crystal Structure Of Glutathione S-Tranferase From Schistosoma Mansoni	34	6.6	23.89	9
45	3.1×10^{-3}	gi|243794|gb|AAB21173.1| glutathione S-transferase, GST [Schistosoma mansoni, Peptide, 218 aa]	56	7.8	25.51	12
46	5.6×10^{-3}	gi|55670478|pdb|1VYG|A Chain A, Schistosoma Mansoni Fatty Acid Binding Protein In Complex With Arachidonic Acid	67	8.0	15.00	9
47	5.5×10^{-3}	gi|10281261|gb|AAG15507.1| thioredoxin peroxidase 1 [Schistosoma mansoni]	37	6.1	21.31	9
48	2.0×10^{-5}	gi|267013 Superoxide dismutase [Cu-Zn]	50	6.1	15.89	6
49	5.5×10^{-5}	gi|605647|gb|AAA57567.1| fructose 1,6 bisphosphate aldolase [Schistosoma mansoni]	45	7.9	39.97	17

APPENDIX D

Solutions and Reagents

D.1 Standard Lysis Buffer, pH 8.4 (20 mL)

(30 mM TrisHCl, 2 M Thiourea, 7 M Urea, 4% (w/v) CHAPS)

0.4 mL 1.5M Tris-HCl pH 8.8

3.04 g thiourea

8.4 g urea

0.8 g CHAPS {3-[(3-cholamidoproply) dimethyl ammonio]-1-propane-sulfonate}

Dissolve in MilliQ and make volume to 20 mL. Make aliquots and store at -20 ^{o}C.

D.2 Rehydration Buffer for IPG DryStrips pI 3-10 and 4-7 (25 mL)

(2 M Thiourea, 7 M Urea, 2% IPG buffer 3-10, 2% DTT, 4% (w/v) CHAPS)

3.8 g thiourea

10.5 g urea

0.5 mL IPG Buffer (3-10)

0.5 g DTT (Dithiothreitol)

1.0 g CHAPS

60 μL bromophenol blue (BPB-used as tracking dye)

Dissolve and make up the volume to 25 mL with MilliQ. Make aliquots and store at -20 ^{o}C.

NOTE: For the above rehydration buffer IPG buffer (4-7) can be used if buffer will be used only for IPG DryStrips 4-7.

D.3 Rehydration Buffer for IPG DryStrips pI 6-11 (20 mL)

(2 M Thiourea, 4 M Urea, 1% IPG Buffer 6-11, 2% (w/v) CHAPS, 10 % Isopropanol, 5% Glycerol)

3.04 g thiourea

8.4 g urea

0.2 mL IPG Buffer (6-11)

0.4 g CHAPS

2.0 mL isoproponal

1.0 mL glycerol

60 μL bromophenol blue (BPB-used as tracking dye)

Dissolve and make up the volume to 20 mL with MilliQ. Make aliquots and store at -20 ^{o}C. Add 2.5 % DTT (For 1 mL rehydration buffer, add 0.025 g DTT) just before rehydration of strips. Add 3.0 % DTT (For 1 mL rehydration buffer, add 0.03 g DTT) for cathodic paper wick.

D.4 Equilibration buffer (500 mL)

(50 mM Tris, 6 M Urea, 30% Glycerol, 2% SDS)

6.7 mL 1.5 M Tris-HCl pH 8.8

72.0 g urea

60.0 mL glycerol

4.0 g SDS (sodium dodecyl sulphate)

60 μL bromophenol blue (BPB-used as tracking dye)

Add 20 mL MilliQ to 250 mL measuring cylinder, and then add 60 mL glycerol. Add 20 mL MilliQ, all above chemicals and stir constantly to dissolve. Add BPB and make volume to 200 mL. Store in bottle at room temperature.

D.5 Fixer (1000 mL)

(50% C_2H_5OH, 3% H_3PO_4)

500 mL C_2H_5OH (ethanol)

30 mL H_3PO_4 (phosphoric acid/orthophosphoric acid)

470 mL MilliQ

Store at room temperature.

D.6 Colloidal staining solution (1000 mL)

(17% $(NH_4)_2SO_4$, 34% CH_3OH, 3% H_3PO_4)

170 g $(NH_4)_2SO_4$ (ammonium sulphate)

340 mL CH_3OH (methanol)

30 mL H_3PO_4 (phosphoric acid/orthophosphoric acid)

Dissolve in MilliQ and make volume to 1000 mL. Store in bottle at room temperature.

D.7 0.06% Coomassie brilliant blue (100 mL)

0.06 g Coomassie G-250 in 100 mL MilliQ.

D.8 50% ACN 0.1% TFA (500 µL)

250 µL ACN (Acetonitrile), 0.5 µL TFA (trifluoroacetic Acid) and 250 µL MilliQ.

D.9 50 mM NH_4HCO_3 50% CH_3OH (500 mL)

2 g NH_4HCO_3 (Ammonium Bicarbonate)

250 mL Methanol

Make up the volume to 500 mL with MilliQ.

D.10 Working CyDye

STOCK: 1 mM (1 nmol/µL)

WORKING CyDye (80 pmol/µL/10 µg protein)

Dimethylformamide (DMF**)** used for reconstitution should be of high quality and open for less than 3 months. DMF should be handled under the hood and a syringe should be used to draw 200 µL in 1.5 mL tube.

1. Reconstitute the stock as directed on the kit (Add 5 µL DMF to each vial of 5 µg CyDye). Vortex vigorously for 30 s and centrifuge at 12000 rpm for 30 s.
2. *For 2 samples* Add 0.16 µL of each stock CyDye to 2 µL DMF.

D.11 10 mM Lysine (10 mL)

Add 0.018 g L-Lysine (MW 182.6) to 10 mL MilliQ, mix and dissolve. Make aliquots and store at 4 ^oC.

D.12 Running Buffer (5X Tris-Glycine-SDS Buffer) (1000 mL)

15 g	Tris
72 g	Glycine
05 g	Sodium Dodecyl Sulphate (SDS)

Dissolve in MilliQ and make volume to 1000 mL

D.13 Western transfer buffer (1000 mL)

(192 mM Glycine, 25 mM Tris Base, 0.037% (w/v) SDS, 20% (v/v) Methanol)

3.03 g	Tris
14.4 g	Glycine
3.75 ml	10% SDS
200 mL	Methanol

Dissolve in MilliQ and make volume to 1000 mL

D.14 Tris Buffered Saline (10X TBS)

(1X composition 0.5 M Tris, 1.5 M NaCl, pH 7.4)

12.1 g	Tris
40.0 g	NaCl
12 mL	1M HCl

Adjust the pH to 7.6 using concentrated HCl and make up the volume to 500 mL with MilliQ.

D.15 TBST buffer

995 mL	1X TBS Buffer
5 mL	Tween-20

D.16 Blocking Buffer

5 g	Skimmed milk powder or 1 g casein
100 mL	T-TBS buffer

D.17 Dovex/ Norit Mixture (Dry powder is stable for years at room temperature)

1. Mix 40 g Dovex (Sigma Aldrich) and 20 g Norit (Activated chatcoal, Sigma Aldrich) in a large beaker, add 6 M HCl and mix well.
2. Transfer the above mix to 800 mL Buchner funnel using #1 Whatman 9.0 cm filter paper and apply suction.
3. Add more 6 M HCl, mix and suction, repeat 2/3 times.
4. Add 95% ethanol, mix and suction, repeat step.
5. Add 100% ethanol, mix and suction, repeat twice.

6. Dry the powder in large drying dish under hood for 48 hours.

D.18 Citrate-Acetate Buffer

57 g NaAcetate.$3H_2O$ (Sigma Aldrich)

37.5 g Na_3Citrate.2H2O (Sigma Aldrich) and

5.5 g H_3Citrate.2H2O (Sigma Aldrich)

385 mL isopropanol (Sigma Aldrich)

make volume to 1000 mL with MilliQ water.

D.19 7% Chloramine-T

7 g Chloramine-T (Sigma Aldrich)

make 100 ml with MilliQ, store in dark bottle at 4 ^{o}C.

D.20 Ehrlich's Reagent

25 g p-dimethylaminobenzaldehyde (Sigma Aldrich), dissolve in

37.5 mL 60% perchloric acid (Sigma Aldrich), store in dark bottle at 4 ^{o}C.

D.21 Solution A (Oxidant Solution) (Always make fresh) (Mix 1 part 7% Chloramine-T with 4 parts Citrate-Acetate buffer)

For 40 samples, add 2 mL 7% Chloramine-T with 8 mL Citrate-Acetate buffer.

For half microplate, add 1 mL 7% Chloramine-T with 4 mL Citrate-Acetate buffer.

D.22 Solution B (Always make fresh) (Mix 3 parts of Ehrlich's Reagent with 13 parts isoproponal)

For 32 samples, add 15 mL of Ehrlich's Reagent with 65 mL isoproponal.

For half microplate, add 1 mL of Ehrlich's Reagent with 4.33 mL isoproponal.

APPENDIX E

Control lysate haemoglobin spot fluorescence comparison

The spot volume fluorescence intensity of haemoglobin spots from control/ uninfected 2D-DIGE maps labelled with either Cy3 or Cy5 dyes was calculated for each experimental design (Table 1 and 2). The difference in spot volume fluorescence intensity showed haemoglobin concentration between the two experimental designs was similar (Table E1) suggesting that the sample set for control samples were similar in physiology. Additionally, indicating that there was no blood contamination during liver sample collection for both experimental designs.

Expt. Design 1 Sample Name with CyDye	**Spot Volume (Fluorescence Intensity)**	**Expt. Design 2 Sample Name with CyDye**	**Spot Volume (Fluorescence Intensity)**
Cy3 C1	833909	Cy5 C2	910275
Cy5 C1	4176331	Cy3 C3	1582513
Cy5 C4	1598374	Cy5C4	3603526
Cy3 C3	1202540	Cy3 C1	1740748
Average	**1952789**	**Average**	**1959266**
		Difference between averages	**6477**

TABLE E1 The difference between the haemoglobin spot volume fluorescence intensity for C=control/uninfected mice from experimental designs 1 and 2.

APPENDIX F

Two-Dimensional Differential In Gel Electrophoresis (2D-DIGE)

Introduction

2D-DIGE is a technique used to study proteomic differences between cells/tissues in different functional states. This was first described by (Ünlü, Morgan et al. 1997) using cyanine dyes or CyDye DIGE fluors or CyDyes, now marketed solely by GE Healthcare Bio-Sciences AB, SE-751 84 Uppsala, Sweden. For experimental purposes three CyDyes are available: Cy2, Cy3 and Cy5, designed with similar charge and molecular weight, so that if a protein labelled with the CyDye, it will migrate to the same position on a 2-D gel. There is a specific excitation wavelength for each CyDye which generates a separate gel image for each CyDye labelled sample, superimposing these images allows the study of proteins that are expressed differentially and consistently. Commercially, two CyDye kits are available, CyDye DIGE Fluor minimal dyes and CyDye DIGE Fluor saturation dyes. The minimal labelling technique is used for multiplexing of 3 samples including the internal standard, as compared to saturation technique which allows multiplexing of 2 samples only.

DIGE chemistry

CyDye DIGE Fluor minimal dyes (GE Healthcare) were used to label the liver and serum samples in this study. The NHS ester reactive group in minimal labelling CyDyes covalently binds to the lysine epsilon amino group of proteins through an amide linkage (Figure F1). The CyDyes label approximately 3 % of the protein sample. This type of labelling has been therefore called minimal labelling as it involves labelling of a single lysine residue per protein. At neutral or acidic pH, the lysine residue in proteins carries an intrinsic +1 charge. The labelling reaction is carried out on ice in dark with the

concentration of 80 pmol CyDye per 10 µg protein, during which the CyDye with +1 charge gets coupled to the lysine on the protein, replacing the lysine's +1 charge with its own, without significantly altering the pI of the protein (Courtesy: GE Healthcare).

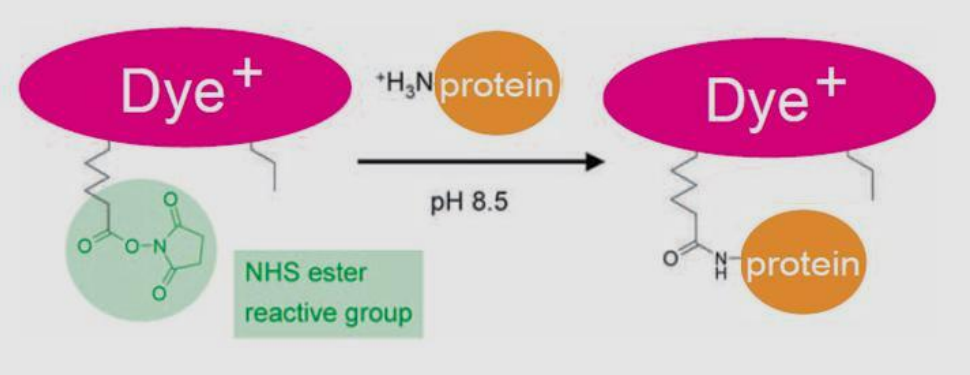

FIGURE F1 Minimal labelling CyDye containing NHS ester active group covalently binds to lysine residue of protein via an amide linkage. (Courtesy: GE Healthcare).

APPENDIX G

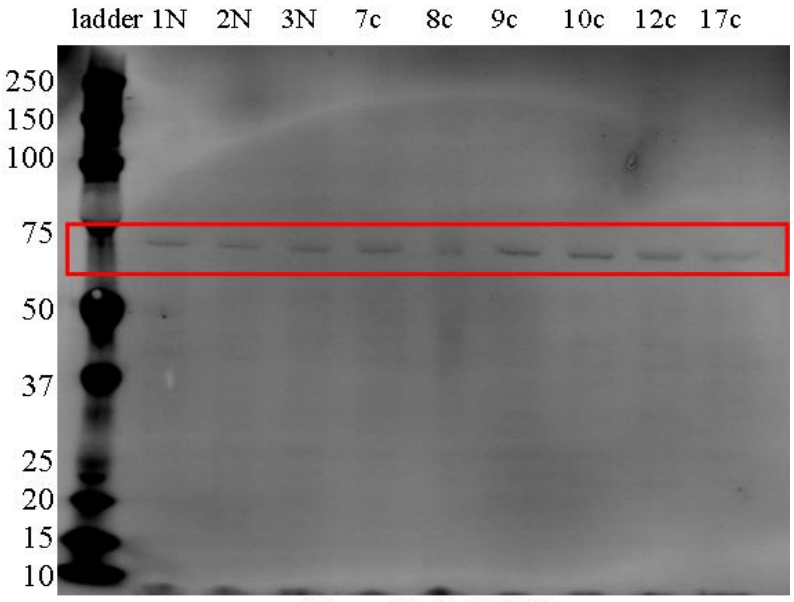

FIGURE G1 Western blot for Mouse liver PEPCK (Control=1N, 2N, 3N; MSS=7c, 8c, 9c; HSS=10c, 12c, 17c)

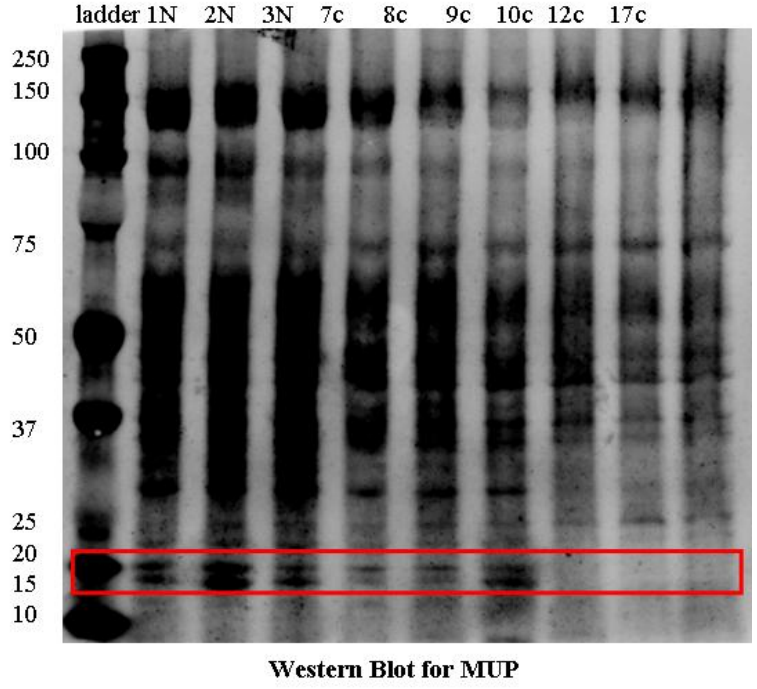

FIGURE G2 Western blot for Mouse liver MUP (Control=1N, 2N, 3N; MSS=7c, 8c, 9c; HSS=10c, 12c, 17c)

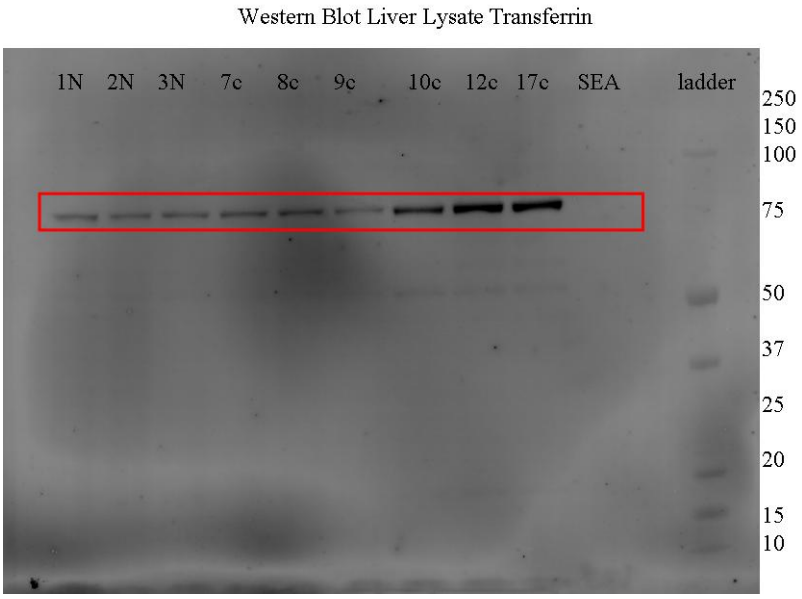

FIGURE G3 Western blot for Mouse liver Transferrin (Control=1N, 2N, 3N; MSS=7c, 8c, 9c; HSS=10c, 12c, 17c; SEA=soluble egg antigen)

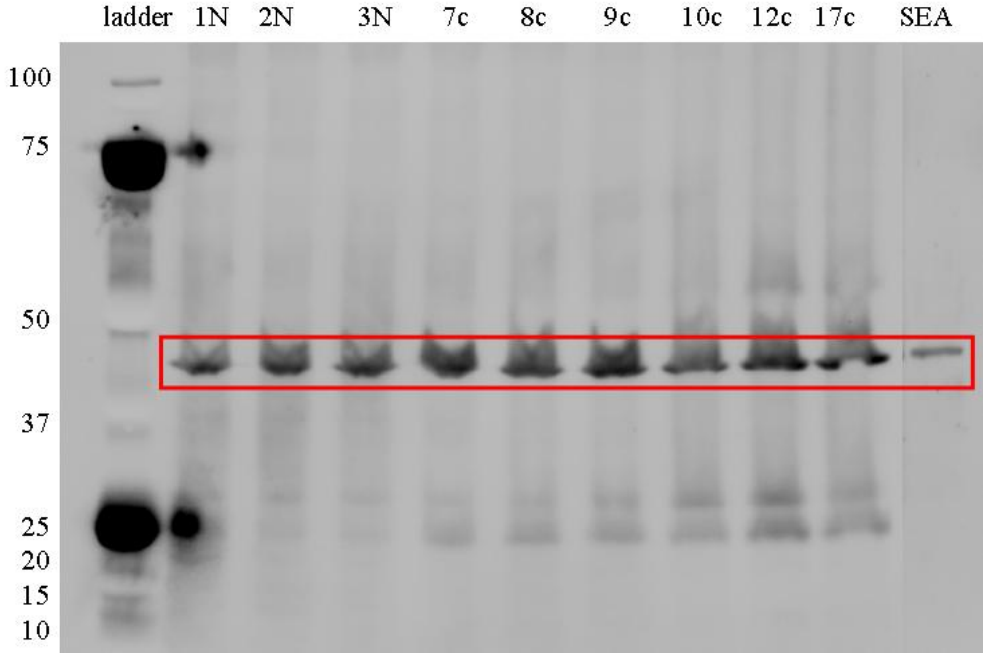

FIGURE G4 Western blot showing actin as loading control (Control=1N, 2N, 3N; MSS=7c, 8c, 9c; HSS=10c, 12c, 17c; SEA= soluble egg antigen)

FIGURE G5-G7 Western blot for Mouse serum Transferrin (Control=1-5N; MSS=1-5M; HSS=1-5H; 8-week infected=801-810; 12-week infected= 1201-1210)

FIGURE G5 (Control mice= 1C-5C)

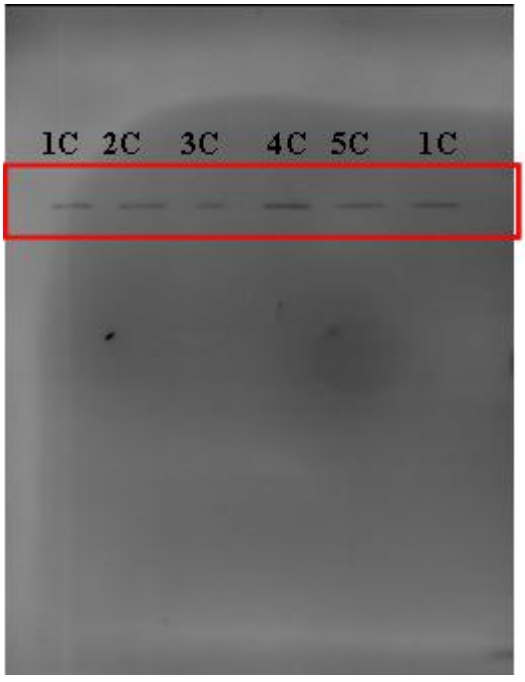

FIGURE G6 (MSS mice=1M-5M; HSS mice=1H-5H)

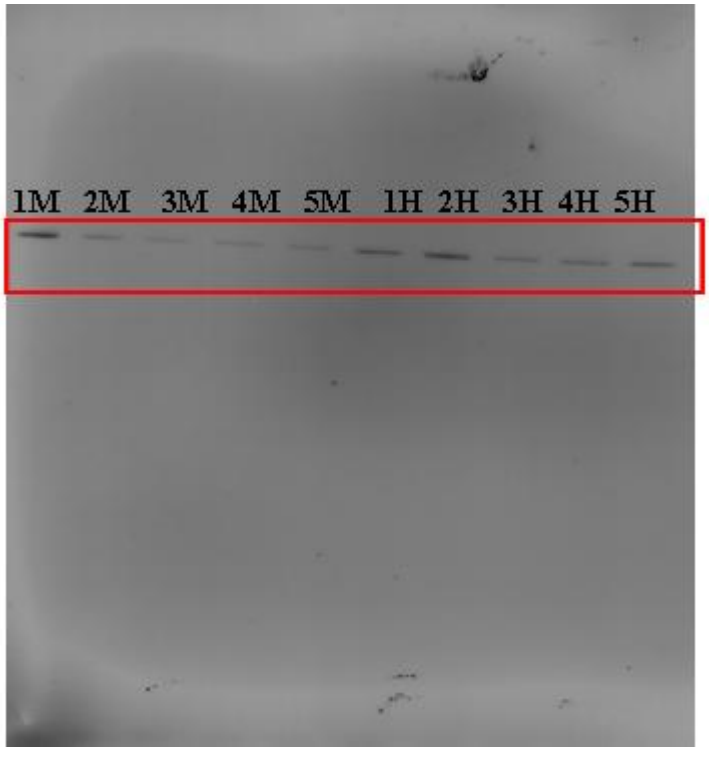

FIGURE G7 (8-week infected=801-810)

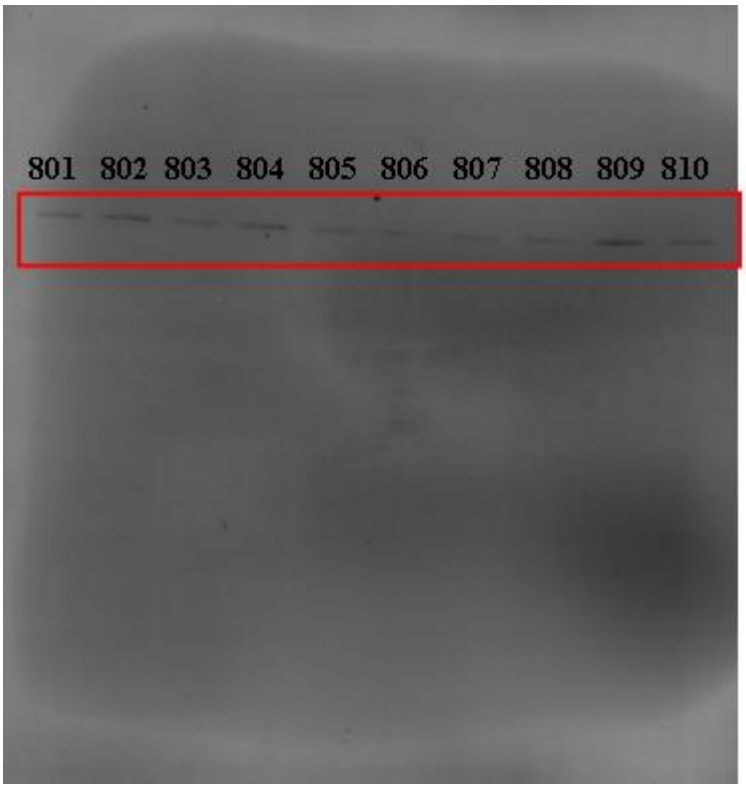

FIGURE G8 (12-week infected=1201-1210)

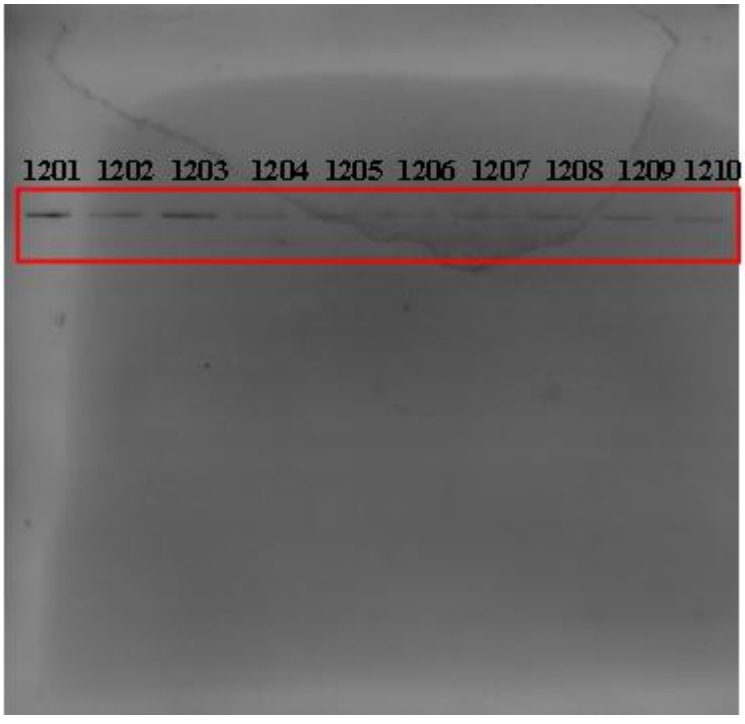

FIGURE G9-G13 Keratin D (cytokeratin 18) western blot analysis for (bands in red box) for mouse and human sera.

FIGURE G9 (INT=human intestinal schistosomiasis, samples INT1-12)

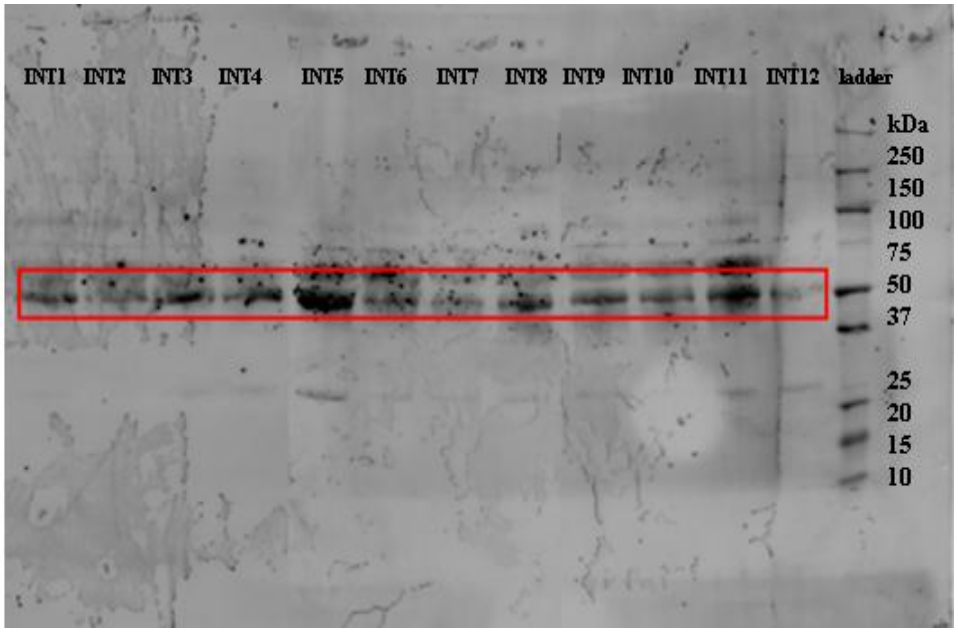

FIGURE G10 (INT=human intestinal schistosomiasis, samples INT13-23; HS= human hepatosplenic schistosomiasis, HS1)

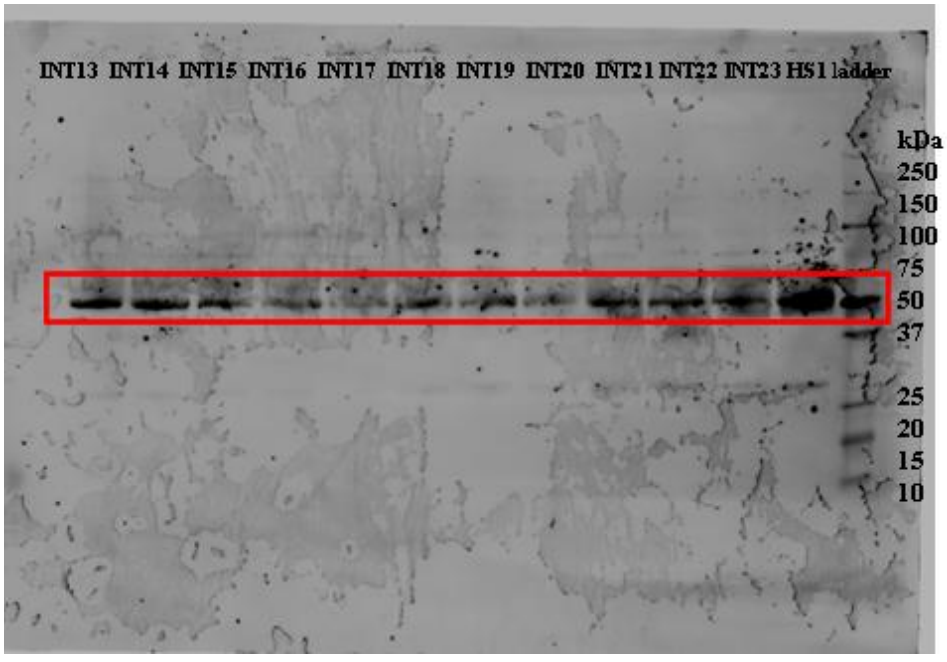

FIGURE G11 (HS= human hepatosplenic schistosomiasis, HS2-14)

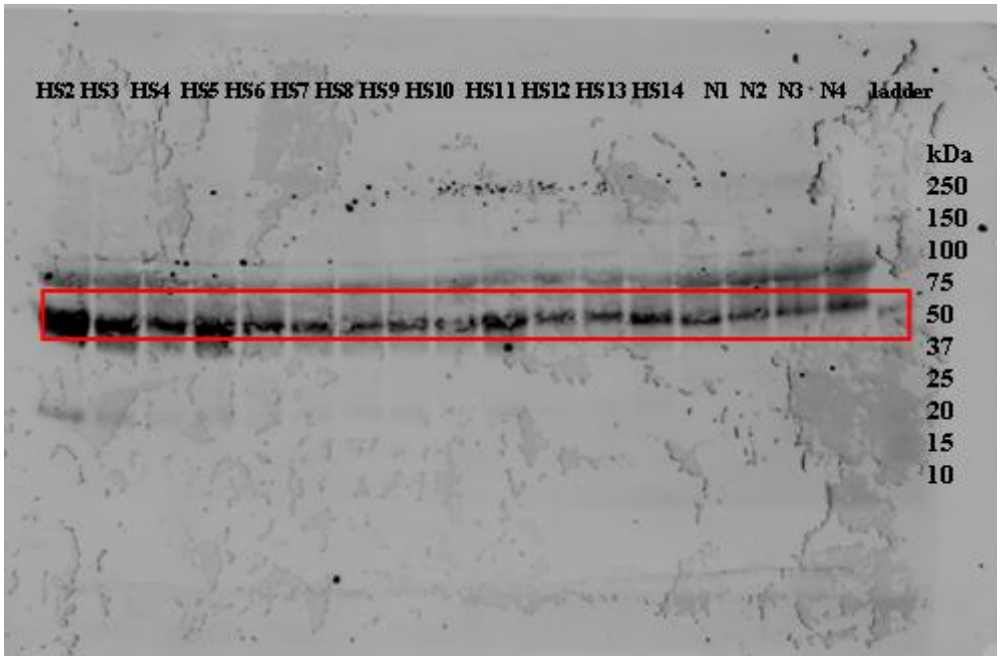

FIGURE G12 (mice control=C, 1-5; mice MSS=M, 1-5; mice HSS= H,1-5)

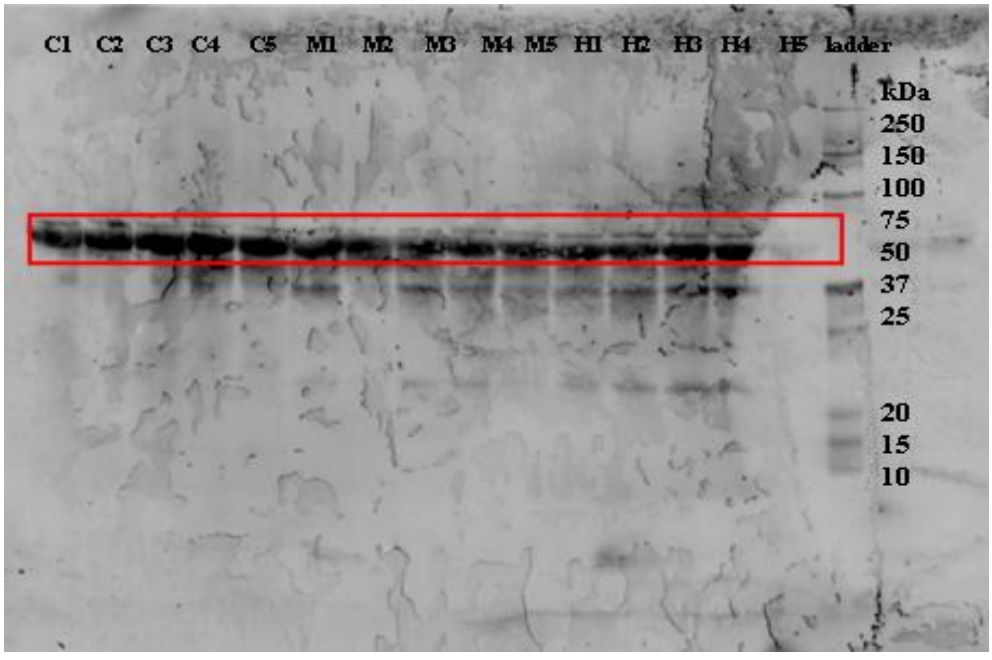

FIGURE G13 (INT=human intestinal schistosomiasis, INT12; HS= human hepatosplenic schistosomiasis, HS1)

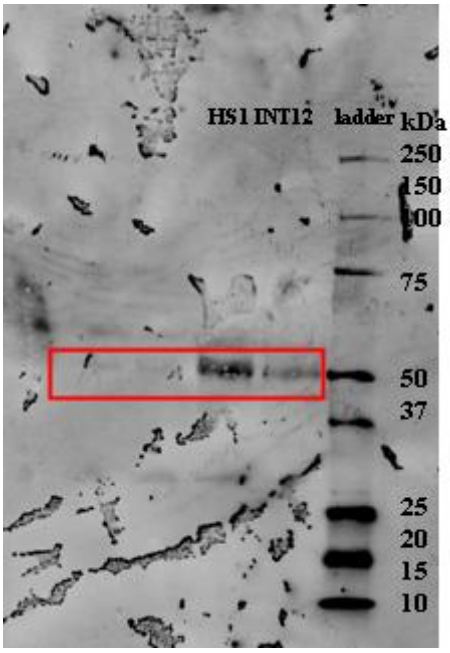

APPENDIX H

Publications:

1. B. Manivannan[1], P. Rawson[1], T. W. Jordan[1], W. E. Secor[2], and A. C. La Flamme[1]. 2010. Differential patterns of liver proteins in experimental murine hepatosplenic schistosomiasis. *Infection and Immunity.* 78: 618–628.

   [1]Centre for Biodiscovery and School of Biological Sciences, Victoria University of Wellington, Wellington, New Zealand, and [2]Centers for Disease Control and Prevention, Atlanta, Georgia (publication attached)

2. Bhagyashree Manivannan[§], Pisana Rawson[§], Thomas William Jordan[§], Diana M. S. Karanja[§§], Pauline N. M. Mwinzi[§§], Daniel G. Colley[¶], William Evan Secor[¶¶] and Anne Camille La Flamme[1*]. A mouse to human study for identification of candidate biomarkers for hepatosplenic schistosomiasis using liver proteome and serum analysis. [§]Centre for Biodiscovery and School of Biological Science, Victoria University of Wellington, Wellington, New Zealand; [§§]Centre for Vector Biology and Control Research, Kenya Medical Research Institute, Kisumu, Kenya; [¶]Centre for Tropical and Emerging Global Diseases and Department of Microbiology, 623 Biological Sciences Building, University of Georgia, Athens, GA, 30602-2606 USA; [¶¶]Centers for Disease Control and Prevention, Atlanta, GA, USA. *Manuscript in preparation*